TARGETING 5-ENOLPYRUVYLSHIKIMATE-3-PHOSPHATE SYNTHASE AND THE SHIKIMATE PATHWAY

By

Todd A. Funke

Submitted to the graduate degree program in Molecular Biosciences
and the Graduate Faculty of the University of Kansas
in partial fulfillment of the requirements for the degree of
Doctorate of Philosophy

_____
Chairperson

Committee Members*

_____*

_____*

_____*

_____*

Date defended: June 23rd 2008

The Dissertation Committee for Todd A. Funke certifies

that this is the approved version of the following dissertation:

Targeting 5-enolpyruvylshikimate-3-phosphate synthase and the shikimate pathway

Committee:

_____
Chairperson

_____

_____

_____

_____

Date defended: June 23rd 2008

Abstract

Bacteria, plants, fungi, and apicomplexan parasites require the functionality of the shikimate pathway for biosynthesis of essential aromatic compounds. Animals lack the enzymes that constitute the shikimate pathway, making these attractive antimicrobial targets.

Glyphosate (the active ingredient in *Roundup* herbicide) inhibits the shikimate pathway enzyme 5-enolpyruvyl-shikimate-3-phosphate synthase (EPSPS), but has limited antimicrobial activity. Several EPSPS point-substitutions can induce glyphosate tolerance, and some species possess EPSPS with intrinsic glyphosate insensitivity.

To aid development of second-generation EPSPS inhibitors, I probed the inhibition of glyphosate-tolerant EPSPS. I examined the effects of mutations at Pro101 and Thr97 on the structure, function, and glyphosate sensitivity of *E. coli* EPSPS; I kinetically characterized the glyphosate-tolerant *Staphylococcus aureus* EPSPS and *Agrobacterium sp.* strain CP4 EPSPS and determined the three-dimensional structure of the CP4 enzyme; I studied the interaction of EPSPS with analogs of the substrate and the tetrahedral intermediate; and I conducted high throughput screening to identify novel EPSPS inhibitors.

Acknowledgements

I would like to thank my mentor, Dr. Ernst Schönbrunn, for his guidance, training, and encouragement; for his willingness to allow me to find my own way and make mistakes; and for his constant support throughout my graduate career.

I would like to thank my co-workers: Dr. Melanie Priestman, Martha Healy-Fried, Dr. Andreas Becker, and Dr. Bernhard Trinczek, for their time and patience in teaching me experimental techniques and for their extensive advice and assistance; and Huijong Han, Katinka Bähr, Jennifer Biery, and Riazul Alam for their assistance, advice, and camaraderie.

I would like to thank my collaborators: Dr. Paul Bartlett and Dr. David Alberg for providing the TI analogs; Dr. Apurba Dutta for providing the shikimate analogs; Dr. Scott Crupper for providing the *S. aureus* EPSPS gene; Dr. Markus Fisher for synthesizing the CP4 EPSPS gene; and Dr. Veena Vasandani for assistance with HTS.

I would like to thank my committee members: Dr. Ernst Schönbrunn, Dr. William Picking, Dr. Susan Egan, Dr. David Davido, and Dr. Emily Scott. Dr. Emily Scott was exceedingly generous with her time and laboratory space, and I would like to thank her and her research group for tolerating my extended presence. Dr. Mark Richter served on my master's committee, and Dr. Kristen Bowman-James and Dr.

Paul Hanson directed the chemical biology training grant which provided funding for two years of my reasearch.

I would also like to note three excellent teachers who fostered my interest in science: James Gaede (Chemistry) and Jerald Hadley (Biology) from Larned High School, and Dr. Craig Martin (Biology) from the University of Kansas. Thank you.

For financial support I thank my mentor, Ernst Schönbrunn who provided support through NIH RO1 GM70633-02, and the NIH *Dynamic Aspects of Chemical Biology* Training Grant, which supported my final two years of graduate school.

Finally, I would like to thank my family. My parents, David and Jodi Funke, provided me with every opportunity to succeed and have always been a source of advice and encouragement. My entire family was very supportive, and I owe a special thanks to my grandfather, Harold Koehn, who encouraged my interest in the sciences. Most importantly, I thank my son, Anton Alonso Funke, who is my inspiration, and my wife, María Alonso Luaces, who has made me a better person and is always my strongest source of support.

Table of Contents

Chpt. 1: Introduction and Background

The 20th century was marked by the introduction of the first synthetic antibiotics, the sulfa drugs, and the first chemical herbicide, 2,4-D (2,4-Dichlorophenoxyacetic acid). The subsequent chemical revolution provided effective strategies to combat human disease and to control agricultural pests. These achievements are threatened by the evolution of drug-resistance in the target organisms, necessitating efforts to combat the development of resistance and strategies toward the discovery of novel chemotherapeutic agents.

Selectivity with respect to bioactivity is the crucial difference between a drug and a poison. To achieve this selectivity, non-conserved biosynthetic pathways are often targeted – for example, β-lactam antibiotics interfere with the crosslinking of peptidoglycan, essential for bacteria but non-existent in mammals. One of the most promising targets for the development of novel non-toxic herbicides and antimicrobial agents is the shikimate pathway.

The shikimate pathway is ancient and highly conserved, found in plants, fungi, and microorganisms, but never in animals (Fig. 1.1)[2, 3]. This seven-step biosynthetic pathway is responsible for the synthesis of chorismate, an essential precursor to the aromatic amino acids and many secondary metabolites. Representatives of each enzyme in the pathway have been purified from both prokaryotic and eukaryotic sources, and representative structures are available for each enzyme (Fig. 1.2). This pathway occurs in the cytosol of bacteria and in the plastids of plants, consistent with

Fig. 1.1: Simplified six-kingdom tree of life[4] – Red coloring indicates the presence of the shikimate pathway. This biosynthetic pathway apparently originated in the common ancestor and was only lost in Animalia (which *ingest* the necessary compounds)[5-8]

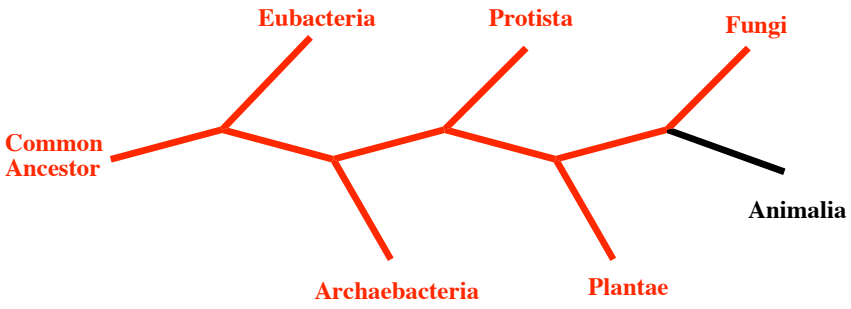

Fig. 1.2: The Shikimate Pathway. These reactions result in the biosynthesis of Chorismate (+ NADH + $NADP^+$ + H_2O + ADP + 4 P_i) from Erythrose-4-phosphate (+ 2 PEP + NAD^+ + NADPH + ATP). Each reaction in this seven-step synthesis is enzyme-catalyzed; since these enzymes are required by microorganisms but absent in mammals, they are attractive drug targets. Enzyme names are listed next to the reaction catalyzed; the names of the corresponding *E. coli* genes are italicized. Representative structures have been determined for each enzyme (cartoon diagrams with PDB IDs shown to the right).

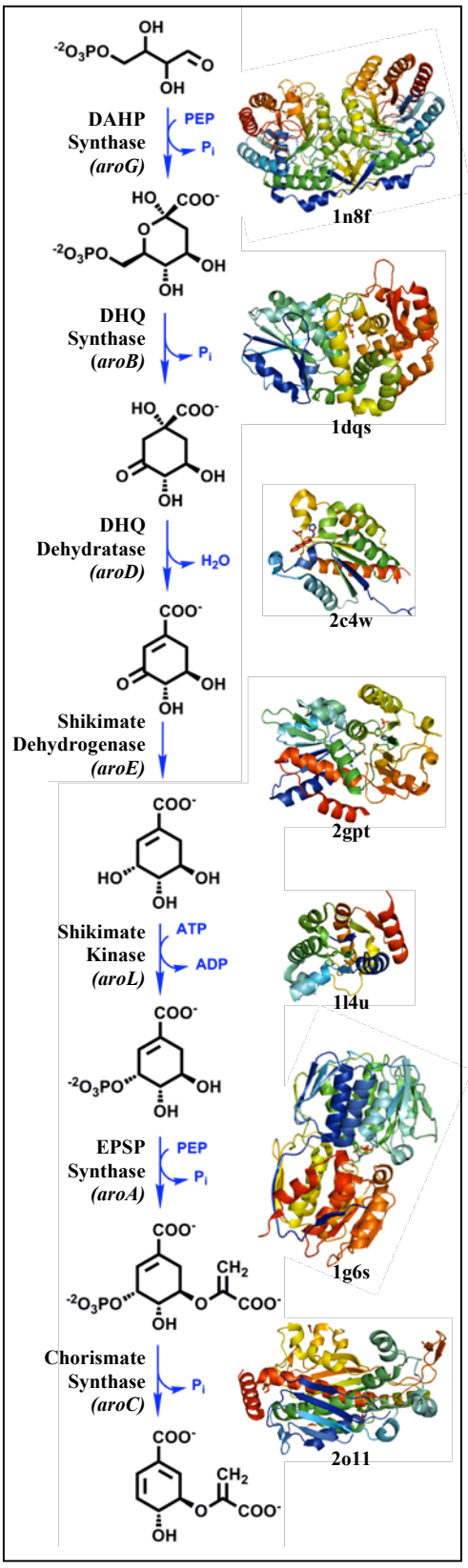

the concept that the eukaryotic shikimate pathway is the product of endosymbiosis. The shikimate pathway has been most extensively studied in bacteria, and the gene names listed in Fig. 1.2 correspond to *Escherichia coli* nomenclature. Substantial amino acid sequence divergence, along with structural and functional dissimilarities, are observed in shikimate pathway orthologs, and some species have various isozymes, but the synthetic steps of this pathway are consistent and conserved. The enzyme catalyzing the sixth step of the shikimate pathway, 5-enolpyruvyl shikimate-3-phosphate synthase (EPSPS; EC 2.5.1.19), has attracted particular attention as the molecular target of the broad-spectrum herbicide, glyphosate[9, 10] (N-phosphonomethylglycine; trade name, *Roundup*).

The reaction catalyzed by EPSPS (Fig. 1.3) results in the transfer of the enolpyruvyl moiety of phosphoenolpyruvate (PEP) to the 5'-hydroxyl of shikimate-3-phosphate (S3P), forming 5-enolpyruvyl shikimate-3-phosphate (EPSP) and inorganic phosphate (P_i). Glyphosate is a reversible inhibitor of this reaction, and shows competitive inhibition with respect to PEP[11]. While no structures of EPSPS from plants have been reported, the structure of *E. coli* EPSPS has been utilized as a model of EPSPS enzymes from plants and from other bacterial species.

A variety of evidence suggests that EPSPS and other shikimate pathway enzymes are attractive drug targets. The product of the shikimate pathway, chorismate, serves as a starting material for the biosynthesis of essential compounds including the aromatic amino acids and cofactors such as ubiquinone, vitamin K, and folate in plants, fungi,

Fig. 1.3: The reaction catalyzed by EPSPS.

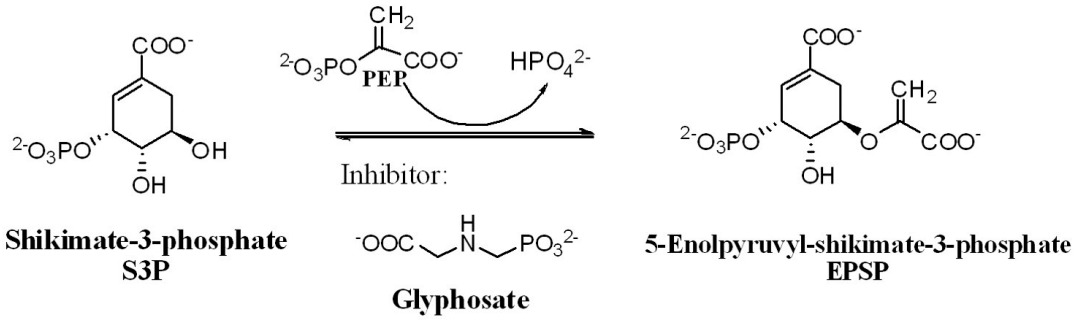

Shikimate-3-phosphate
S3P

Glyphosate

5-Enolpyruvyl-shikimate-3-phosphate
EPSP

and microorganisms, while mammals instead obtain the necessary aromatic compounds from their diets[12-14]. The deletion of the gene encoding EPSPS has been shown to result in attenuated virulence in *Staphylococcus aureus*, *Streptococcus pneumoniae*, and *Bordetella bronchiseptica*[15-17]. Many organisms, including *Mycobacterium tuberculosis*, *Pseudamonas aeruginosa*, *Vibrio cholerae*, and *Yersinia pestis*, require the production of chorismate-derived siderophores for pathogenicity[18, 19]. Further, the EPSPS inhibitor, glyphosate, has been shown to inhibit the *in vitro* growth of apicomplexan parasites including *Toxoplasma gondii*, *Plasmodium falciparum*, and *Cryptosporidium parvum*[20].

EPSPS in plants and bacteria is a 44-48 kDa enzyme composed of two globular domains connected by a short "hinge" region (Fig. 1.4). Binding of the first substrate, S3P, induces a global conformational change, with the N-terminal and C-terminal globular domains approaching each other to form the active site at the interdomain cleft. Several orthologs of EPSPS have known structures (Fig. 1.5); these include the EPSPS enzyme from *E. coli*, as mentioned, and also EPSPS enzymes from bacterial pathogens *Streptococcus pneumoniae*[21] and, recently, *Mycobacterium tuberculosis* (*unpublished*). The global structures and folding pattern are quite similar, with each globular domain composed of a three repeats of a βαβαββ-unit; each of these enzymes also exhibit the global induced fit as shown in *E. coli* EPSPS. The structure of the EPSPS active site, depicted in Fig. 1.6a, shows the inhibitor, glyphosate, bound adjacent to the substrate S3P, where PEP has been observed in other structures.

Fig. 1.4: Global conformational change: "open" to "closed" conformational change of EPSPS is induced by S3P binding[22].

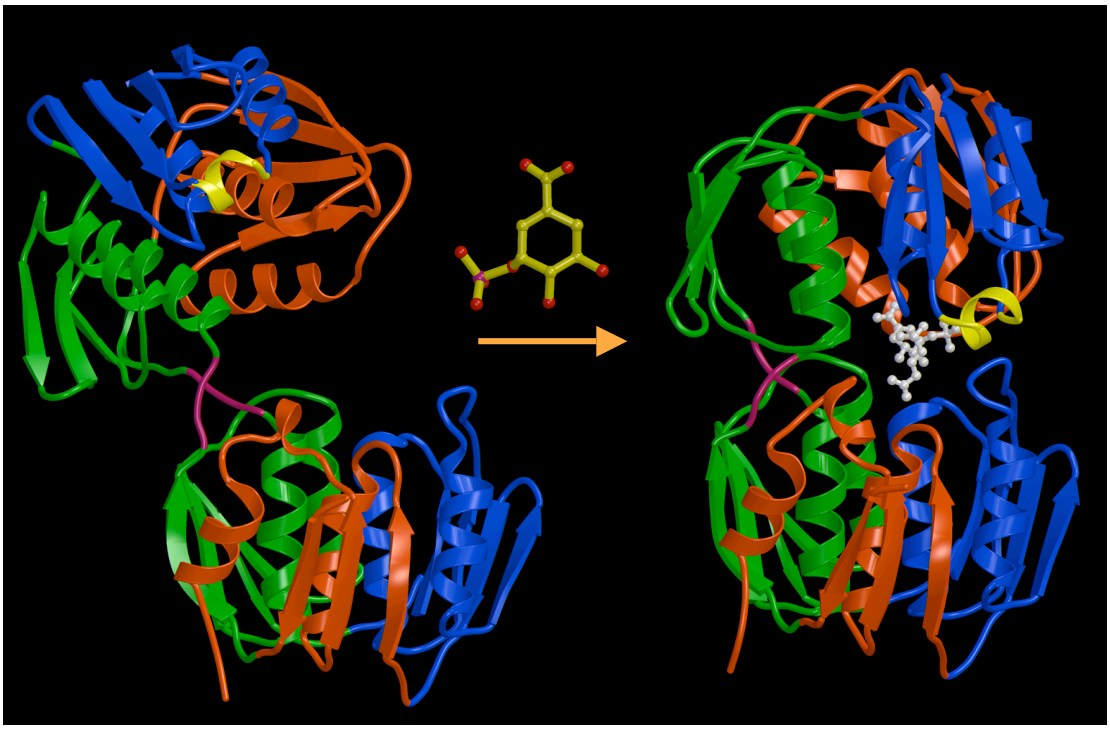

Fig. 1.5: Known structures of EPSPS. All show similar folding pattern and global induced-fit mechanism.

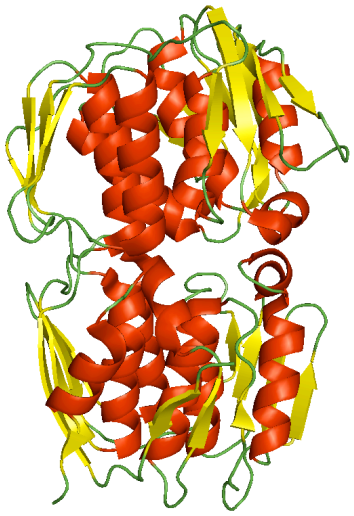

E. coli EPSPS
Open-form: Stallings *et al.* (1991) PDB ID 1eps[23]
Closed-form : Schönbrunn *et al.* (2001) PDB ID 1g6s[22]

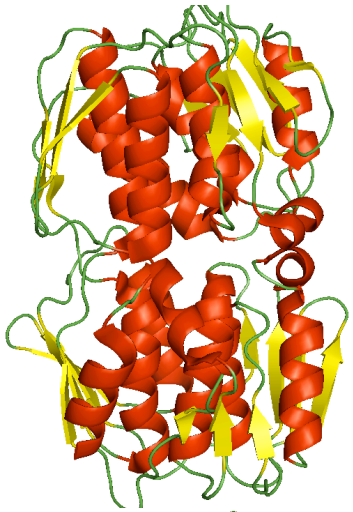

S. pneumoniae EPSPS
Open- and Closed-forms: Park *et al.* (2004) Respective PDB IDs are 1rf4 and 1rf6[21]

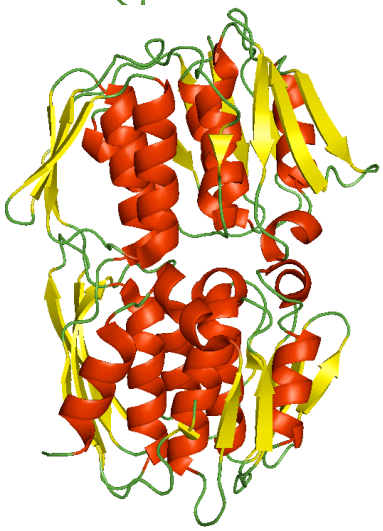

M. tuberculosis EPSPS
Open-form: Bourenkov *et al.* (2006) PDB ID 2bjb
Closed-form: Kachalova *et al.* (2008) PDB ID 2o0e
(*Unpublished; structures deposited to the PDB*)

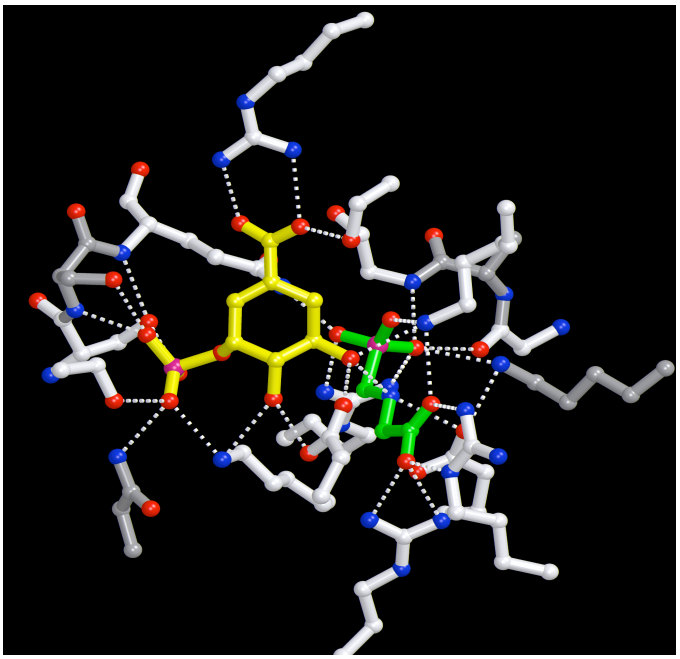

Fig. 1.6a: Structure of *E. coli* EPSPS active-site (E•S•I ternary complex; PDB ID 1g6s[1]). Glyphosate (green) binds in the active site adjacent to S3P (yellow). White dotted lines indicate hydrogen bonding interactions; water molecules and Tyr-200 are omitted for simplicity.

Fig. 1.6b: Hydrogen bonding interactions in *E. coli* EPSPS (E•S•I ternary complex[1]). Exploded active-site diagram shows hydrogen bonding to S3P and glyphosate (black dotted lines). Glyphosate occupies the binding site of the substrate, PEP (structure shown on right).

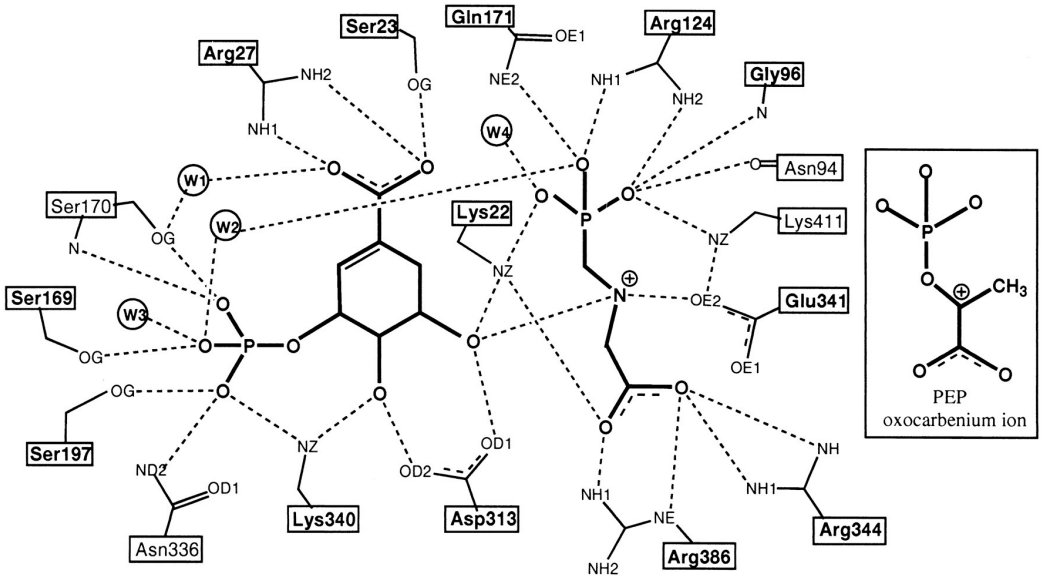

The hydrogen bonding interactions and active site architecture of EPSPS enzymes is highly conserved, even in enzymes with divergent amino acid sequences. Fig. 1.6b shows an exploded view of the active site hydrogen bonding interactions as found in the *E.coli* EPSPS•S3P•glyphosate active site; the PEP oxacarbenium ion is shown in the inset, next to the bound glyphosate molecule, to emphasize the structural similarities. The catalytic mechanism of the enzyme-catalyzed enolpyruvyl transfer is not completely understood. The mutation of active-site residue Asp313 (*E. coli* EPSPS D313A mutant) allowed trapping of the tetrahedral reaction intermediate (TI) bound to the enzyme[24]. This result, supported by the results obtained by chemical synthesis of the TI[25], demonstrated that the addition-elimination reaction proceeds through an (*S*)-configured tetrahedral intermediate (Fig. 1.7a). The possible mechanisms of this reaction are described and shown in more detail in Fig. 1.7b; the base responsible for the initial nucleophilic attack leading to the addition reaction is unknown, while the crystallographic results demonstrated that Asp313 proton-extraction results in the elimination reaction.

The structural information obtained has thus far not lead to the development of novel EPSPS inhibitors. The confined, highly charged nature of the active site limits the binding of many molecules, and the global induced-fit mechanism and flexibility of this enzyme have frustrated molecular modeling experiments. In fact, all potent inhibitors of this reaction are ground-state, product, or TI analogs, and the most potent known inhibitors are select TI analogs[26-28]. Extensive efforts to modify the

Fig. 1.7a: The enolpyruvyl transfer catalyzed by EPSPS is an addition/elimination reaction, proceeding through an S-configured tetrahedral intermediate[24]

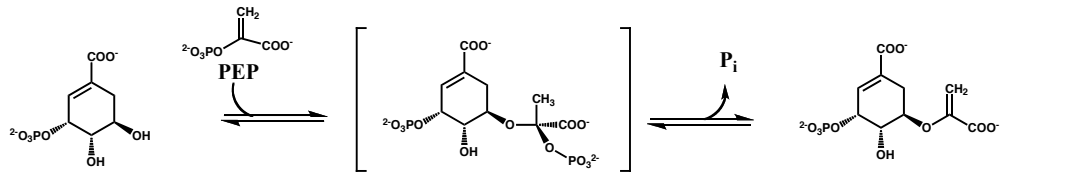

Shikimate-3-phosphate
S3P

(*S*)- Tetrahedral reaction intermediate
TI

5-Enolpyruvyl-shikimate-3-phosphate
EPSP

Fig. 1.7b: Proposed catalytic mechanism: Addition mechanism is not well known, elimination proceeds via proton abstraction by Asp313[24]

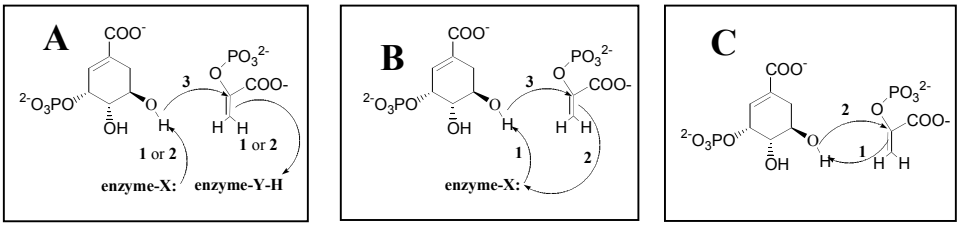

(*Above*) Three conceivable mechanisms for the addition reaction of enolpyruvyl transfer. **A**: If two residues are involved, then a base (X:) abstracts a proton from the target OH and an acid (Y-H) donates a proton to PEP. **B**: If one residue acts as a general acid-base catalyst, then it is likely to be a strong base, first abstracting a proton from the 5-OH of S3P and subsequently donating a proton to PEP. **C**: If no residue is involved at all, then the active site environment of S3P in the binary complex puts significant strain on the S3P molecule, making the 5-OH an acid, which first donates its proton to PEP followed by nucleophilic attack of the resulting oxyanion of PEP.

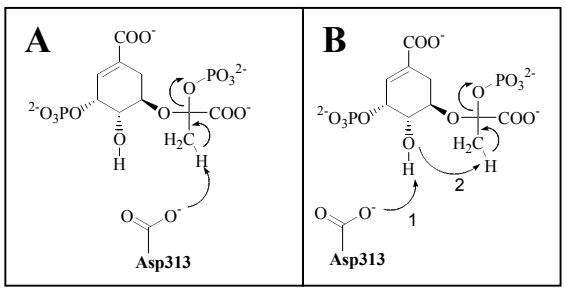

(*Left*) Two conceivable mechanisms for the elimination reaction of enolpyruvyl transfer.
A: Asp313 abstracts a proton from the PEP C-3 methyl group of the intermediate structure directly.
B: Asp313 abstracts a proton from the 4-OH of S3P; the resulting oxyanion then abstracts a proton from the C-3 of the PEP moiety.

structure of glyphosate showed that essentially any modification of this molecule resulted in decreased activity against EPSPS[29]. Glyphosate has excellent herbicidal properties and very low human and environmental toxicity[30, 31]. These attributes, together with the existence and widespread adoption of commercial varieties of glyphosate-tolerant crops (52% of corn, 70% of cotton, and 91% of soybeans planted in the United States in 2007 were glyphosate-resistant varieties[32]), have made glyphosate the most-used pesticide in the world.

While the success of glyphosate as a herbicide demonstrates proof-of-concept for the targeting of the shikimate pathway, glyphosate itself has poor antimicrobial properties, and a number of bacteria have intrinsically glyphosate-insensitive EPSPS synthases[33-37]. On the basis of their catalytic efficiency in the presence of glyphosate, EPSPS enzymes from bacteria including *Staphylococcus aureus*, *Agrobacterium sp.* strain CP4, and *Pseudomonas sp.* strain PG2982, have been termed "class II" EPSPS enzymes. The sequence of *aroA* genes isolated from plants or bacterial species such as *E. coli*, *Klebsiella pneumonia,* or *Salmonella typhimurium* are quite similar; based on their sensitivity to inhibition by glyphosate, these "plant-like" enzymes are termed "class I" EPSPS.

Richards *et al.* (2006) examined the phylogenetic relationship of shikimate pathway genes from a variety of organisms[5]. The phylogeny of *aroA* genes (Fig. 1.8) suggests a genetic basis for some of the observed functional differences. The genes encoding plant EPSPS enzymes are clustered in the upper branch of this phylogenetic tree,

Fig. 1.8: Phylogenetic tree of *aroA* genes (taken from ref [5]). The length of the horizontal connecting lines represents the degree of sequence divergence observed (longer line = more substitutions).

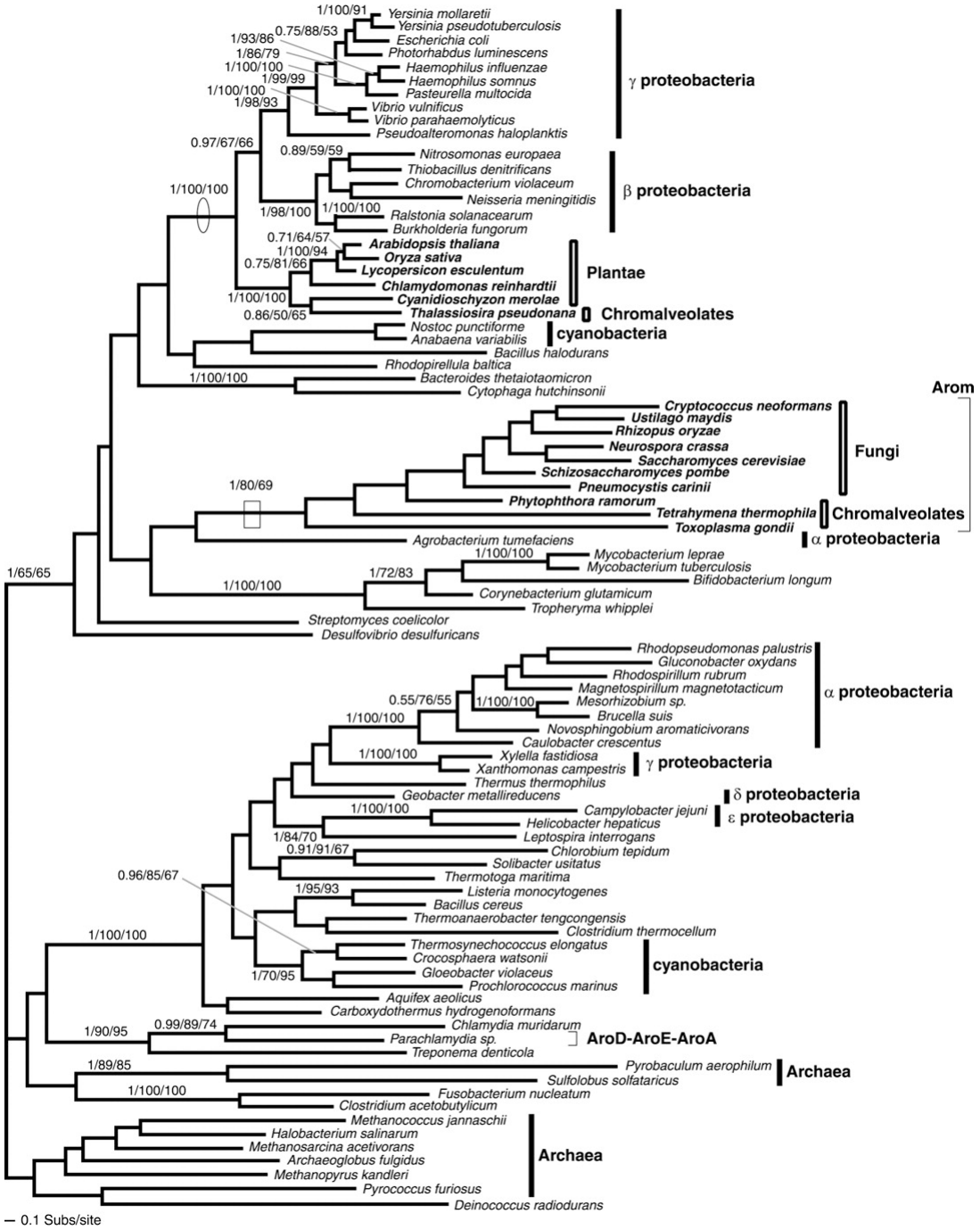

together with *aroA* genes from proteobacterial species, including *E. coli*. The genes encoding EPSPS enzymes from Fungi, *Mycobacterium spp*., and apicomplexan parasites seem to form a clade and appear to be related to the class I EPSPS enzymes. Substantial sequence diversity is observed within class II EPSPS enzymes, and while these glyphosate-tolerant enzymes cannot be easily defined or distinguished by amino acid sequence, it appears likely that organisms with Class II EPSPS genes comprise a subset of the largest and most diverse clade (the lower branch of this phylogenetic tree). To confirm this would require examination of the glyphosate-sensitivity of each organism's EPSPS enzyme. Overall, phylogenetic analysis indicates that the *aroA* genes encoding class I and class II EPSPS enzymes diverged long ago and have undergone substantial sequence differentiation. The diversity of Class I EPSPS enzymes is very limited compared to the overall diversity of EPSPS enzymes, and few pathogenic species have Class I enzymes. Some organisms knows to possess class II EPSPS enzymes are human pathogens, but essentially no data are available concerning the structure, activity, or inhibition of the class II EPSPS enzymes. Such data are desired, along with detailed structure-function studies, in order to facilitate the development of broad-spectrum antimicrobial compounds.

The effectiveness of antibiotic drugs characteristically deteriorates due to the emergence of drug-resistant bacterial strains. A great deal of genetic variation exists between bacterial species; in combination with the massive number of individual bacteria, this represents an enormous reservoir of genetic diversity. Utilization of antibacterial agents effectively screens this genetic reservoir, selecting for drug-

resistant organisms. The short generation time of bacteria, coupled with horizontal gene-transfer mechanisms, facilitates the relatively rapid emergence of drug-resistant bacterial strains. L.C. McDonald (2006) examined the emergence of penicillin-resistant and methicillin-resistant strains of *S. aureus* (Fig. 1.9)[38]. Drug-resistant *S. aureus* strains emerge first in hospital settings, then in the general population. In each case, the percentage of antibiotic-resistant *S. aureus* isolates increased at an exponential rate, quickly diminishing the utility of the antibiotic agent and demonstrating the need for novel drugs. The maintenance of effective therapies to combat bacterial infections thus requires on-going research into potential drug targets and the continual development of novel antimicrobial agents.

The development of resistance is also observed in plants. From the introduction of glyphosate-based herbicides in 1974 until 1996, no evolved glyphosate-resistant weed species were described. R.F. Service (2007) plotted the evolution of glyphosate-resistant plants (Fig. 1.10)[39]. These data show that since 1996, the number of plant species with evolved glyphosate-resistance has increased at an exponential rate. The scale of modern chemical agriculture is such that the question is not *whether* pesticides will be used, but *which* pesticides will be used. In light of glyphosate's broad-spectrum phytoxicity, minimal environmental persistence, and lack of animal toxicity, coupled with the increasing utilization of glyphosate-dependent soil conservation practices (such as no-till farming), and the efficiency and market dominance of glyphosate-tolerant (*Roundup Ready*) crops varieties, the widespread

Fig. 1.9: Evolution of antimicrobial resistance in *S. aureus* (taken from ref [38]). Grey lines indicate percentage of resistant bacteria isolated from healthcare settings, black lines indicate percentage of resistant bacteria in the general population. The left-side plots show occurrence of penicillin-resistant isolates, while the right-side plots show the occurrence of methicillin-resistant isolates.

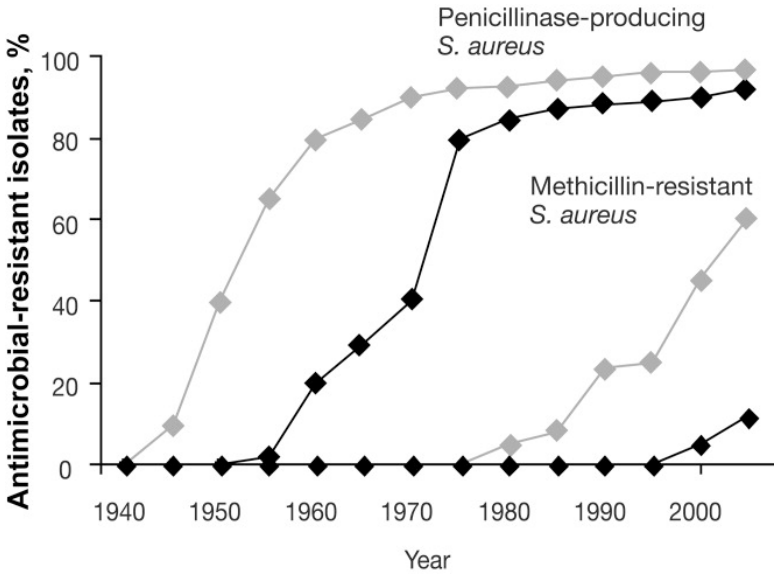

Fig. 1.10: Evolution of glyphosate-resistant weed species (taken from ref [39]). The first field-evolved glyphosate-resistant weed species was described in 1996; the number of such species appears to be increasing at an exponential rate.

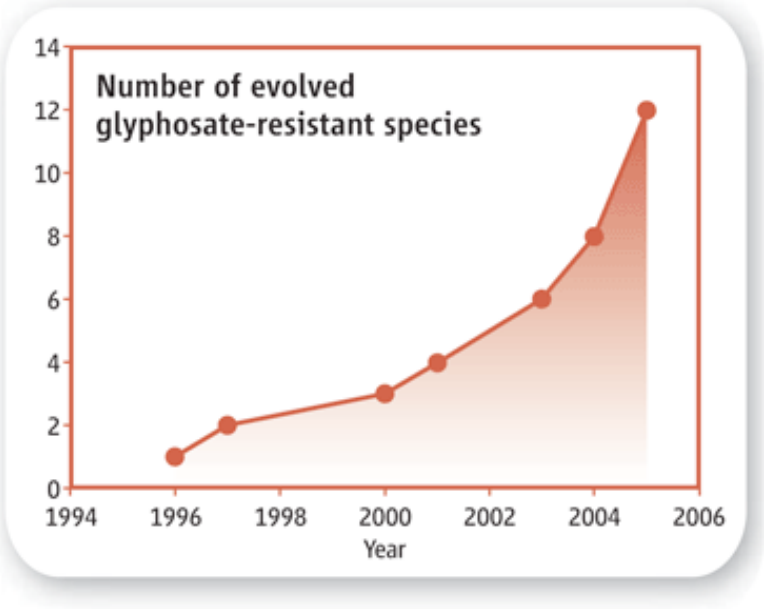

emergence of glyphosate-resistant weeds constitutes a significant threat to agriculture and the environment[39-42].

We believe that the targeting of shikimate pathway enzymes is an efficient strategy toward the development of the required novel antimicrobial and herbicidal agents. Here, we describe our progress in understanding the inhibition of EPSPS and our efforts toward development of second-generation EPSPS inhibitors.

List of Abbreviations

2,4-D	2,4-Dichlorophenoxyacetic acid
2F-TI	(*R*)-difluoromethyl TI analog
Abs	Absorbance
Ala, A	Alanine
Amp	Ampicillin
ANS	1-anilino-8-naphthalene sulfonate
Arg, R	Arginine
APS	Ammonium persulfate
a.u.	Arbitrary units
AUC	Area-under-the-curve
BSA	Bovine serum albumin
CP4	*Agrobacterium sp.* strain CP4 EPSPS
CV	Column volume
Cys, C	Cysteine
DMSO	Dimethysulfoxide
DNA	Deoxyribonucleic acid
DTT	Dithiothreitol
E. coli	*Escherichia coli*
EDTA	Ethylenediaminetetraacetic acid
EPS	5-enolpyruvylshikimate
EPSP	5-enolpyruvylshikimate-3-phosphate
EPSPS	5-enolpyruvylshikimate-3-phosphate synthase

EtOH	Ethanol
F_c	Calculated structure factors
F_L	Fluorescence intensity observed in presence of ligand
F_o	Observed structure factors
F_O	Original fluorescence intensity observed
FPLC	Fast protein liquid chromatography
Glp	Glyphosate
Glu, E	Glutamic acid
HCl	Hydrochloric acid
HEPES	N-[2-Hydroxyethyl] piperazine-N'-[2-ethanesulfonic acid]
HPLC	High pressure liquid chromatography
HTS	High throughput screening
IC_{50}	50% inhibitory concentration
ID	Identification number
Ile, I	Isoleucine
IPTG	Isopropyl-β-D-thiogalactoside
Kb	Kilobase
k_{cat}	Catalytic rate constant
K_d	Dissociation constant
K_i	Inhibition constant
K_m	Michaelis constant
kDa	Kilodalton
LB	Luria-Bertani
Leu, L	Leucine

M. jannaschii	*Methanococcus jannaschii*
M. tuberculosis	*Mycobacterium tuberculosis*
MES	2-[N-Morpholino] ethanesulfonic acid
NAD^+	Nicotinamide adenine dinucleotide
NADPH	Nicotinamide adenosine dinucleotide phosphate
OD	Optical density
PEP	Phosphoenolpyruvate
PDB	Protein data bank
Phe, F	Phenylalanine
P_i	Inorganic phosphate
Q-seph	Q-sepharose
r.m.s.d.	Root mean squared deviation
rpm	Revolutions per min
RP-TI	(*R*)-phosphonate TI analog
S3P	Shikimate-3-phosphate
S. aureus	*Staphylococcus aureus*
S. pneumoniae	*Streptomyces pneumoniae*
Ser, S	Serine
SDS	Sodium dodecyl sulfate
SDS-PAGE	Sodium dodecyl sulfate polyacrylamide gel electrophoresis
SK	Shikimate Kinase
SP-TI	(*S*)-phosphonate TI analog
TAE	Tris, Acetic acid and EDTA buffer
TEAB	Triethylammonium bicarbonate

TEMED	N,N,N',N'-Tetra-methylethylenediamine
TI	Tetrahedral reaction intermediate
Tris	Tris hydroxymethyl aminomethane
U/mg	micromoles product formed per minute, per milligram of enzyme
UV	Ultraviolet
(v/v)	Volume/volume
(w/v)	Weight/volume
WT	Wild-type enzyme

General Protocols

All chemicals and equipment were purchased from Sigma (St. Louis, MO) or Fisher (Springfield, NJ) unless otherwise noted. A Labconco Water Pure Plus System was used to purify all ddH_2O used for research. Deviations from the standard procedures, as well as additional specific procedures, are noted in the Experimental procedures section of each research chapter.

Media- All media was autoclaved and stored at 4 ˚C. Antibiotic stocks were added to the media just prior to use.

LB Media:

10 g tryptone

7.5 g yeast extract

5 g NaCl

Fill to 1 L with H_2O

LB Agar:

20 g granulated agar

Fill to 1 L with LB media

LB agar was autoclaved and allowed to cool to 30 °C before addition of appropriate antibiotic stocks, then was poured into Petri dishes and stored at 4 °C.

Antibiotics- Ampicillin stocks at 100 mg/ml in H_2O or Kanamycin stocks at 30 mg/ml were sterile filtered with a 0.45 μm filter and stored at -20 ˚C. Amp and Kan

stocks were diluted 1:1000 for all purposes (final [Amp] = 100 μg/ml; final [Kan] = 30 μg/ml).

DNA Electrophoresis- One-percent (w/v) agarose gels were utilized to separate DNA on the basis of size; 500 mg of agarose was heated in 50 ml of 1X TAE until dissolved, 1 μl of ethidium bromide (5 mg/ml) was added to the solution and the gel was cast using a DNA mini-submarine gel electrophoresis unit (GE Healthcare, Piscataway, NJ). DNA samples were prepared by addition of 1 μl of 10X Bluejuice and 1-9 μl of DNA to 0-8 μl of H_2O, for total sample volume = 10 μl. Electrophoresis of gels was typically performed at 120 mV for 45 min. A 50X concentrated solution of TAE was stored at room temperature and diluted to 1X prior to use.

50X TAE:

242 g Tris (pH 8.5)

57.1 ml glacial acetic acid

100 ml 0.5 M EDTA (pH 8.0)

Fill to 1 L with H_2O

Following electrophoresis, the ethidium bromide-intercalated DNA was visualized with UV light and compared to a molecular ladder containing 10, 7, 5, 4, 3, 2.5, 2, 1.5 and 1 Kb markers, prepared by adding 5 μl Low-Range DNA marker (Cambrex Bio Science, Rockland, ME) and 2 μl 10X Bluejuice (Invitrogen) to 3 μl H_2O.

SDS-PAGE- Protein samples for SDS-PAGE were denatured by addition of 5x SDS-PAGE loading buffer to the protein sample to effect a final concentration of 1x, followed by incubation for 10 min at 100˚C. The samples were loaded onto the SDS gel by pipetting 20 μl into each lane. Electrophoresis of gels was conducted in a reservoir of 1x Running Buffer using a mini PROTEAN 3 cell (Biorad) at 160 V for 1 hour. To visualize protein samples, SDS gels were soaked in the coomassie-based staining solution for ~ 15 minutes followed by removal of excess coomassie dye by soaking SDS gels for several hours in the destaining solution. Sample migration in SDS-PAGE experiments was monitored visually by comparison to the known-MW protein ladder. Acrylamide/Bis Solution, 30% 19:1 crosslinker ratio (Biorad), APS, TEMED (Biorad) and Tris buffers were stored at 4 ˚C. The Low Range MW ladder was stored at -20˚C. All other solutions were stored at room temperature. SDS-PAGE gels were made in-lab and stored at 4˚C for up to 2 weeks. The resolving portion of the gel was cast and allowed to solidify first, then topped by a ~ 1.5 cm stacking portion. The list of ingredients for each solution follows:

Resolving portion, SDS Gel:

4 ml 30 % Acrylamide/Bis solution

100 μl 10 % (w/v) SDS

2.5 ml 1.5 M Tris (pH 8.8)

3.36 ml H_2O

80 μl 10 % (w/v) APS

10.0 μl TEMED

Stacking Portion, SDS gel:

650 µl 30 % Acrylamide/Bis solution

50 µl 10 % SDS

1.25 ml 0.5 M Tris (pH 6.8)

3.05 ml H_2O

40 µl 10 % APS

5 µl TEMED

5X SDS-PAGE Loading Buffer:

1.82 g Tris (pH 8.5)

5 g SDS

12.5 ml β-mercaptoethanol

25 ml glycerol

1.28 ml HCl

0.028 g bromophenol blue

Fill to 50 ml with H_2O

Low-Molecular-Weight Marker:

50 µl concentrated Low-Range marker (Biorad)

100 µl 5X loading dye

350 µl H_2O

Heat 5 min at 100˚C.

Store at -20˚C.

Apply 5 μl marker to visualize ladder.

MW of ladder bands correspond to 97.4, 66.2, 45, 31, 21.5 and 14.4 kDa.

10X SDS-PAGE Running Buffer:

30 g Tris (pH 8.5)

144 g glycine

10 g SDS

Fill to 1 L with H_2O

Coomassie Staining Solution:

1.25 g Coomassie brilliant blue R-250

500 ml 95 % EtOH

450 ml H_2O.

50 ml 100 % acetic acid.

Filtered and stored in a dark bottle.

Destaining Solution:

500 ml EtOH

100 ml acetic acid

400 ml H_2O

Competent cells- *E. coli* chemically competent cell strains utilized were: BL21(DE3), BL21 Star (DE3), and DH5α (Invitrogen). Commercial stocks of competent cells were generally utilized; in-house stocks of $CaCl_2$ competent cells were generously

provided by Dr. Melanie Priestman, Dr. Bernhard Trinczek, Katinka Bahr, and Jennifer Biery.

Transformations- Competent cells were transformed by adding 50 to 250 ng of plasmid to 95 μl of a glycerol stock of chemically competent cells. This mixture was incubated on ice for 30 min, heat-shocked for 45 sec at 42˚C and incubated again on ice for 2 min. After adding 900 μl of LB media, the mixture was incubated 1 h at 37°C with shaking at 250 rpm. The cells were then centrifuged for 4 min at 5,000 rpm and 900 μl of supernatant was removed. The pellet was resuspended in the remaining broth, plated on LB agar plates containing the appropriate antibiotic and incubated overnight at 37˚C.

Plasmid preparation- Plasmids were isolated from cultures and purified using the Mini-Prep kit (Qiagen), according to the manufacturer's protocol. Plasmid and DNA fragments were isolated from agarose gels using Gel Extraction kits (Qiagen) according to the manufacturer's protocol. In either case, DNA was typically eluted in 30 μl sterile H_2O.

DNA Sequencing- DNA sequences were verified by sequencing at the University of Kansas Medical Center's Biotech Research Support Facility or at the Idaho State University Molecular Reaseach Core Facility, using appropriate primers.

Mutagenesis- Site-directed mutagenesis was performed to introduce desired mutations using the QuikChange II site-directed mutagenesis kit (Stratagene),

according to the manufacturer's instructions. Appropriate primers were synthesized by MWG Biotech. Following *Dpn*I digestion, products were transformed into DH5α competent cells, plated to agar, and incubated overnight. Colonies were selected for overnight cultures, plasmids were isolated as described, and the presence of the mutations were verified by DNA sequencing.

Induction Studies- To assay soluble over-expression, positively sequenced plasmids were transformed into competent cell lines, colonies were picked from each transformation plate, and incubated in 5 ml LB media and the appropriate antibiotic overnight at 37°C with shaking. A 50 µl aliquot of the overnight culture was used to inoculate 5 ml of fresh LB-antibiotic media, and the culture was again incubated at 37˚C while shaking at 250 rpm. After reaching an OD_{600} of 0.4 - 0.6, a 1 ml aliquot was removed to serve as a control, and the cells were induced with IPTG to a final concentration of 0.5 mM. After induction, cells were incubated for 4-6 hours at 37˚C with shaking. A 1 ml aliquot was subsequently removed and all aliquots were centrifuged at 13,000 rpm for 1 minute. The supernatant was discarded and each cell pellet was resuspended in 200 µl extraction buffer then sonicated to lyse the cells. Following sonication, the uninduced control samples were set aside and the pellet solution from the induced samples were again centrifuged for 1 min at 13,000 rpm. The supernatant (containing soluble proteins) was removed, and the pellet (containing insoluble protein and cell debris) was resuspended in 200 µl of extraction buffer. The uninduced control, induced supernatant, and induced pellet samples were mixed with 50 µl 5X loading dye, vortexed briefly, and heated for 10 min at 100°C. The levels of

soluble over-expression were visualized with SDS-PAGE. As needed, the induction studies were repeated with adjustments to the time and temperature of incubation, the cell density at the time of induction, and the final concentration of IPTG, in attempts to increase the amount of soluble protein.

Glycerol stocks- A 900 µl aliquot of an overnight cell culture was mixed with 100 µl sterile 80% glycerol and stored at -80°C for use in future experiments.

Protein overexpression- Typically, overexpression of protein was achieved by using 50 µl of the appropriate glycerol stock to start a 50 ml overnight culture at 37°C, in LB media with the appropriate antibiotic. The following day, 5 ml aliquots of the overnight culture were added to each of 6 flasks containing 500 ml each of LB media with the appropriate antibiotic and 1 drop of antifoam solution (Triton-X100). These cultures were incubated with shaking at 37°C until log phase (OD_{600} of 0.4-0.8) was reached, then protein overexpression was induced by addition of IPTG to a final concentration of 0.5 mM. After induction, the cells were allowed to grow 4-6 hours at 37°C, then the cells were pelleted by centrifugation (6,000 rpm for 10 minutes). The cell pellets were collected, weighed, and stored at -80°C.

Protein extraction and purification buffers- All buffers for protein purification were prepared at 4°C using purified H_2O, pH-adjusted with NaOH or HCl, filtered with a 0.45 µm filter, and stored at 4°C.

Extraction Buffer:

50 mM Tris-Cl (pH 7.8)

2.5 mM DTT

1 mM EDTA

0.1 % (v/v) Tween 20

Phenyl-sepharose Buffer A:

50 mM Tris-Cl pH 7.8

1 mM EDTA

1 mM DTT

Phenyl-sepharose Buffer B:

50 mM Tris-Cl pH 7.8

1 mM EDTA

1 mM DTT

1 M $(NH_4)_2SO_4$

Phenyl-sepharose cleaning solutions:

a) 2 CV 1 M NaOH

b) 2 CV 20 % Ethanol

c) 2 CV 1 M HCl

d) 2 CV H_2O

Q-sepharose Buffer A:

50 mM Tris-Cl pH 7.8

1 mM EDTA

1 mM DTT

Q-sepharose Buffer B:

50 mM Tris-Cl pH 7.8

1 mM EDTA

1 mM DTT

0.4 M KCl or NaCl

Q-sepharose cleaning solutions:

a) 2 CV 1 M NaOH

b) 2 CV 20 % Ethanol

c) 2 CV 2M NaCl

d) 2 CV H_2O

Resource-Q Buffer A:

50 mM Tris-Cl pH 7.8

1 mM EDTA

1 mM DTT

Resource-Q Buffer B:

50 mM Tris pH 7.8

1 mM EDTA

1 mM DTT

0.4 M KCl or NaCl

Resource-Q cleaning solutions:

a) 5 CV 1 M NaCl

b) 5 CV H_2O

c) 5 CV 1 M NaOH

d) 5 CV H_2O

e) 5 CV 1 M HCl

f) 5 CV H_2O

g) 5 CV 1 M NaCl

h) 5 CV H_2O

Size-exclusion chromatography protocol:

Utilized pre-equilibrated gel filtration columns,

Maximum flow rate = 0.5 ml/min,

Isocratic elution of samples

Specific buffer conditions as described.

Size-exclusion cleaning procedure:

a) 2 CV 1 M NaOH

b) 2 CV 20 % Ethanol

c) 2 CV 2M NaCl

d) 2 CV H_2O

Standard protein purification- Enzymes were purified at 4°C using ÄKTA FPLC systems and prepacked columns, typically according to standard procedures described by Eschenburg *et al*. (2002)[43]. Cell pellets obtained from overexpression cultures were resuspended in extraction buffer plus lysozyme and stirred for 1 hour at 4°C, using 10 ml extraction buffer and 1 mg lysozyme per 1 g of cell pellet weight. The solution was then sonicated on ice for 2x30 seconds. After sonication, insoluble cell debris was removed by centrifugation for 30 min at 14,000 rpm. The supernatant was pooled and undesired proteins were precipitated by stirring for 1 hour at 4°C in the presence of a 25% saturating concentration of $(NH_4)_2SO_4$. Following the $(NH_4)_2SO_4$ precipitation, samples were clarified by centrifugation at 18,000 rpm for 1 hour. The supernatants were then applied to a Phenyl Sepharose 26/10 hydrophobic interaction column, pre-equilibrated with Buffer B (50 mM Tris, 1 mM DTT, 1 mM EDTA, pH 7.8 + 1 M $(NH_4)_2SO_4$, and protein fractions were eluted from the column by decreasing the salt concentration in the mobile phase (gradient: 0 % Buffer A to 100% Buffer A over 10 CV). The fractions containing the target protein were identified by size using SDS-PAGE, or by enzymatic activity using the appropriate assay. The fractions containing the target protein were combined, and removal of salt was accomplished by concentrating samples on an Amicon protein concentration cell (with the appropriately-sized Millipore filter) with serial addition of Q-sepharose Buffer A until salinity readings were less than 10 mS/cm^2 were recorded using a conductivity meter. This desalted and concentrated protein solution was loaded onto a Q-Sepharose 26/10 and the protein was eluted from the column by increasing the salt

concentration in the mobile phase (gradient: 100% Buffer A to 0% Buffer A over 10-15 CV). As previously, fractions containing the target protein were pooled, concentrated, and buffer exchanged using to reach a conductivity of < 10 mS/cm^2. The protein was then applied to a 6 ml Resource-Q column and subjected to a secondary anion-exchange purification. Again, the protein was eluted by increasing the salt in the mobile phase (gradient: 100 % Buffer A to 0% Buffer A over 25 CV). Fractions containing the target protein were identified by SDS-PAGE or enzymatic activity, and homogeneity of at least 95% was verified by coomassie-stained SDS-PAGE. For kinetic analysis, the purified proteins were aliquoted, shock-frozen in liquid nitrogen, and stored at -80°C**.** For crystallographic analysis, the purified proteins were concentrated in 50 mM Tris-Cl pH 8.0 and 2 mM dithiothreitol using Centricon-30 devices (Millipore) at 4°C. Again, these were aliquoted, shock-frozen in liquid nitrogen, and stored at -80°C**.**

Protein concentration determination- Protein concentrations were determined spectroscopically using coomassie reagent (Pierce) according to the Bradford[44] method, with bovine serum albumin as a standard. For cuvette-based assays, 5 µl protein sample, 95 µl H_2O, and 900 µl coomassie reagent were utilized. For microtiter-plate-based assays, 5 µl protein sample, 15 µl H_2O, and 180 µl coomassie reagent were utilized. Absorbance was measured at 595 nm and the data were fit to a BSA standard curve to determine the protein concentration.

Standard Production of S3P- The enzymatic synthesis of S3P was typically achieved according to the protocol described by Priestman *et al.* (2005)[45] using a His_6-tag-*Methanococcus jannaschii* SK[46] (gift from Integrated Genomics Inc.). For all experiments, the *M. jannachii* SK enzyme was provided by Dr. Melanie Priestman or Martha Healy-Fried.

Briefly, to obtain the SK, a pET-derived vector with ampicillin resistance containing the *M. jannaschii* SK gene was transformed into BL21(DE3) *E. coli* cells, large-scale cultures were grown to log phase (OD_{600} = 0.4 to 0.6) at 37ºC , induced by the addition of IPTG, and grown an additional 24 hours at 20ºC. Cells were collected by centrifugation, resuspended and lysed. The supernatant was clarified, loaded onto Ni-NTA resin, and eluted by an imidazole gradient. Fractions containing purified SK were detected by SDS-PAGE and were stored at -80ºC.

Typically, S3P was enzymatically synthesized in a reaction mixture containing 100 mM magnesium chloride, 75 mM shikimic acid, 50 mM ATP, 2 mM DTT, and 7 µg/mL SK. The pH was adjusted to 6.0 with concentrated sodium hydroxide and the reaction was allowed to proceed at RT for 16 hours.

To purify S3P by anion exchange, the reaction mixture was diluted 1 to 10 with H_20 to reduce the conductivity to < 10 mS/cm and loaded onto a Q-Sepharose 26/10 column (Amersham Biosciences) which had been equilibrated with H_2O. The column was washed with 5 CV of H_2O to wash any unbound sample from the resin, then the S3P was eluted by a Triethylammonium bicarbonate (TEAB) gradient from 0

to 0.4 M over 20 CV. S3P-containing samples were detected by catalytic activity upon addition of PEP and EPSPS (malachite green indicator used to detect phosphate release). S3P and ADP were found to partially co-elute; to remove greater amounts of ADP, only the fractions in the front half of the elution peak were combined. These fractions were again diluted with H_20 to reduce the conductivity to < 10 mS/cm and loaded onto a Q-Sepharose 26/10 column, repeating all procedures as just described. The S3P-containing fractions were pooled and concentrated by rotary evaporation. The volatile TEAB buffer was removed by rotary evaporation and/or lyophilization and an ammonium salt of S3P was obtained. The S3P was redissolved in water, the purity of the samples was examined by UV scanning, and the concentration was determined using the enzymatic reaction with EPSPS. Because of difficulty in removing ADP, the overall yield of this process was typically *ca.* 25%.

Malachite green phosphate indicator solution- To prepare this reagent, used for the detection and quantification of inorganic phosphate[47], 4.25 g of ammonium molybdate was fully dissolved in 41 ml 12 *N* HCl, then diluted with 81 ml water. Seperarately, 169 mgs of malachite green were dissolved in 375 ml water. These solutions were then combined and stirred for 1 hour at room temperature, then filtered though a 0.45 μm filter. The solution was stored at 4 °C in the dark. The change in absorbance at ~ 660 nm is proportional to the amount of inorganic phosphate in the sample, within the constraints of Lambert-Beers law. Visually, this can be observed by a color change from brown-yellow to emerald green in the presence of inorganic

phosphate. The enzymatic release of inorganic phosphate was compared to a phosphate standard curve to obtain EPSPS activity data.

Kinetic analysis of enzymes- These procedures varied substantially and were performed as described for each experiment. In every case, enzyme activity is expressed as micromoles of product (P_i for EPSPS or ADP in the case of SK) produced per minute of reaction time per milligram of enzyme. All activity data were fit to the appropriate equations using the program SigmaPlot (SPSS Science).

Standard crystallization of *E. coli* EPSPS- "Closed"-form *E. coli* EPSPS was crystallized by hanging-droplet vapor diffusion, using 4.5 M sodium formate as the precipitant according to standard procedures described by Eschenburg *et al*. (2002)[43]. Briefly, the enzyme was concentrated to 75 mg/ml in 50 mM Tris–HCl pH 8.0, desired ligands were added to a concentration of ~ 10 mM, and 5 μl of this enzyme preparation was mixed on a cover slide with 5 μl of the precipitant solution, then sealed over a reservoir containing 500 μl of the precipitant solution. The initial droplets of 10 μl each thus contained 37.5 mg/ml EPSPS (= 810 μM), 5 mM ligand, and 2.25 M sodium formate. The crystals were found to be stable in a harvesting buffer containing 5 M sodium formate with the presence of 2 mM of each ligand, and this harvesting buffer provided cryoprotection.

Standard data collection procedure- X-ray diffraction data were recorded at −180°C using the rotation method on single flash-frozen crystals [Detector: R-axis IV++

image plate detector (MSC) X-rays: CuKα, focused by mirror optics (MSC); generator: Rigaku RU300 (MSC)].

Standard structure determination- Individual steps within the structure determination process were performed variously by Dr. Ernst Schönbrunn, Dr. Andreas Becker, Huijong Han, Martha Healy-Fried, or Todd Funke. Except as otherwise described, indexing and data reduction were performed with XDS[48] or HKL2000[49], the program package CNS[50] was used for phasing and refinement, and model building was performed with program O[51]. The structures were solved by molecular replacement using *E. coli* EPSPS (PDB ID 1g6s[22]), *S. pnumoniae* EPSPS (PDB ID 1rf5[21]), or CP4 EPSPS (PDB IDs 2gg4 or 2gg6[52]), stripped of solvent molecules, ions, and ligands, as search models. Refinement was performed using data to the highest resolution with no cut-off applied. Solvent molecules were added to the models at reasonable positions, and ligands were modeled according to the clear electron density maps. Several rounds of minimization, simulated annealing (2500 K starting temperature), and restrained individual B-factor refinement were carried out. Data collection and refinement statistics are summarized in the representative publications, as cited. Structure figures were prepared by Todd Funke with Pymol[53] or by Dr. Schönbrunn using MolScript[54], BobScript[55], and Raster3D[56].

Chpt. 2: Shikimate as a Substrate of *E. coli* EPSPS: Structural Bases for Glyphosate Insensitivity and Catalytic Activity

Portions of this work were included in: Priestman M.A.; Healy M.L.; Funke T.; Becker A.; and Schönbrunn E., Molecular basis for the glyphosate-insensitivity of the reaction of 5-enolpyruvylshikimate 3-phosphate synthase with shikimate. *FEBS Letters* **2005**, 579, 5773-80.

Introduction:

In final three steps of the shikimate pathway, shikimate kinase converts shikimate to S3P, EPSP synthase converts S3P to EPSP, and chorismate synthase converts EPSP to chorismate (Fig. 2.1a). EPSP synthase, or EPSPS, preferentially binds its substrate, S3P[57], and while this selectivity ensures that this enzyme is monofunctional *in vivo*, the molecular recognition mechanism is presently not well understood. EPSPS is composed of two globular domains connected by a short "hinge" region, and S3P-binding induces a global conformational change (the "open-closed" transition)[21-24, 52]. S3P apparently first forms a transient "collision complex" with the N-terminal domain of the "open"-form EPSPS[58]. Upon S3P binding, the enzyme undergoes a global conformational change, and the two globular domains approach each other, forming the active site at the interdomain cleft (of "closed"-form EPSPS). This two-step process requires that, for full binding, any analog of S3P must first interact favorably with the apo-enzyme in the collision complex, and additionally must trigger the global open-closed transition. Only the genuine substrate (S3P) and select substrate[57, 59-61] and tetrahedral reaction intermediate (TI) analogs[28, 62] have

Fig. 2.1a: The final three steps of the shikimate pathway.
(*Left*) Shikimate kinase catalyzes the phophorylation of shikimate to form S3P (shikimate-3-phosphate). (*Middle*) EPSP synthase catalyzes the transfer of the enolpyruvyl moiety of PEP, forming EPSP (5-enolpyruvylshikimate-3-phosphate). This reaction is inhibited by glyphosate. (*Right*) Chorismate synthase catalyzes elimination of the phosphate to produce chorismate, a precursor to essential aromatic metabolites.

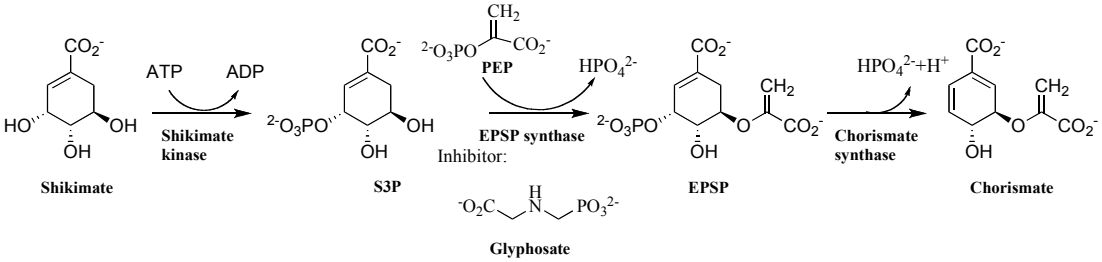

Fig. 2.1b: Shikimate as a substrate of EPSPS. EPSPS can also utilize shikimate as a substrate for the enolpyruvyl transfer, resulting in the formation of EPS and P_i; this reaction is glyphosate-insensitive.

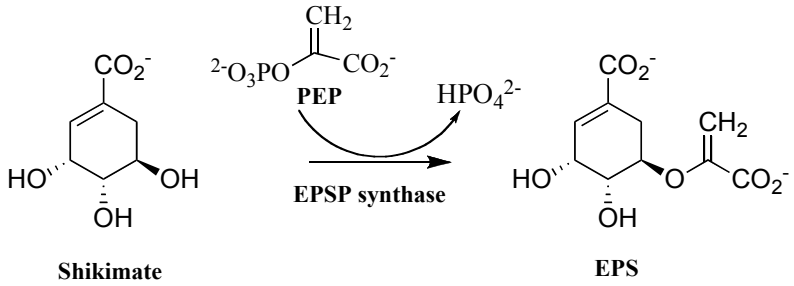

been demonstrated to induce formation of closed-form EPSPS. Of these non-substrate ligands, the enolpyruvyl transfer reaction was only demonstrated to occur when utilizing shikimate (the precursor to shikimate-3-phosphate) or select ring-contracted shikimate-3-phosphate analogs.

EPSPS utilization of shikimate as a substrate for the enolpyruvyl transfer reaction results in formation of enolpyruvylshikimate (EPS) (Fig. 2.1b); this reaction was examined previously and found to be glyphosate insensitive[57, 61]. Lacking from the previous work was a structural basis for catalysis of this reaction or the insensitivity to inhibition by glyphosate. The effect of ions on this reaction had not been probed, and no structures were available showing the alternate products or substrates bound to the active site. Here, the reaction of EPSPS with shikimate as a substrate was probed using steady-state kinetics and the reaction product was produced, purified, and analyzed. EPSPS was co-crystallized with shikimate, with and without glyphosate, and these structures were utilized to explain the observed kinetic characteristics. We assess the broader implications of these studies.

Experimental Procedures:

Materials- Chemicals and reagents were purchased from Sigma (St. Louis, MO) unless otherwise noted. S3P was synthesized and purified by Dr. Melanie Priestman according to the standard procedure described[45]. *E. coli* EPSPS was overexpressed and purified by Dr. Melanie Priestman according to the standard procedure

described[43]. Protein concentration was determined spectroscopically according to the standard procedure described (see Chapter 1, General Protocols).

Kinetics- Steady-state enzyme activity assays were performed by Dr. Melanie Priestman and Todd Funke. The activity of EPSPS was calculated by determining the amount of inorganic phosphate produced in the reaction using a colorimetric malachite green phosphate indicator[47]. The effect of anions on the reaction of EPSP synthase with shikimate was assayed with saturating concentrations of the substrates (10 mM PEP and 250 mM shikimate) and 100 mM of the respective ion. The reaction of EPSPS with either shikimate or S3P as substrate was typically assayed in 100 µl of 500 mM Na-MES pH 5.5 with 2 mM DTT in the absence or presence of 100 mM $NaHCO_3$ or 100 mM KCl. For the titration with carbonate, assays were carried out in 100 µl of 500 mM Tris, pH 8.0 + 2 mM DTT. The substrate concentrations considered saturating for these assays were 250 mM shikimate with 10 mM PEP, or 1 mM S3P with 1 mM PEP. The IC_{50} comparison was performed using 0.1 mM PEP in the case of the S3P-utilizing reaction or 1 mM PEP for the shikimate-utilizing reaction. The concentration of EPSPS was 22 nM for all assays utilizing S3P, 220 nM for assays utilizing shikimate and carbonate, and 1.1 µM for all other shikimate-utilizing reactions (chloride ion, varied salts or no salt). The reactions were started by the addition of enzyme and stopped after 3 minutes by the addition of 800 µl of the malachite green reagent, and color development was arrested after 5 minutes by the addition of 100 µl of a 34% w/v sodium citrate solution (final sample volume = 1 ml). The absorbance at 660 nm was determined spectroscopically and product formation

was determined by comparison to inorganic phosphate standards. Enzyme activity is expressed as micromoles of phosphate produced per minute of reaction time per milligram of EPSPS (U/mg). To determine the steady-state kinetic parameters of the reaction of EPSPS, the concentration of enzyme and one substrate were held constant while concentrations of the other substrate were varied as shown. The K_m and V_{max} values were determined by fitting the data to

Equation 1: $v = V_{max} * [S] / (K_m + [S])$

where v is the initial velocity, V_{max} is the maximum velocity, K_m is the Michaelis constant and $[S]$ is the concentration of the varied substrate (Shikimate, S3P, or PEP). To determine the glyphosate-sensitivity of these reactions, enzyme activity was measured in the presence of saturating concentrations of S3P or Shikimate, near-K_m concentrations of PEP, and varied concentrations of glyphosate (Glp). IC_{50} values for EPSPS inhibition were determined by fitting data to

***Equation 2*:** $$v = V_{min} + \frac{V_{max} - V_{min}}{1 + \left(\frac{[I]}{IC_{50}} \right)^n}$$

where v is the initial velocity, V_{max} is the maximum velocity, V_{min} is the minimum velocity, $[I]$ is the concentration of glyphosate and n is the Hill slope.

Synthesis of alternate product- On the basis of the kinetic results, an enzymatic synthesis was designed for the production of the alternate product. The 1 mL synthesis reaction mixture contained 100 mM MES, 2 mM DTT, 250 mM shikimate, 10 mM PEP, and 100 mM sodium bicarbonate. After adjusting the pH to 5.5, the

reaction was started by addition of 100 µg *E. coli* EPSPS and allowed to proceed at ambient temperature for 16 hours.

Purification of alternate product- Purification of the alternate product was accomplished with the assistance of Dr. Andreas Becker. Protein was removed by passing the crude mixture was passed through a 30 kDa-Centricon membrane, followed by a short C_{18} column, and the reaction substrates and products were then separated by HPLC using a Hi-Trap QFF anion exchange column subjected to a 40 min, 0 to 1 M NaCl gradient with flow rate set to 1 ml per minute. EPS was detected by monitoring UV absorbance at 213 nM. A small sample was examined by analytical HPLC, performed according to the same procedure, to estimate purity and yield.

Identification of alternate product- Analysis by mass spectrometry (MS) necessitated removal of the NaCl, so the sample was re-applied to the anion-exchange column and subjected to a NH_4HCO_3 gradient. The EPS-containing fractions were collected and concentrated via lyophilization. Mass spectra were acquired by Dr. Todd Williams using an electrospray time of flight mass spectrometer equipped with a lock spray reference probe. The sample was analyzed for exact mass formula confirmation using electrospray ionization with time of flight mass analysis. Spectra were mass corrected using a standard infused in a reference channel on a dual spray source.

Crystallization and structure determination- Protein crystals were produced by Todd Funke and Dr. Melanie Priestman using the standard crystallization conditions

previously described[43]. *E. coli* EPSPS was crystallized in the presence of 100 mM NaCl or $NaHCO_3$ and 10 mM shikimate, ± 30 mM glyphosate, with sodium formate as a precipitant, using hanging-droplet vapor diffusion. Crystallography was performed according to standard procedures (see Chapter 1, General Protocols); data collection and refinement statistics table included in the publication[59].

Results and Discussion:

Seeking a fuller understanding of the substrate recognition, induced fit mechanism, and catalytic potential of EPSPS, we used kinetic and structural approaches to investigate the reaction of EPSPS utilizing shikimate as a substrate.

Enzyme activity and ion-sensitivity- Steady-state kinetics analyses were performed utilizing a phosphate-release activity assay. The optimal buffer and pH as determined for the shikimate-utilizing reaction (Na-MES, pH 5.5) were used throughout our studies, and the reaction with S3P was analyzed in parallel to aid direct comparison. The reaction with shikimate proceeds very slowly compared to the S3P-utilizing reaction. In an attempt to increase the rate of this reaction, the activity was measured in the presence of 100 mM of diverse salts. While the S3P-utilizing reaction is insensitive to ions, the rate of the shikimate-utilizing reaction was increased by select anions. A more detailed examination of the anion effect was performed using 100 mM of each anion and combining the data obtained with various counter-ions (i.e., 50 mM $MgCl_2$ was considered equivalent to 100 mM KCl, and all activity data obtained using chloride salts were averaged together to describe the effect of 100 mM Cl^-). A

substantial increase in activity was observed in the presence of certain anions (Fig. 2.2a). The most marked effect was seen with carbonate, which increased the rate of the shikimate-utilizing reaction by 340-fold (without salt activity = 0.02 U/mg; with 100 mM carbonate activity = 6.8 U/mg). Enzyme activity was then analyzed as a function of carbonate concentration; while enzyme activity was decreased under the high buffer concentrations utilized in the assay, normal enzyme saturation behavior was observed (Fig. 2.2b). These data were fit to Equation 1 to derive the dissociation constant (K_d carbonate = 17 mM). Carbonate concentrations are not stable in solution due to the formation of carbon dioxide and further kinetic analysis was performed in the presence of 100 mM KCl or 100 mM $NaHCO_3$.

Substrate binding- The activity of EPSPS measured as a function of substrate concentration (Fig. 2.3) displayed normal Michaelis-Menten kinetics and the data were fit to Equation 1 to obtain the values for kinetic parameters listed in Table 2.1. The activity (V_{max}) observed with 100 mM $NaHCO_3$ was approximately 6-fold that observed in the presence of 100 mM KCl, but similar K_m values were observed for shikimate and PEP using either salt. Compared to the kinetic parameters obtained from the parallel S3P-utilizing substrate saturation experiments the utilization of shikimate by EPSPS results in both decreased substrate binding and lower catalytic activity. Compared to the S3P-utilizing reaction, the optimal (HCO_3^--activated) shikimate-utilizing reaction had 7-fold lower specific activity. The K_m shikimate was 500-fold the K_m S3P, and the K_m PEP was increased 8-fold in the shikimate-utilizing reaction (Table 2.1). If the substrate affinity is considered as inversely proportional to

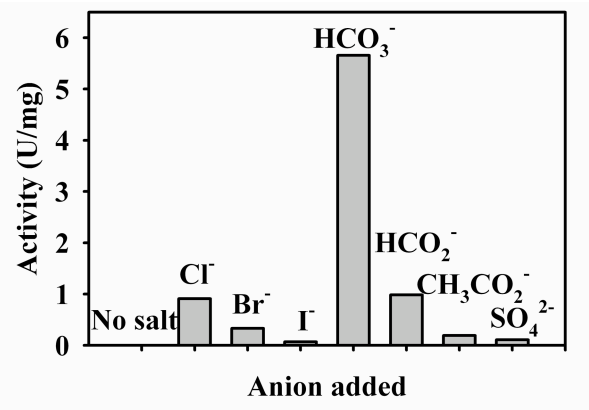

Fig. 2.2a: Ion Sensitivity. Select anions increase the rate of the EPSPS reaction with shikimate utilized as a substrate.

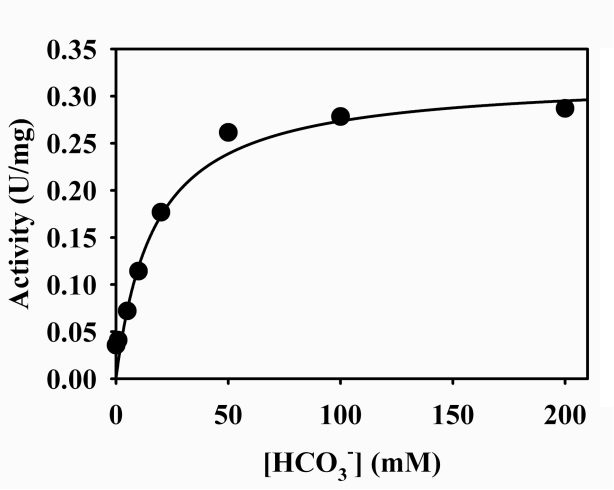

Fig. 2.2b: Carbonate Saturation. EPSPS activity was plotted as a function of [HCO_3^-]. Data were fit to Equation 1 to derive a K_d of 17 mM.

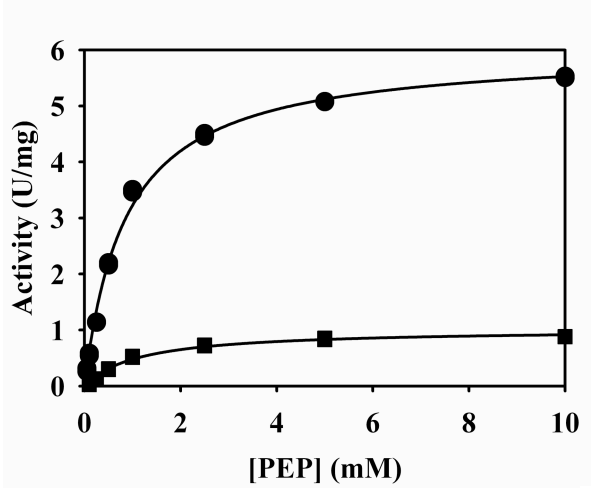

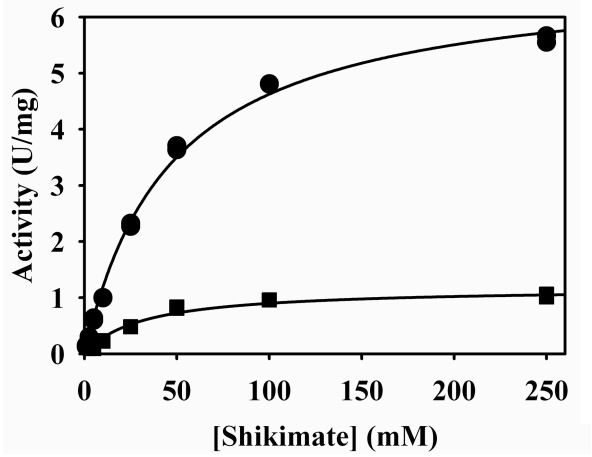

Fig. 2.3: Substrate Saturation.
(Top) EPSPS activity was plotted as a function of PEP concentration in the presence of Cl^- (■) or HCO_3^- (●). *(Bottom)* EPSPS activity was plotted as a function of shikimate concentration in the presence of Cl^- (■) or HCO_3^- (●). Data were fit to Equation 1 to determine the parameters shown in Table 2.1.

Table 2.1: Summary of kinetic data. Steady-state kinetic parameters for the reaction of EPSPS with S3P or shikimate were determined by fitting the activity data to the appropriate equation.

Substrate (S_1)	K_m (S_1) (mM)	V_{max} (S_1) (U/mg)	k_{cat}/K_m (S_1) (M^{-1} s^{-1})	K_m (PEP) (mM)	V_{max} (PEP) (U/mg)	k_{cat}/K_m (PEP) (M^{-1} s^{-1})	IC_{50} (Glp) (mM)
S3P	0.09 ± 0.005	53 ± 3.0	$4.5*10^5$ ± $0.25*10^5$	0.10 ± 0.004	58 ± 2.3	$4.5*10^5$ ± $0.18*10^5$	0.006 ± 0.0001
Shikimate + HCO_3^-	47 ± 2.9	6.8 ± 0.15	$1.1*10^2$ ± $0.07*10^2$	0.86 ± 0.05	6.0 ± 0.09	$5.4*10^3$ ± $0.33*10^3$	1.7 ± 0.11
Shikimate + Cl^-	31 ± 4.1	1.2 ± 0.04	$2.5*10^1$ ± $0.28*10^1$	1.1 ± 0.12	1.0 ± 0.03	$84*10^2$ ± $1.2*10^2$	1.2 ± 0.13

the K_m, these data indicate that the 3'-phosphate of S3P contributes substantially to substrate binding, while the activity data show that the phosphate moiety is not required for the induced-fit mechanism or catalytic activity. Notably, the moderate decrease in specific activity of the shikimate-utilizing reaction is not proportionate to the dramatically reduced affinity for shikimate; it is also not immediately evident why the PEP-binding affinity appears to decrease.

Glyphosate sensitivity- Parallel glyphosate-inhibition studies were performed utilizing either shikimate or S3P as a substrate for the enolpyruvyl transfer reaction. Relative enzyme activity as function of glyphosate concentration is shown in Fig. 2.4, and the inhibition data were fit to Equation 2 to derive the IC_{50} values reported in Table 2.1. Glyphosate is not an effective inhibitor of EPSPS when shikimate is used as a substrate. The IC_{50} data show that the shikimate-utilizing reaction is about 200 times less sensitive to glyphosate, independent of the anion used for activation, but these data do not explain the basis for this loss of glyphosate sensitivity.

Alternate product synthesis and purification- To verify that EPS was, in fact, the product of the shikimate-utilizing reaction (as shown in Fig. 2.1b), we synthesized, purified, and analyzed the reaction product. An enzymatic synthesis utilizing EPSPS was designed according to the optimal kinetic parameters determined in the preceding section. Saturating concentrations of shikimate, PEP, and $NaHCO_3$ were used, along with an excess of the enzyme and an extended reaction time. Purification was accomplished using anion-exchange HPLC with a 40 minute, 0 to 1 M NaCl gradient

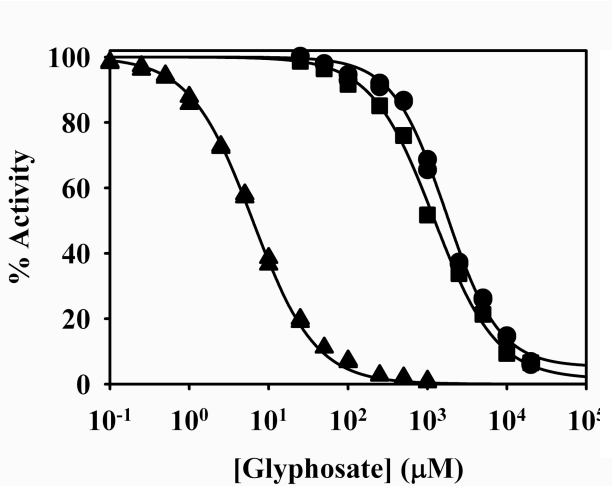

Fig. 2.4: Glyphosate inhibition. EPSPS activity was assayed with 1 mM S3P and 0.1 mM PEP (▲), or with 250 mM shikimate, 1.0 mM PEP plus either 100 mM $NaHCO_3$ (●) or 100 mM NaCl (■). Data were fit to Equation 2 to yield the IC_{50} values shown in Table 2.1.

(flow rate = 1 ml/min). A representative chromatogram is shown in Fig. 2.5a, with time on the X-axis plotted against Abs_{214} on the Y-axis. The unreacted substrate elutes in the major peak at 5.84 minutes, while EPS elutes in the minor peak at 13.26 minutes. The EPS-containing fractions were reapplied to examine purity. Fig. 2.5b shows the product eluting in the major peak at 11.27 minutes, while shikimate impurity is seen in the minor peak at 5.98 minutes. Area-under-the-curve (AUC) analysis indicated 92% purity, and, based on the extinction coefficient of shikimate, the estimated yield was *ca.* 3 μmoles of EPS.

Alternate product identification- The purified product was analyzed using an electrospray time of flight mass spectrometer. The most abundant signals, in mass regions corresponding to M+H+, M+Na+, or M-H- are 245.667 (+0.6mmu), 267.0477 (+0.5mmu) and 243.0492 (-1.3mmu), provide positive identification of the product (EPS molecular weight = 242.183) (mass spectra shown in Fig. 2.6). This purification and analysis procedure should be applicable to other shikimate or EPSP analogs as well, and with AUC analysis, this procedure provides an alternative (non-phosphate-based) method for measurement of enzyme activity.

Crystal structure analysis- The sodium formate crystallization conditions previously described for closed-form *E. coli* EPSPS were utilized in ultimately unsuccessful attempts to obtain an EPSPS•EPS co-crystal structure. The EPSPS•shikimate and EPSPS•shikimate•glyphosate complexes did crystallize, allowing the structures to be solved at 1.5 Å resolution. This analysis revealed that the enzyme–shikimate complex

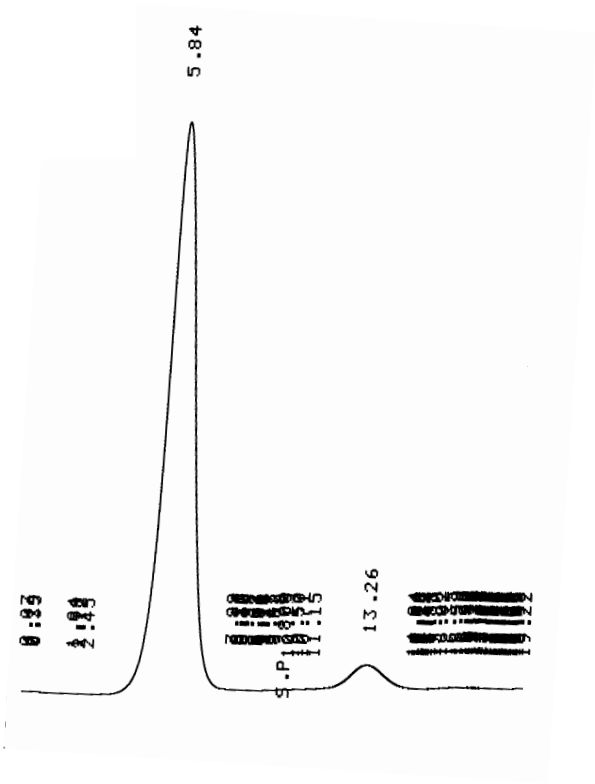

Fig. 2.5a: EPS purification. This chromatograph displays time (min) on the X-axis and Abs_{214} (a.u.) on the Y-axis. EPS elutes at 13.26.

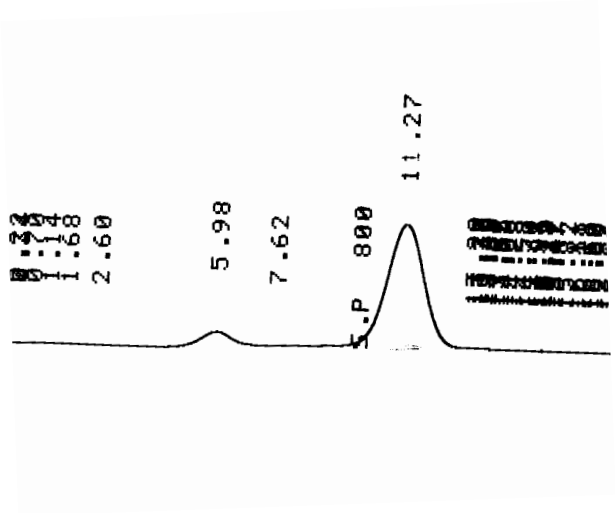

Fig. 2.5b: Analytical HPLC. This chromatograph displays time (min) on the X-axis and Abs_{214} (a.u.) on the Y-axis. EPS elutes at 11.27.

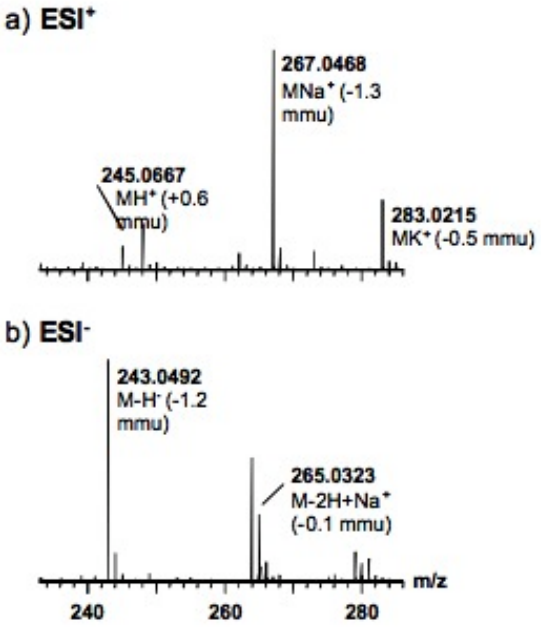

Fig. 2.6: Product Identification. The isolated product was subjected to electrospray time of flight mass spectrometry resulting in these spectra, which confirm that the product is EPS.
(a) Positive ion mode
(b) Negative ion mode

exists in the closed state, providing further evidence that the 3'-phosphate of S3P is not required for substrate binding or to induce the EPSPS open-closed transition. It was hypothesized that shikimate may shift slightly in the active site relative to S3P, impeding the binding of PEP and glyphosate and accounting for the functional changes, but this was not observed in comparisons of binary EPSPS•shikimate and EPSPS•S3P complexes. Instead, comparison of the active sites complexes of EPSPS•shikimate•glyphosate and EPSPS•S3P•glyphosate (Fig. 2.7) revealed that the binding of shikimate induces changes around the backbone of the active site, which in turn impacts the efficient binding of glyphosate. Comparison of the root mean square deviations (rmsd) of the shikimate- and S3P-liganded structures revealed that the greatest structural change occurred around Val168 (Fig. 2.8, *Top*). The corresponding portions of the ternary structures are overlaid in the stereofigure (Fig. 2.8, *Bottom*) to illustrate the shift of active site residues toward the shikimate-occupied active site. This appears to constitute the major basis for the glyphosate insensitivity of the reaction of EPSPS with shikimate.

Basis of ion sensistivity- It was hypothesized that the observed ion effect (see Fig. 2.2) could result from anions occupying the portion of the EPSPS active site that normally binds the phosphate moiety. To probe this, carbonate and chloride were included in the crystallization buffers; neither of these were observed in the active site. However, formate ions also activated shikimate-utilizing reaction (Fig. 2.2a) and two formate ions are, in fact, observed in place of the missing phosphate (Fig. 2.8); these likely out-compete the "preferred" ions due to their much higher concentration

Fig. 2.7: Active site ternary structure. Stereofigures show shikimate and S3P in yellow, glyphosate in orange, formate ions are in green, water molecules are aqua spheres and hydrogen bonds are indicated by dashed lines. (*Top*) Structure of EPSPS•Shikimate•Glyphosate complex. (*Bottom*) Structure of EPSPS•S3P•Glyphosate complex.

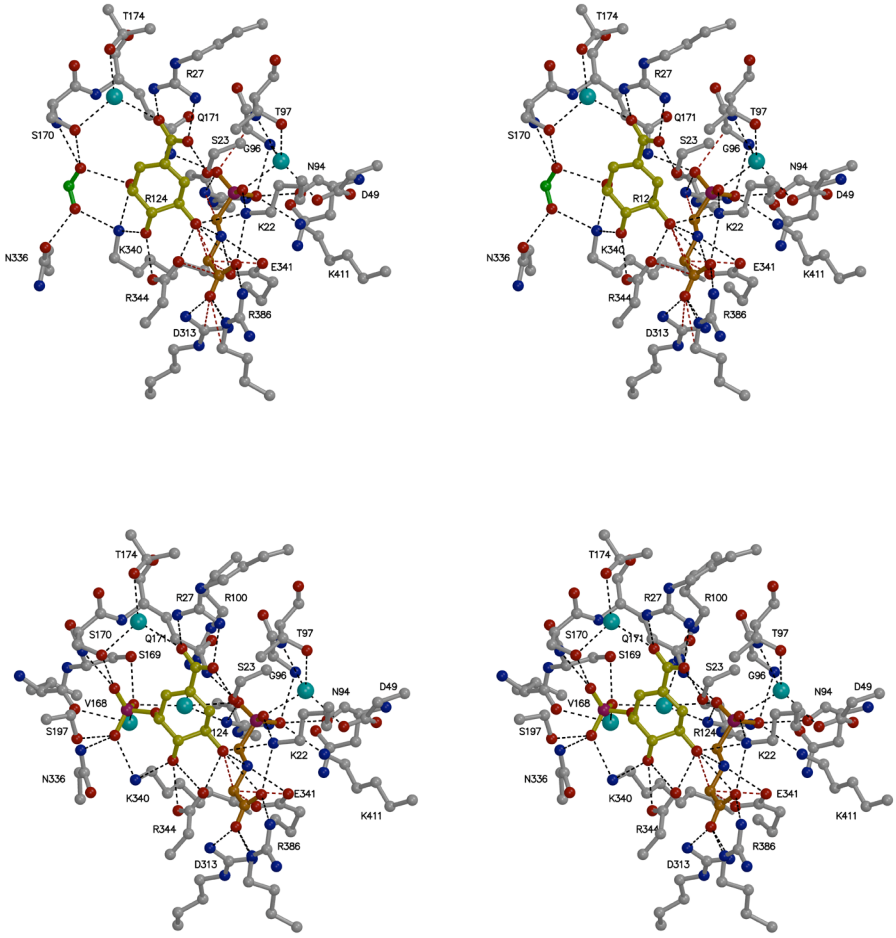

Fig. 2.8: Alterations in enzyme structure from shikimate binding. *(Top)* Comparison of the root mean square deviations (rmsd) of the Cα-atoms of EPSPS liganded with S3P or S3P/glyphosate (black line; average rmsd = 0.1 Å) and that of EPSPS liganded with shikimate or shikimate/glyphosate (dotted line; average rmsd = 0.13 Å).
(Bottom) Stereo view of the hydrophobic pocket built up by Pro125/Val168/Val339, altered upon binding of shikimate to the enzyme. EPSPS residues in the complex with S3P and glyphosate are shown in yellow; residues in the complex with shikimate and glyphosate in cyan. S3P and glyphosate are displayed in grey, hydrogen bonding interactions as black dotted lines and hydrophobic interactions as green dotted lines.

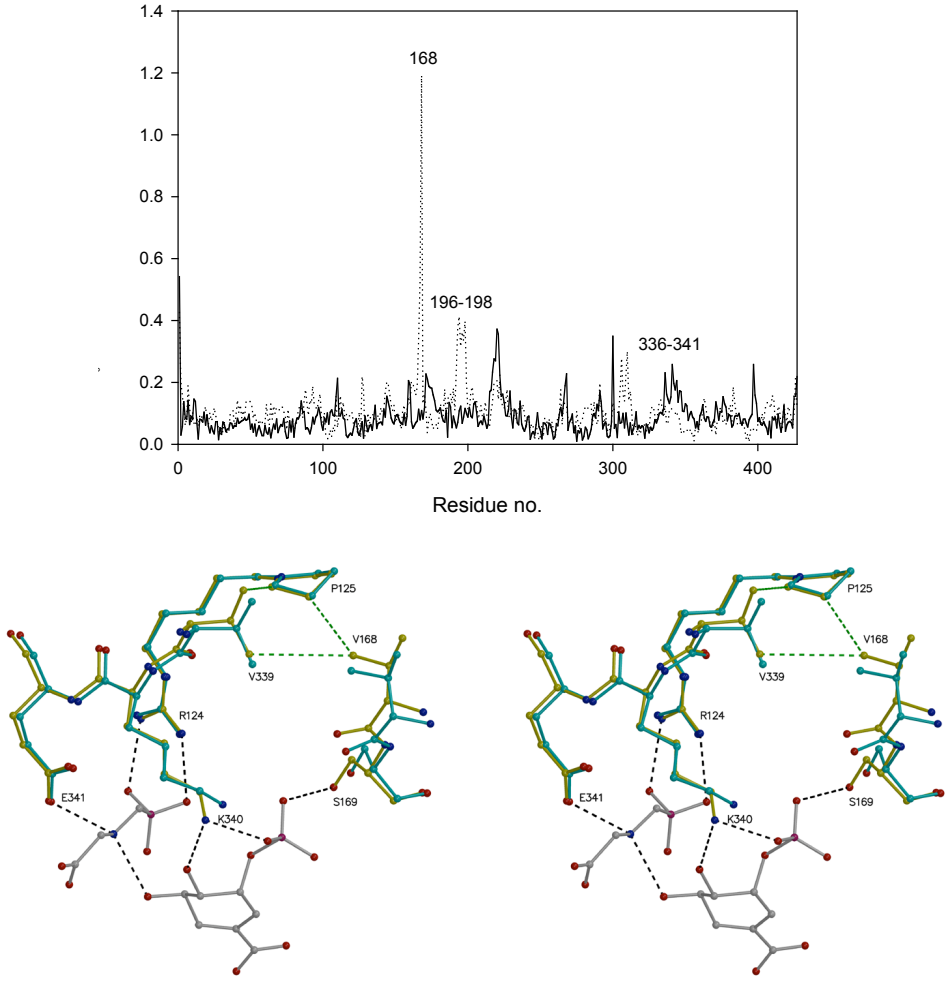

in the crystallization solution. The observed stimulation of catalytic activity by anions likely does result from binding at the positions occupied by formate ions in this structure.

Conclusions:

A full understanding of substrate recognition, the open-closed transition, and the catalytic potential of EPSPS is desired to facilitate the design of novel inhibitors. Enzyme inhibition is often achieved with competitive inhibitors (such as glyphosate), which occupy the substrate-binding site, and it is thus desirable to understand the molecular bases for substrate recognition. From these results, it appears that shikimate alone can induce the open-closed transition of *E. coli* EPSPS; while the 3-phosphate moiety of S3P is not required, select anions do appear to aid in the induced fit mechanism (as indicated by the observed stimulation of catalytic activity). Apparently these anions bind to the EPSPS active site in place of the 3'-phosphate of S3P. Competitive or allosteric inhibitors could potentially be designed to disrupt the global induced-fit mechanism of EPSPS, trapping the enzyme into non-productive "dead-end" complexes (for example, $E{\bullet}S{\bullet}I_{open}$, or $E{\bullet}I_{closed}$). Additionally, the products formed by the alternate-substrate reactions may themselves be useful as probes or inhibitors of downstream enzymes. Chorismate synthase utilizes the 3'-phosphate of EPSP as a leaving group, suggesting that EPS may inhibit chorismate synthase; this remains to be tested.

The procedures established for the production, purification, and identification of EPS

should be useful for the production and purification of other substrate, product, or TI analogs. Our structural data illuminate the subtle changes responsible for the observed differences in kinetic behavior for the reactions of EPSPS with shikimate and S3P. Overall, these results should facilitate and stimulate further research concerning the global induced fit mechanism of EPSPS.

Chpt. 3: Expression, Purification, Kinetic Characterization, and Glyphosate Insensitivity of *S. aureus* EPSPS

Portions of this work were included in: Priestman M.A.; Funke T.; Singh I.M.; Crupper S.S.; Schönbrunn E., 5-Enolpyruvylshikimate-3-phosphate synthase from *Staphylococcus aureus* is insensitive to glyphosate. *FEBS Letters* **2005**, 579, 728-32.

Introduction:

The pathogen *Staphylococcus aureus* is a major cause of death due to nosocomial infections[63, 64]. The increasing frequency of multi-drug resistance, including methicillin-resistant *S. aureus*[38], is particularly worrisome given the paucity of novel classes of antibiotic introduced in the last decades[65, 66]. Novel antimicrobial agents are required (see Fig. 1.9), so detailed characterization of suitable *S. aureus* drug targets is desirable. The shikimate pathway is essential for the growth and survival of plants, bacteria, fungi, and apicomplexan parasites[12-14, 20], and inhibitors of the *S. aureus* shikimate pathway are sought as potential antimicrobial drugs.

The herbicide glyphosate[10] (active ingredient in *Roundup*) specifically targets EPSPS[9] (see Fig. 1.6), but the patent record suggested that *S. aureus* EPSPS was insensitive to glyphosate[35], but no kinetic, inhibition, or structural data were available in the peer-reviewed literature. While glyphosate has generally poor antimicrobial properties, EPSPS-null mutants of *S. aureus* are not pathogenic, indicating that this enzyme is required for the growth and/or pathogenicity of this organism[15]. *S. aureus* EPSPS exhibits substantial amino acid sequence variation compared to the model enzyme from *E. coli* and the optimal global alignment (Fig. 3.1) shows only 27% amino acid

Fig. 3.1: *S. aureus* and *E. coli* EPSPS sequence alignment. Amino acid sequence alignment (PAM250 similarity matrix) reveals that the EPSPS enzymes from *E. coli* and *S. aureus* share 27% amino acid sequence identity and 56% similarity. Boxes indicate conserved amino acids.

sequence identity. This sequence variation may account for substantial structural or functional differences, but the structure of *S. aureus* EPSPS is not known. To facilitate the development of novel chemotherapies, we report the expression, purification, and biochemical characterization of *S. aureus* EPSPS and explore the implications of our findings.

Experimental Procedures

Materials- Chemicals and reagents were purchased from Sigma (St. Louis, MO) unless otherwise noted. Dr. Priestman utilized the shikimate kinase from *Methanococcus jannaschii*[46] to produce S3P from shikimate and ATP, and purified the product by anion exchange chromatography, as described[45]. DNA of *S. aureus* EPSPS (Japan strain) in a pT7 Blue3 plasmid was provided by Scott Crupper (Emporia State University, Emporia, KS). The target gene was excised and inserted into the desired pET-24d (Novagen) by Dr. Priestman. This construct was transformed into *E. coli* Stbl2(DE3) (Invitrogen) cells. On the basis of induction studies performed by Dr. Priestman, large scale cell cultures were incubated at 37°C initially, with the temperature reduced to 20°C prior to induction by the addition of 0.5 mM IPTG. Cell cultures were incubated at 20°C for 16-20 hours post-induction. *S. aureus* EPSPS was originally purified by Dr. Priestman using a slightly altered protocol: the crude extract was subjected to a preliminary anion-exchange column (Q-sepharose resin from GE Healthcare). EPSPS-containing fractions were collected and pooled and applied to a hydrophobic interactions column (P-sepharose resin from GE Healthcare). A secondary anion-exchange column (Resource-Q column from GE

Healthcare) was then utilized. Subsequently, the standard protein purification procedures described[43] were utilized and produced similar results. EPSPS from *E. coli* was produced by Dr. Priestman, according to the standard procedures described[43].

Activity and salt sensitivity- Steady-state activity assays were performed by Dr. Priestman and Todd Funke. The activity of EPSPS was calculated by determining inorganic phosphate production using the malachite green phosphate indicator[47]. The effect of specific cations and anions on the activity of *E. coli* and *S. aureus* EPSPS was assayed in 100 µl of 150 mM HEPES-NaOH (pH 7.0), 2 mM DTT + 100 mM salt. To determine the concentration of KCl required for optimal activity of *S. aureus* EPSPS, assays were carried out in 100 µl of 500 mM Tris pH 8.0 + 2 mM DTT with varied concentrations of KCl. The substrate binding of *E. coli* EPSPS and *S. aureus* EPSPS were assayed in 100 µl of 50 mM HEPES-NaOH (pH 7.0), 2 mM DTT ± 100 mM KCl. The final concentration of enzyme in the assay mixture was 660 nM and 1.65 µM for *S. aureus* EPSPS with and without KCl, respectively. In every case, reactions were started by the addition of enzyme and stopped after 3 minutes by addition of the malachite green reagent (800 µl); color development was arrested after an additional 5 min by the addition of 100 µl 34% (w/v) sodium citrate (1 ml total sample volume). The optical density was measured at 660 nm and the amount of inorganic phosphate formed in each reaction was determined by comparison to phosphate standards.

Substrate binding- To find the steady-state kinetic parameters, the concentration of enzyme and one substrate were held constant while the concentration of the other substrate were varied (as shown). The K_m and V_{max} values were determined by fitting the data to

Equation 1: $v = V_{max} * [S] / (K_m + [S])$

where v is the initial velocity, V_{max} is the maximum velocity, K_m is the Michaelis constant and $[S]$ is the concentration of the varied substrate.

Glyphosate sensitivity- The IC_{50} values for EPSPS inhibition were determined by fitting data to

Equation 2: $$v = V_{min} + \frac{V_{max} - V_{min}}{1 + \left(\frac{[I]}{IC_{50}} \right)^n}$$

where v is the initial velocity, V_{max} is the maximum velocity, V_{min} is the minimum velocity, $[I]$ is the concentration of glyphosate and n is the Hill slope.

Fluorescence- Fluorescence spectroscopy studies were also conducted utilizing *S. aureus* EPSPS. For intrinsic fluorescence experiments, the excitation wavelength was 280 nm, and emission spectra were recorded between 290 and 400 nm. Experiments were conducted in a buffer consisting of 50 mM Na-HEPES pH 7.0, 2 mM DTT, ± 100 mM KCl with 150 μg of *S. aureus* EPSPS per 1 ml sample. Emission spectra were recorded prior to the addition of ligands, and again after the addition of each ligand (S3P, PEP, KCl, or glyphosate). Final concentration of each ligand was 1 mM. Extrinsic fluorescence experiments were conducted the utilizing the fluorophore

ANS. The assay was performed in 50 mM Na-HEPES pH 7.0, 2 mM DTT, ± 100 mM KCl, and 50 μg of *S. aureus* EPSPS was used for each 1 ml sample. For ANS fluorescence, the excitation wavelength was set to 366 nm and emission spectra were recorded between 400 and 600 nm. The ANS fluorescence emission spectra were recorded prior to the addition of enzyme or ligands and this free-ANS fluorescence signal was subtracted from that obtained after addition of enzyme, so that the fluorescence intensity reported is proportional to the amount of ANS•EPSPS complex in the sample. The maximum fluorescence intensity ($\lambda = 475$) was recorded, plotted as a function of ANS concentration, and fit to

Equation 3: $y = Y_{max} * [ANS] / (K_d + [ANS])$

where y is the observed fluorescence intensity, Y_{max} is the maximal fluorescence intensity, K_d is the dissociation constant and $[ANS]$ is the concentration of the fluorophore.

Crystallization- Extensive crystallization trials were performed, utilizing a variety of *S. aureus* EPSPS preparations. Commercial sparse-matrix screens Crystal Screen I and II (Hampton Research) and Wizard Screen I and II (Emerald Biosystems) were utilized along with in-house screening conditions (listed in Fig. 3.2). Hanging drop vapor diffusion trials were set up by combining 2 μl of the enzyme preparation and 2 μl of the precipitant solution on a siliconized cover slide, forming a 4 μl droplet. The cover slides were inverted and sealed over reservoirs containing 500 μl of the precipitant solution, and the crystal setups was stored at 19 °C indefinitely. All crystallization screens were inspected regularly for the formation of protein crystals.

Fig. 3.2a: Formulation of in-house crystallization screen, Ernst I

Number	Buffer	Precipitant
1	None	1 M ammonium sulfate
2	None	2 M ammonium sulfate
3	0.5 M 1:2 NaH_2PO_4/K_2HPO_4	1 M ammonium sulfate
4	0.5 M 1:1 NaH_2PO_4/K_2HPO_4	1 M ammonium sulfate
5	0.5 M 1:2 NaH_2PO_4/K_2HPO_4	1 M ammonium sulfate
6	0.5 M 2:1 NaH_2PO_4/K_2HPO_4	2 M ammonium sulfate
7	0.5 M 1:1 NaH_2PO_4/K_2HPO_4	2 M ammonium sulfate
8	0.5 M 1:2 NaH_2PO_4/K_2HPO_4	2 M ammonium sulfate
9	None	0.5 M Mg formate
10	None	1 M Mg Formate
11	None	1 M Na formate
12	None	2 M Na formate
13	None	1 M 1:2 NaH_2PO_4/K_2HPO_4
14	None	1 M 1:1 NaH_2PO_4/K_2HPO_4
15	None	1 M 2:1 NaH_2PO_4/K_2HPO_4
16	None	2 M 1:2 NaH_2PO_4/K_2HPO_4
17	None	2 M 1:1 NaH_2PO_4/K_2HPO_4
18	None	2 M 2:1 NaH_2PO_4/K_2HPO_4

Fig. 3.2b: Formulation of in-house crystallization screen, Ernst II

Number	Buffer	Precipitant
2_1	None	10 % PEG 300
2_2	None	10 % PEG 400
2_3	None	10 % PEG 600
2_4	None	10 % PEG 1000
2_5	None	10 % PEG 1500
2_6	None	10 % PEG 3350
2_7	None	10 % PEG 4000
2_8	None	10 % PEG 6000
2_9	None	10 % PEG 8000
2_10	None	10 % PEG 10000
2_11	None	10 % PEG 20000
2_12	None	10 % PEG MME 2000
2_13	0.1 M MES	10 % PEG 300
2_14	0.1 M MES	10 % PEG 400
2_15	0.1 M MES	10 % PEG 600
2_16	0.1 M MES	10 % PEG 1000
2_17	0.1 M MES	10 % PEG 1500
2_18	0.1 M MES	10 % PEG 3350
2_19	0.1 M MES	10 % PEG 4000
2_20	0.1 M MES	10 % PEG 6000
2_21	0.1 M MES	10 % PEG 8000
2_22	0.1 M MES	10 % PEG 10000
2_23	0.1 M MES	10 % PEG 20000
2_24	0.1 M MES	10 % PEG MME 2000

Number	Buffer	Precipitant
2_25	0.1 M PIPES	10 % PEG 300
2_26	0.1 M PIPES	10 % PEG 400
2_27	0.1 M PIPES	10 % PEG 600
2_28	0.1 M PIPES	10 % PEG 1000
2_29	0.1 M PIPES	10 % PEG 1500
2_30	0.1 M PIPES	10 % PEG 3350
2_31	0.1 M PIPES	10 % PEG 4000
2_32	0.1 M PIPES	10 % PEG 6000
2_33	0.1 M PIPES	10 % PEG 8000
2_34	0.1 M PIPES	10 % PEG 10000
2_35	0.1 M PIPES	10 % PEG 20000
2_36	0.1 M PIPES	10 % PEG MME 2000
2_37	0.1 M HEPES	10 % PEG 300
2_38	0.1 M HEPES	10 % PEG 400
2_39	0.1 M HEPES	10 % PEG 600
2_40	0.1 M HEPES	10 % PEG 1000
2_41	0.1 M HEPES	10 % PEG 1500
2_42	0.1 M HEPES	10 % PEG 3350
2_43	0.1 M HEPES	10 % PEG 4000
2_44	0.1 M HEPES	10 % PEG 6000
2_45	0.1 M HEPES	10 % PEG 8000
2_46	0.1 M HEPES	10 % PEG 10000
2_47	0.1 M HEPES	10 % PEG 20000
2_25	0.1 M HEPES	10 % PEG MME 2000

Results and Discussion:

The expression system and purification protocol developed enabled isolation and characterization of highly purified, catalytically active *S. aureus* EPSPS enzyme.

Salt-sensitivity- Preliminary assays showed substantially decreased enzyme activity compared to our model enzyme, *E. coli* EPSPS. Based on reports of ion-sensitive EPSPS isolated from organisms such as *Bacillus subtilis*[67] and *Streptococcus pneumoniae*[68], EPSPS activity was examined in the presence of 100 mM of diverse salts. Preliminary screening (data not shown) indicated that while *E. coli* EPSPS activity was ion-independent, *S. aureus* EPSPS activity was stimulated by select cations. *S. aureus* EPSPS was re-tested with 100 mM of each cation (100 mM of salts with monovalent anions, and 50 mM of salts with divalent anions) and the data obtained with different counter-ions was combined (i.e., 50 mM $(NH_4)_2SO_4$ was considered equivalent to 100 mM NH_4Cl, and all activity data obtained using ammonium salts were averaged together to isolate the effect of 100 mM NH_4^+). Several monovalent cations effected a substantial increase in *S. aureus* EPSPS activity (see Fig. 3.3a), and nearly 8-fold rate enhancement was observed with the preferred cation, K^+. To further examine the cation effect, the enzyme activity was assayed in the presence of varied KCl concentrations (Fig. 3.3b). Normal enzyme saturation behavior was observed and the activity data were fit to Equation 1, yielding a dissociation constant (K_d) of 58 mM for the potassium ion.

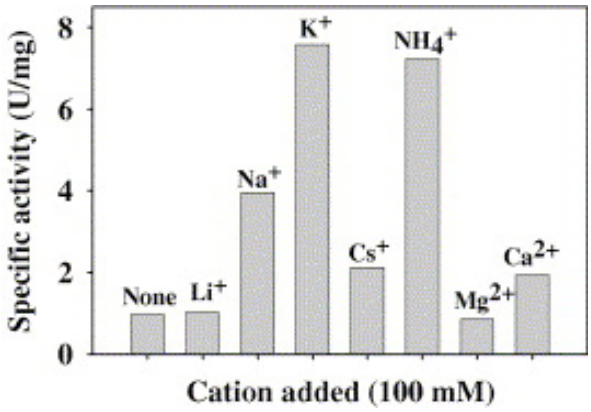

Fig. 3.3a: Ion sensitivity. The activity of *S. aureus* EPSPS is increased in the presence of specific monovalent cations.

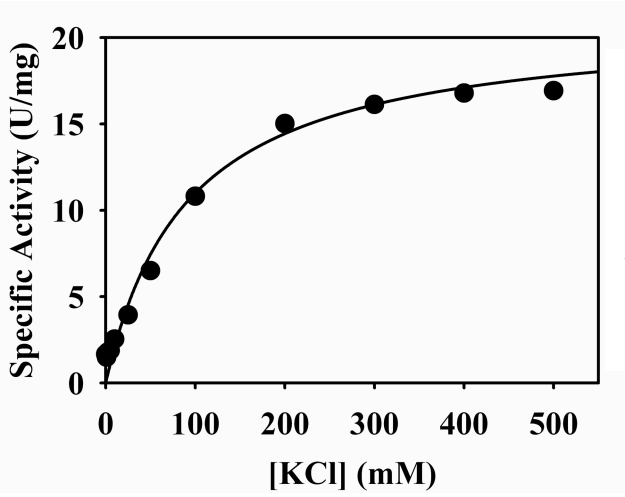

Fig 3.3b: Potassium Saturation. EPSPS activity plotted as a function of $[K^+]$ shows normal enzyme saturation behavior. These data were fit to Equation 1, yielding a K_d of 58 mM for K^+.

Substrate binding and catalytic activity- The binding of S3P and PEP and production of EPSP by *S. aureus* EPSPS (±100 mM KCl) and *E. coli* EPSPS were examined in parallel steady-state kinetic experiments. Activity was plotted as a function of substrate concentration (Fig. 3.4) and these data were fit to Equation 1 to obtain the kinetic parameters shown in Table 3.1. The specific activity (k_{cat}) varies dramatically; *E. coli* EPSPS is 13-fold more active than *S. aureus* EPSPS + KCl, and 260-fold more active than salt-free *S. aureus* EPSPS. The substrate saturation curves, in contrast, are remarkably similar. The Michaelis constant (K_m) of S3P ranges from 0.14 mM (*E. coli* EPSPS) to 0.18 mM (salt-free *S. aureus* EPSPS); similarly, the K_m PEP ranges from 0.14 mM for the *E. coli* enzyme to 0.18 mM (for *S. aureus* EPSPS + KCl) (Table 3.1). The inverse of the K_m is often used as a proxy for substrate affinity; in this case, the minor variations observed in substrate binding do not account for the substantial decrease in catalytic activity, suggesting that substrate binding may not constitute the rate-limiting step for the *S. aureus* EPSPS.

Glyphosate sensitivity- Parallel inhibition experiments were conducted to determine the IC_{50} of glyphosate for *S. aureus* EPSPS (± 100 mM KCl) and *E. coli* EPSPS (see Fig. 3.5). The data were fit to Equation 2 to obtain the IC_{50} values reported in Table 3.1. These experiments demonstrated that glyphosate is a poor inhibitor of *S. aureus* EPSPS, and this glyphosate-insensitivity is essentially cation-independent. The IC_{50} values indicate that, compared to *E. coli* EPSPS, *S. aureus* EPSPS (± KCl) is 100- to 180-fold less sensitive to inhibition by glyphosate. Since glyphosate occupies the PEP-binding site of EPSPS, enzymes with decreased glyphosate sensitivity often

Fig. 3.4: Steady-state kinetics of *E. coli* and *S. aureus* EPSPS. *(Left) S. aureus* EPSPS activity was plotted as a function of substrate concentration: with 100 mM KCl (*left axis* - ●) or without KCl (*right axis* - ■). (*Right) E. coli* EPSPS activity was plotted as a function of substrate concentration. Data were fit to Equation 1 to derive the parameters shown in Table 3.1.

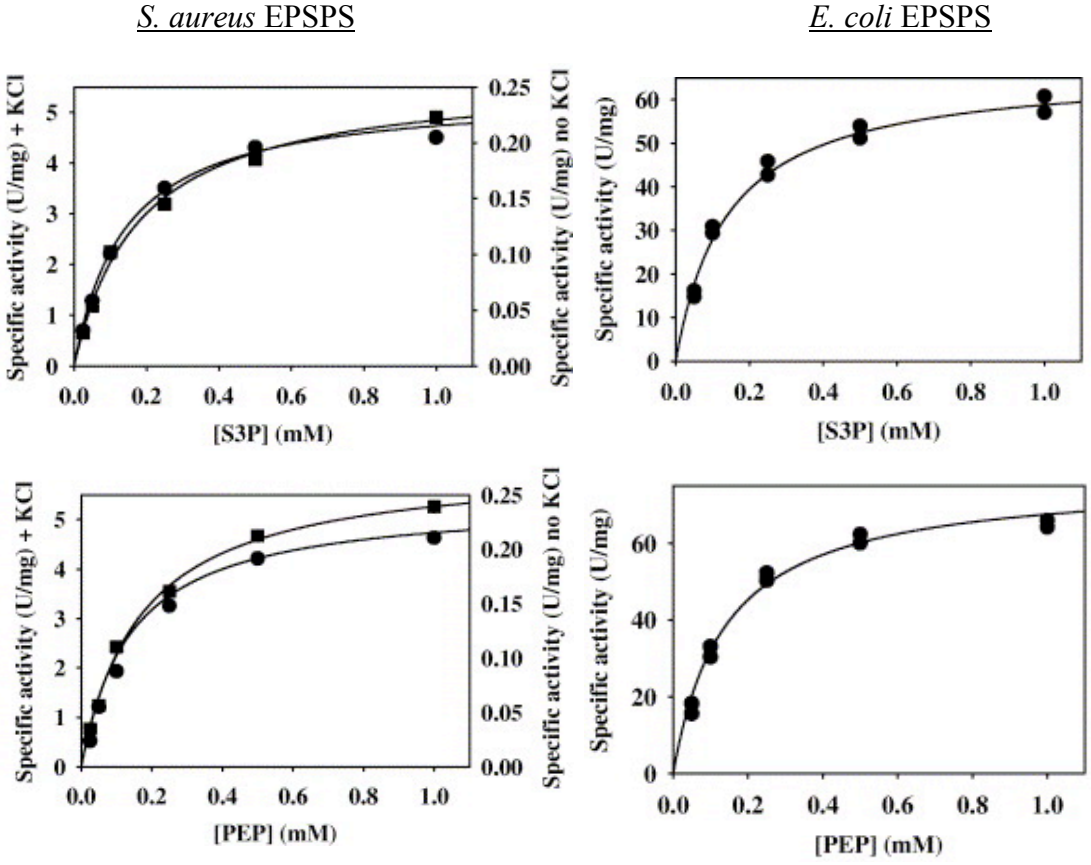

Table 3.1: Summary of steady-state enzyme kinetic parameters.

	K_m (PEP) (mM)	k_{cat} (PEP) (s^{-1})	k_{cat}/K_m (PEP) ($M^{-1}\ s^{-1}$)	K_m (S3P) (mM)	k_{cat} (S3P) (s^{-1})	k_{cat}/K_m (S3P) ($M^{-1}\ s^{-1}$)	IC50 (Glp) (mM)
E. coli EPSPS	0.14 ± 0.02	59 ± 1.9	$4.2 \times 10^5 \pm 0.5 \times 10^5$	0.14 ± 0.01	51 ± 1.5	$3.7 \times 10^5 \pm 0.4 \times 10^5$	0.0086 ± 0.0003
S. aureus EPSPS + KCl	0.18 ± 0.02	4.3 ± 0.02	$2.4 \times 10^4 \pm 0.3 \times 10^4$	0.14 ± 0.02	4.2 ± 0.02	$3.0 \times 10^4 \pm 0.3 \times 10^4$	0.9 ± 0.006
S. aureus EPSPS no KCl	0.17 ± 0.02	0.22 ± 0.006	$1.3 \times 10^3 \pm 0.2 \times 10^3$	0.18 ± 0.02	0.20 ± 0.008	$1.1 \times 10^3 \pm 0.1 \times 10^3$	1.6 ± 0.005

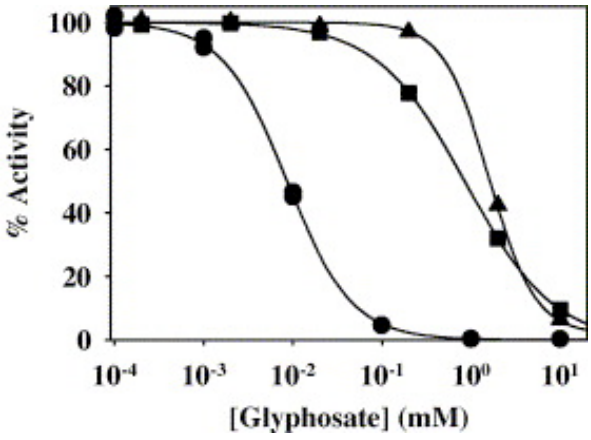

Fig. 3.5: Glyphosate inhibition. IC_{50} determination for *E. coli* (●), and *S. aureus* EPSPS, with 100 mM KCl (■) or without salt (▲). Data were fit to Equation 2 to obtain the values reported in Table 3.1.

exhibit a corresponding decrease in PEP affinity, but this is not observed for the *S. aureus* enzyme. These data indicate that *S. aureus* EPSPS preferentially binds PEP, sustaining substantial catalytic activity even in the presence of 1 mM glyphosate.

S. aureus EPSPS fluorescence- Intrinsic and extrinsic fluorescence trials were conducted with *S. aureus* EPSPS. Intrinsic fluorescence was observed, but no change in signal could be detected upon addition of up to 1 mM substrate or 200 mM KCl (data not shown). ANS, an extrinsic fluorophore utilized to probe ligand-induced conformational change in other enolpyruvyltransferases[1] was also utilized. An increase in ANS fluorescence signal upon addition of *S. aureus* EPSPS indicates formation of an ANS•EPSPS complex, so fluorescence spectra were collected in the presence of increasing concentrations of ANS (Fig. 3.6a). The fluorescence intensities at 475 nm, replotted as a function of ANS concentration, showed normal enzyme saturation behavior (Fig. 3.6a) and these data were fit to Equation 3 to determine the dissociation constant. For *S. aureus* EPSPS, the calculated K_d ANS was 5.2 μM. ANS•EPSPS fluorescence was monitored upon sequential addition of ligands (1 mM S3P, 100 mM KCl, 1 mM glyphosate, and 1 mM PEP) (Fig. 3.6b), but no substantial change was observed, precluding further ANS-based ligand-binding studies. The saturation curve indicates that there is a discreet ANS binding site, but the lack of fluorescence quench with substrate addition implies that ANS binding (or the ANS-binding site) is not sensitive to the induced fit confomational change. Other fluorophores or experimental systems may be better suited for characterization of the conformational change in this enzyme.

Fig. 3.6a: *S. aureus* EPSPS extrinsic fluorescence. Fluorescence intensity was plotted as a function of ANS concentrations and fit to Equation 3, yielding K_d ANS = 5.2 μM for *S. aureus* EPSPS.

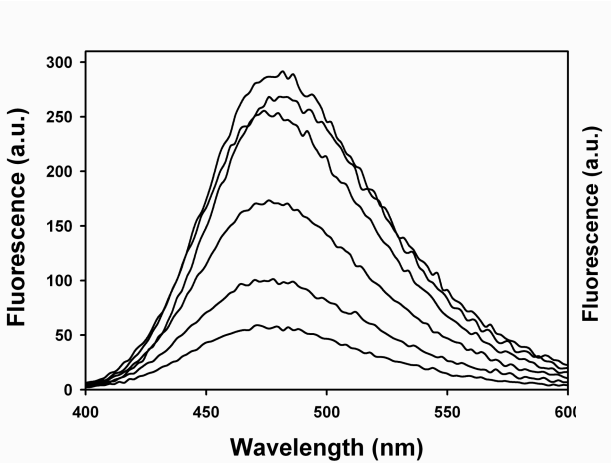

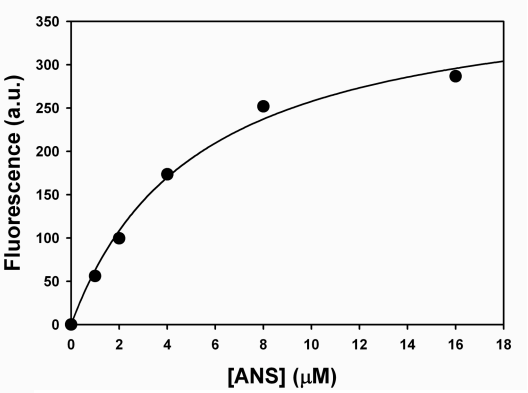

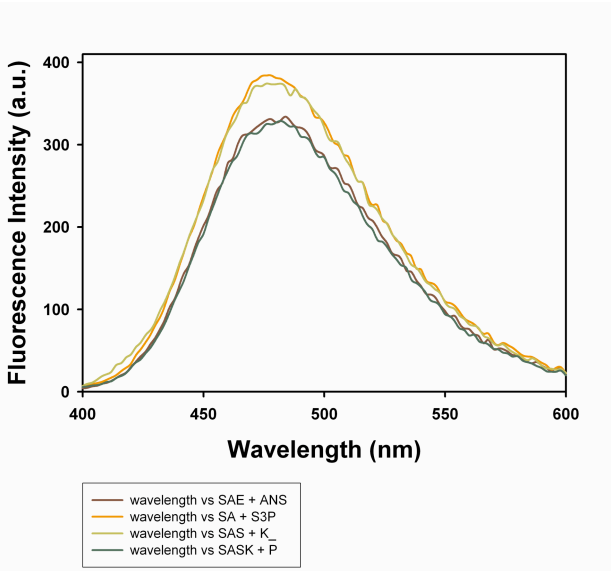

Fig. 3.6b: Fluorescence quench trials. The addition of ligands did not substantially affect ANS•EPSPS fluorescence.

Crystallization- Substantial efforts were made to obtain crystals of *S. aureus* EPSPS. Commercial and in-house precipitant solutions were used (as described in the Experimental Procedures section) to screen the various enzyme preparations listed in Fig. 3.7. Protein crystals were not observed, and the structural details of *S. aureus* EPSPS are still unknown.

Conclusions:

Catalytically active *S. aureus* EPSPS was expressed, purified, and characterized by steady-state kinetics. *E. coli* EPSPS was utilized as a control and for comparison, and substantial differences were observed in catalytic activity, ion sensitivity, and glyphosate sensitivity. In contrast binding of the substrates, PEP and S3P, appeared to be quite similar for both enzymes. The basis for the observed cation-activation of the *S. aureus* enzyme is not known - based on the steady-state kinetic parameters, cations likely aid the global induced fit mechanism. This interpretation would be consistent with the observation that ions affect the rate of catalysis, but do not appear to influence substrate or glyphosate binding. In retrospect, the KCl saturation plot (Fig. 3.3b) indicates that 100 mM KCl was sub-saturating and insufficient for maximal catalytic activity. Higher salt concentrations should be used in future experiments. Elucidation of the specific basis for the ion sensitivity likely requires knowledge of the three-dimensional atomic structure of *S. aureus* EPSPS.

Structural data are also required to fully explain the glyphosate tolerance of EPSPS from *S. aureus*. An inspection of the sequence alignment (Fig. 3.1) reveals a leucine

Fig. 3.7: *S. aureus* EPSPS preparations used for crystal screens:

[enzyme]	Buffer (+ 2 mM DTT)	Additives, etc
1. 40 mg/ml	50 mM Tris-Cl	-
2. 40 mg/ml	50 mM Tris-Cl	5 mM S3P
3. 40 mg/ml	50 mM Na/K Phosphate	5 mM S3P, 100 mM KCl
4. 10 mg/ml	50 mM Na/K Phosphate	5 mM S3P, 100 mM KCl, post gel-filtration
5. 24 mg/ml	50 mM Na/K Phosphate	5 mM S3P, 100 mM KCl
6. 8 mg/ml	50 mM Na/K Phosphate	5 mM S3P, 100 mM KCl
7. 8 mg/ml	50 mM Na-HEPES	5 mM S3P, 100 mM KCl
8. 8 mg/ml	50 mM Tris-Cl	5 mM S3P, 100 mM KCl
9. 8 mg/ml	50 mM Na/K Phosphate	5 mM S3P, 5 mM glyphosate, 2 mM ANS, 100 mM KCl
10. 8 mg/ml	50 mM Na/K Phosphate	5 mM S3P, 100 mM KCl, 2% DMSO

residue at the site corresponding to Pro101 in the *E. coli* enzyme. Mutations at this conserved Pro101 residue are known to result in moderate levels of glyphosate tolerance[69-71], but other unknown features likely contribute to the high levels of glyphosate insensitivity observed in *S. aureus* EPSPS.

Other EPSPS with intrinsic glyphosate tolerance have been described as "class II" EPSPS[29, 72], and were utilized to produce transgenic glyphosate resistant (*Roundup Ready*) crop lines. Class II EPSPS are characterized by the ability to maintain catalytic efficiency in the presence of glyphosate; they typically exhibit substantial sequence dissimilarity compared to the EPSPS found in plants or *E. coli*; and they tend to be ion-sensitive. On the basis of these criteria, *S. aureus* EPSPS can be considered a prototypical class II EPSPS.

Inhibitors and structural data remain unavailable for class II EPSPS enzymes, including *S. aureus* EPSPS. The work described here should facilitate further examination of this important enzyme.

Chpt. 4: CP4 EPSPS: Catalysis, Inhibition, and Structural Basis for the Glyphosate Insensitivity of transgenic *Roundup Ready* Crops

Portions of this work were included in: Funke T.; Han H.; Healy-Fried M.L.; Fischer M.; Schönbrunn E., Molecular Basis for the Herbicide Resistance of Roundup Ready Crops. *PNAS* **2006***,* 103, 13010-15.

Introduction:

Glyphosate, the active ingredient in *Roundup*, is the world's most-used pesticide[73]. Glyphosate possesses broad-spectrum herbicidal activity and kills essentially all plants upon foliar application[10, 29, 42]. This phytotoxicity is a result of the specific and potent inhibition of EPSPS, the penultimate enzyme of the shikimate pathway[9, 29, 74]. The toxicological and herbicidal profiles of glyphosate are very favorable[29-31, 42]. To broaden the utility of this herbicide, a degree of selectivity was desired to facilitate application during the growing season - killing weeds without damaging crops. Substantial efforts to create a selective herbicide by modifying the chemical structure of glyphosate were unsuccessful – the herbicidal activity of glyphosate analogs was either broad-spectrum or non-existent[27, 29]. The identification of EPSPS as the molecular target of glyphosate spurred extensive research into the structure, function, and inhibition of this enzyme by scientists seeking to engineer glyphosate tolerant crop varieties[22, 23, 33, 35, 71, 75-80].

EPSPS catalyzes the transfer of the enolpyruvyl moiety of PEP to the 5'-hydroxyl of S3P to produce EPSP (See Fig. 1.3). Glyphosate is a reversible inhibitor of this

reaction, binding competitively with respect to PEP[11]; structural studies have confirmed that PEP and glyphosate share a common binding site[21, 22, 24]. In plants, EPSPS is a soluble, nuclear encoded, plastid localized, *ca.* 44-48 kDa enzyme[14, 29]. Two classes of EPSPS have been described based on the intrinsic glyphosate sensitivity of the enzyme. Glyphosate-sensitive EPSPS enzymes are termed "Class I" and have been isolated from plants (*Petunia x hybrida, Zea mays, etc.*)[29, 80-82] and bacteria (*E. coli, Salmonella typhimurium, Klebsiella pneumoniae, etc.*)[29, 71, 76, 83]. In constrast, bacterial EPSPS enzymes, isolated from species including *Staphlococcus aureus, Pseudomonas sp*. strain PG2982, and *Agrobacterium sp.* strain CP4, show substantial sequence divergence compared to the prototypical class I EPSPS enzymes and are not sensitive to inhibition by glyphosate. On the basis of their ability to maintain catalytic efficiency in the presence of glyphosate, these enzymes were termed "class II" EPSPS[29, 35, 36, 72, 82].

A number of glyphosate resistance mechanisms have been demonstrated, including *1)* reduced glyphosate uptake and/or translocation (non-target site mechanisms)[70, 84-86]; *2)* overproduction of the target (class I EPSPS)[76, 79, 87-89]; *3)* alteration of the target (mutated class I EPSPS)[71, 75, 82, 90-92]; *4)* utilization of a glyphosate-degrading enzyme (*e.g.,* glyphosate oxidoreductase)[93-96]; and *5)* utilization of an intrinsically glyphosate-insensitive target (Class II EPSPS)[29, 35, 72, 82, 97]. Of these, mechanisms *1)* and *3)* have been significant in the development of glyphosate tolerant weeds, while methods *3)* and *5)* have been significant in the development of glyphosate tolerant crops. Notably, a prototypical class II enzyme isolated from *Agrobacterium sp.* strain CP4

EPSPS, was utilized to produce commercially successful transgenic glyphosate-resistant crop varieties (*Roundup Ready 2* corn; *Roundup Ready* soybeans, canola, and cotton) that currently dominate North and South American agriculture (52% of corn, 70% of cotton, and 91% of soybeans planted in the United States in 2007 were such transgenic glyphosate-resistant varieties[32]). Despite being widely used and commercially significant, little was known about the structure or glyphosate-tolerance mechanism of CP4 EPSPS; in fact, no structural data was available for any class II EPSPS enzyme. Using the published amino acid sequence, a synthetic CP4 EPSPS gene was constructed with codon-usage optimized for bacterial expression. We produced, purified, and analyzed the structural and kinetic properties of CP4 EPSPS. We describe the structural basis of glyphosate insensitivity and discuss the implications of our results.

Experimental Procedures:

Materials- Chemicals and reagents were purchased from Sigma (St. Louis, MO) unless otherwise noted. S3P was synthesized and purified according to the standard procedure described[45]. The amino acid sequence of *Agrobacterium sp.* strain CP4 EPSPS was obtained from U.S. Patent 5633435[72].

Molecular Biology- This gene's codon usage was optimized for bacterial expression, a synthetic gene was produced, and this was inserted into the plasmid pNCO113 by Dr. Markus Fischer, as described[52]. This construct was subjected to restriction digest using *Hind*III and *Nde*I restriction endonucleases in NEB Buffer 2 (New England

BioLabs), according to the manufacturer's instructions. The products of the digest were separated by size using agarose gel electrophoresis and the CP4 EPSPS gene was isolated using the QIAquick Gel Extraction Kit (Qiagen), according to the manufacturer's instructions. The pET-21a vector (Novagen) was linearized by the same restriction digest purification process, and the CP4 EPSPS gene was ligated into this pre-digested vector using T4 DNA polymerase from the Quick Ligation kit (New England BioLab), again according to the manufacture's instructions. The product of this cohesive-end ligation was utilized directly for transformation of chemically competent *E. coli* DH5-α cells. These cells were plated on LB-Agar plates containing 100 μg/ml ampicillin and incubated overnight. The resulting bacterial colonies with ampicillin-resistance were picked and grown in LB media overnight and the plasmids were isolated using the QIAprep Spin Miniprep kit (Qiagen) according the manufacturer's instructions. Samples of the isolated plasmids were subjected again to restriction digest by *Hind*III and *Nde*I and analyzed by agarose gel electrophoresis. Several of the restriction digest analyses displayed a CP4-sized gene; one of these was submitted for sequence analysis at the University of Kansas Medical Center biotech research support facility. The sequence obtained utilizing the T7 primer confirmed the presence of the CP4 EPSPS open reading frame, and this CP4 EPSPS-pET-21a construct was transformed into *E. coli* BL21(DE3) cells.

Expression and Purification- Small-scale studies showed that soluble expression of CP4 EPSPS could by induced at 37°C by addition of 0.5 mM IPTG. Large scale cultures were grown to log stage (OD_{600} = 0.4 to 0.6) at 37°C in LB media in the

presence of 100 μg/ml ampicillin, induced with 0.5 mM IPTG, and cells were harvested by centrifugation 4 to 6 hours post-induction and stored at -80 °C. CP4 EPSPS was originally purified using a protocol similar to that used by Dr. Priestman for *S. aureus* EPSPS[45]: briefly, the cell pellet was resuspended in extraction buffer with lysozyme, sonicated 2x 30 seconds, and centrifuged for 60 min at 18,000 RPM. The crude extract was subjected to a preliminary anion-exchange column (Q-sepharose resin from GE Healthcare). EPSPS-containing fractions were collected and pooled and applied to a hydrophobic interactions column (P-sepharose resin from GE Healthcare). A secondary anion-exchange column (Resource-Q column from GE Healthcare) was then utilized. Subsequently, standard EPSPS purification procedures[43] (25% ammonium sulfate precipitation, P-sepharose column, and Q-sepharose) were utilized and produced similar results. The resulting highly purified CP4 EPSPS was used for kinetic characterization and crystallization. EPSPS from *E. coli* was produced and purified according to the standard protocol[43]. The Ala100Gly mutant CP4 EPSPS was produced by site-directed mutagenesis with the Quik Change II mutagenesis kit (Stratagene) according to the manufacturer's instructions, using appropriate primers (MWG Biotech), and overexpressed and purified according to the standard protocol[43]. Coomassie reagent (Pierce, Rockford, IL) with BSA as a standard was used to determine protein concentrations.

Kinetics- CP4 EPSPS activity assays were typically conducted at 25 °C in 100 μl of 50 mM HEPES-NaOH, pH 7.5 with 2 mM DTT ± KCl (as indicated), in parallel with *E. coli* EPSPS. *E. coli* EPSPS is salt-insensitive and assays utilized 0.001 mg/ml

enzyme, and 1 mM PEP or S3P were considered saturating substrate concentrations. CP4 EPSPS activity is salt sensitive; assays performed in the presence of 100 mM KCl used 0.002 mg/mL enzyme with 1 mM PEP or 1 mM S3P for saturation, while the experiments performed in the absence of salt required increased enzyme (0.0075 mg/ml CP4 EPSPS) and increased PEP (10 mM PEP considered saturating). The 100 µl reactions were started by the addition of enzyme, stopped after 3 minutes by the addition of 800 µl malachite green reagent, and color development was arrested after 5 minutes by the addition of 100 µl 34% w/v sodium citrate (final assay volume = 1 ml). Enzyme activity was determined by the amount of inorganic phosphate produced, as determined in comparison to phosphate standards.

Salt-sensitivity- The salt sensitivity test utilized saturating substrate concentrations (1 mM S3P, 1 mM PEP) ± 100 mM various salts (as shown) in Na-HEPES with 0.002 mg/mL CP4 EPSPS and was performed as described for *S. aureus* EPSPS (Chapter 3).

Optimal pH- The pH sensitivity test utilized saturating substrate concentrations (1 mM S3P, 1 mM PEP), 100 mM KCl, and 100 mM of a variety of sulfonate buffers, adjusted to the pH indicated. The heat sensitivity test was performed by Huijong Han by incubating the enzyme at various temperatures (as shown) for increasing times (as shown) in 50 mM HEPES, 100 mM KCl, 2 mM DTT, pH 7.5. Standard assays were then performed according to the method above at 25ºC in HEPES buffer and reactions were started by addition of heat-treated enzyme.

Substrate saturation- Enzyme activities were measured as a function of substrate concentration and the K_m and V_{max} values were determined by fitting the data to

Equation 1: $v = V_{max} * [S] / (K_m + [S])$

where v is the initial velocity, V_{max} is the maximum velocity, K_m is the Michaelis constant and $[S]$ is the substrate (S3P or PEP) concentration.

Glyphosate sensitivity- Enzyme activity as a function of glyphosate concentration was measured and the reported IC_{50} values for EPSPS inhibition were determined by fitting the data to

Equation 2: $$v = V_{min} + \frac{V_{max} - V_{min}}{1 + \left(\frac{[I]}{IC_{50}} \right)^n}$$

where v is the initial velocity, V_{max} is the maximum velocity, V_{min} is the minimum velocity, $[I]$ is the concentration of glyphosate and n is the Hill slope. Enzymatic activities at increasing PEP and varied glyphosate concentrations were recorded and the data were fit to Equation 1, and the K_i was determined by linear regression of the replot of the $K_{m(obs)}$ values versus the concentration of glyphosate, $[I]$ according to

Equation 3: $K_{m(obs)} = (K_m / K_i) * [I] + K_m$

where $K_{m(obs)}$ is the observed Michaelis constant in the presence of inhibitor, K_m is the true Michaelis constant, and K_i is the inhibition constant.

Fluoroescence studies- Fluorescence spectroscopy studies were also conducted utilizing CP4 EPSPS. For intrinsic fluorescence experiments, the excitation wavelength was 280 nm, and emission spectra were recorded between 290 and 400

nm. Experiments were conducted in 50 mM Na-HEPES pH 7.0, 2 mM DTT, with 150 µg of CP4 EPSPS per 1 ml sample. Emission spectra were recorded prior to the addition of ligands, and again after the addition of each ligand (S3P, PEP, KCl or glyphosate) to a final concentration of 1 mM (except in the case of KCl, which was added to a final concentration of 100 mM). Extrinsic fluorescence experiments were conducted utilizing ANS as a fluorophore. The assays were performed in 50 mM Na-HEPES pH 7.0, 2 mM DTT, and 150 µg of CP4 EPSPS was used for each 1 ml sample. For ANS fluorescence, the excitation wavelength was set to 366 nm and emission spectra were recorded between 400 and 600 nm. The ANS fluorescence emission spectra were recorded prior to the addition of enzyme or ligands and this free-ANS fluorescence signal was subtracted from that obtained after addition of enzyme, so that the fluorescence intensity reported is proportional to the amount of ANS•EPSPS complex in the sample. To determine the K_d ANS, maximum fluorescence intensity (λ = 475 nm) was recorded, plotted as a function of ANS concentration, and fit to

Equation 4: $y = Y_{max} * [ANS] / (K_d + [ANS])$

where y is the observed fluorescence, Y_{max} is the maximal fluorescence, K_d is the dissociation constant and $[ANS]$ is the concentration of the fluorophore. To determine the K_d of S3P, KCl, PEP, and glyphosate using this assay, ANS concentration was held constant at 200 µM. Fluorescence spectra were recorded after addition of 150 µg of CP4 EPSPS to the 1 ml sample to obtain F_O, the "original" fluorescence intensity. Varied concentrations of the ligands were then added and the spectra were again

recorded to obtain the F_L, the "liganded" fluorescence intensity. The addition of ligands resulted in fluorescence quench as ANS was displaced from the enzymes; to fit this to the K_d equation, the raw fluorescence intensity data were converted to the relative change in fluorescence intensity (equal to: 1- F_L/ F_O). This relative change in fluorescence intensity was plotted as a function of substrate concentration and fit to

Equation 5: $y = Y_{max} * [L] / (K_d + [L])$

where y is the observed relative change in fluorescence, Y_{max} is the maximal relative change in fluorescence, K_d is the dissociation constant and $[L]$ is the concentration of the ligand.

Crystallization screens- CP4 EPSPS was concentrated to 40 mg/ml in 50 mM Tris·HCl, pH 8.0 with 2 mM DTT and crystallized by hanging drop vapor diffusion. Initial crystallization trials were conducted in parallel using enzyme at 40 mg/ml and 20 mg/ml, ± 5 mM S3P, with 200 mM KCl included in every case. Crystallization conditions were found and optimized for both the "closed-form" (found with CP4 EPSPS + S3P ± glyphosate) and the substrate-free "open-form" (apo-enzyme) CP4 EPSPS.

Open-form CP4 EPSPS crystallization- For the open-form crystallization conditions, an enzyme mixture containing 20 mg/ml CP4 EPSPS, 100 mM KCl, 5% DMSO, 50 mM Tris-Cl pH 8.0, and 2 mM DTT and a precipitant solution consisting of 100 mM Tris-Cl pH 8.5 and 25% w/v PEG 4000 were mixed in a 1:1 ratio (4 μl + 4 μl), and the droplet was sealed over a reservoir containing 500 μl of the precipitant solution.

Needle-like crystals typically formed spontaneously after several days and persisted for several months in the crystallization droplet; stable harvesting conditions were not identified. Just prior to freezing for data collection, the crystals were soaked briefly (< 10 sec) in a cryoprotection buffer consisting of 50 mM KCl, 50 mM Tris-Cl pH 8.5, 25% w/v PEG 200, 25% w/v PEG 4000, and 2% DMSO. Since the resolution of individual open-form crystals varied substantially and cracks were frequently observed, particularly in larger crystal specimens, multiple open-form CP4 EPSPS crystals were typically screened prior to data collection.

Closed-form CP4 EPSPS crystallization- For the closed form crystallization conditions, an enzyme mixture containing 5-10 mg/mL CP4 EPSPS, 0.2 M KCl, 50 mM Tris-Cl, 10 mM S3P, and 2 mM DTT and a precipitant solution consisting of 2% PEG 400, 0.1 M Na-HEPES pH 7.5, and 2.0 M $(NH_4)_2SO_4$ were mixed in a 1:1 ratio (4 μl + 4 μl) and the droplet was sealed over a reservoir containing 500 μl of the precipitant solution. Blade-like crystals formed spontaneously after several days, or more rapidly with microseeding. These crystals were stable in a harvesting buffer consisting of 2.25 M $(NH_4)_2SO_4$, 0.1 M KCl, 1 mM S3P, and 50 mM Tris-Cl. Just prior to freezing for data collection, the crystals were soaked briefly (< 10 sec) in a cryoprotection buffer consisting of harvesting buffer diluted by addition of 25% v/v glycerol. These crystals showed better diffraction, greater stability, and less variability compared to the open-form CP4 EPSPS crystals. The best resolution was observed with the largest crystals, the growth of which can be favored by utilization of low concentrations of CP4 EPSPS and longer crystal growth times without

microseeding. To achieve the co-crystallization of CP4 EPSPS with glyphosate, the previously-described enzyme mixture and a small amount of the precipitant solution were prepared in a 0.5 M glyphosate solution (used in place of water). The concentration of glyphosate in the crystal droplet was approximately 80 mM.

Structure determination- X-ray diffraction data were collected according to the standard procedures described. The data were reduced with XDS[48] or HKL-2000[49]. The structures were solved by molecular replacement. With the unliganded *S. pneumoniae* EPSPS (PDB 1rf5) as search model, the structure of the unliganded (open-form) CP4 EPSPS was determined at 2.1-Å resolution. Subsequently, the structure of the S3P-liganded CP4 EPSPS was determined at 1.64-Å resolution with both globular domains of the open-form CP4 enzyme utilized as search models. This binary complex served as the search model for the determination of the ternary complexes of the WT and A100G CP4 EPSPS enzymes. Refinement and structure building were performed as previously described. Data collection and structure refinement statistics are included in the publication[52]. *Ab initio* energy calculations of the two glyphosate conformations were performed by Huijong Han with GAMESS using MP2/6–31+G*[98].

Results and Discussion:

The highly purified product of the synthetic CP4 EPSPS gene showed catalytic activity and glyphosate insensitivity. Parallel experiments were performed to compare the characteristics of the prototypical class I EPSPS enzyme from *E. coli* and the

prototypical class II EPSPS from CP4. The global sequence alignment between CP4 EPSPS and *E. coli* EPSPS (Fig. 4.1) indicates that the amino acid sequences of these orthologs share only 27% identity and 48% similarity. By comparing CP4 and *E. coli* EPSPS amino acid sequences, kinetic properties, and 3-dimensional structures, we illuminate the differences between these EPSPS enzymes and describe the structural basis for the glyphosate insensitivity of CP4 EPSPS.

Catalytic activity and salt effect- The catalytic activity observed in preliminary experiments was much decreased compared to the *E. coli* EPSPS, prompting experiments to test the effect of ions on this prototypical class II EPSPS. Much like the EPSPS enzyme from *S. aureus*[45], the CP4 enzyme is sensitive to ions, showing an increase in catalytic activity in the presence of specific monovalent cations (Fig. 4.2). The greatest activation was seen with potassium ions, and the enzyme activity plotted as a function of KCl concentration (Fig. 4.2) shows that this effect is saturable; these data were fit to Equation 1 to derive the dissociation constant for K^+ (K_d = 26 μM). To examine the basis of the cation-activation of CP4 EPSPS, we examined the steady-state kinetic properties in the presence and absence of 100 mM KCl (Fig. 4.3). Enzyme activity was plotted as a function of substrate concentration and fit to Equation 1 to derive the kinetic parameters reported in Table 4.1. In the presence of KCl, the specific activity of CP4 EPSPS was about 30 U/mg, half that of *E. coli* EPSPS. In the presence of KCl, the substrate binding affinity of CP4 EPSPS (K_m S3P = 140 μM; K_m PEP = 200 μM) appeared very comparable to that of *E. coli* EPSPS. In

Fig. 4.1: Optimal global alignment of CP4 and *E. coli* EPSPS. The prototypical class I and class II EPSPS synthases, from *E. coli* and CP4, respectively, share 27% amino acid sequence identity and 48% similarity. Boxes residues are identical.

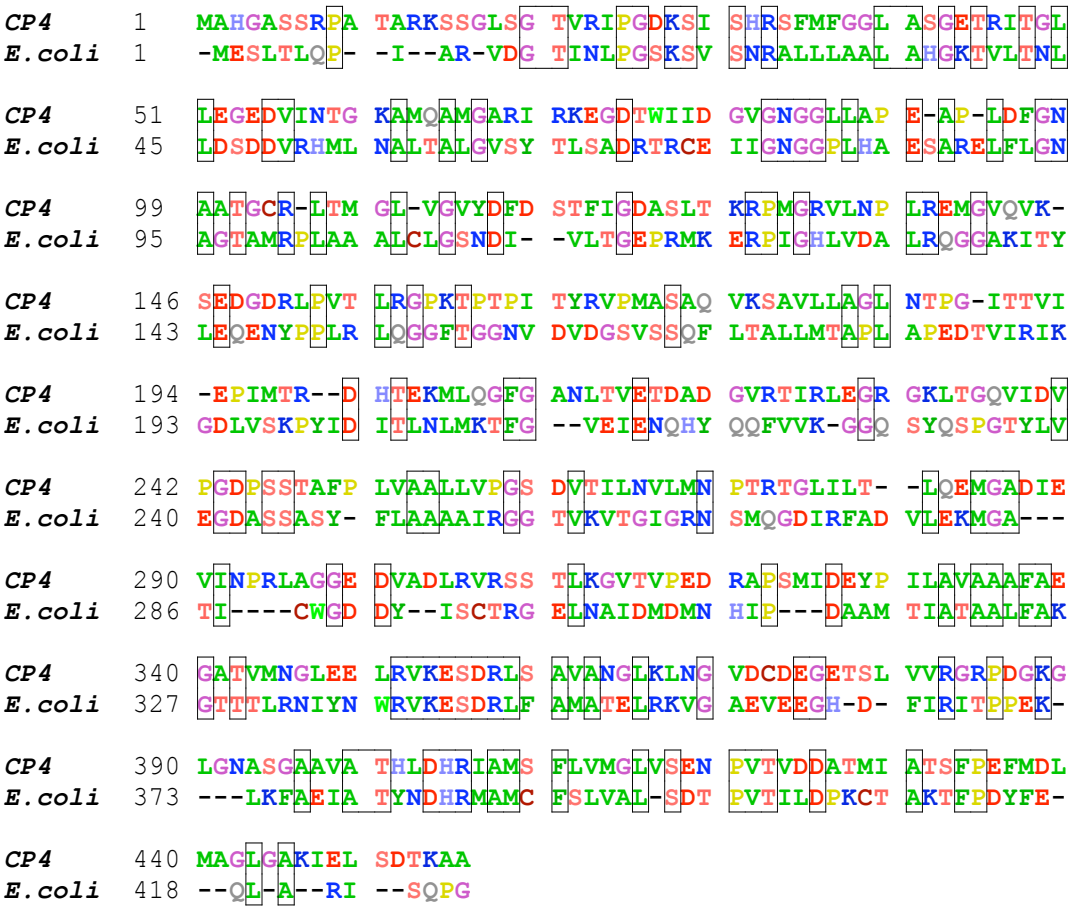

Fig. 4.2: The cation sensitivity of CP4 EPSPS (*Top*) The activity of CP4 EPSPS depends strongly on the presence of cations, such as NH_4^+, Rb^+, and K^+. (*Bottom*) Activation by K^+ is saturable with an apparent dissociation constant of 26 mM.

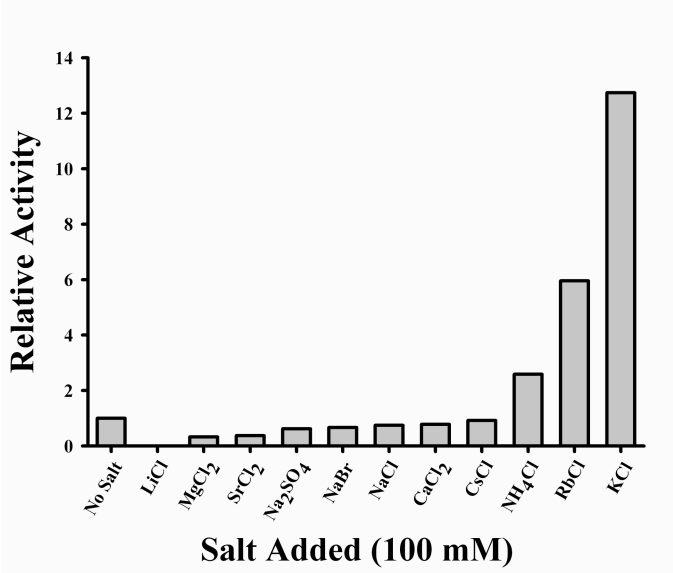

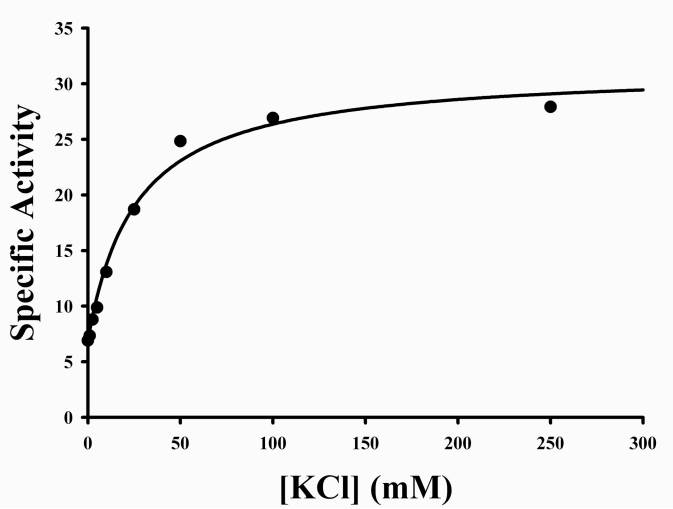

Fig. 4.3: CP4 EPSPS steady state kinetics: The effect of K^+. Steady-state kinetics of CP4 EPSPS (*Top*) The activity of CP4 EPSPS at various concentrations of PEP was assayed in the presence (filled circles) or absence (filled squares) of 100 mM KCl. Data were fit to Equation 1, yielding K_m PEP = 0.20 mM in the presence of 100 mM KCl and K_m PEP = 3.5 mM in the absence of salt. (*Bottom*) The activity of CP4 EPSPS at various [S3P] was assayed in the presence of 100 mM KCl (filled circles) or 10 mM PEP in the absence of salt (filled squares). Data were fit to Equation 1, yielding K_m S3P = 0.14 mM in the presence of 100 mM KCl, and K_m S3P = 0.18 mM in the absence of salt.

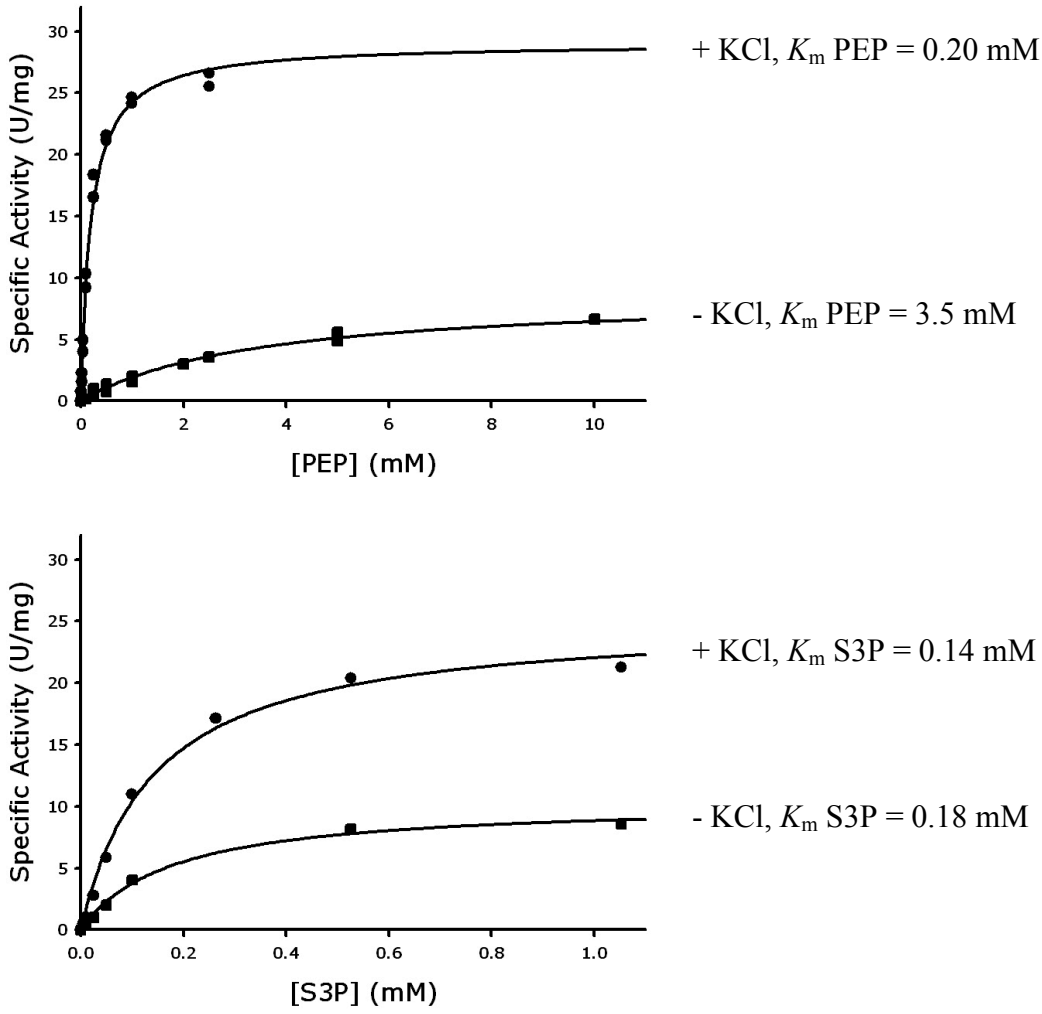

Table 4.1: Steady-state kinetic constants.

EPSPS Enzyme	K_m S3P (mM)	k_{cat}/K_m S3P (M^{-1} sec^{-1})	K_m PEP (mM)	k_{cat}/K_m PEP (M^{-1} sec^{-1})	IC_{50} Glp (mM)	K_i Glp (mM)
WT *E. coli* No KCl	0.16	$2.8* 10^5$	0.17	$2.8* 10^5$	0.0025	0.40
WT CP4 + KCl	0.14	$1.4 * 10^5$	0.20	$1.0 * 10^5$	11	6.4
A100G CP4 + KCl	0.28	$8.2 * 10^4$	0.18	$1.4 * 10^5$	0.16	0.092

the absence of salt, the specific activity of CP4 EPSPS decreased by 3-fold, while the binding of S3P by CP4 EPSPS was not substantially affected (K_m S3P = 180 μM). The K_m PEP was increased by 17-fold in the absence of salt, (K_m PEP = 3500 μM) suggesting that the cations facilitate the binding of PEP at the active site of CP4 EPSPS to produce the observed increase in specific activity. The concentration of potassium in plant cells is reportedly sufficient to produce the cation-activation of this enzyme *in situ*[99].

pH sensitivity- The log plot of enzyme activity as a function of sulfonate buffer pH (Fig. 4.4) shows that while both enzymes maintain activity over a broad pH range, the CP4 EPSPS is inhibited by more acidic conditions, while the *E. coli* EPSPS activity is decreased under more basic conditions.

Heat sensitivity- Thermal denaturation assays performed by Huijong Han (Fig. 4.5) indicated that CP4 EPSPS more thermally stable than the *E. coli* enzyme. The activity of the enzyme was measured after incubation at the temperature listed for the length of time indicated. Studies performed at 45 °C and 60 °C demonstrated that the CP4 enzyme is at least 17-fold more stable than EPSPS from *E. coli*. These results indicate that CP4 EPSPS is well-suited to harsh environmental conditions and suggest that the CP4 enzyme is much more rigid than *E. coli* EPSPS.

Glyphosate inhibition- The glyphosate-sensitivity of CP4 EPSPS was assessed by determining the K_i of glyphosate with respect to PEP (Fig. 4.6). Enzyme activity as a function of PEP concentration was measured in the presence of varied glyphosate

Fig. 4.4: Comparison of *E. coli* and CP4 EPSPS pH dependence. This plot shows the log of the activity of *E. coli* EPSPS (filled circles) and CP4 EPSPS (open circles) as a function of pH. The reactions were performed in 100 mM of various sulfonate buffers in the presence of 1 mM S3P, 1 mM PEP, and 100 mM KCl.

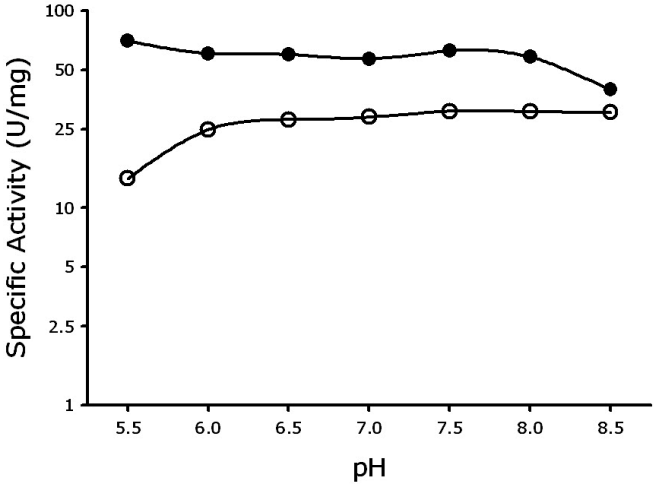

Fig. 4.5: Heat sensitivity of CP4 and *E. coli* EPSPS. (*Top*) The decline in activity of CP4 EPSPS (filled circles) and *E. coli* EPSPS (open circles) was assayed at 45 °C. Data were fit to a single exponential equation, yielding $T_{0.5}$ = 133 min for CP4 EPSPS and $T_{0.5}$ = 11 min for *E. coli* EPSPS. (*Bottom*) The decline in activity of CP4 EPSPS (filled circles) and *E. coli* EPSPS (open circles) was assayed at 60 °C. Data were fit to a single exponential equation, yielding $T_{0.5}$ = 6.8 min for CP4 EPSPS and $T_{0.5}$ = 0.2 min for *E. coli* EPSPS.

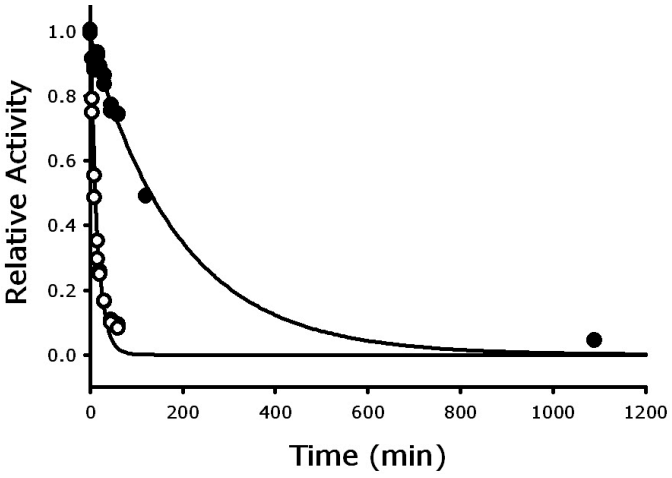

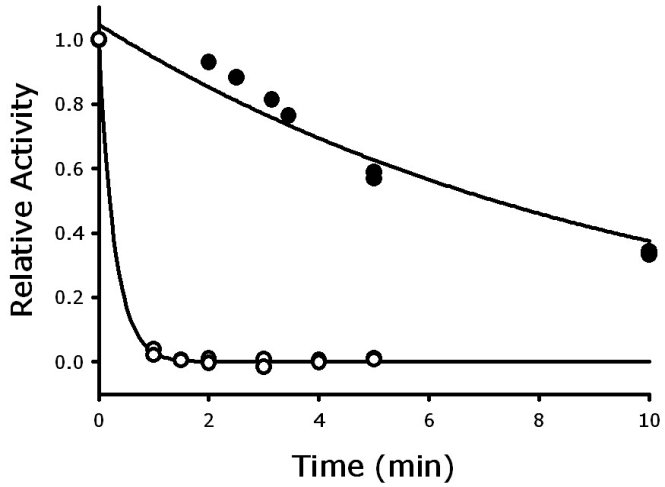

Fig. 4.6: Inhibition of CP4 EPSPS by glyphosate. (*Top*) The activity of CP4 EPSPS at various concentrations of PEP was assayed in the presence of 100 mM KCl with varied glyphosate concentrations: 0 mM (filled circles), 0.1 mM (filled diamonds), 0.5 mM (filled inverted triangles), 2.5 mM (filled triangles), 10 mM (filled squares), and 25 mM (open squares). The V_{max} and $K_{m(obs)}$ PEP were determined by fitting the data to Equation 1. (*Bottom*) Replot of the $K_{m(obs)}$ PEP as a function of glyphosate concentration. Data were fit to Equation 3, yielding a K_i of 6.4 mM.

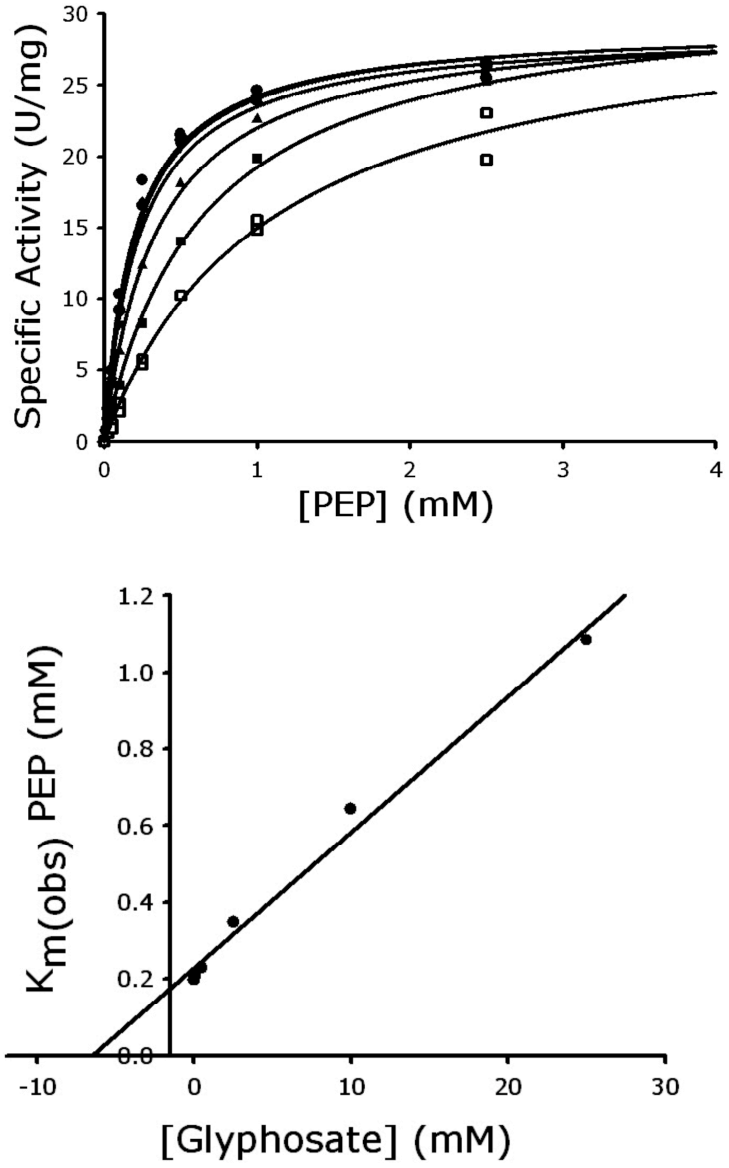

concentrations. These data were fit to Equation 1 to determine the $K_{m(obs)}$. The $K_{m(obs)}$ values were replotted as a function of glyphosate concentration and the data were fit to Equation 3 to determine the K_i values for glyphosate. Class I EPSPS enzymes are typically inhibited by low-micromolar-range concentrations of glyphosate, as demonstrated by *E. coli* EPSPS (K_i = 0.4 μM glyphosate). As expected, the class II EPSPS enzyme from CP4 is insensitive to glyphosate (K_i = 6.4 mM). This 16,000-fold difference in glyphosate-sensitivity roughly corresponds to the herbicide application window, or the difference between the minimum glyphosate concentrations required to kill weeds, and the maximum glyphosate concentrations that can be applied without damage to (the CP4 EPSPS-expressing) *Roundup Ready* crops.

Crystal structures- To examine the mechanism by which CP4 EPSPS discriminates between PEP and glyphosate to selectively binds PEP, crystallization conditions were discovered and optimized, enabling determination of apo-enzyme (unliganded CP4 EPSPS), binary complex (CP4 EPSPS•S3P), and ternary complex (CP4 EPSPS•S3P•glyphosate) structures. The gross morphology and folding pattern of CP4 EPSPS is similar to the *S. pneumoniae*[21] and *E. coli*[22] EPSPS enzymes; as observed in the other EPSPS enzymes, the binding of S3P to the active site of CP4 EPSPS induces a global conformational change (the open-closed transition) (Fig. 4.7). Despite the relatively low overall sequence conservation between *E. coli* and CP4 EPSPS, the active-site residues appear quite well conserved. The S3P-complexed active sites of CP4 and *E. coli* EPSPS are compared in Fig. 4.8. One obvious

Fig. 4.7: Global CP4 EPSPS structures. The open-closed transition is shown in this cartoon diagrams of CP4 EPSPS. Unliganded CP4 EPSPS exists in an open conformation (*Left*). The binding of S3P to the enzyme's active site induces a global conformational change to form the closed-form enzyme (*Right*).

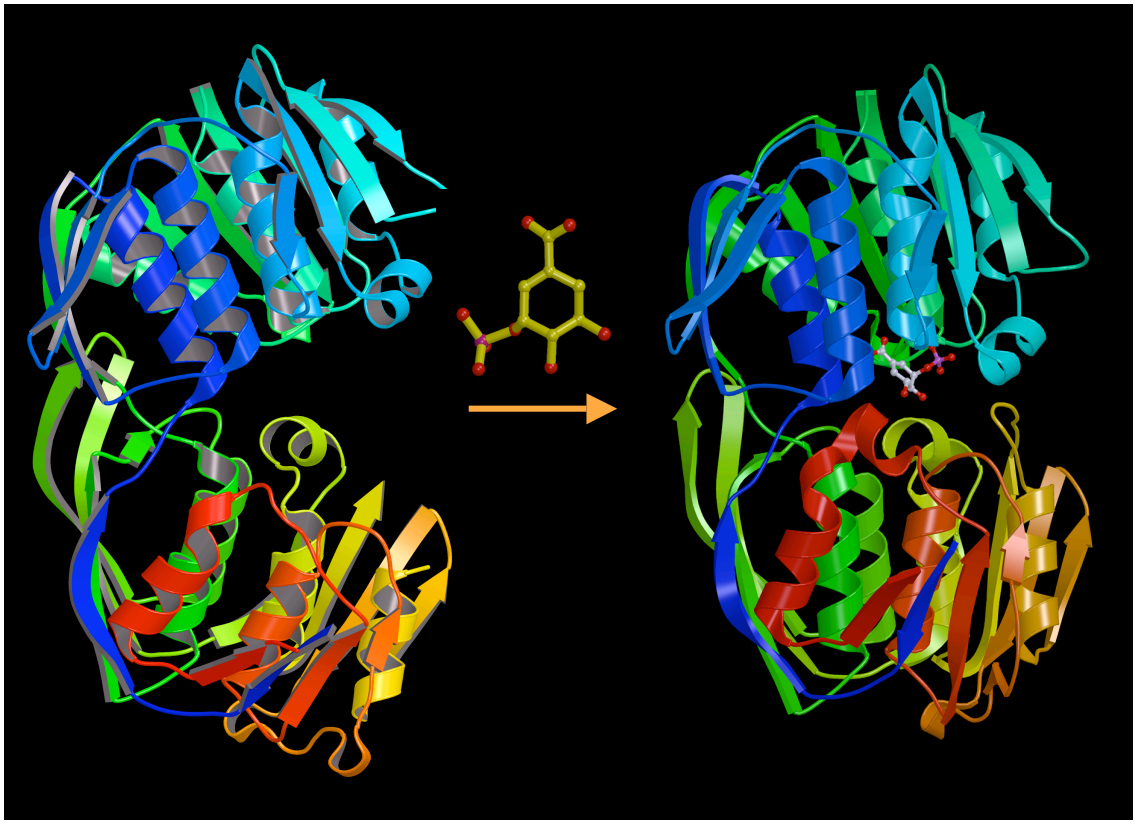

Fig. 4.8: Comparison of binary active-site structures of EPSPS.
(*Top*) S3P-complexed CP4 EPSPS; (*Bottom*) S3P-complexed *E. coli* EPSPS.

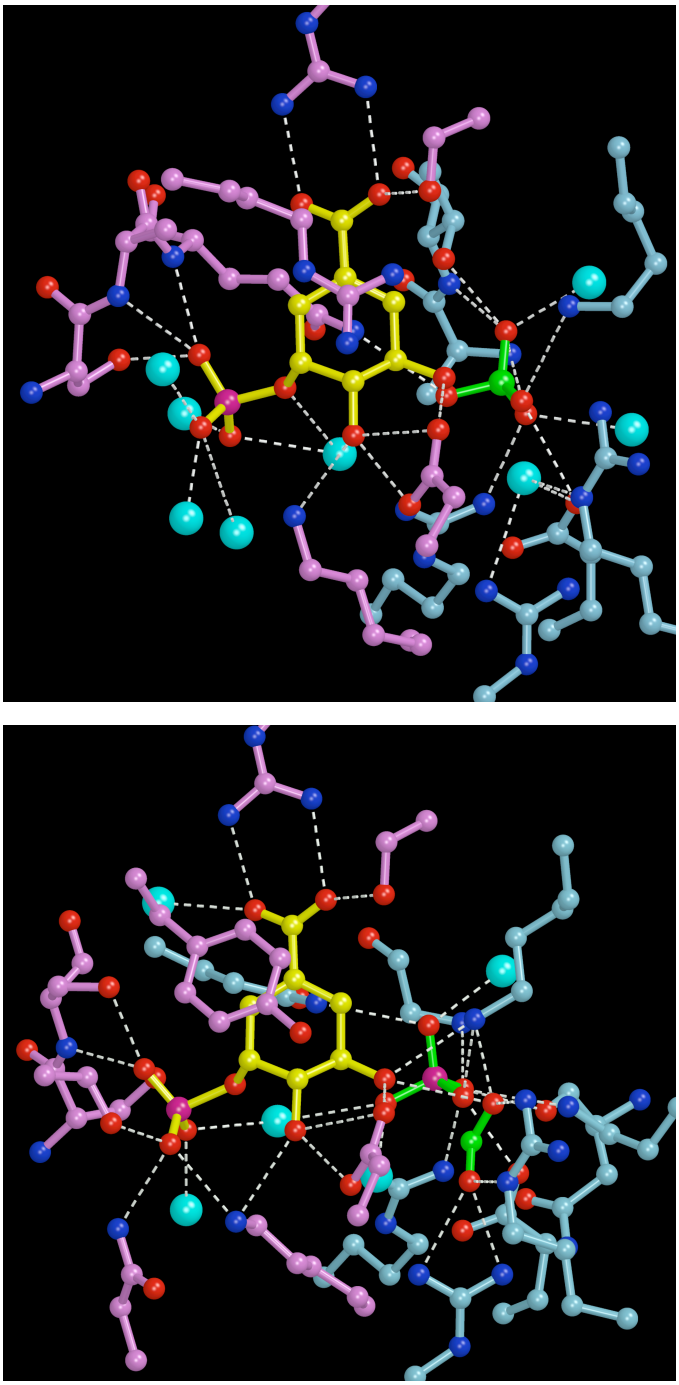

S3P (yellow) binds to the magenta-colored residues through multiple hydrogen-bonding/electrostatic interactions (shown as white dotted lines). Light-blue-colored residues constitute the PEP/glyphosate binding site. Water molecules are shown as cyan spheres.

The accumulation of positive charges in the space normally occupied by the phosphate moiety of PEP or the phosphonate moiety of glyphosate attracts anions (shown green) from the crystallization solutions (sulfate ions in CP4 EPSPS structure (*upper*), or formate ions in the *E. coli* EPSPS structure (*lower*)).

difference in the active site of these enzymes is that the front face of the S3P-binding pocket in the CP4 enzyme is formed by an arginine residue (Arg200) instead of the tyrosine residue (Tyr200) observed in *E. coli* EPSPS; additionally, in the CP4 enzyme, the phosphate moiety of S3P is predominantly hydrogen-bonded to water molecules, rather than directly to amino acid residues as observed in *E. coli* EPSPS. Less noticeable in this view is the presence of an alanine residue in position 100, replacing a strictly conserved glycine residue (corresponding to Gly96 of the *E. coli* EPSPS). The Gly96Ala mutation in *E. coli* EPSPS has been shown to result in glyphosate insensitivity[43, 90]; we therefore hypothesized that the glyphosate insensitivity of CP4 EPSPS is largely a result of the substitution of this alanine residue for the conserved, active-site glycine. To test this hypothesis, A100G CP4 EPSPS was produced, and we analyzed the activity, inhibition, and structure of the mutant enzyme.

A100G CP4 EPSPS Kinetics- The steady-state kinetic properties of A100G CP4 EPSPS are very similar to those of the WT CP4 EPSPS (Fig. 4.9). Compared to the WT CP4 enzyme, the S3P-binding affinity appears to be slightly decreased for this A100G mutant EPSPS (K_m S3P = 0.28 mM in the presence of 100 mM KCl; K_m S3P = 0.23 mM in the absence of salt). The binding of PEP to this enzyme is, again, influenced by the presence of potassium ions, with the PEP-binding affinity slightly increased (K_m = 0.18 mM) in the presence of 100 mM KCl or slightly decreased (K_m PEP = 5.0 mM) in the absence of salt as compared to WT CP4 EPSPS. These data are notable, because the reverse mutation at the equivalent site (Gly96Ala) in *E. coli*

Fig. 4.9: Steady-state kinetics of A100G CP4 EPSPS (*Top*) The activity of A100G CP4 EPSPS at various concentrations of PEP in the presence (filled circles) or absence (filled squares) of 100 mM KCl. Data were fit to Equation 1, yielding K_m PEP = 0.18 mM in the presence of 100 mM KCl and K_m PEP = 5.0 mM in the absence of salt. (*Bottom*) The activity of A100G CP4 EPSPS at various S3P concentrations was assayed in the presence of 100 mM KCl (filled circles), or in the absence of salt (filled squares). Data were fit to Equation 1, yielding K_m S3P = 0.28 mM in the presence of 100 mM KCl and K_m S3P = 0.23 mM in the absence of salt.

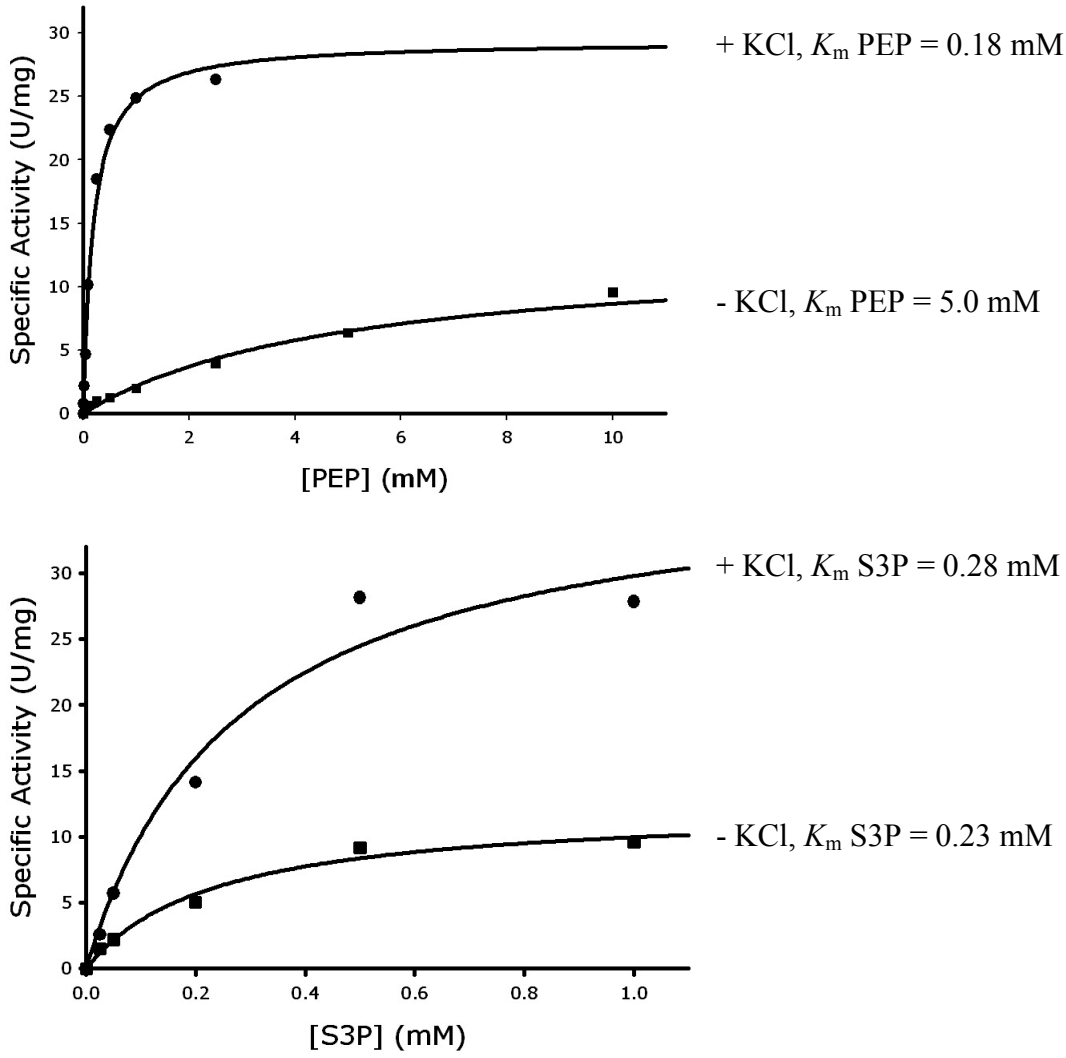

EPSPS resulted in dramatically decreased affinity for PEP[43]. If the Ala-100 residue of CP4 EPSPS interfered with PEP-binding, one would expect the A100G mutant to show higher affinity for PEP. Based on the conserved active-site architecture observed in the crystal structures and the consistent K_m values for PEP obtained with all three enzymes, it appears that subtle structural differences exist in WT CP4 EPSPS to compensate for the presence of the Ala-100 side chain and maintain PEP binding affinity. The specific activities observed for A100G CP4 EPSPS are, in every case, comparable to those of WT CP4 EPSPS. Overall, the substrate binding and catalytic activity of CP4 EPSPS appear unaffected by the A100G mutation.

A100G CP4 EPSPS Inhibition by Glyphosate- The glyphosate sensitivity of WT CP4, A100G CP4, and WT *E. coli* EPSPS enzymes are directly compared in Fig. 4.10, with relative enzyme activity measured as a function of glyphosate concentration. These plots show that the A100G mutation results in a substantially increased glyphosate sensitivity. These data were fit to Equation 2 to determine the IC_{50} values, revealing that the IC_{50} of the A100G mutant enzymes is decreased by nearly 2 orders of magnitude compared to WT CP4 EPSPS, suggesting that the presence of this alanine residue in the active site of CP4 EPSPS is, in large part, responsible for the observed glyphosate-insensitivity. For a more precise analysis, we determined the K_i of glyphosate with respect to PEP for A100G EPSPS (Fig. 4.11). The results are similar to the IC_{50} data, with the A100G K_i glyphosate = 0.092 mM. We conclude that the

Fig. 4.10: IC_{50} of Glyphosate. Studies with WT CP4 EPSPS (filled squares), A100G CP4 EPSPS (open circles), and WT *E. coli* EPSPS (closed circles) reveal that CP4 EPSPS is inhibited only by high millimolar concentrations of glyphosate (IC_{50} = 11 mM). The A100G CP4 EPSPS is approximately two orders of magnitude more sensitive to glyphosate (IC_{50} = 160 μM). The *E. coli* enzyme is inhibited by much lower glyphosate concentrations (IC_{50} = 2.5 μM).

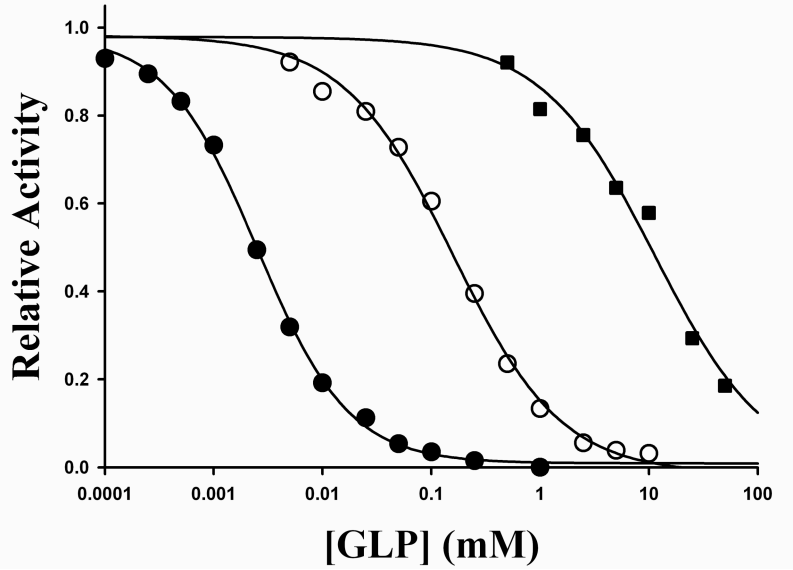

Fig. 4.11: Inhibition of Ala100Gly CP4 EPSPS by glyphosate. (*Top*) The activity of A100G CP4 EPSPS was assayed at various concentrations of PEP in the presence of 100 mM KCl, with varied glyphosate concentrations: 0 mM (filled circles), 0.01 mM (filled diamonds), 0.025 mM (filled inverted triangles), 0.05 mM (filled triangles), 0.1 mM (filled squares), and 0.25 mM (open squares). The V_{max} and $K_{m(obs)}$ PEP were determined by fitting the data to Equation 1. (*Bottom*) Replot of the $K_{m(obs)}$ PEP as a function of glyphosate concentration. Data were fit to Equation 3, yielding a K_i of 0.092 mM.

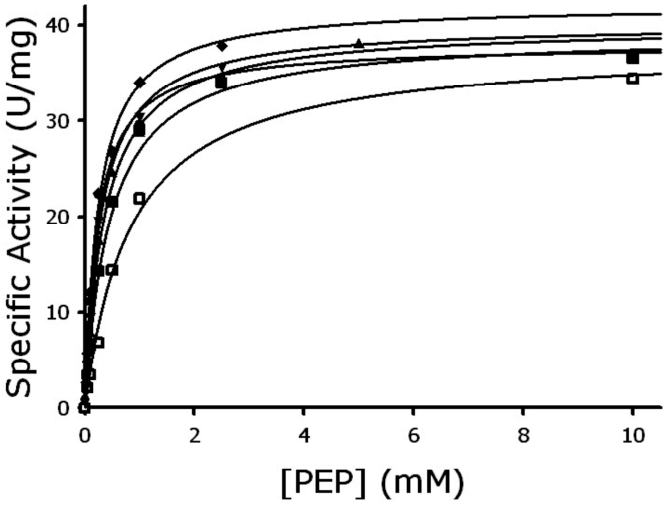

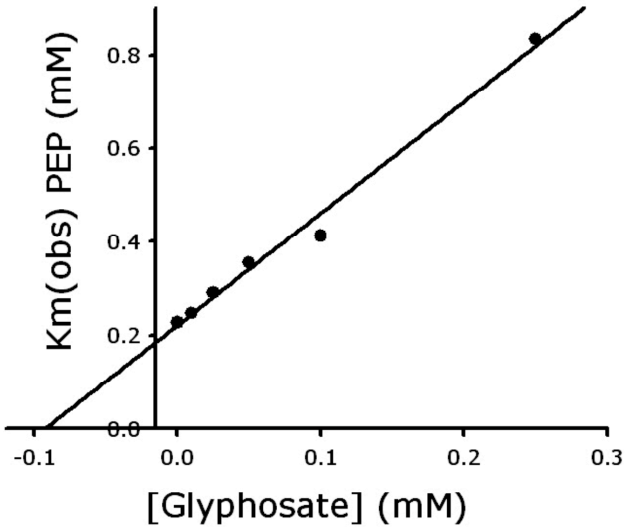

steric bulk of the Ala-100 side chain contributes substantially to the glyphosate insensitivity of CP4 EPSPS.

A100G CP4 EPSPS Crystallization- To further analyze the basis of glyphosate tolerance, we crystallized the A100G CP4 EPSPS enzyme in the presence of S3P and glyphosate and compared this structure to the WT CP4 EPSPS ternary complex (Fig. 4.12). This analysis revealed that the active site of CP4 EPSPS is very stable; aside from the alanine-to-glycine mutation, all amino acid residues are in essentially identical positions. In fact, the major change observed is in the conformation of the glyphosate molecule itself (shown green). The presence of the Ala-100 side chain effectively shortens the glyphosate binding site; the glyphosate molecule must adopt an alternate, condensed conformation in order to bind. In this condensed conformation, the carbon atom of glyphosate's phosphonate moiety is positioned very close to the glutamate side chain of residue Glu-354, introducing a steric clash. Thus, not only is glyphosate unable to bind CP4 EPSPS in the normal, extended conformation, but even binding of the condensed conformation is disfavored due to interactions with residue Glu-354. The conformational change of glyphosate is further explored in Fig. 4.13, which displays the fitting of the glyphosate structure into the electron density maps. The condensed conformation on the left side was observed only in CP4 EPSPS, while the extended conformation on the right side is observed in A100G CP4 EPSPS, *E. coli* EPSPS[22], and *S. pneumoniae* EPSPS[21], and indeed is the lower energy conformation that exists in solution[29]. Ab initio energy calculations (by Huijong Han) showed that the condensed conformation of glyphosate has an

Fig. 4.12: Ternary active-site structures of CP4 EPSPS.
Glyphosate (green) binds adjacent to S3P (yellow) in the active site of EPSPS. Hydrogen bonding/electrostatic interactions are indicated by white dashed lines; Steric clashes shown as red dotted lines; Water molecules shown as cyan spheres.

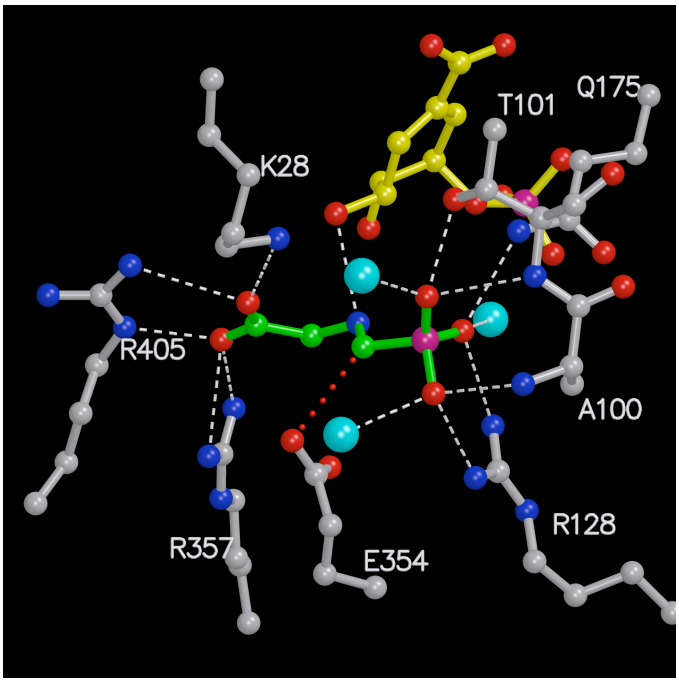

(*Top*) WT CP4 EPSPS: Glyphosate adopts a condensed conformation as a the result of a clash between the Ala-100 side chain and oxygen atoms of glyphosate's phosphonate group. This alternate conformation causes the carbon atom of the phosphonate group to clash with the side chain of Glu-354 (red dotted line).

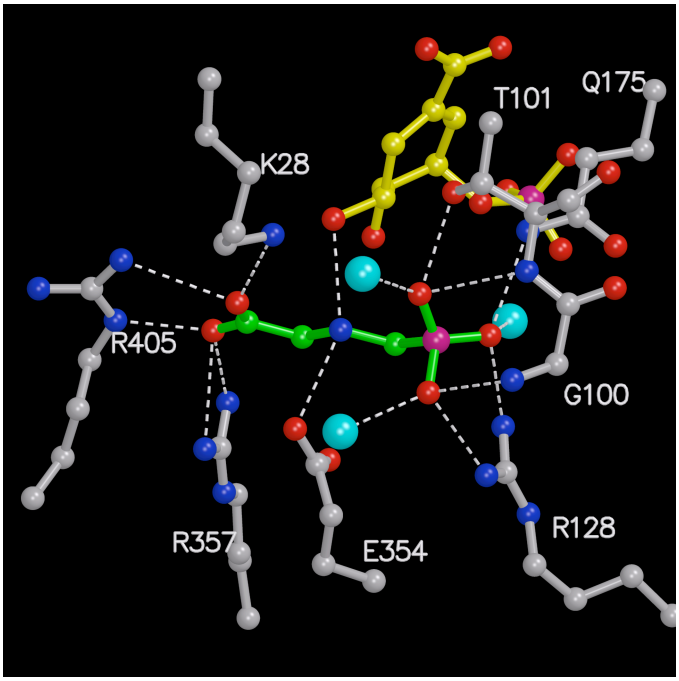

(*Bottom*) A100G CP4 EPSPS: Replacing Ala-100 with a glycine residue allows glyphosate to bind in the extended conformation that it adopts in solution and as observed in other crystal structures. In this extended conformation, the nitrogen atom of glyphosate is equidistant from the 5'-hydroxyl of S3P and the carboxyl of Glu-354.

Fig. 4.13: Conformational change of glyphosate. Two distinct conformations of glyphosate. Displayed are the electron densities, contoured at 3σ, derived from $1F_o - 1F_c$ Fourier syntheses to 1.7-Å resolution, omitting the model of glyphosate during the refinement of the ternary complexes of CP4 EPSPS (*Left*) and A100G CP4 EPSPS (*Right*). (*Right*) The conformation of glyphosate upon interaction with the A100G CP4 EPSPS is identical to the one observed in the *E. coli* or *S. pneumoniae* enzymes. (*Left*) With an Ala residue in position 100, the glyphosate molecule is ~ 0.6 Å shorter, mainly because of a rotation around the CN bond next to the carboxyl group.

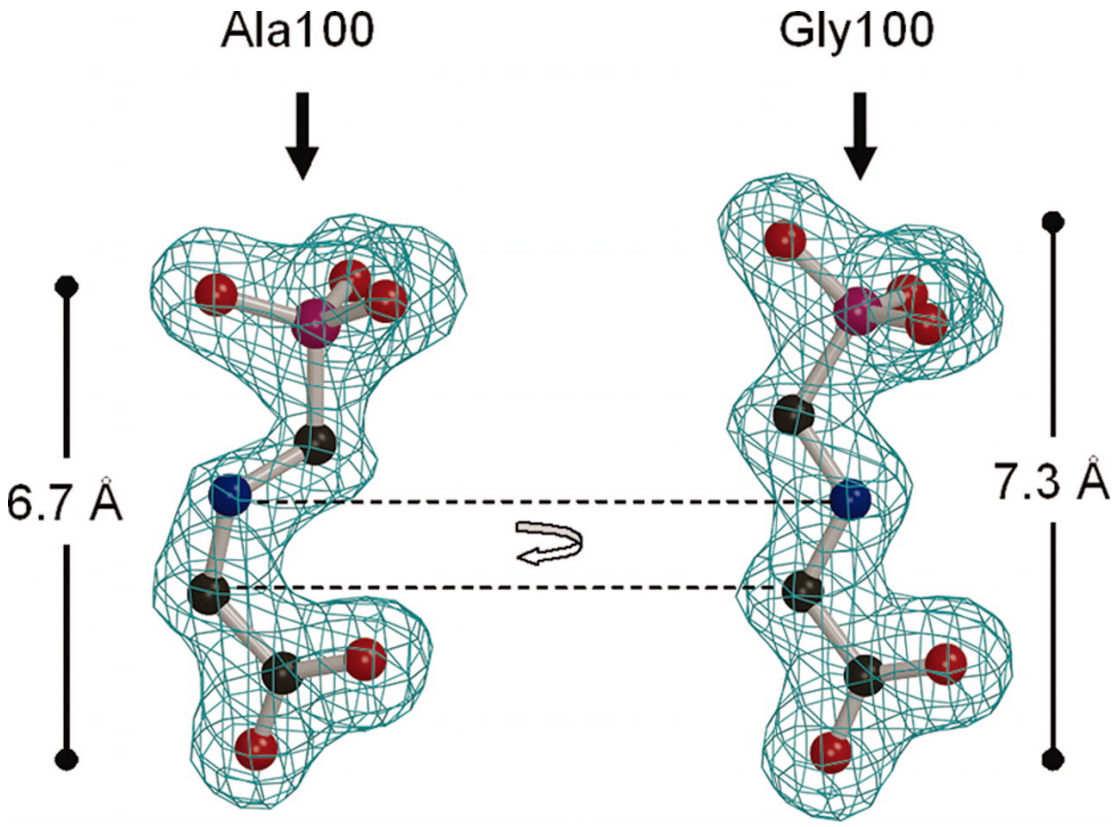

estimated 17 kcal/mol higher energy than the extended conformation. It is not clear whether glyphosate adopts this condensed conformation prior to interacting with CP4 EPSPS or upon binding to the enzyme. Since higher energy conformations are statistically disfavored in solution, only a small percentage of the glyphosate molecules would occupy the condensed conformation at any given moment. Thus, if only a high-energy conformation is able to bind to the enzyme, then the actual concentration of the ligand (the glyphosate molecules in the high-energy, condensed conformation) is much lower than the molarity of glyphosate in the solution, and high glyphosate concentrations may be needed to obtain moderate concentrations of the active confomer. Alternatively, CP4 EPSPS may initially interact with the low energy, "extended" glyphosate molecule, and induce the conformational change upon binding. If this transition to the higher-energy conformation were enzyme-induced, the free energy required for binding would be increased, thereby disfavoring formation of the EPSPS•glyphosate complex. Either explanation seems to account for the observed conformational change of glyphosate and both provide a rationale for the insensitivity of CP4 EPSPS to this inhibitor.

Fluorescence Studies- Intrinsic and extrinsic fluorescence trials were conducted with CP4 EPSPS. This enzyme exhibits intrinsic fluorescence (Fig. 4.14, top), but the addition of saturating amounts of salt or substrates (colored lines) did not alter the fluorescence signal, and these experiments were discontinued. CP4 EPSPS extrinsic fluorescence trials were performed using the fluorophore ANS (Fig. 4.14, bottom). The brown line shows the fluorescence signal of ANS alone; the black line shows the

Fig 4.14: CP4 EPSPS fluorescence trials.

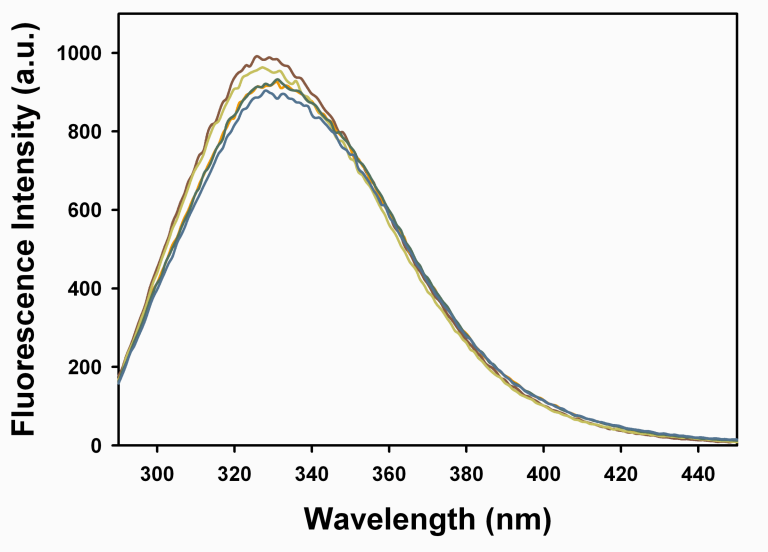

(*Top*) CP4 EPSPS shows intrinsic fluorescence, but no change is observed upon addition of ligands (colored lines).

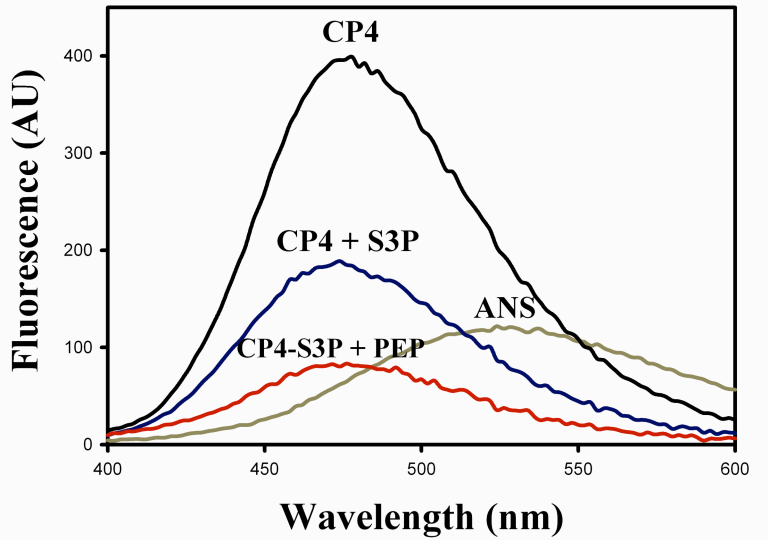

(*Bottom*) The extrinsic fluorophore ANS shows a fluorescence increase upon binding to CP4, and the addition of ligands results in fluorescence quench.

increase in fluorescence observed upon addition of CP4 EPSPS, due to formation of a CP4 EPSPS•ANS complex. The CP4 EPSPS•ANS fluorescence signal was quenched upon addition of 1 mM S3P, and further decreased by addition of 1 mM PEP, suggesting that ANS fluorescence quench assays may be useful for examination of the ligand binding and induced fit mechanism of CP4 EPSPS. The results of the extrinsic fluorescence experiments are shown in Figs. 4.15a-e. In Fig. 4.15a, the maximum fluorescence intensity was replotted as a function of ANS concentration. Normal enzyme saturation behaviour was observed and these data were fit to Equation 4 to derive the dissociation constant for ANS (K_d = 42 μM). The ANS fluorescence experiments summarized in Fig. 4.15b-e were performed in the absence of salt, with constant concentrations of enzyme and fluorophore, and varied concentrations of ligands (S3P, PEP, glyphosate, or KCl), as indicated. Fig. 4.15b shows the quenching of CP4 EPSPS•ANS fluorescence upon addition of S3P. The relative change in fluorescence intensity was replotted as a function of S3P concentration and data were fit to Equation 5, yielding K_d S3P = 2.4 μM. This is nearly two orders of magnitude lower than the K_m S3P determined from the activity assays. Fig. 4.15c shows the quenching of CP4 EPSPS•ANS fluorescence upon addition of PEP. The relative change in fluorescence intensity was replotted as a function of PEP concentration and data were fit to Equation 5, yielding K_d PEP = 8.6 μM. This result was unexpected, as S3P-induced conformational change is thought to result in formation of the PEP-binding site at the interdomain cleft of closed-form EPSPS. It is remarkable that PEP binds to CP4 EPSPS with such high affinity in the

Fig 4.15a-e: CP4 extrinsic fluorescence: K_d determinations.
Fig 4.15a: Fluorescence intensity as a function of [ANS]. ANS K_d = 35 μM

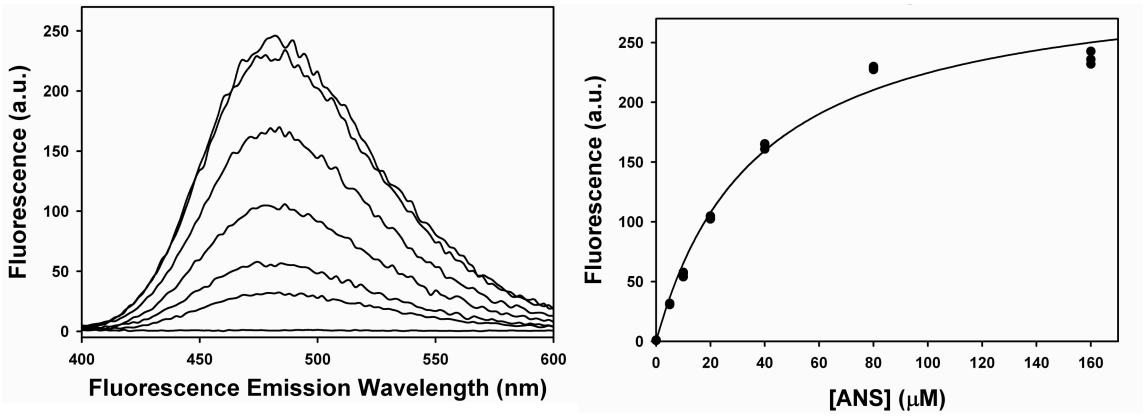

Fig. 4.15b: Dashed line displays average CP4 + ANS fluorescence (F_O). Solid lines display CP4 + ANS + S3P fluorescence (F_L). K_d S3P = 2.4 μM

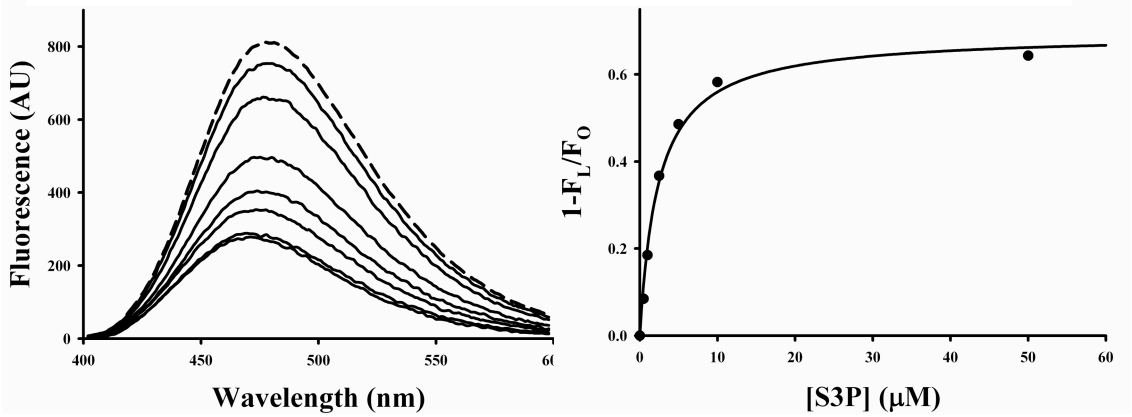

Fig. 4.15c: Dashed line displays average CP4 + ANS fluorescence (F_O). Solid lines display CP4 + ANS + PEP fluorescence (F_L). K_d PEP = 8.6 μM

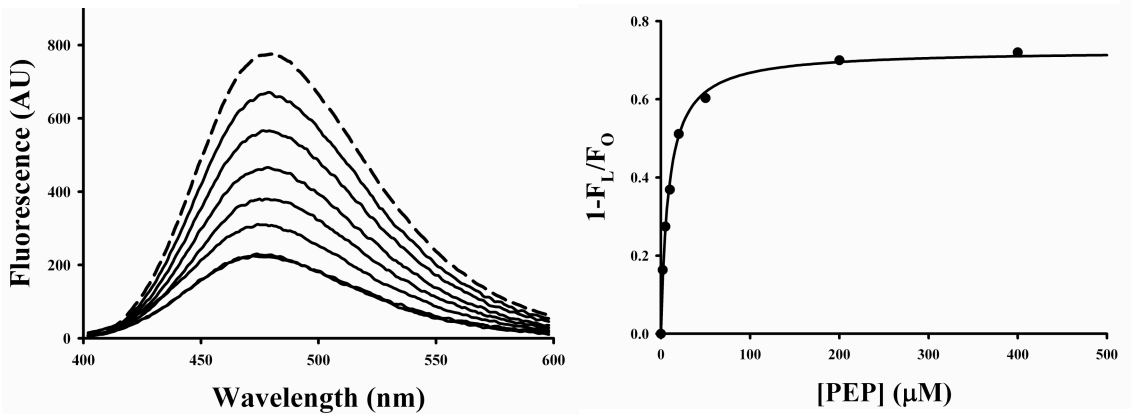

Fig 4.15: CP4 extrinsic fluorescence: K_d determinations, *cont.*

Fig 4.15d: Dashed line displays average CP4 + ANS fluorescence (F_O). Solid lines display CP4 + ANS + KCl fluorescence (F_L). K_d KCl = 11.2 mM

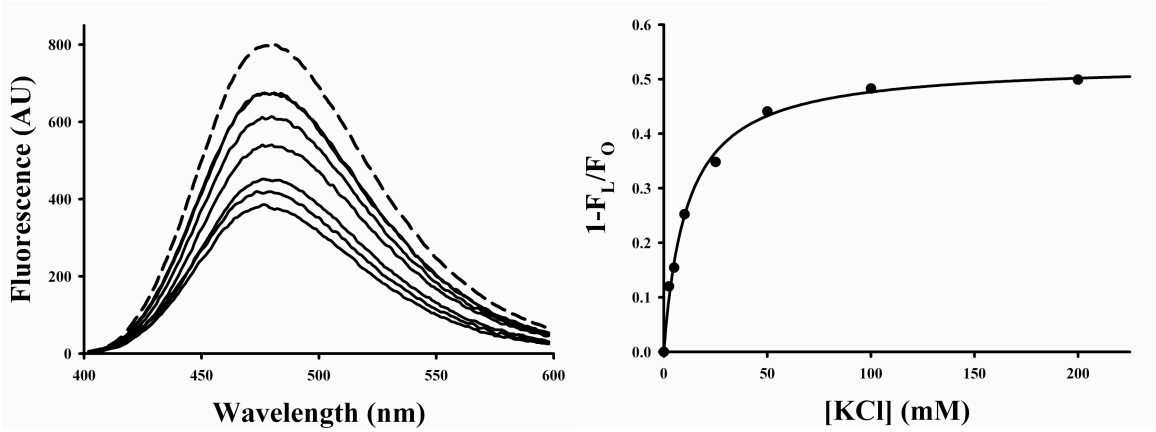

Fig. 4.15e: Dashed line displays average CP4 + ANS fluorescence (F_O). Solid lines display CP4 + ANS + glyphosate fluorescence (F_L).
K_d glyphosate= 2.1 mM

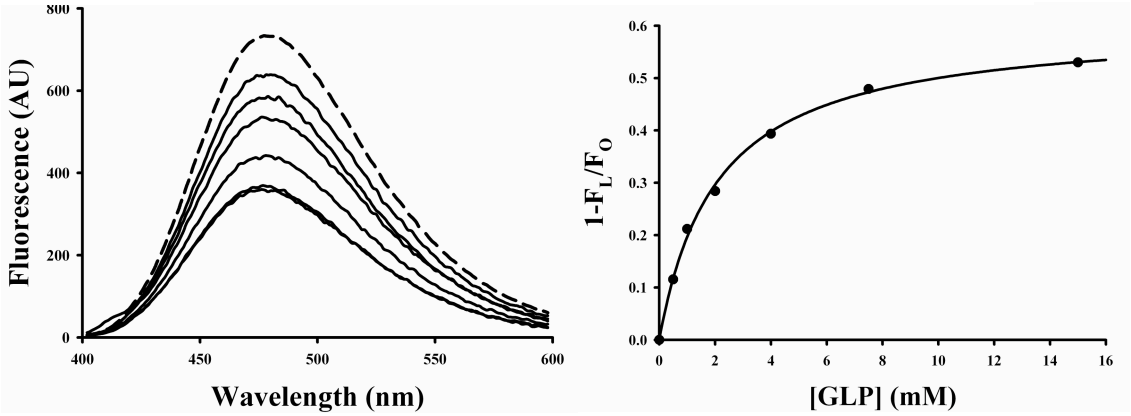

absence of S3P when the activity assays performed in the absence of salt showed that the K_m for PEP was in the low millimolar range. Fig. 4.15d shows the quenching of CP4 EPSPS•ANS fluorescence upon addition of KCl. The relative change in fluorescence intensity was replotted as a function of KCl concentration and data were fit to Equation 5; in this case, the K_d value of 11.2 mM agrees relatively well with that determined in the activity assays (26 mM). Finally, Fig. 4.15e shows the quenching of CP4 EPSPS•ANS fluorescence upon addition of glyphosate – again, the observed fluorescence quenching was somewhat unexpected; like PEP, the glyphosate binding site was not expected to exist in the absence of S3P. The relative change in fluorescence intensity was replotted as a function of glyphosate concentration and data were fit to Equation 5, yielding a K_d of 2.1 mM for glyphosate, roughly comparable to the K_i for glyphosate previously determined.

Further crystallization trials- To better explain the effect of cations on CP4 EPSPS, we attempted to define the cation-binding site by crystallization in the presence of the more electron-dense Rb^+ ion. To better explain the ANS fluorescence quench data, we attempted to define the ANS-binding site by crystallization of CP4 EPSPS in the presence of ANS. Neither cations nor ANS were observed in the resulting crystal structures. These experiments were not entirely uninformative, however. In the unliganded state, the CP4 EPSP synthase contains a highly flexible, 12-residue loop in the C-terminal domain around the strictly conserved active site residue E354 (shown orange in Fig. 4.16). In the open-form crystal structure, this loop is only barely visible in the electron density map. In the closed-form crystal structure, this

Fig. 4.16: Putative ANS/cation binding site. Shown in orange is a loop spanning residues 347–358, which is highly flexible in the open conformation but becomes ordered in the closed conformation. This loop contains the strictly conserved EPSP synthase residues Glu-354 and Arg-357, which are involved in PEP/glyphosate binding. Monovalent cations may influence the conformation of this loop and facilitate binding of PEP.

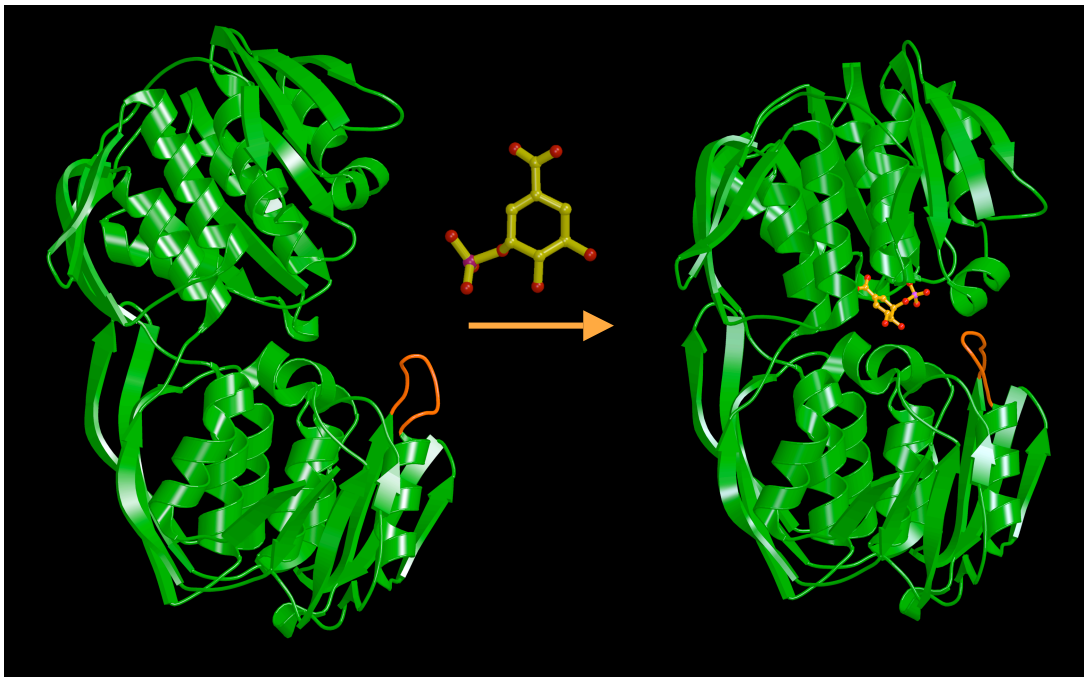

loop becomes ordered and interacts with the N-terminal domain, forming a portion of the active site. The structures of the open-form CP4 EPSPS crystallized in the presence of ANS or with high concentrations of cations show this loop adopting a less flexible, more ordered structure, suggesting that ANS or cations may bind at this loop, essentially acting as chaperones to restructure the loop region. While neither the cations nor the ANS are observed at this site in the crystal structures, it may be the case that they essentially act as chaperones to restructure the loop; once the loop adopts a more regular conformation, the binding sites may be lost. The interaction of this loop with PEP and glyphosate, and putatively with ions and ANS, would account for the fluorescence quench data and could explain the dissociation constants for PEP and glyphosate that we obtained in the absence of S3P.

Crystallization and inhibition experiments with DMSO- CP4 EPSPS co-crystallization trials were conducted with newly-identified inhibitors of the *E. coli* EPSPS (see chapter 8). The DMSO solution used to solubilize the inhibitors prevented crystallization of *E. coli* EPSPS but resulted in formation of closed-form CP4 EPSPS crystals even in the absence of S3P. Instead of finding the inhibitor bound at the active site, it was observed that the enzyme, while indeed in the closed conformation, was largely "empty" (Fig. 4.17). Several conserved water molecules were observed at the positions normally found, and several additional water molecules and two sulfate ions were also observed. Strong additional electron density was observed (yellow balls in Fig. 4.17) which could not be definitively identified,

Fig. 4.17: Closed-form "Apo"-CP4 EPSPS active site structure. Waters shown in cyan, sulfates in green, and unmodeled electron density in yellow.

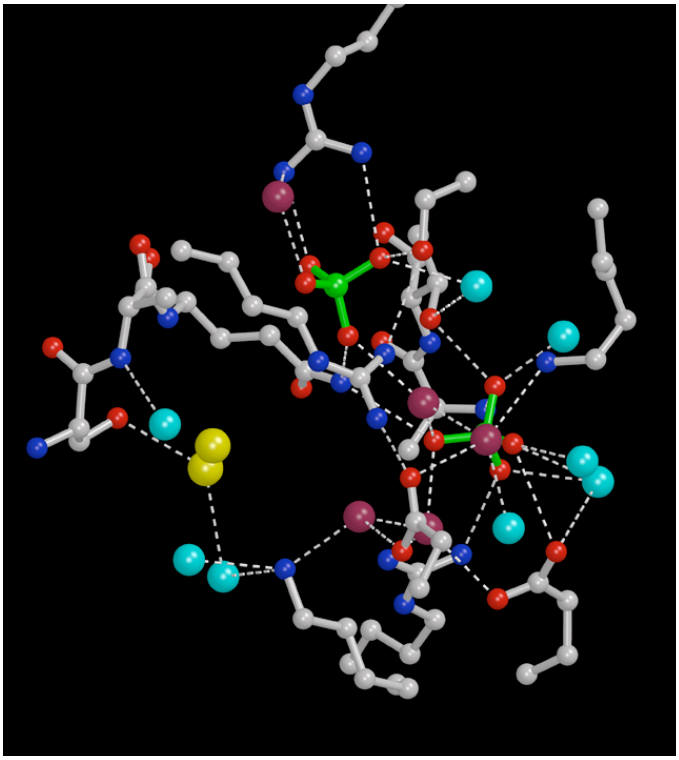

but may be DMSO or glycerol. Further experiments are underway. The crystals were reproducible in the absence of S3P and inhibitors by including 5 to 8 % DMSO in the precipitation buffer (2.5 to 4% DMSO in the crystal droplet). The basis for the formation of the closed-form apo-CP4 EPSPS in the absence of S3P is unknown, but this structure demonstrates that S3P is not required to induce the open-closed transition in this enzyme, and may be particularly useful for purposes of fragment-based drug design. The sensitivity of CP4 EPSPS to DMSO was subsequently tested (Fig. 4.18) and fit to Equation 2 to determine an IC_{50} for DMSO of 1.4 M, or about 10% v/v, as shown in the figure. In the crystallization droplet, only about 4% DMSO was present, suggesting that the DMSO is not directly responsible for the substrate-free open-closed conformational change of CP4 EPSPS. It may be that the role of DMSO is simply to keep the apo-form CP4 EPSPS enzyme in solution under the closed-form crystallization conditions. In this case, the open-closed transition could be induced either spontaneously or by the binding of anions, and the closed-form of the enzyme could be "trapped" and removed from the solution by crystal formation. Further experiments may illuminate the basis for this phenomenon and the identity of molecule responsible for the unmodeled electron density.

Conclusions:

We determined the catalytic activity, steady-state kinetic constants, cation-dependence, multiple crystal structures (apo-open, apo-closed, binary, and ternary complexes) and the major structural basis for glyphosate tolerance of CP4 EPSPS, a representative class II enzyme. The activity and substrate binding appear similar to *E.*

Fig. 4.18: CP4 EPSPS DMSO sensitivity. CP4 EPSPS is inhibited by DMSO. The IC_{50} for DMSO is 1.4 M (approximately 10% v/v).

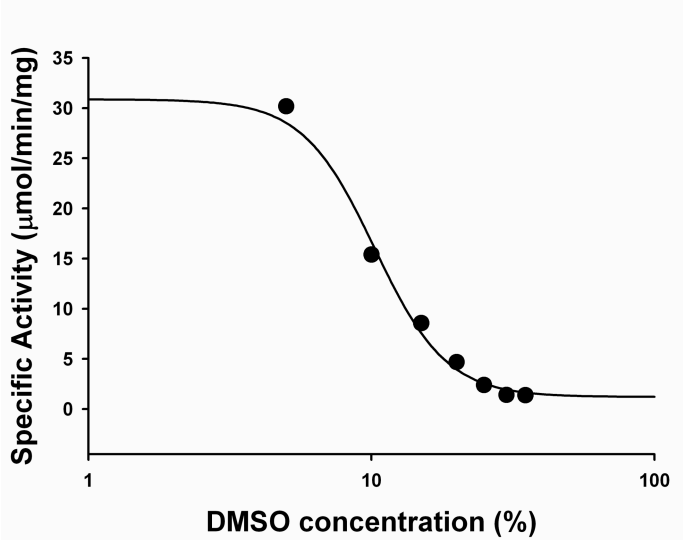

coli EPSPS and other class I enzymes. The glyphosate-tolerance and cation-dependence of CP4 EPSPS are markedly different. The steric bulk added by the methyl group of the alanine residue (A100), found in CP4 EPSPS in place of a conserved active-site glycine residue, appears to be largely responsible for the glyphosate insensitivity. The added bulk at this position forces the glyphosate molecule to adopt a higher-energy condensed conformation that has not been observed previously. The mutation of this alanine back to glycine (A100G CP4 EPSPS) largely, but not completely, restored glyphosate sensitivity, without altering the binding of PEP. It seems that other, more subtle changes must also occur in CP4 EPSPS to account for the residual glyphosate insensitivity of the A100G CP4 EPSPS and to facilitate PEP-binding in the WT CP4 enzyme. Glyphosate insensitivity has also been reported due to mutations of the residue corresponding to Pro101 of *E. coli* EPSPS[69, 71, 100], and the CP4 EPSPS contains a leucine at the equivalent position (see Fig. 4.2); this residue may also contribute toward the ability of CP4 EPSPS to distinguish between PEP and glyphosate.

Overall, these data explain the agricultural success of *Roundup Ready* crops at a molecular level. The continued presence of glyphosate in the environment will favor the accumulation of mutations that reduce the glyphosate sensitivity of EPSPS while maintaining catalytic efficiency. The speed at which glyphosate resistance develops depends on the organisms' generation time and fidelity of gene replication. It is perhaps therefore not surprising that the CP4 gene was isolated from bacteria found in a glyphosate-production facility. The current low rate of appearance of plants with

evolved glyphosate resistance may be attributed to the relatively high-fidelity replication and long generation times of most plants, along with glyphosate's phytotoxicity and lack of persistence or residual activity in the environment. However, extensive use of glyphosate increases the likelihood that glyphosate-resistant weeds will emerge on a large scale. Indeed, the introduction of glyphosate-tolerant crops resulted in greatly increased application of glyphosate, and this has coincided with an exponential increase in the number of weed species with evolved glyphosate resistance[39].

It appears that the confined space of the active site of EPSPS prohibits even slight alterations of the glyphosate molecule. More than 1,000 analogs of glyphosate were produced and tested, but relatively minor structural alterations resulted in dramatically reduced potency, and no compound superior to glyphosate was identified for inhibition of class I EPSPS enzymes[29, 42]. Further, while EPSPS is considered a promising target for the treatment of diseases caused by pathogenic bacteria or eukaryotic parasites[101, 102], glyphosate displays little antimicrobial activity[6, 16, 29]. Together, these findings demonstrate the need for entirely new inhibitors that target this agriculturally and medicinally significant enzyme.

Chpt. 5: Kinetic Effects and Structural Bases of Glyphosate Tolerance Resulting from Mutations at Pro101 of *E. coli* EPSPS

This work was included in: Healy-Fried M.L.; Funke T.; Priestman M.A.; Han H.; Schönbrunn E., Structural basis of glyphosate tolerance resulting from mutations of Pro101 in Escherichia coli 5-enolpyruvylshikimate-3-phosphate synthase. *J. Biol. Chem.* **2007**, 282, 32949-55.

Introduction:

Glyphosate exhibits broad-spectrum herbicidal activity, yet is essentially nontoxic to animals and does not persist in the environment[30, 31]. These characteristics have made it the world's most popular herbicide, and usage continues to increase with the adoption of glyphosate-utilizing technologies, such as herbicide-tolerant crops and minimal tillage (no-till) agriculture[40, 103]. The enormous reliance on glyphosate and the absence of suitably safe alternative herbicides mean that the widespread emergence of glyphosate-tolerant weeds could have devastating agricultural and environmental consequences[39, 41, 42].

EPSPS catalyzes the transfer of the enolpyruvyl moiety of PEP to the 5-hydroxy position of S3P (See Fig 1.3). Structures of the EPSPS•S3P•glyphosate complex show glyphosate bound to the PEP-binding site of EPSPS[21, 22, 24, 52], corroborating early kinetic data indicating that glyphosate inhibition is competitive with respect to PEP[11, 83]. Before bacterial enzymes with innate glyphosate tolerance (class II EPSPS) were discovered and used to produce *Roundup Ready* crops, scientists described

several mutations that decreased glyphosate sensitivity in the "plant-like" EPSPS from *Escherichia coli, Klebsiella pneumoniae,* and *Salmonella typhimurium*[29, 71, 75, 90, 104]. However, these mutant enzymes typically exhibited an increased K_m for PEP and a correspondingly decreased catalytic efficiency, indicative of decreased fitness in the absence of glyphosate, and were thus considered unsuitable for the development of commercial glyphosate-tolerant crops[29, 82].

Glyphosate-resistant organisms have developed both through natural evolution in situ and by directed evolution or mutagenesis in vitro, and glyphosate tolerance can be induced by either target-site or non-target-site mechanisms. Non-target-site tolerance mechanisms include overexpression of EPSPS[76, 87, 88] and decreased uptake or translocation of glyphosate[70, 84-86]. Target-site glyphosate tolerance can be induced by specific EPSPS point mutations including T42M[105]; G96A[43, 90, 104]; T97I[106, 107]; P101L, P101T, P101A, and P101S[71, 85, 86, 100, 108, 109]; and A183T[92, 110]; (all numbering according to *E. coli* EPSPS). Notably, field-evolved plants exhibiting target-site glyphosate tolerance invariably contain single-residue substitutions at the site corresponding to Pro101 of *E. coli* EPSPS.

Pro101 is not directly involved in glyphosate binding (see Fig. 5.1), and the basis for Pro101-mutation-induced glyphosate tolerance has remained unclear in the absence of further kinetic and structural characterization. To probe the effects of mutations at this site, a series of *E. coli* EPSPS mutant enzymes were produced with glycine, alanine, serine, or leucine substituted for Pro101. These mutant enzymes were analyzed by steady-state kinetics, and the crystal structures of the substrate binary and

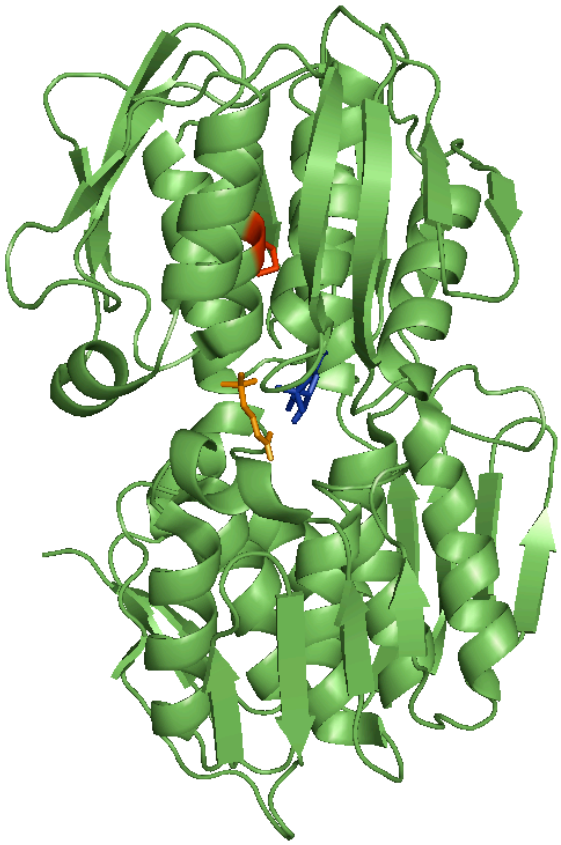

Fig 5.1: Global structure of *E. coli* EPSPS. Cartoon diagram shows the location of Pro101 (shown in red) relative to the location of S3P (blue) or glyphosate (orange).

substrate·glyphosate ternary complexes of P101S and P101L EPSPS were determined to between 1.5- and 1.6-Å resolution. The results indicate that any substitution at this site causes small but significant structural changes in the active site. The implications of our findings concerning the development and spread of glyphosate-resistant weeds are discussed.

Experimental Procedures:

Materials- Chemicals and reagents were purchased from Sigma (St. Louis, MO) unless otherwise noted. S3P was synthesized and purified as described previously[45]. The pET-24d vector (Novagen) containing the open reading frame of WT EPSPS from *E. coli* was used as a template for the mutations. Single-site Pro101 mutations were introduced by Martha Healy-Fried and Dr. Melanie Priestman using the QuikChange mutagenesis kit (Stratagene) and appropriate primers (MWG Biotech). Pro101 mutant EPSPS enzymes were over-expressed in BL21(DE3) competent cells (Invitrogen) and purified according to the general protocol previously described[43].

Steady-state kinetics- The enzymatic activities of WT and Pro101 mutant EPSPS enzymes were measured in 96-well microtiter plates by Todd Funke and Martha Healy-Fried at 25 °C using a colorimetric phosphate-release assay. Each 60 µl reaction mixture contained 50 mM HEPES (pH 7.5), 100 mM KCl, 2 mM dithiothreitol, and varied concentrations of S3P, PEP, or glyphosate, as indicated. The reactions were initiated by addition of enzyme (3.4 nM WT; 8.5 nM P101S, P101G, and P101A; or 34 nM P101L) and allowed to proceed for 30 minutes. The reactions

were stopped by addition of 140 μL malachite green phosphate indicator[47] and samples were incubated for ten minutes to allowed for color development. Change in absorbance at 650 nm was measured on a Spectra-Max 340PC plate reader, and product formation was determined by comparison to phosphate standards. The K_m and V_{max} values were determined by fitting the data to

Equation 1: $v = V_{max} * [S] / (K_m + [S])$

where v is the initial velocity, V_{max} is the maximum velocity, K_m is the Michaelis constant and $[S]$ is the concentration of the varied substrate. The K_i values for glyphosate inhibition were derived by determining the $K_{m(obs)}$ of PEP in the presence of increasing concentrations of glyphosate. The resulting data were fit to

Equation 2: $K_{m(obs)} = (K_m / K_i) * [I] + K_m$

where $K_{m(obs)}$ is the Michaelis constant for PEP in the presence of glyphosate, $[I]$ is the glyphosate concentration, and K_m is the Michaelis constant for PEP in the absence of glyphosate.

Crystallization and Structure determination- P101S and P101L EPSPS enzymes were crystallized using the standard protocol for *E. coli* EPSPS, as described[43], in the presence of 5 mM S3P, ± 5 mM glyphosate. X-ray diffraction data was collected according to standard procedures previously described. The collected data were reduced with XDS[48] or HKL2000[49]. Crystallography was performed as previously described (see General Protocol, Chpt. 1); data collection and refinement statistics table included in the publication[69].

Results and Discussion:

Four single-site mutations were introduced into *E. coli* EPSPS, replacing Pro101 with glycine, alanine, serine, or leucine, to examine the structural and function effects of Pro101 mutations.

Catalytic activity- All four mutant enzymes were catalytically active and were analyzed by steady-state kinetics. Enzyme activity asssayed as a function of substrate concentration (data not shown) showed normal saturation kinetics and the data obtained were fit to Equation 1 to derive the kinetic parameters listed in Table 5.1. In every case, the Pro101-mutations result in decreased catalytic activity. WT EPSPS is 6 times more active than P101L and over twice as active as P101S. P101A and P101G show the highest activity, about 60% that of WT EPSPS. Similarly, PEP binding is slightly decreased as a result of these mutations; the K_m PEP for P101S, P101A, and P101G is increased slightly compared to WT EPSPS, and P101L shows the most increase (K_m = 150 μM, compared to 60 μM for WT EPSPS). S3P binding appears little affected by these mutations; again, P101L show the most substantial change (K_m = 100 μM, compared to 60 μM for WT EPSPS). The catalytic efficiencies (k_{cat}/K_m) of the mutant enzymes are 2–10-fold lower than those of WT EPSPS, with P101L EPSPS having the lowest catalytic efficiency. Based on these data, it appears that residues smaller than leucine may be substituted for Pro101 without substantially altering the substrate affinity or catalytic activity of EPSPS.

Table 5.1. Summary of steady-state kinetic parameters.

EPSPS Enzyme	K_m S3P (µM)	Vmax (U/mg)	$k_{cat}/K_{m(S3P)}$ ($M^{-1}s^{-1}$)	K_m PEP (µM)	$k_{cat}/K_{m(PEP)}$ ($M^{-1}s^{-1}$)	K_i (µM)	$K_{m(PEP)}/K_i$
WT	60 ± 6	50 ± 1	6.4×10^5	60 ±6	6.4×10^5	0.4 ± 0.06	150
Pro101Ser	80 ± 6	22 ± 0.4	2.0×10^5	70 ± 5	2.9×10^5	5.5 ± 0.3	13
Pro101Gly	60 ± 10	28 ± 1	3.9×10^5	90 ± 10	2.4×10^5	12 ± 4	7.5
Pro101Ala	60 ± 4	31 ± 0.5	3.9×10^5	80 ± 5	2.8×10^5	19 ± 3	4.2
Pro101Leu	100 ± 7	8 ± 0.2	6.2×10^4	150 ± 20	4.1×10^4	66 ± 2	2.3

Inhibition by glyphosate- The glyphosate sensitivity of each enzyme was examined by K_i determination. Since glyphosate is a competitive inhibitor with respect to PEP, EPSPS activity as a function of PEP concentration was assayed in the presence of varied concentrations of glyphosate. The data were fit to Equation 1 to derive the $K_{m(obs)}$ PEP, and the $K_{m(obs)}$ PEP, plotted as a function of glyphosate concentration, was fit to Equation 2 to determine the K_i glyphosate for each enzyme, reported in Table 5.1. The substrate saturation plots and the data replots used for K_i determinations are shown in Fig. 5.2a-e. Unlike WT EPSPS, which is very sensitive to glyphosate (K_i = 0.4 μM), these mutant enzymes are 10–165-fold less sensitive. The most glyphosate-sensitive mutant enzyme is P101S (K_i = 5.5 μM) and the most glyphosate-tolerant mutant is P101L (K_i = 66 μM). The $K_{m(PEP)}/K_i$ ratio provides a measure of the selectivity of each enzyme, and indicates that P101L is the most discriminating of these mutants.

Summary of kinetic characterization: These data show that substitution of any of these residues for Pro101 decreased the binding affinity of glyphosate, reducing the potency of this inhibitor. Overall, the substitution of residues smaller than leucine for Pro101 results in a glyphosate-tolerant, catalytically efficient enzyme.

Crystallization- In WT EPSPS from *E. coli*, Pro101 is part of an internal helix (residues 97–105) in the N-terminal globular domain, ~ 9 Å distant from glyphosate (Fig. 5.1), so it is not obvious how glyphosate binding at the active site is affected by Pro101 mutations. To probe the specific effects, the binary (EPSPS•S3P) and ternary

Fig. 5.2a: WT *E. coli* EPSPS inhibition by glyphosate. (*Left*) PEP saturation curves in the presence of increasing concentrations of glyphosate: 0 (●), 0.16 (○), 0.31 (▲), 0.63 (Δ), 1.25 (■), 2.5 (□), 5 (▼), and 10 (∇) mM glyphosate. The concentration of S3P was 1 mM. Data were fit to the Equation 1. (*Right*) Replot of the observed K_m values as a function of glyphosate concentration. Data were fit to equation 2, yielding a K_i of 0.4 ± 0.06 μM.

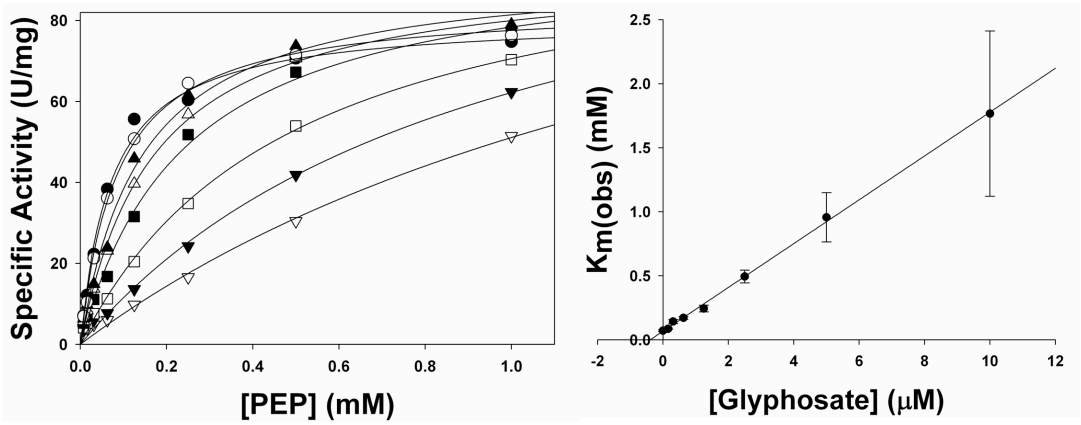

Fig. 5.2b: Pro101Ser *E. coli* EPSPS inhibition by glyphosate. (*Left*) PEP saturation curves in the presence of increasing concentrations of glyphosate: 0 (●), 0.31 (○), 0.63 (▲), 1.25 (Δ), 2.5 (■), 5 (□), 10 (▼), 53 (∇), and 106 (♦) μM glyphosate. The concentration of S3P was 1 mM. Data were fit to Equation. 1. (*Right*) Replot of the observed K_m values as a function of glyphosate concentration. Data were fit to equation 2, yielding a K_i of 5.5 ± 0.3 μM.

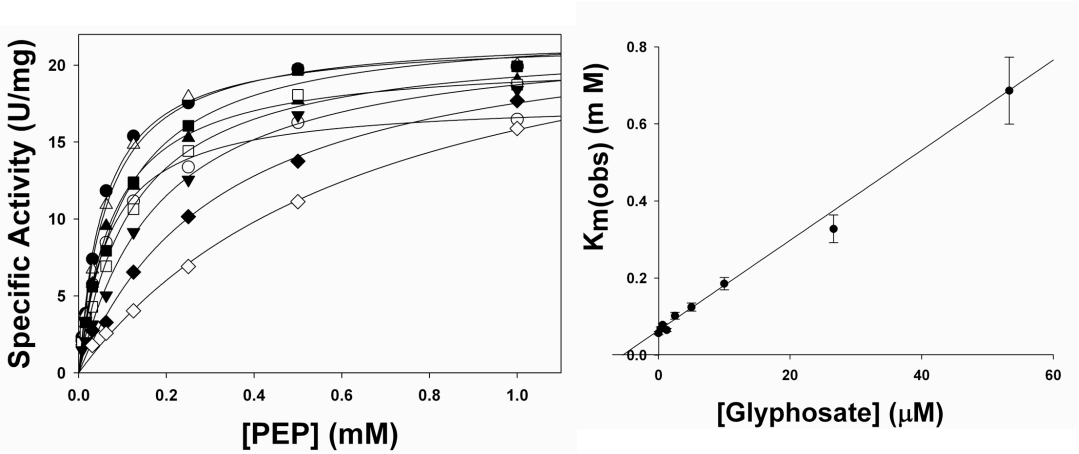

Fig. 5.2c: Pro101Leu *E. coli* EPSPS inhibition by glyphosate. (*Left*) PEP saturation curves in the presence of increasing concentrations of glyphosate: 0 (●), 0.31 (○), 0.63 (▲), 10 (Δ), 20 (■), 40 (□), 53 (▼), and 106 (∇) μM glyphosate. The concentration of S3P was 1 mM. Data were fit to Equation 1. (*Right*) Replot of the observed K_m values as a function of glyphosate concentration. Data were fit to Equation 2, yielding a K_i of 66 ± 2 μM.

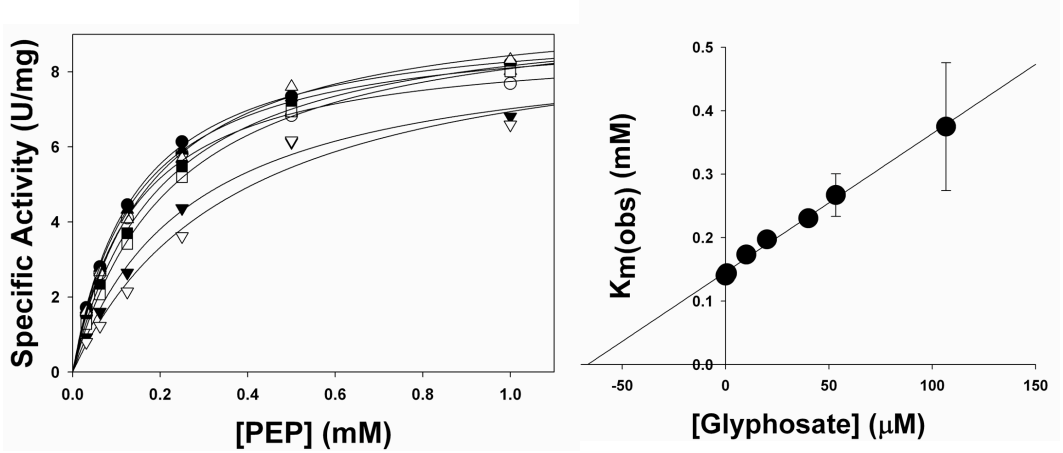

Fig. 5.2d: Pro101Ala *E. coli* EPSPS inhibition by glyphosate. (*Left*) PEP saturation curves in the presence of increasing concentrations of glyphosate: 0 (●), 0.07 (○), 0.13 (▲), 0.26 (Δ), 0.53 (■), 1.0 (□), 2.1 (▼), 4.2 (▽), 8.3 (♦), 16.6 (◊), 50 (●) and 200 (○) μM glyphosate. The concentration of S3P was 1 mM. Data were fit to Equation 1. (*Right*) Replot of the observed K_m values as a function of glyphosate concentration. Data were fit to Equation 2, yielding a K_i of 19 ± 3 μM.

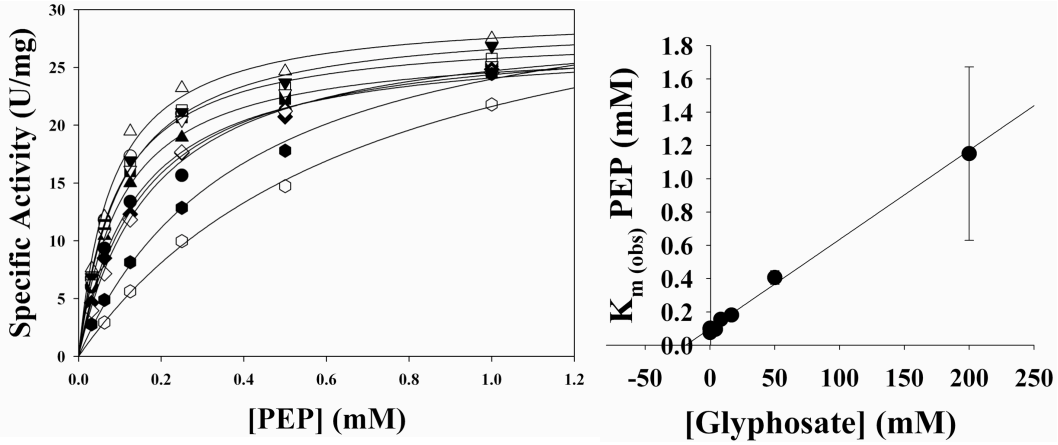

Fig. 5.2e: Pro101Gly *E. coli* EPSPS inhibition by glyphosate. (*Left*) PEP saturation curves in the presence of increasing concentrations of glyphosate: 0 (●), 0.13 (○), 0.26 (▲), 0.52 (Δ), 4.2 (■), 8.3 (□), 16.6 (▼), 33.3 (∇), 100 (♦), and 300 (◊) μM glyphosate. The concentration of S3P was 1 mM. Data were fit to equation 1. (*Right)*: Replot of the observed K_m values as a function of glyphosate concentration. Data were fit to equation 2, yielding a K_i of 12 ± 4 μM.

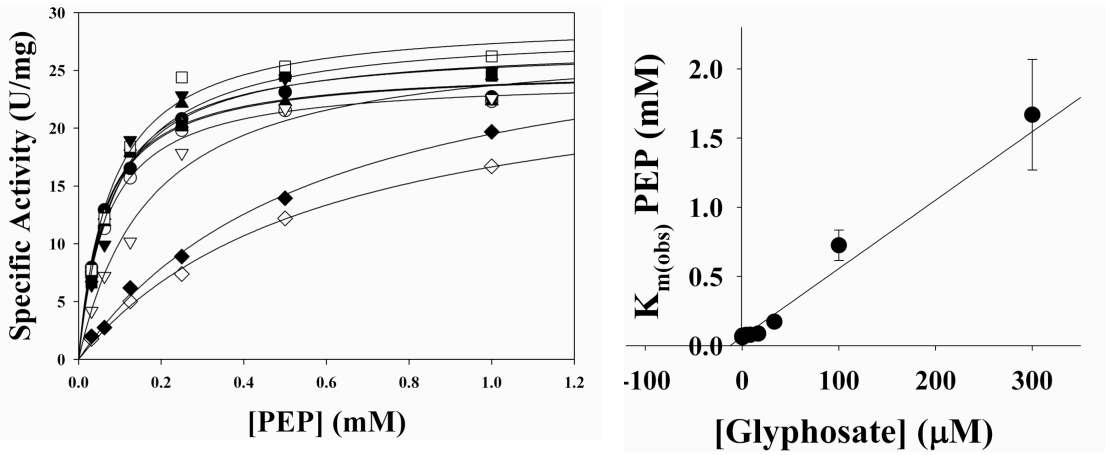

(EPSPS•S3P•glyphosate) complexes of P101S and P101L EPSPS were crystallized, and the structures were determined to between 1.5- and 1.6-Å resolution.

Structural analysis- The structures of the P101S and P101L mutant enzymes are nearly identical to that of WT EPSPS. To highlight the subtle changes induced by these mutations, the main chain atoms of the P101S and P101L EPSPS ternary complexes were compared to WT EPSPS. The root mean square deviation (rmsd), values are plotted in Fig. 5.3, with the inset showing rmsd values for residues 93-106 relative to the overall rmsd. The largest differences are observed in the backbone of Gly96, Thr97, and Ala98. Figs. 5.4 and 5.5 display this region (residues 95-102) with the increased r.m.s.d. The altered amino acids, Ser101 and Leu101, are shown modeled into the respective electron density from the $1F_o$ - $1F_c$ Fourier syntheses (Fig. 5.4). Fig. 5.5 displays the electron density from the $1F_{o(\mathrm{WT})}$ - $1F_{o(\mathrm{mutant})}$ Fourier syntheses. These $F_o - F_o$ maps show difference peak heights of 23σ and 18σ in the backbone around Thr97 for the P101S and P101L enzymes, respectively, suggesting that the Pro101 mutations affect glyphosate binding through a shift in the position of the active-site reside Thr97. Fig. 5.6 shows residues 96-102 with S3P and glyphosate bound to the active site. Based on the α-helix backbone trace, it appears that the mutation of Pro101 does not disrupt the secondary structure; instead, the mutation of Pro101 disrupts the side chain bonding patterns. The hydrophobic interactions between Pro101 and the carbonyl oxygen of Thr97 observed in the WT EPSPS are absent in the P101S and P101L structures, and the backbone of Thr97 reorients, shifting Gly96 and Thr97 slightly toward glyphosate. Glyphosate binding is sterically

Fig. 5.3: Structural differences between WT and mutant EPSPS. Shown is the rmsd comparison of the main chain atoms of WT EPSPS and the P101L (*solid line*) and P101S (*dotted line*) mutant enzymes complexed with S3P and glyphosate. The *inset* shows the rmsd values of residues 93–106 in multiples of the overall rmsd.

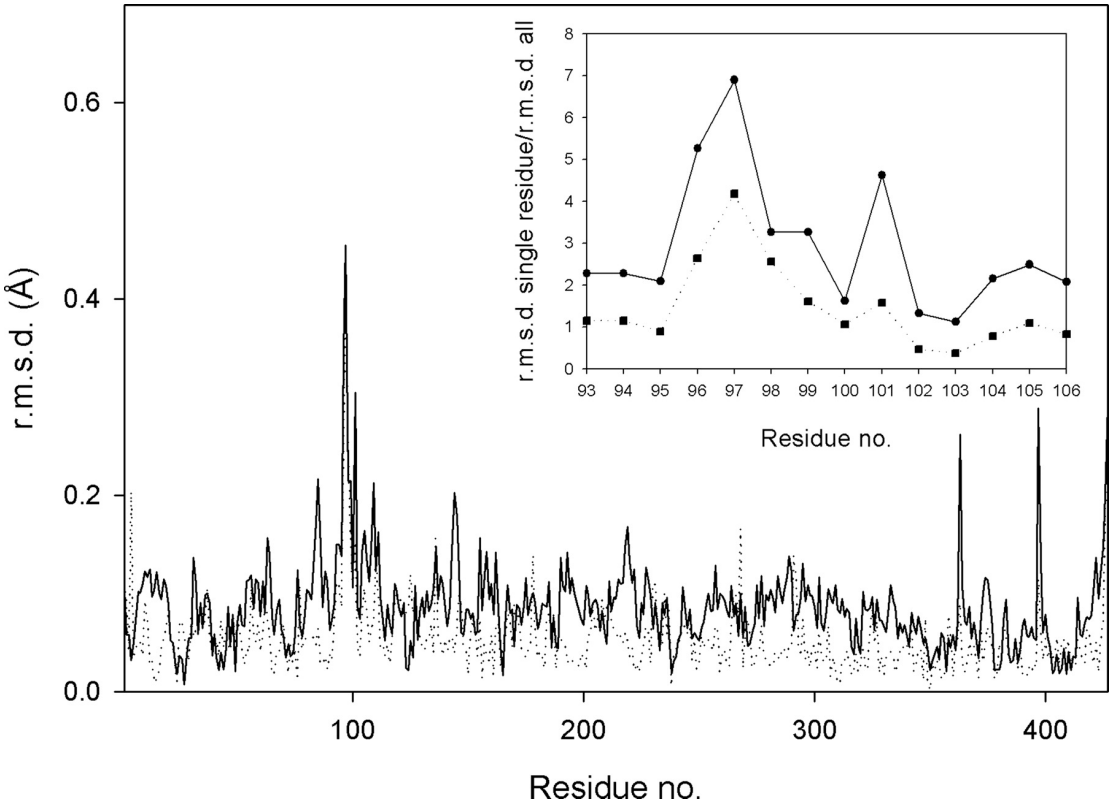

Fig. 5.4: F_o-F_c density map of P101S and P101L mutant EPSPS. Electron density (contoured at 3σ) derived from $1F_o$ - $1F_c$ Fourier syntheses, omitting residues 96–101 during refinement of the P101S enzyme (*left*) or the P101L enzyme (*right*). For clarity, only the density of Gly^{96}, Thr^{97}, and Ser^{101} is displayed.

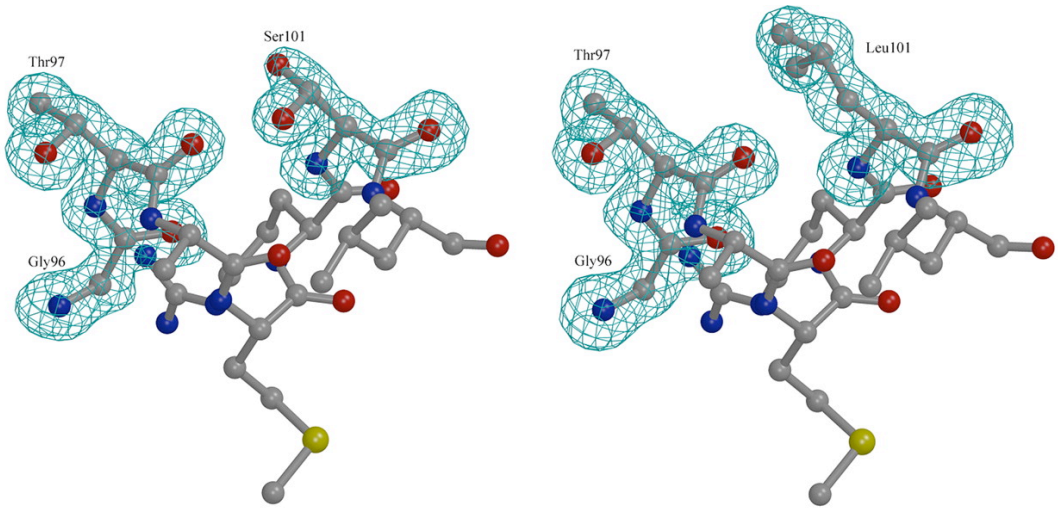

Fig. 5.5: F_o –F_o density map of P101S and P101L mutant EPSPS. Electron density (contoured at 4σ) derived from $1F_{o(WT)}$ - $1F_{o(mutant)}$ Fourier syntheses using the coordinates of P101S (*left*) or P101L (*right*) as reference. The highest peaks (of 23 and 18 sigma) correspond to the position of the carbonyl oxygen of Thr^{97} in WT EPSPS, which shifts substantially as a result of the mutation. The difference density to the right of Thr^{97} corresponds to the carbon atoms of the Pro^{101} ring.

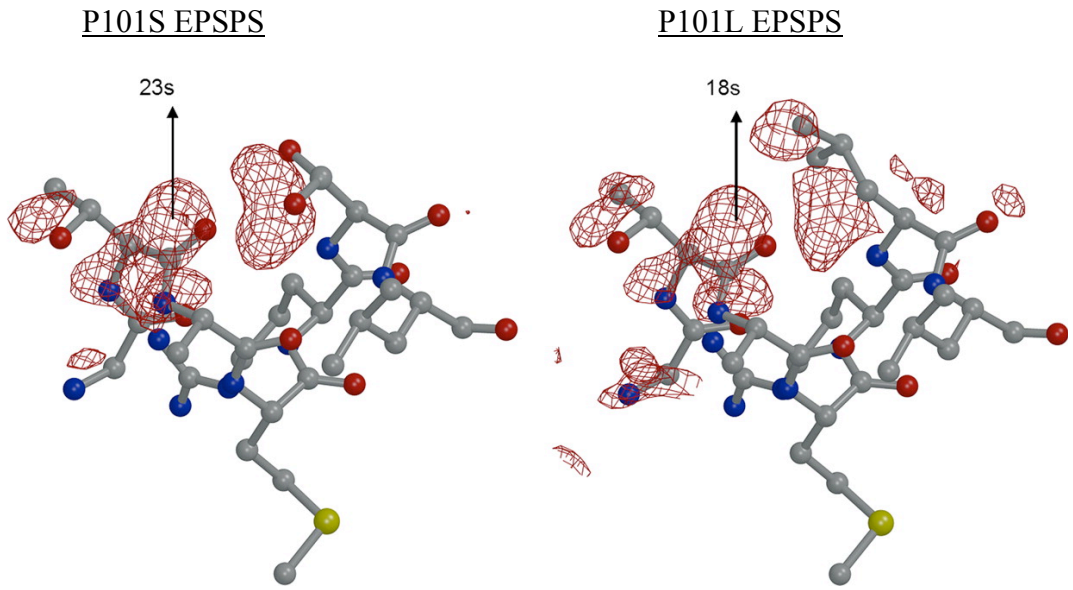

Fig. 5.6: Effects of Pro101 mutations on ternary *E. coli* EPSPS structure. Stereo view of E•S•I structures: Orange traces show backbone, green lines indicate hydrophobic interactions, black dashed lines mark hydrogen bonding, and red lines denote clash distances. (*Top*) WT EPSPS; (*Middle*) P101S mutant EPSPS; (*Bottom*) P101L mutant EPSPS.

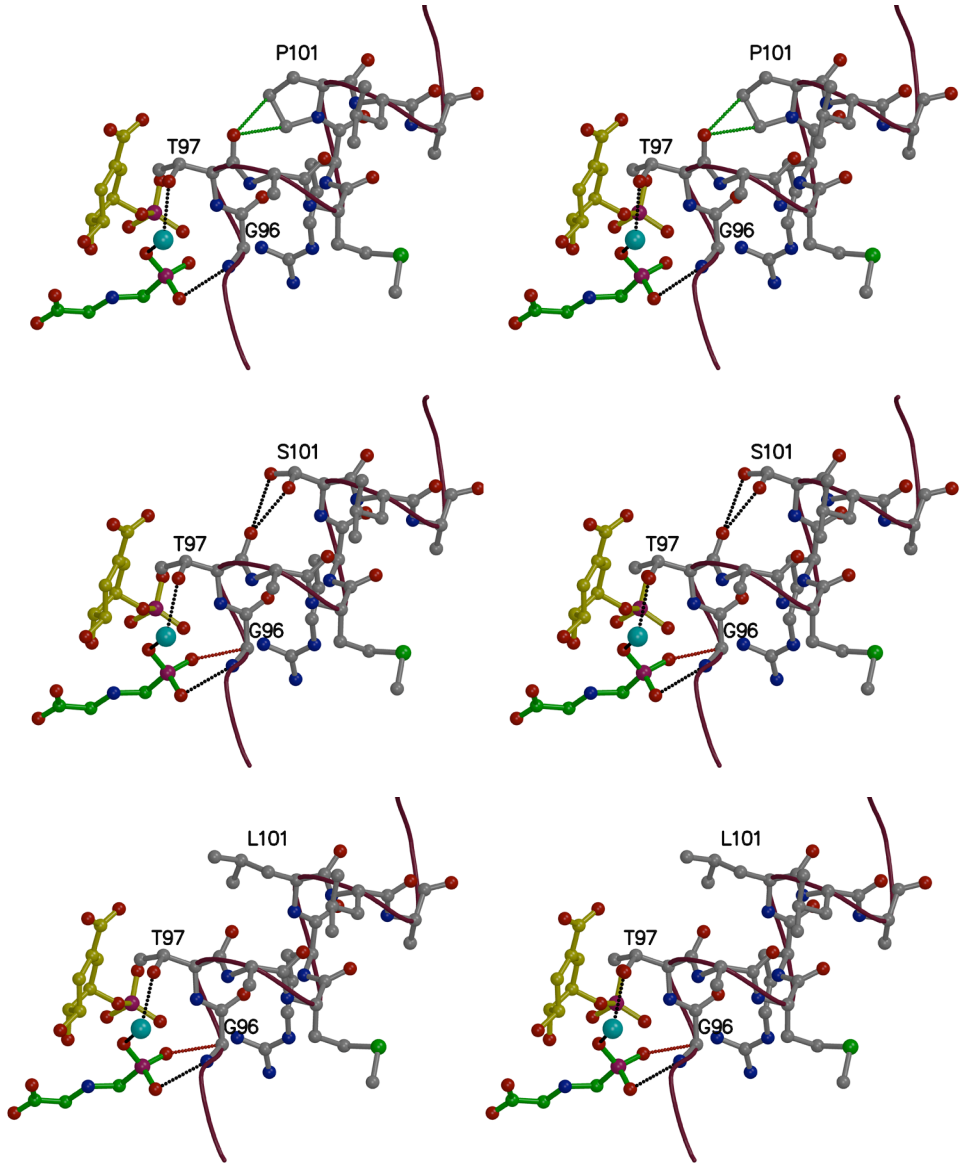

hindered by this narrowed glyphosate binding site. The subtlety of these effects results in retention of binding affinity for the (slightly shorter) PEP molecule. Together, these structural data indicate that the glyphosate tolerance of Pro101 mutant EPSPS enzymes results from long-range alteration of the spatial orientation of Gly96 and Thr97 in the active site of the mutant EPSPS enzymes.

Conclusions:

The removal of undesired plant species (weeds) to increase nutrient availability and crop yields is an intrinsic component of agriculture. The current enormous (and growing) reliance on glyphosate indicates that the development and spread of glyphosate-resistant weeds would have far-reaching negative consequences[39-42]. Glyphosate-tolerant mutant EPSPS enzymes typically show decreased fitness in the absence of glyphosate (decreased substrate binding and/or decreased catalytic activity). Mutations at sites corresponding to Pro101 appear to incur the least fitness cost, and because point mutations are far more evolutionarily accessible than multiple mutations, target-site glyphosate tolerance seems most likely to arise via mutations of this residue. With continued selective pressure from glyphosate application, the evolution of weedy plants expressing such enzymes appears inevitable. Our study indicates that the structural basis for the glyphosate tolerance of such Pro101 mutant EPSPS enzymes is due to long-range alterations in the active site of the enzyme, in particular impacting the spatial orientation of Gly96 and Thr97. It has long been known that Gly96 is critical for the efficient binding of glyphosate. For *E. coli* EPSPS, mutation of Gly96 to alanine results in a complete loss of inhibitory potency

because of the methyl group protruding into the glyphosate-binding site; however, this glyphosate tolerance comes at the expense of a drastically lowered affinity for PEP and poor catalytic efficiency[43]. In general, because the degree of glyphosate tolerance depends on the extent to which the inhibitor-binding site is perturbed and because the catalytic efficiency depends on the extent to which the substrate-binding site is left intact, it appears that the Pro101 substitution is favorable precisely because the changes in the enzyme active-site structure are so slight. Residues other than proline substituted at position 101 reduce glyphosate binding, while residues smaller than leucine at this position essentially do not alter the S3P- and PEP-binding sites, retaining catalytic efficiency.

To prevent the expected deterioration of the herbicidal properties of glyphosate, aggressive strategies for combating glyphosate-tolerant weeds should be implemented. Our data indicate that plants with these target-site mutations likely remain susceptible to glyphosate at high concentrations, but non-target-site mutations may act synergistically[70, 85, 109], drastically decreasing the effectiveness of glyphosate. On the basis of the extensive structure-activity relationship studies performed with glyphosate analogs[29] and the subtlety of the structural changes observed in glyphosate-tolerant enzymes, glyphosate analogs may not represent suitable replacements for glyphosate. Because plants with target-site glyphosate tolerance mutations remain susceptible to herbicides targeting enzymes other than EPSPS, herbicide rotation practices may delay the development and spread of glyphosate-tolerant weeds, and integrated weed management programs should be encouraged[111].

The engineering of crops with resistance to other herbicides, such as dicamba[112], holds some promise, but such crops are not yet commercially available, and glyphosate has unique advantages because of its very low toxicity to animals and its broad-spectrum activity against plants. In the long run, the development of completely new inhibitors of EPSPS or other shikimate pathway enzymes is desirable, as new nontoxic herbicides will be required.

Chpt. 6: Kinetic and Structural Analysis of Glyphosate Insensitive *E. coli* EPSPS T97I and T97I/P101S Mutant Enzymes

Manuscript in preparation

Introduction:

The safety and efficacy of glyphosate[10, 30, 31, 42], coupled with the existence of glyphosate resistant crop varieties[72, 91, 97], have made glyphosate the most-used herbicide in the world[73]. Glyphosate binds in the PEP-binding site of EPSPS[21, 22, 24], preventing catalysis of the enolpyruvyl transfer reaction (Fig. 6.1)[9]. EPSPS enzymes from different organisms have been divided into two classes according to intrinsic glyphosate sensitivity: in Class I enzymes, found in all plants and in bacteria such as *Escherichia coli* and *Salmonella typhimurium*, catalytic activity is inhibited at low micromolar concentrations of glyphosate[11, 29, 83]. Class II enzymes, found in bacterial species including *Staphylococcus aureus, Pseudomonas spp.,* and *Agrobacterium sp.* strain CP4, are distinguished by their ability to sustain efficient catalysis in the presence of glyphosate[29, 37, 45, 52, 72, 113].

Glyphosate insensitivity has been achieved in Class I EPSPS enzymes through natural selection, directed evolution and site-directed mutagenesis. As suggested by the fact that glyphosate and PEP bind to the same site, EPSPS mutants with substantially decreased affinity for the inhibitor glyphosate typically also exhibited decreased affinity for the substrate PEP[29, 43, 82]. Single-site mutations such as T42M[105], G96A[43, 90, 104] and P101S[69, 71, 75] were found to be advantageous but insufficient for commercial development of glyphosate tolerant crops. Multi-site mutations with more

favorable properties were sought and discovered, including *Petunia hybrida* EPSPS mutants G101A/G137D and G101A/P158S[82]; the *E. coli* EPSPS mutant G96A/A183T[92, 110] and the *Zea mays* EPSPS mutant TI02I/P106S[91, 107, 114]. The TI02I/P106S double mutant EPSPS (corresponding to T97I/P101S in *E. coli*; here abbreviated as TIPS EPSPS) had particularly favorable characteristics. The TIPS mutations were introduced into the endogenous EPSPS enzyme of *Z. mays* (field corn) to produce *Roundup Ready* corn (GA21 event[80, 115]), the first commercial varieties of glyphosate-resistant maize. The Class II EPSP synthase from *Agrobacterium sp.* strain CP4 was eventually utilized to create the transgenic glyphosate-resistant crops (such as *Roundup Ready 2* corn, NK603 event[72, 97]) that currently dominate the market.

We have utilized EPSPS from *E. coli* as a model to investigate the unique properties of TIPS EPSPS in parallel with the single site mutant T97I EPSPS. Both of these mutant enzymes exhibit glyphosate insensitivity, but also decreased catalytic activity compared to wild-type EPSPS. We consider the implications of our results concerning the development of glyphosate resistance in weeds or crops via these mutations.

Experimental Procedures:

Materials- Chemicals and reagents were purchased from Sigma (St. Louis, MO) unless otherwise noted. S3P was synthesized and purified according to standard methods as described previously[45]. The pET-24d vector (Novagen) containing the

open reading frame of EPSPS from *E. coli* was used as a template for the mutations. Single-site T97I mutations were introduced in the wild-type EPSPS and in the P101S mutant EPSPS from *E. coli* using the QuikChange II site-directed mutagenesis kit (Stratagene) and appropriate primers (MWG Biotech). The presence of the mutations was verified by DNA sequencing. The single-mutant T97I and double mutant TIPS EPSPS enzymes were overexpressed in BL21(DE3) competent cells (Novagen) and purified according to the standard methods previously described[43]. P101S and WT EPSPS enzymes were used as controls, and these kinetic constants were redetermined to facilitate direct comparisons.

Enzyme activity assays- The catalytic activities of WT, T97I, and TIPS EPSP synthases were measured at 25°C using a colorimetric phosphate-release assay. The 60 µl reactions were performed in 50 mM HEPES (pH 7.5), 2 mM DTT, with S3P, PEP and glyphosate concentrations varied as indicated. The reactions were initiated by addition of enzyme and allowed to proceed for 3 - 30 minutes. The reactions were stopped by addition of the malachite green phosphate indicator[47] and the samples were incubated for five minutes to allow for color development. Change in absorbance at 650 nm was measured on a Spectra-Max 340PC plate reader, and product formation was determined by comparison to inorganic phosphate standards. The K_m and V_{max} values were determined by fitting the data to

Equation 1: $v = V_{max} * [S] / (K_m + [S])$

where v is the initial velocity, V_{max} is the maximum velocity, K_m is the Michaelis constant and $[S]$ is the substrate (S3P or PEP) concentration. The IC_{50} values for

EPSPS inhibition were determined by fitting data to

Equation 2: $$v = V_{\min} + \frac{V_{\max} - V_{\min}}{1 + \left(\frac{[I]}{IC_{50}} \right)^{n}}$$

where v is the initial velocity, $V_{\max}$ is the maximum velocity, $V_{\min}$ is the minimum velocity, [I] is the inhibitor concentration and n is the Hill slope.

Crystallization and Structure determination- EPSPS enzymes were crystallized at 19°C by the hanging-drop vapor diffusion method in the presence of 5 mM S3P, with or without 5 mM glyphosate, using the standard sodium formate crystallization conditions described previously[43]. X-ray diffraction data were collected and structures were solved as previously described[69] (see also General Protocols, Chapter 1).

Results and Discussion:

The residues corresponding to 90 through 104 of *E. coli* are strictly conserved in representative species Class I EPSPS synthases (Fig. 6.1). Residues Pro101 and Thr97 are both part of an N-terminal helix (see Fig. 6.2), but only Thr97 is an active site residue. Both T97I and the TIPS mutant enzymes showed catalytic activity and increased glyphosate tolerance; their activity, inhibition, and structure were examined.

Enzyme activity- The results of substrate saturation experiments are shown in Fig. 6.3. The data from these studies were fit to Equation 1 to derive the K_m values shown

Fig. 6.1: Alignment of strictly conserved region of Class I EPSPS.

EPSPS Source	start **Amino Acid Residues** stop
Escherichia coli	90 **LFLGN AGTAM RPLAA** 104
Klebsiella pneumoniae	90 **LFLGN AGTAM RPLAA** 104
Salmonella typhimurium	90 **LFLGN AGTAM RPLAA** 104
Zea mays	95 **LFLGN AGTAM RPLTA** 109
Petunia hybrida	167 **LFLGN AGTAM RPLTA** 181

Fig. 6.2: Global structure of *E. coli* EPSPS. Position of residues Pro101 and Thr97 (shown red), relative to glyphosate (orange) and S3P (blue). Both residues are part of an internal, N-terminal helix. Thr97 (lower red reside) is an active site residue, while Pro101 (upper red residue) is ~9 Å distant from the active site.

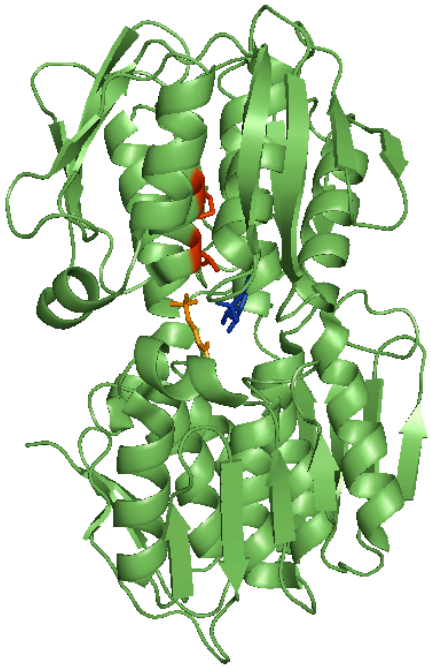

Fig. 6.3: Substrate K_m determinations. (*Top*) PEP saturation plot; (*Bottom*) S3P saturation plot. WT (●) P101S (○) T97I (▼) and TIPS (△) EPSPS. Data were fit to Equation 1 to derive kinetic parameters shown in Table 6.1.

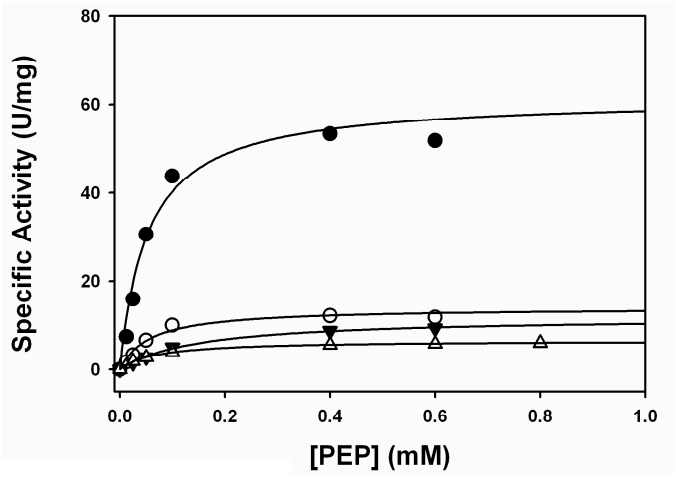

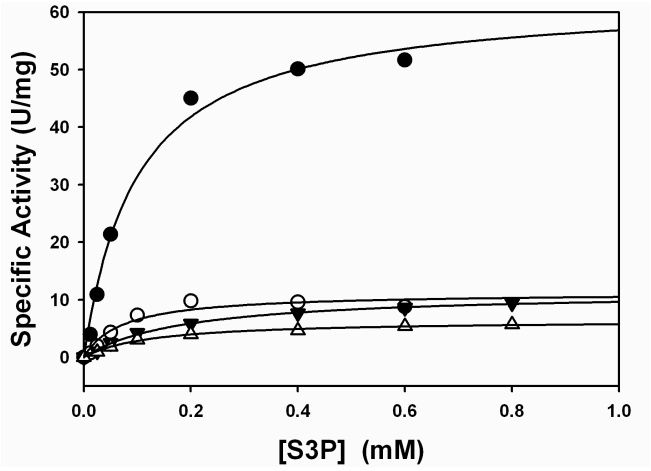

in Table 6.1. The WT EPSPS was clearly the most active enzyme, showing specific activity of over 60 U/mg. The activity of the single-site mutants T97I and P101S enzyme was decreased 5-fold compared to the WT enzyme, and the activity of TIPS EPSPS was decreased nearly 10-fold compared to WT EPSPS. Substrate binding affinity, assessed as the inverse of the K_m values, was maintained in the P101S and TIPS mutants, but the T97I mutant shows decreased catalytic efficiency due to increased K_m for both PEP and S3P.

Glyphosate inhibition- To assess the glyphosate sensitivity of these mutants, parallel IC_{50} experiments were performed (see Fig. 6.4) and these data were fit to Equation 2 to obtain the values listed in Table 6.1. All the mutant enzymes show decreased glyphosate sensitivity. P101S EPSPS (IC_{50} = 4.5 μM). exhibits only moderate glyphosate tolerance, with the IC_{50} of glyphosate increased by 7-fold compared to WT EPSPS (IC_{50} = 0.62 μM). The T97I glyphosate sensitivity is decreased by 3 orders of magnitude compared to WT EPSPS (IC_{50} = 620 μM), and the TIPS mutant is essentially insensitive to glyphosate (IC_{50} = 4500 μM).

T97I and TIPS EPSPS kinetic summary- The glyphosate tolerance exhibited by the TIPS enzyme is on the same order of magnitude observed for the class II EPSPS enzymes from *S. aureus* and CP4 EPSPS. However, the low specific activity of this enzyme suggests that it is not ideal for the development of glyphosate-resistant weeds or crops. To maintain levels of EPSPS activity *in planta*, any decrease in specific activity should be compensated by an increase in expression levels. Overexpression

Table 6.1: Comparison of steady-state kinetic parameters

E. coli EPSPS	K_m S3P (mM)	V_{max} S3P (U/mg)	K_m PEP (mM)	V_{max} PEP (U/mg)	Average K_{cat}/K_m (M^{-1} sec^{-1})	IC_{50} GLP (µM)
WT	**0.080 ± 0.02**	**61.1 ± 4**	**0.053 ± 0.01**	**61.6 ± 4**	**$7.1 * 10^6$**	**0.62 ± 0.05**
P101S	**0.070 ± 0.02**	**13.2 ± 0.7**	**0.057 ± 0.01**	**12.9 ± 0.8**	**$1.6 * 10^5$**	**4.5 ± 0.1**
T97I	**0.18 ± 0.01**	**11.4 ± 0.3**	**0.15 ± 0.01**	**11.8 ± 0.3**	**$5.4 * 10^4$**	**620 ± 50**
TIPS	**0.12 ± 0.01**	**6.46 ± 0.2**	**0.067 ± 0.003**	**6.50 ± 0.08**	**$5.3 * 10^4$**	**4500 ± 100**

Fig. 6.4: WT, P101S, T97I and TIPS EPSPS: glyphosate inhibition. IC_{50} comparison of WT EPSPS (●); P101S EPSPS (▲); T97I EPSPS (■); and TIPS EPSPS (◆). Data were fit to Equation 2 to derive the IC_{50} values displayed in Table 6.1.

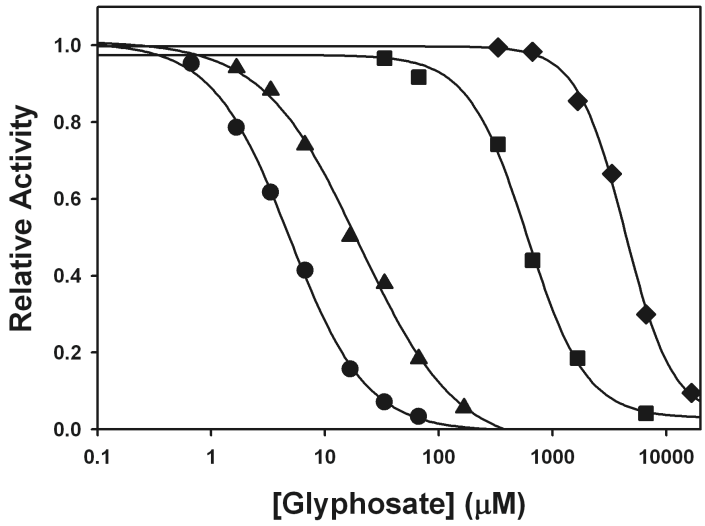

of even an unaltered EPSPS enzyme has resulted in glyphosate-resistance in a number of organisms[76, 88, 89, 116], but high-level, plastid-localized overexpression is reportedly difficult to achieve[82], and to maintain functioning of the shikimate pathway, these high expression levels would need to be maintained in all plant tissues, and even in the absence of glyphosate. Mutations of the residue corresponding to Pro101 of *E. coli* EPSPS have been reported in a number of field-evolved glyphosate resistant weeds[70, 100, 109]. Such a T97I mutation has never been observed in a naturally occurring plant population - in fact, BLAST analysis revealed this residue is strictly conserved - only EPSPS from *Chlaymydia* spp. were observed to contain an isoleucine at the equivalent position. The decreased catalytic efficiency of the T97I mutant EPSPS may explain why it has not been observed in glyphosate-resistant weeds. The moderate levels of glyphosate tolerance resulting from Pro101-mutations are often enhanced by synergistic, non-target-site glyphosate resistance mechanisms, such as decreased uptake and translocation of glyphosate[84, 86]; it may be that these mechanisms are more efficient that the high-level overexpression of a more glyphosate-tolerant enzyme with low catalytic efficiency.

Structural analysis- To better understand the effect of the T97I mutation and the mechanism by which subsequent mutation of P101S results in greater substrate affinity yet less glyphosate sensitivity, the T97I and TIPS mutant EPSPS enzymes were crystallized and the structures were compared to the those of WT EPSPS[1] and the single-site P101S[69] mutant. Figure 6.5 shows a stereoview of the active site architecture of T97I and TIPS EPSPS. The T97I mutation does not alter the backbone

Fig. 6.5: The glyphosate binding sites of TIPS and T97I EPSPS
(*Top stereofigure*) Glyphosate (shown in green) bound to T97I EPSPS reveal potential clashes between a phosphonate oxygen and the Cα atom of Gly96 (d=3.13 Å) and between a carbon atom of glyphosate and a carboxylate oxygen of Glu341 (d=2.93 Å) (red dotted lines).
(*Bottom stereofigure*) In TIPS EPSPS these clashes are more pronounced (Gly96: d=3.02 Å; Glu341: d=2.82 Å) and additional unfavorable interactions occur between glyphosate and S3P (d=3.02 Å) and between glyphosate's carboxylate and the Cδ atom of Arg386 (d=3.11 Å). S3P is shown in yellow. The helix between residues 97 to 101 is indicated in orange. Black dotted lines indicate polar interactions. The cyan spheres denote water molecules.

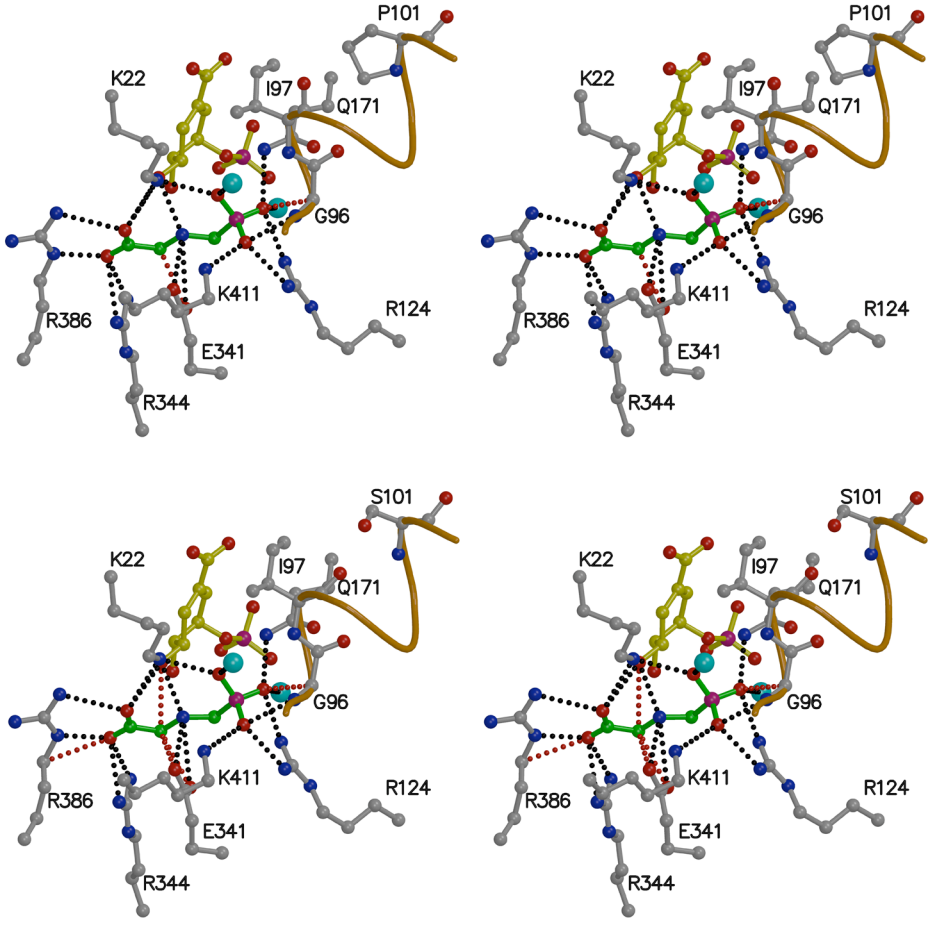

of the α-helix but disfavors glyphosate binding due to the shortened distance between the Cα of Gly96 and the phosphate oxygen of glyphosate, and between the carboxylate side chain of Glu341 and a carbon atom of glyphosate. The TIPS mutation produces more dramatic effects, further shortening the distances between Gly96 and glyphosate and Glu341 and glyphosate, and causing additional clashes between glyphosate and Arg386, and between glyphosate and S3P. It appears to be these steric effects that reduce the binding of glyphosate. To observe the change effected by T97I in more detail, Fig. 6.6 shows an overlay of the structures of the TIPS and the P101S EPSPS. In WT or P101S EPSPS enzymes, the side chain of T97I is hydrogen-bonded with the side chain of Asn26. Upon mutation (P101S), this residue shifts away from Asn26, resulting in a shift of Gly96 toward glyphosate. The S3P molecule is also shifted slightly downward in the TIPS mutant due to the hydrophobic side chain of Ile97. This shift causes a steric clash between glyphosate and the 5'-hydroxyl of S3P.

Structural comparison- Fig. 6.7, turned 90 degrees to the left from the previous structure, shows an overlay of the structures of the T97I and the TIPS EPSPS. In the T97I mutant, the Ile97 and Pro101 establish hydrophobic interactions and the location of the Ile97 side chain results in a slight shifting away of the S3P molecule, apparently causing the observed increase in the K_m of S3P; In the TIPS enzyme, the hydrogen bonding interactions between in Ser101 and the Ile97 shifts the Ile97 back away from the S3P molecule, restoring the S3P-binding site, while maintaining the altered position of Gly96, which distorts the glyphosate binding site. The binding of

Fig. 6.6: Effect of T97I mutation on the structure of EPSPS.
Displayed is an overlay of active-site residues and ligands (S3P and glyphosate) of P101S (orange) and TIPS (cyan). The side chain hydroxyl of Thr97 in P101S and WT EPSPS is in hydrogen bonding interaction with the side chain of Asn26 (white dotted line). The hydrophobicity of the Ile97 side chain results in a shift of this residue away from Asn26 (green dotted line); at the same time Gly96 shifts towards glyphosate and causes a steric clash with glyphosates phosphonate moiety (red dotted line). In addition, the side chain of Ile97 forces S3P to shift towards the glyphosate binding site (green dotted line), which gives rise to a potential steric clash between the target hydroxyl of S3P and one of glyphosate's carbon atoms (red dooted line).

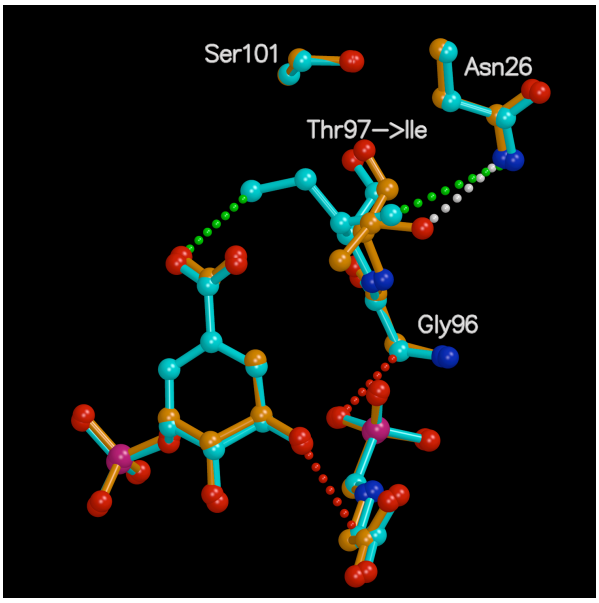

Fig. 6.7: Effect of P101S mutation on the structure of T97I EPSPS.
Displayed is an overlay of active-site residues and ligands (S3P and glyphosate) of T97I (orange) and TIPS EPSPS (cyan). The Pro101 ring in the T97I enzyme exerts hydrophobic forces on the carbonyl oxygen of Ile97; the Ile97 side chain comes close to the S3P carboxylate causing the S3P molecule to shift away (green dotted lines). In the TIPS enzyme, the Ile97 carbonyl oxygen establishes a hydrogen bond with the Ser101 side chain, which causes the Ile97 side chain to shift away from S3P. These effects may explain the difference in binding of S3P to both enzymes as indicated by the different Km values. In both mutant enzymes Gly96 shifts slightly towards the glyphosate binding site resulting in clash distances (red dotted line) towards the phosphonate moiety of glyphosate.

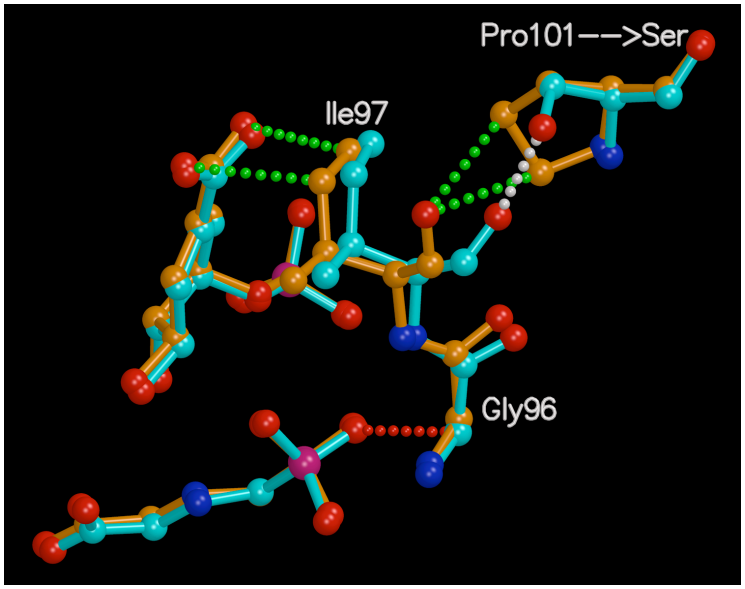

the shorter PEP molecule (which binds in the same site as glyphosate) is apparently not affected by the very slight shift of Gly96.

Inhibition by TI analogs- The TIPS EPSPS is very insensitive to glyphosate. We hypothesized that analogs of the tetrahedral reaction intermediate (TI analogs), previously described as potent inhibitors of WT *E. coli* EPSPS[26, 28, 62, 117] (See also chapter 8), would still act as potent inhibitors of this mutant enzyme due to their more global coverage of the active site and the maintained substrate binding affinity of TIPS EPSPS. Fig. 6.8 shows the inhibition of TIPS EPSPS and WT EPSPS by the (*R*)-difluoro-TI analog (2F-TI), the (*R*)-phosphonate-TI analog (RP-TI), and the (*S*)-phosphonate-TI analog (SP-TI). Since these TI analogs are quite potent and are competitive inhibitors with respect to S3P, all reactions utilized equal amounts of enzyme (the greater specific activity of WT EPSPS was compensated for with shorter reaction times), with concentrations of S3P corresponding to the K_m, in the presence of saturating concentrations of PEP. As hypothesized, the TIPS and WT EPSPS enzymes show nearly equal sensitivity to these inhibitors, with the greatest difference the almost 2-fold increased tolerance of TIPS toward 2F-TI. These data support our hypothesis that inhibitors with more global coverage of the active site are not as affected by these mutations.

Conclusions:

T97I and TIPS EPSPS from *E. coli* were produced and analyzed structurally and kinetically and compared to the WT and P101S EPSPS enzymes to isolate the effect

Fig. 6.8: Inhibition of TIPS by the tetrahedral intermediate analogs

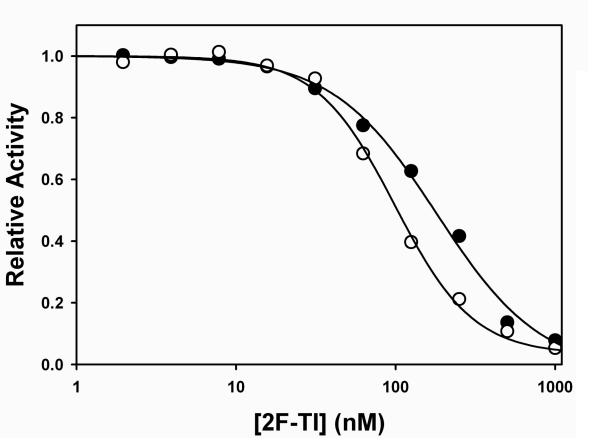

(*Top*) 2F-TI inhibition
IC_{50} TIPS (●) = 180 nM
IC_{50} WT EPSPS (○) = 99 nM

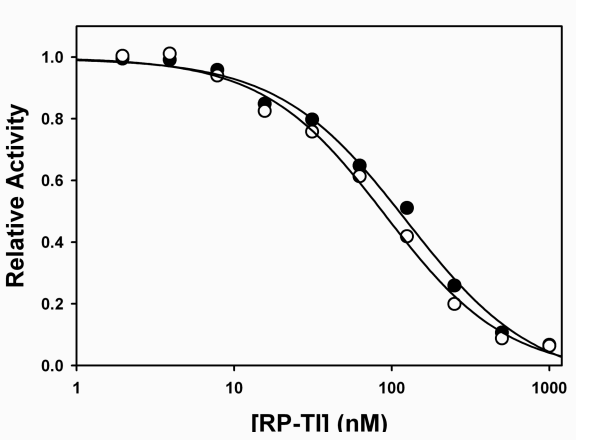

(*Center*) RP-TI inhibition
IC_{50} TIPS (●) = 120 nm
IC_{50} WT EPSPS (○) = 91 nm

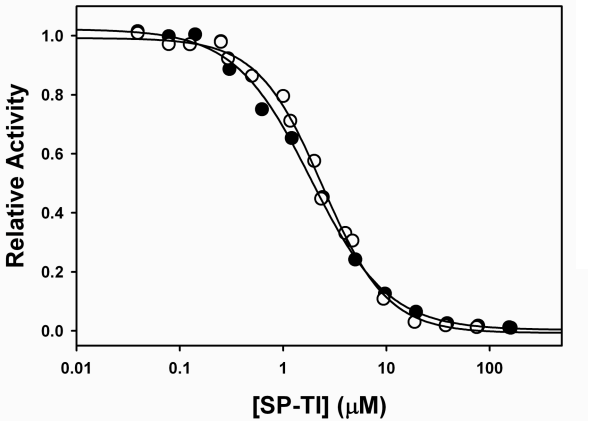

(*Bottom*) SP-TI inhibition
IC_{50} TIPS (●) = 1.9 μM
IC_{50} WT EPSPS (○) = 2.4 μM

of each mutation. The TIPS EPSPS enzyme shows high levels of glyphosate tolerance while maintaining affinity for its substrates, PEP and S3P. The single site T97I mutation is also glyphosate insensitive, but, in the absence of the compensating P101S mutation, exhibits decreased affinity for PEP and S3P. These phenomena can be attributed to specific structural features in the active site. Less clear is the molecular basis for the decreased catalytic activity observed in these mutant enzymes. It appears that substrate binding is not the rate-limiting step, at least for the P101S and TIPS EPSPS enzymes. It may be the case that mutation of these residues somehow affects the rate or induction of the open-closed transition. Further experiments may reveal the details of this effect, but for now it seems unlikely that plants exhibiting these mutations with be successful on a large scale due to the decreased catalytic activity. Overall, the structures illustrate how the mutations produce glyphosate tolerant enzymes but the kinetics illuminate why they are not optimal for the production of glyphosate resistant organisms. Our results also indicated that resistance to substrate analogs may occur more readily than the development of resistance toward TI analogs. Such phenomena should be taken into account in the design of second-generation EPSPS inhibitors.

Chpt. 7: High Throughput Screening for Inhibitors of E. coli EPSPS: Identification of Diverse and Novel Chemical Scaffolds

(*unpublished*)

Introduction:

The enzymes of the shikimate pathway represent attractive drug targets[2, 14, 20, 27, 29, 101, 102]. EPSPS is well known as the target of glyphosate, but this inhibitor has little antimicrobial activity. All EPSPS inhibitors described are analogs of substrate, product, tetrahedral reaction intermediate, or glyphosate (itself analogous to PEP)[14, 26, 27, 29, 60, 118-121], and of these, only a few fluorinated analogs of shikimate have shown potent antimicrobial activity[101, 122]. Identification of additional inhibitors could lead to the development of novel antibiotic drugs[27, 102].

High Throughput Screening (HTS) can facilitate identification of inhibitors by rapidly assaying a chemical library of compounds for activity against a given drug target. We conducted HTS using *E. coli* EPSPS with the goal of identifying novel chemical scaffolds of EPSPS inhibitors; since crystallization conditions are known for *E. coli* EPSPS, co-crystal structures can potentially be obtained with these compounds to aid in structure-based lead optimization.

Experimental Procedures:

Materials- The screen was conducted at the University of Kansas High Throughput Screening Laboratory, using the in-house compound collection composed of 45,000 compounds from the *ChemBridge* library, 56,000 compounds from the *ChemDiv*

library, and 880 compounds from the *Prestwick* library. Training, assistance, and collaboration were provided by Dr. Veena Vasandani. *E. coli* EPSPS and S3P were produced according to the standard methods previously described. We utilized the malachite green reagent previously described to detect the production of inorganic phosphate.

Activity assay and primary screening- The cuvette-based phosphate-release activity assays previously utilized were down-scaled and the screen was conducted in a manner similar to the previously performed HTS for MurA inhibitors (Huijong Han, *unpublished*, and Dr. Melanie Priestman, *unpublished*). The assay was performed in 384-well microtiter plates having a maximum volume of 100 µl per well. Prior to the primary screen, 20 µl of each compound to be screened was added to the testing plates. In the primary screen, all compounds were dissolved in 2.5 % DMSO, and the concentration of all compounds was 25 mg/ml. Next, 20 µl of *E. coli* EPSPS, at 0.45 µg/ml (in 50 mM Na-HEPES pH 7.5, 50 mM KCl, and 2 mM DTT) was added to each well using a multidropper apparatus. The reaction was started by addition of 20 µl of a substrate mixture containing 600 µM PEP and 300 µM S3P (in 50 mM Na-HEPES pH 7.5, 50 mM KCl, and 2 mM DTT), again using a multidropper apparatus. The testing plates were centrifuged briefly to ensure that each sample was mixed. Two columns on each plate contained no compound; to one column (18 wells), no inhibitor was added (volume replaced by 2.5% DMSO); to the other column (18 wells), 0.1 mM glyphosate was added (in 2.5% DMSO); these rows served as controls to monitor the assay. In each case, the assay volume was 60 µl, and contained: testing

compound, at 8.3 mg/ml; *E. coli* EPSPS, at 0.15 μg/mL; PEP, at 200 μM; and S3P, at 100 μM; the buffer for the reaction contained 33.3 mM Na-HEPES pH 7.5, 33.3 mM KCl, 1.33 mM DTT, and 0.83% DMSO. After addition of the substrate, the reactions were allowed to proceed for 30 minutes at room temperature. The assays were stopped by the addition of 40 μl of the malachite green reagent, 10 minutes was allowed for color development (no sodium citrate was used) and the absorbance at 650 nm was measured on a SpectraMax 340C plate reader. Every 2 hours, fresh substrate and enzyme stock solutions were remade to limit the effects of PEP hydrolysis (which can result in false negatives) or enzyme denaturation (which can result in false positives).

Secondary screening- The data from the primary screen were analyzed by Dr. Vasandani. Secondary screening, consisting of automated IC_{50} determination, was carried out for all compounds that showed greater than 40% inhibition of *E. coli* EPSPS – this corresponded to 83 samples, less than 1 out of every 1,000 compounds tested. These compounds were hit-picked from the daughter plates and 12 concentrations of 2-fold dilutions were prepared in 2.5% DMSO. The highest inhibitor concentration in each case was 16.7 mg/ml. Enzyme and substrate was added to each dilution of each inhibitor using a multidropper apparatus, the microtiter plates were centrifuged to ensure mixing of the reactants, and enzyme reactions were allowed to proceed 30 minutes at room temperature, all as previously described. The reactions were stopped by the addition of 40 μl of the malachite green reagent and the absorbance at 650 nm was measured after 10 minutes.

Results:

According to the automated IC_{50} determination, only 28 of the samples had IC50 values of lower than 10 μM; of these, 18 of the most potent were selected as the lead compounds for further study. The vendor, vendor identification number, IC_{50} values determined in the secondary screening, and the in-house abbreviated name of these lead compounds are listed in Table 7.1, along with the chemical structures of these inhibitors (Fig. 7.1-3). Dry compounds were ordered from the supplier listed, stock solutions were resuspended in DMSO, and these compounds were subjected to in-house hit verification and co-crystallization trials. Hit verification and co-crystallization trials with these compounds are still underway.

Conclusions:

The lead compounds selected for further testing had IC_{50} values between 10.2 and 2.4 μM. The molecular weights were between 222 and 432 g/M. These compounds appear significantly larger than glyphosate and it seems unlikely that they bind in the PEP-binding site, like glyphosate. The mode of action of these inhibitors is still unknown, and they may inhibit the open-closed transition of EPSPS. Alternatively, the six-carbon ring moieties could mimic S3P-binding, resulting in formation of a "dead-end" complex. Co-crystallization and K_i determination will be helpful in determining the basis for EPSPS inhibition by these compounds.

Using the standard cuvette-based assay, the *E. coli* EPSPS stock utilized here was previously determined to have specific activity of 40 U/mg; K_m S3P = 150 μM; K_m

Table 7.1: Inhibitors of *E. coli* EPSPS identified by HTS. The IC_{50} values listed correspond to those obtained in the secondary screen in the KU HTS laboratory. The abbreviated identification numbers were used to identify the compounds ordered from the suppliers, and roughly corresponds to the molecular weights.

Vendor	Vendor ID #	IC_{50} (uM)	Abbr. ID:	Structure
ChemBridge	5140900	6.8	396	Fig. 7.1
ChemBridge	5180253	7.2	230	Fig. 7.1
ChemBridge	5222121	2.3	322	Fig. 7.1
ChemBridge	5457980	10.2	241	Fig. 7.1
ChemBridge	5465249	6.7	336	Fig. 7.1
ChemBridge	5552585	7.2	428	Fig. 7.1
ChemBridge	5651052	4.5	433	Fig. 7.2
ChemBridge	6003431	2.4	222	Fig. 7.2
ChemBridge	6520475	5.0	351	Fig. 7.2
ChemBridge	6540479	4.5	298	Fig. 7.2
ChemBridge	6648723	9.0	317	Fig. 7.2
ChemBridge	6696755	3.8	345	Fig. 7.2
ChemDiv	0263-0421	6.5	432	Fig. 7.3
ChemDiv	2389-1031	3.1	429	Fig. 7.3
ChemDiv	3976-0242	4.4	304	Fig. 7.3
ChemDiv	4361-0397	4.2	325	Fig. 7.3
ChemDiv	4456-2362	5.6	326	Fig. 7.3
ChemDiv	5863-2113	3.6	306	Fig. 7.3

Fig. 7.1: Structures of *E. coli* EPSPS inhibitors identified by HTS:

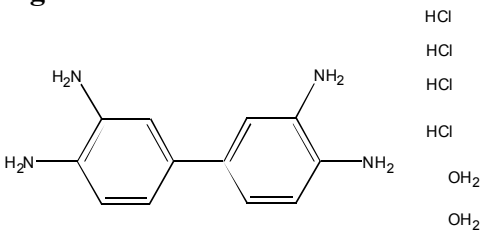

Abbr. ID

396

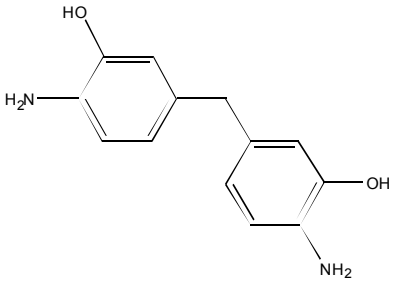

230

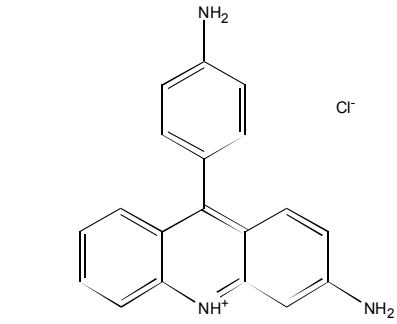

322

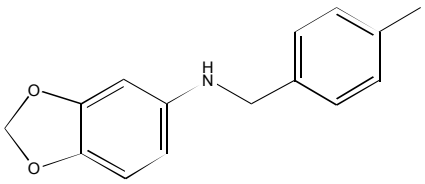

241

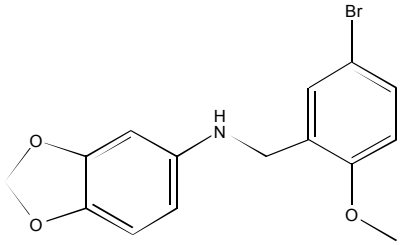

336

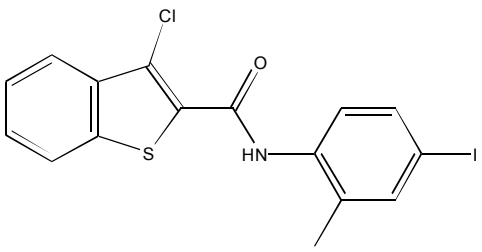

428

Fig. 7.2: Structures of *E. coli* EPSPS inhibitors identified by HTS:

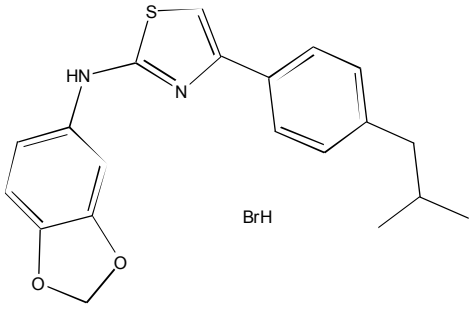

Abbr. ID

433

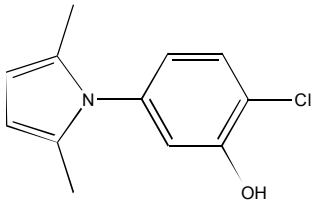

222

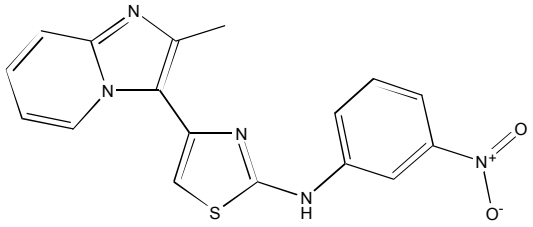

351

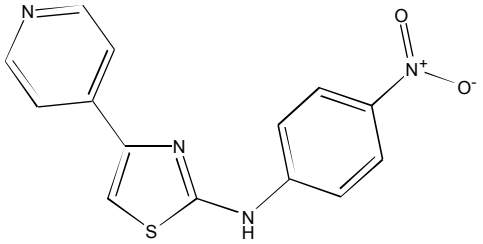

298

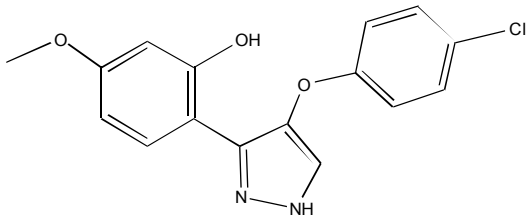

317

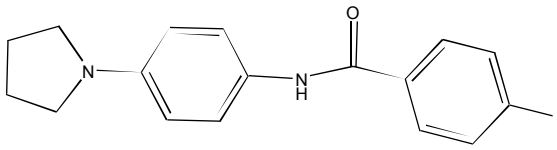

345

Fig. 7.3: Structures of *E. coli* EPSPS inhibitors identified by HTS:

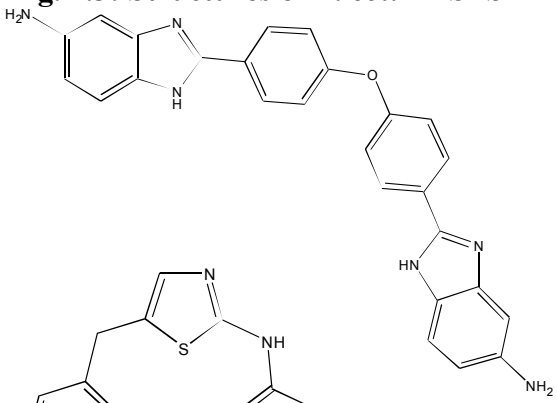

Abbr. ID

432

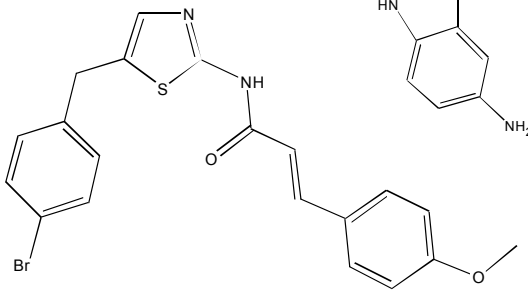

429

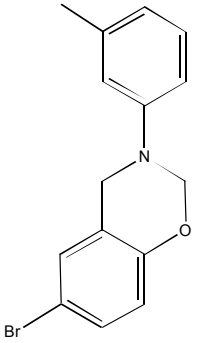

304

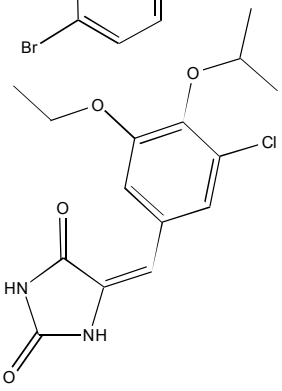

325

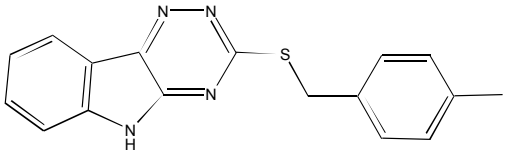

326

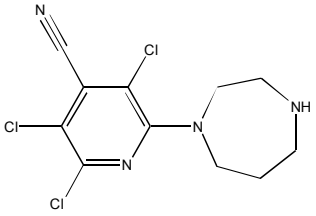

306

PEP = 150 μM; and IC_{50} glyphosate = 1 μM. Subsequent 96-well microtiter kinetic analyses revealed that the K_m values observed in the plate-based assay are lower than those estimated by the cuvette-based experiment. In the plate-based assay, the K_m S3P and the K_m PEP are both approximately 50 μM[69]. These data suggest that for greater sensitivity to competitive inhibitors, future HTS with this enzyme should utilized less substrate, with more enzyme added if necessary to achieve sufficient signal.

Small amounts of DMSO appear to prevent the crystallization of *E. coli* EPSPS. The development of alternate enzyme crystallization conditions (or the utilization of alternate enzymes - see chapter 8) may be useful for future screens. In particular, due to the global induced fit mechanism of EPSPS[21-23, 52], it would be useful to utilize an enzyme with reproducible "open"- and "closed"-form crystallization conditions.

These experiments proved useful as the conceptual basis of utilization of microtiter plate-based assays for the determination of IC_{50}, K_m, and particularly K_i values, which were employed variously in Chapters 5[69], 6, 8[62], and 9.

Chpt. 8: Differential Inhibition of E. coli, S. aureus and CP4 EPSPS Enzymes by Analogs of the Tetrahedral Reaction Intermediate

This work was included in: Funke T.; Healy-Fried M.L.; Han H.; Alberg D.G.; Bartlett P.A.; and Schonbrunn E., Differential Inhibition of Class I and Class II 5-Enolpyruvylshikimate-3-phosphate Synthases by Tetrahedral Reaction Intermediate Analogues. *Biochemistry* **2007**, 46, 13344-51.

Introduction:

While glyphosate has proven to be a potent inhibitor of EPSPS from plants and *Escherichia coli*, several glyphosate-tolerant forms of EPSPS have been identified[43, 45, 71, 75, 104]. EPSPS with intrinsic glyphosate insensitivity were isolated from organisms including *S. aureus*, *S. pneumoniae*, *Pseudomonas* sp. strain PG2982, and *Agrobacterium* sp. strain CP4[29, 52, 72, 113]. These glyphosate tolerant enzymes are termed class II enzymes, while glyphosate sensitive plant and *E. coli* enzymes are considered prototypical class I EPSPS enzymes. A search of the literature reveals little concerning inhibition of class II EPSPS, and concerted efforts to identify novel EPSPS inhibitors have relied exclusively on class I enzymes[26, 29]. Intensive efforts to find a molecule better than glyphosate at inhibiting class I EPSPS largely failed; only a few analogues of the TI have been identified as more potent inhibitors (Fig. 8.1)[26, 27, 29, 117]. Glyphosate itself has poor antimicrobial properties; detailed inhibition and structural data concerning are desired for non-glyphosate-based compounds to aid in the design and development of novel EPSPS inhibitors with potential antimicrobial activity.

Fig. 8.1: The TI analogs used in this study.

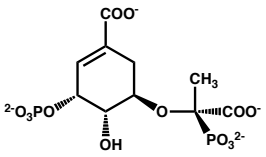

(*S*)-phosphonate TI-analog
SP-TI

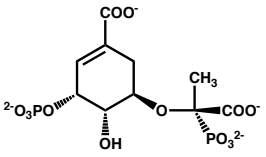

(*R*)-phosphonate TI-analog
RP-TI

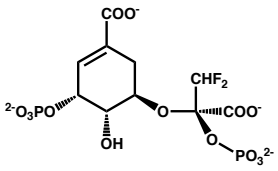

(*R*)-difluoromethyl TI-analog
2F-TI

Crystallographic and chemical studies using *E. coli* EPSPS demonstrated that the addition-elimination reaction catalyzed by EPSPS proceeds through an (*S*)-configured tetrahedral reaction intermediate (TI) (See Fig. 1.7)[24, 25]. The most potent of the synthetic TI analogs, the (*R*)-difluoromethyl TI analog (2F-TI) and the (*R*)-phosphonate TI analog (RP-TI), inhibit EPSPS at nanomolar-range concentrations[26, 28].

Previously, the structure of *E. coli* EPSPS was examined in complex with RP-TI and the (*S*)-phosphonate TI analog (SP-TI) to explain the molecular basis for the much higher potency of RP-TI compared to SP-TI (which reflects the stereochemistry of the genuine TI). To further examine inhibition by these TI analogs, and to probe inhibition of the Class II EPSPS, here we investigated the molecular modes of action of RP-TI, SP-TI, and 2F-TI using representative class II EPSPS enzymes from *S. aureus* and *Agrobacterium* sp. strain CP4 in parallel with the prototypic class I EPSPS from *E. coli*. Our kinetic data indicate that class II EPSPS are generally less susceptible to inhibition by these TI analogues. We determined the crystal structures of the *E. coli* EPSPS in complex with 2F-TI and the CP4 EPSPS in complex with 2F-TI and RP-TI to understand the structural basis for the inhibition data.

Experimental Procedures:

Materials- Chemicals and reagents were purchased from Sigma (St. Louis, MO) unless otherwise noted. S3P was synthesized and purified as described previously[45]. The stable TI analogs (2F-TI, RP-TI, and SP-TI) were provided by Dr. Paul Bartlett.

E. coli EPSPS[43], *Agrobacterium sp.* strain CP4 EPSPS[52], and *S. aureus* EPSPS[45] enzymes were overexpressed and purified as previously described.

Enzyme activity assays- Colorimetric enzyme activity assays were conducted by Todd Funke and Martha Healy-Fried at 25 °C in using 96-well microtiter plates. The reactions, performed in 60 µL of 50 mM Na-HEPES, pH 7.5, 100 mM KCl, and 2 mM DTT, were started by the addition of enzyme (final concentration of the EPSPS was 1.4 nM for E. coli, 3.2 nM for both the wild-type CP4 and the Ala100Gly CP4, and 13 nM for S. aureus), and stopped by addition of 140 µl of the malachite green phosphate indicator[47] after 20 min (S. aureus EPSPS) or 30 min (E. coli, wild-type CP4, and Ala100Gly CP4 EPSPS). Samples were incubated for ten minutes to allow for color development, change in absorbance at 650 nm was measured on a Spectra-Max 340PC plate reader, and product formation was determined by comparison to phosphate standards. Enzymatic activities at increasing S3P and varied inhibitor concentrations were recorded, and the data were fit to

Equation 1: $v = V_{max} * [S] / (K_m + [S])$

K_i values for 2F-TI, RP-TI, and SP-TI were determined by linear regression of the replot of the $K_{m(obs)}$ values versus the concentration of the inhibitor [*I*], according to

Equation 2: $K_{m(obs)} = (K_m / K_i) * [I] + K_m$

where $K_{m(obs)}$ is the observed Michaelis constant in the presence of inhibitor, K_m is the true Michaelis constant, and K_i is the inhibition constant. To ensure that the results were directly comparable, the kinetic constants previously determined for *E. coli* EPSPS inhibition by RP-TI and SP-TI were redetermined using the plate-based assay.

Protein concentrations were determined on a Spectra-Max 340PC plate reader (Molecular Devices, Sunnyvale, CA) using Pierce (Rockford, IL) coomassie reagent with bovine serum albumin as a standard.

Crystallization- CP4 EPSPS crystals and *E. coli* EPSPS crystals were grown as previously described (see Chapter 4 Experimental Procedures, and Chapter 1 General Protocols)[43, 52]. The structures were solved for E. coli EPSPS, crystallized in the presence of 10 mM 2F-TI, and WT CP4 and Ala100Gly CP4 EPSPS crystallized in the presence of 5 mM 2F-TI or 5 mM RP-TI. X-ray diffraction data were collected, and structure determination was performed as previously described (see General Protocols, Chapter 1). Data collection and structure refinement statistics are reported in the publication[62].

Results and Discussion:

Comparison of these EPSPS enzymes- These orthologs of EPSPS have been studied, separately, previously in our lab. *E. coli* EPSPS and CP4 EPSPS are model Class I and Class II enzymes, respectively, with known structures. *S. aureus* EPSPS is a class II enzyme from a pathogenic source. Since CP4 and *S. aureus* EPSPS are insensitive to glyphosate, we examined their sensitivity to the TI analogs previously found to be the most potent EPSPS inhibitors. The amino acid sequences of these enzymes show substantial divergence (Fig. 8.2). Pairwise alignments (data not shown; matrix: EBlosum62) reveal that the orthologous enzymes from *E. coli* and CP4 share 27%

Fig. 8.2: Sequence alignment of EPSPS enzymes used in this study.
Three-way amino acid sequence alignment of CP4, *S. aureus*, and *E. coli* EPSPS.

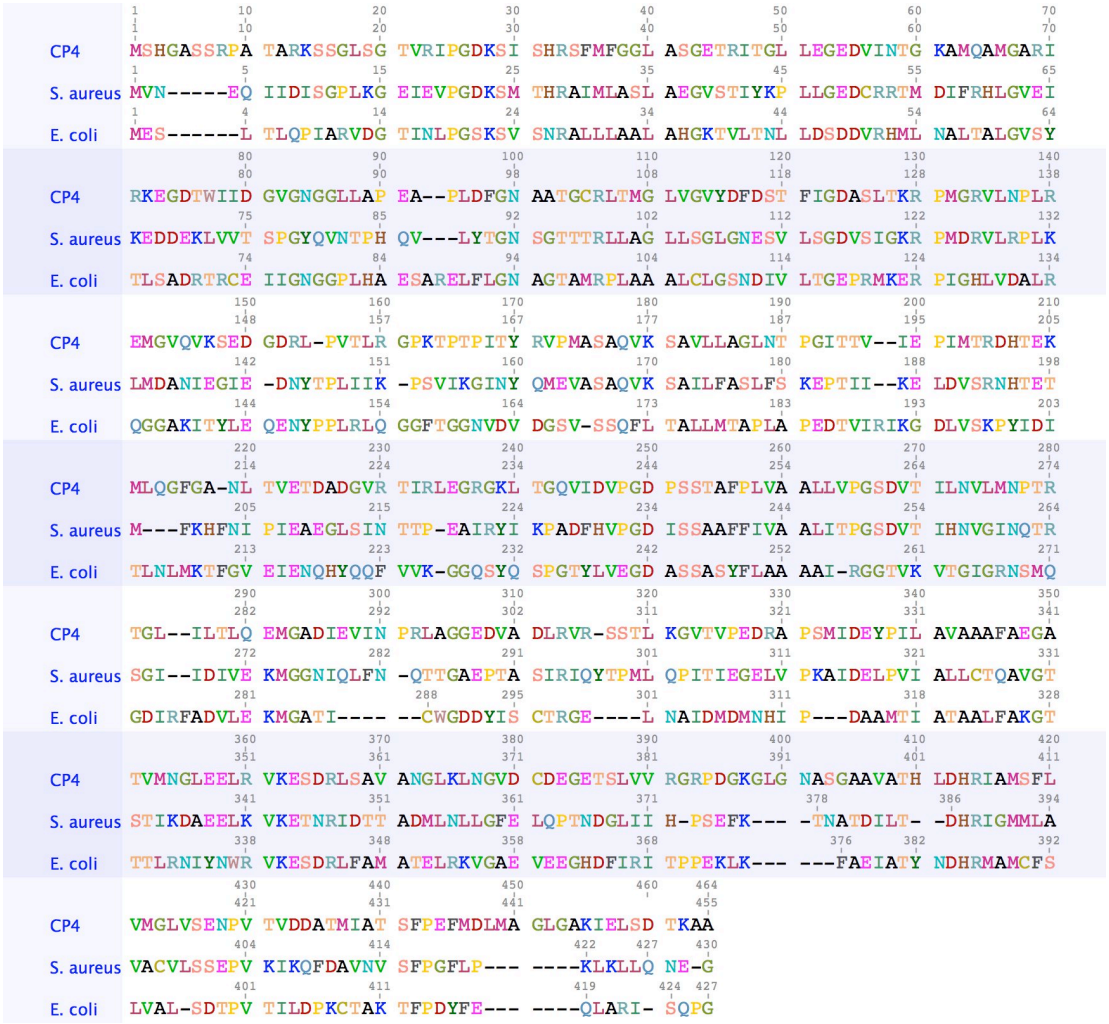

identity and 45% similarity; CP4 and *S. aureus* share 32% identity and 50% similarity, and *E. coli* and *S. aureus* share 27% identity and 46% similarity.

Kinetic characteristics- The functional properties of these enzymes are compared in Fig. 8.3. The specific activity is highest in the *E. coli* EPSPS and lowest in the *S. aureus* EPSPS, which is approximately one order of magnitude less active. The substrate binding affinity is well conserved, as evinced by the comparable K_m values obtained from all three mutants. The biggest differences are observed in the IC_{50} glyphosate; *S. aureus* EPSPS is 430-fold less sensitive than *E. coli* EPSPS, and CP4 is over 5000-fold less sensitive to glyphosate than *E. coli*.

Inhibition by TI analogs- For each of these EPSPS enzymes, we determined the K_i of 2F-TI, RP-TI, and SP-TI using steady state kinetics. The substrate saturation plots and the $K_{m(obs)}$ replots utilized for K_i determination are shown in figure 8.4a-c, and the calculated K_i values are displayed in Table 8.1. Previously, Alberg *et al.* (1992) found both 2F-TI (K_i = 4 nM) and RP-TI (K_i = 15 nM) to be nanomolar-range inhibitors of *Petunia hybrida* EPSPS[26], and Priestman *et al.* (2005) determined that RP-TI exhibits similar potency against *E. coli* EPSPS (K_i = 16 nM)[28]. Our results with the *E. coli* EPSPS enzyme correlate well with these previous findings, but substantial differences are observed in both the rank order and the magnitude of inhibition of the class II EPSPS from *S. aureus* and CP4. RP-TI is the most potent inhibitor of *E. coli* EPSPS, with K_i = 3.9 nM. However, this inhibitor is 120-fold less potent against *S. aureus* (K_i = 450 nM) and 460-fold less potent against CP4 EPSPS (K_i = 1800 nM). The potency

Fig. 8.3: Kinetic properties of EPSPS enzymes used in this study: S3P, PEP, and glyphosate binding comparisons.

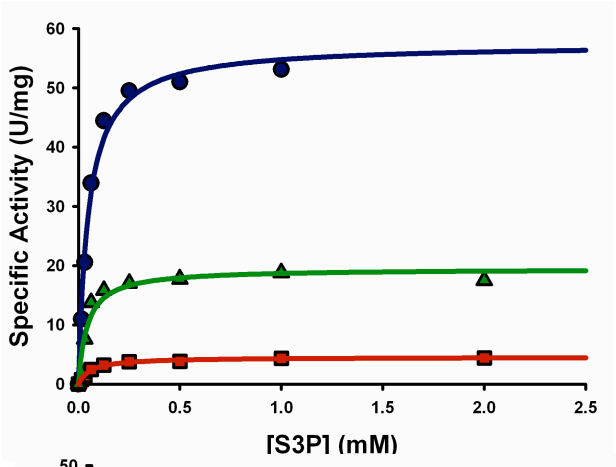

EPSPS K_m S3P:
E. coli (●)= .05 mM,
CP4 (▲) = .04 mM;
S. aureus (■) = .06 mM

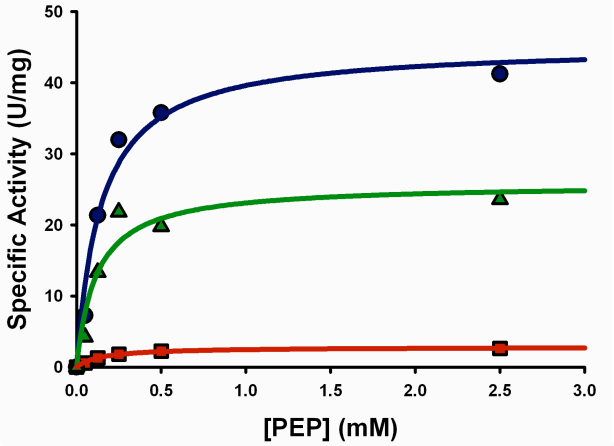

EPSPS K_m PEP:
E. coli (●)= 0.14 mM;
CP4 (▲) = 0.12 mM;
S. aureus (■) = . 0.15 mM

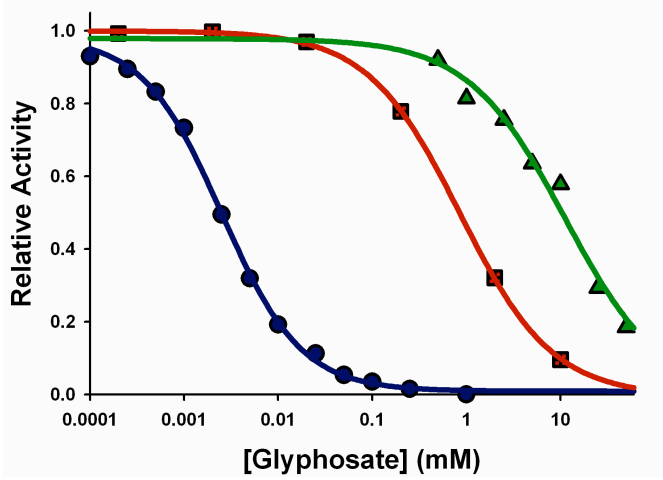

EPSPS IC_{50} GLP:
E. coli (●)=0.002 mM;
CP4 (▲) = 11 mM
S. aureus (■) = 0.86 mM

Fig. 8.4a: *E. coli* EPSPS inhibition by TI analogs (see following page):

(***Top***) S3P saturation curves in the presence of increasing concentrations of 2F-TI: 0 (●), 1.9 (○), 3.8 (▲), 7.5 (Δ), 15 (■), and 30 (□) nM 2F-TI. The concentration of PEP was 1 mM. Data were fit to Equation 1.
(*Right*) Replot of the observed K_m values as a function of 2F-TI concentration. Data were fit to Equation 2, yielding a K_i of 7.8 ± 0.5 nM.

(***Center***) S3P saturation curves in the presence of increasing concentrations of RP-TI: 0 (●), 0.9 (○), 3.8 (▼), 7.5 (∇), 15 (■), and 30 (□) nM RP-TI. The concentration of PEP was 1 mM. Data were fit to Equation 1.
(*Right*) Replot of the observed K_m values as a function of RP-TI concentration. Data were fit to Equation 2, yielding a K_i of 3.9 ± 0.6 nM

(***Bottom***) S3P saturation curves in the presence of increasing concentrations of SP-TI: 0 (●), 0.47 (○), 0.94 (▼), 2.5 (∇), 5 (■), and 10 (□) μM SP-TI. The concentration of PEP was 2 mM. Data were fit to Equation 1.
(*Right*) Replot of the observed K_m values as a function of SP-TI concentration. Data were fit to Equation 2, yielding a K_i of 0.76 ± 0.2 μM.

Fig. 8.4a: *E. coli* EPSPS inhibition by TI analogs

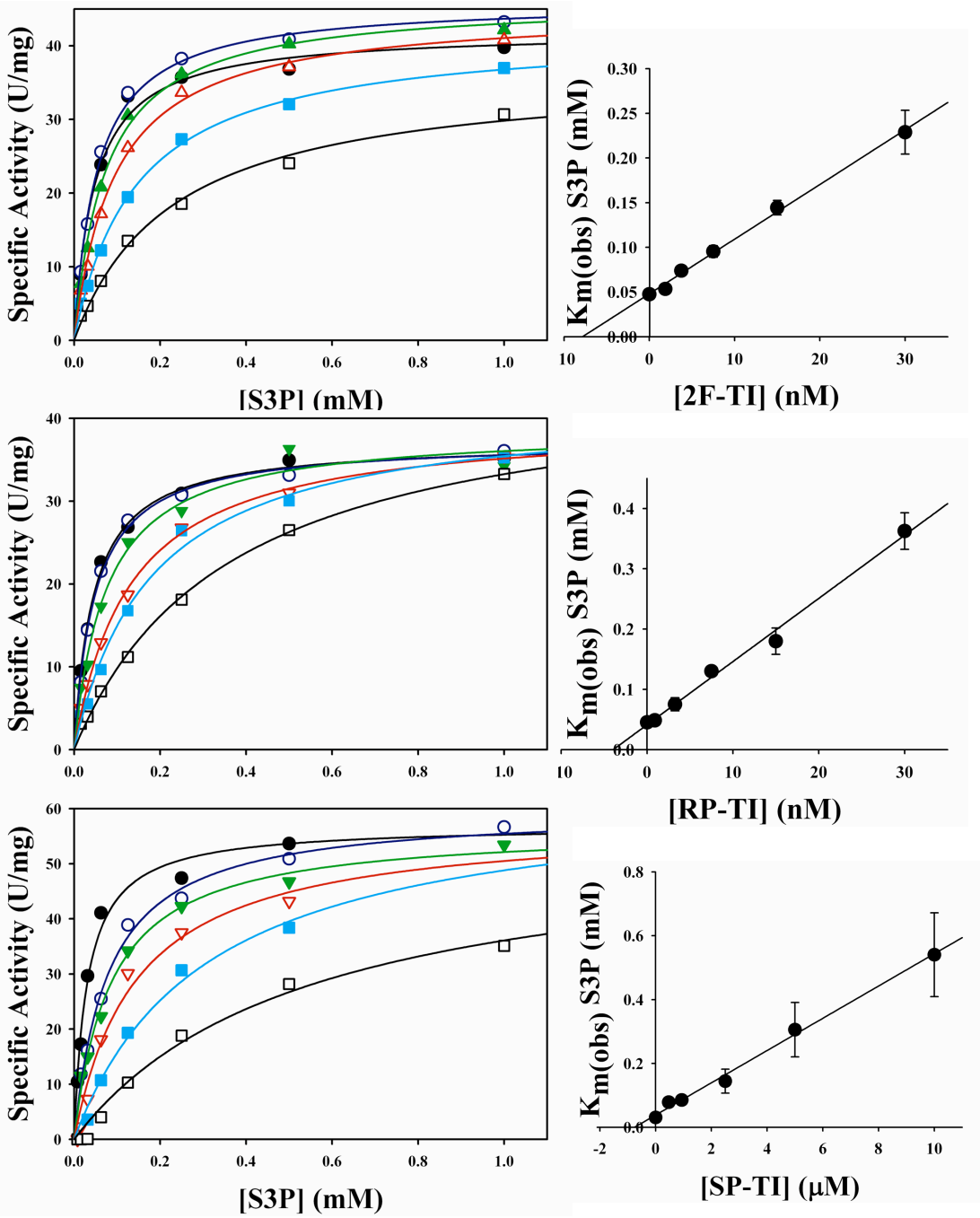

Fig. 8.4b: *S. aureus* EPSPS inhibition by TI analogs (see following page):

(***Top***) S3P saturation curves in the presence of increasing concentrations of 2F-TI: 0 (●), 4.7 (○), 9.4 (▲), 18.8 (Δ), 37.5 (■), 75 (□), and 150 (▼) nM 2F-TI. The concentration of PEP was 1 mM. Data were fit to Equation 1.
(*Right*) Replot of the observed K_m values as a function of 2F-TI concentration. Data were fit to Equation 2, yielding a K_i of 30 ± 6 nM.

(***Center***) S3P saturation curves in the presence of increasing concentrations of RP-TI: 0 (●), 0.16 (○), 0.31 (▼), 0.63 (∇), 1.3 (■), and 2.5 (□) μM RP-TI. The concentration of PEP was 1 mM. Data were fit to Equation 1.
(*Right*) Replot of the observed K_m values as a function of RP-TI concentration. Data were fit to Equation 2, yielding a K_i of 0.45 ± 0.07 μM.

(***Bottom***) S3P saturation curves in the presence of increasing concentrations of SP-TI: 0 (●), 3.1 (○), 6.3 (▲), 12.5 (Δ), 25 (■), 50 (□), 100 (▼), and 200 (∇) μM SP-TI. The concentration of PEP was 1 mM. Data were fit to Equation 1.
(*Right*) Replot of the observed K_m values as a function of SP-TI concentration. Data were fit to Equation 2, yielding a K_i of 11.0 ± 2 μM.

Fig. 8.4b: *S. aureus* EPSPS inhibition by TI analogs:

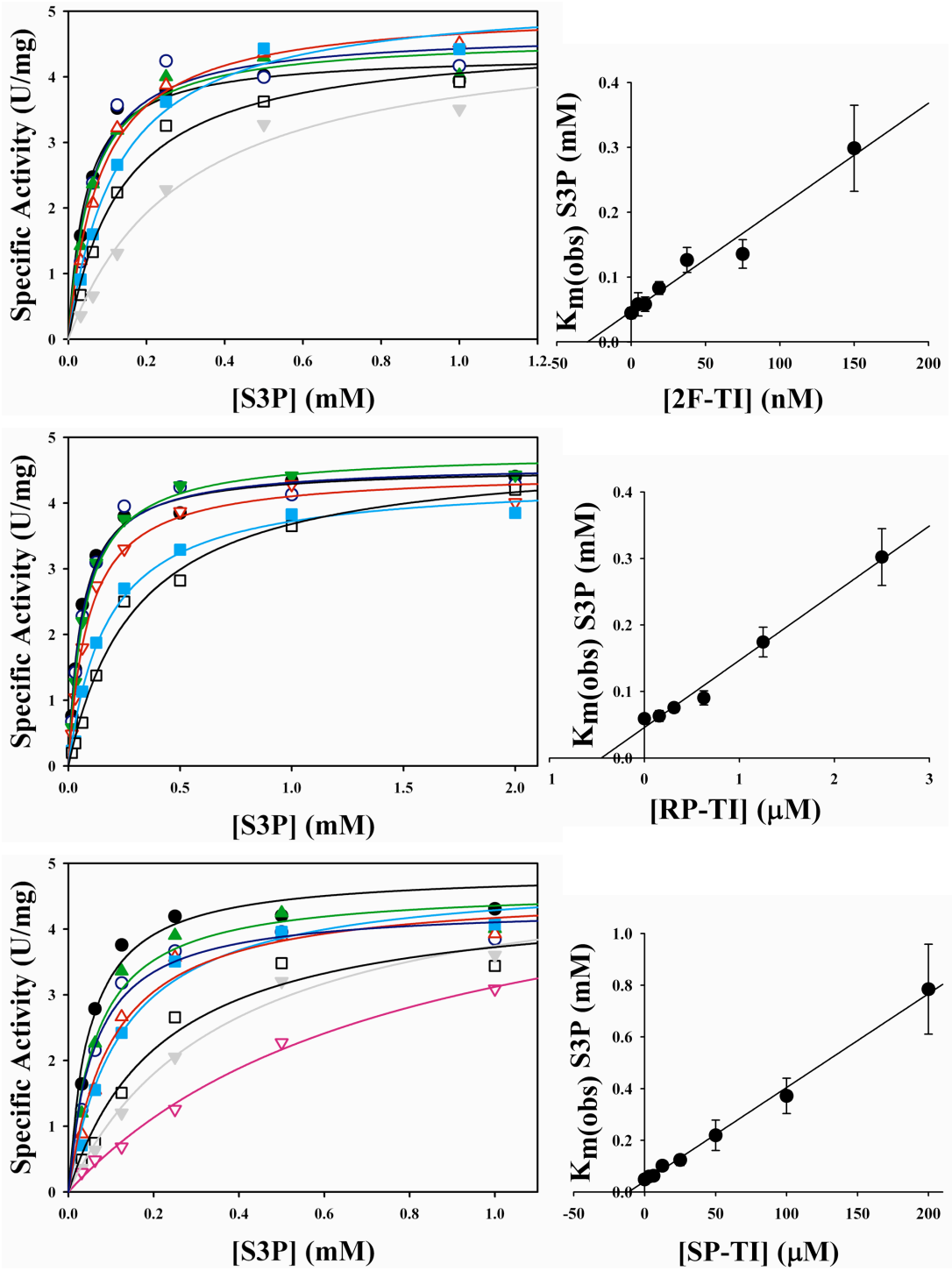

Fig. 8.4c. CP4 EPSPS inhibition by TI analogs (see following page):

(***Top***) S3P saturation curves in the presence of increasing concentrations of 2F-TI: 0 (●), 60 (○), 120 (▼), 240 (▽), and 480 (■) nM 2F-TI. The concentration of PEP was 2 mM. Data were fit to Equation 1.
(*Right*) Replot of the observed K_m values as a function of 2F-TI concentration. Data were fit to Equation 2, yielding a K_i of 63 ± 15 nM.

(***Center***) S3P saturation curves in the presence of increasing concentrations of RP-TI: 0 (●), 2.5 (○), 5 (▲), 10 (Δ), and 20 (■) μM RP-TI. The concentration of PEP was 2 mM. Data were fit to Equation 1.
(*Right*) Replot of the observed K_m values as a function of RP-TI concentration. Data were fit to Equation 2, yielding a K_i of 1.8 ± 0.6 μM.

(***Bottom***) S3P saturation curves in the presence of increasing concentrations of SP-TI: 0 (●), 25 (○), 50 (▼), 100 (Δ), 200 (■), and 400 (□) μM SP-TI. The concentration of PEP was 2 mM. Data were fit to Equation 1.
(*Right*) Replot of the observed K_m values as a function of SP-TI concentration. Data were fit to Equation 2, yielding a K_i of 76 ± 9 μM.

Fig. 8.4c. CP4 EPSPS inhibition by TI analogs:

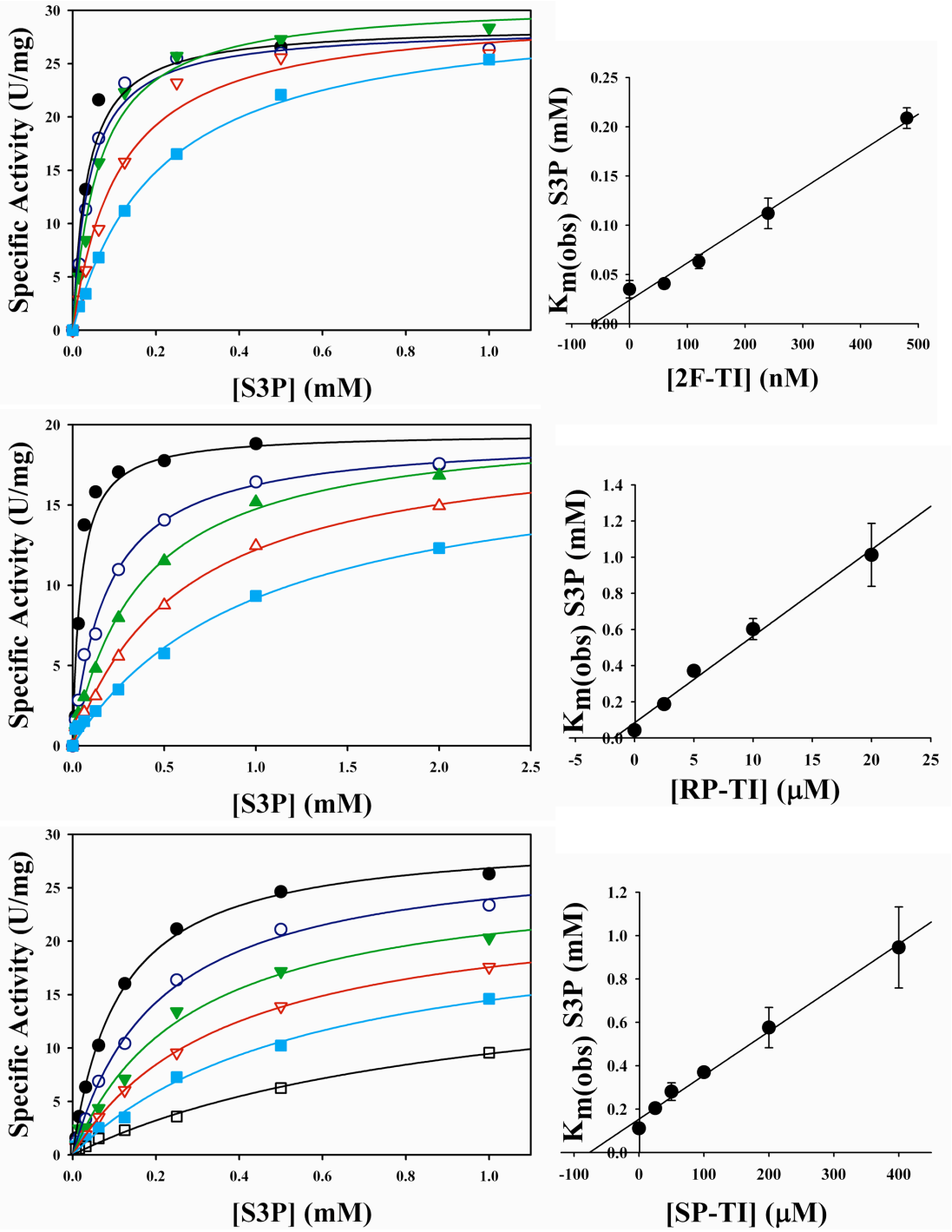

Table 8.1: TI analogs: *E. coli*, CP4, and *S. aureus* EPSPS inhibition. Inhibition constants (K_i) of TI analogs with respect to S3P (see Figs. 8.4a-c).

EPSPS Enzyme	K_i 2F-TI (nM)	K_i RP-TI (nM)	K_i 2F-TI (nM)
E. coli	7.8 ± 0.5	3.9 ± 0.6	760 ± 200
CP4	63 ± 15	1800 ± 600	76000 ± 9000
S. aureus	30 ± 6	450 ± 70	11000 ± 2000

of 2F-TI against the class II EPSPS is also decreased (by 3- to 7-fold) compared to *E. coli* EPSPS; despite this, 2F-TI is the most potent inhibitor of the Class II enzymes (*S. aureus* K_i = 30 nM; CP4 K_i = 63 nM). Of these three inhibitors, the SP-TI is the most similar to the genuine TI, yet shows the least potency. The inhibitory potency of SP-TI against the class II EPSPS is, again, decreased (by 14- to 100-fold) compared to the class I *E. coli* EPSPS. Together, these findings indicate that class II enzymes such as *S. aureus* or CP4 EPSPS are tolerant not only toward glyphosate but are also considerably less susceptible to inhibition by these analogues of the TI.

Crystallization- To probe the basis of the observed differential inhibition, we determined the structures of the dead-end complexes. The *E. coli* EPSPS•2F-TI structure was determined at 1.6 Å resolution, the CP4 EPSPS•2F-TI complex at 1.8 Å resolution, and the CP4 EPSPS•RP-TI complex at 1.6 Å resolution. Despite repeated efforts, we were unable to obtain crystals of the CP4 EPSPS•SP-TI complex, and crystallization conditions for the *S. aureus* enzyme are, as of yet, unknown. We utilized the previously determined *E. coli* EPSPS•TI[24], *E. coli* EPSPS•RP-TI, and *E. coli* EPSPS•SP-TI structures[28] to enable fuller comparison.

Comparison of 2F-TI co-crystal structures- The active sites of the *E. coli* EPSPS•2F-TI and the CP4 EPSPS•2F-TI structures are shown, in stereo, in Fig. 8.5. In the case of the *E. coli* EPSPS structure, the most prominent change (compared to the S3P-bound binary complex) is seen in the side chain of residue Glu341, which swings away from the active site in the 2F-TI complex. The position of this glutamate side

Fig. 8.5: 2F-TI, active site structures and bonding interactions. Stereofigure shows inhibitor (yellow) bound to active site of EPSPS enzymes. (*Top*) 2F-TI•*E. coli* EPSPS; (*Bottom*) 2F-TI•CP4 EPSPS. Green residues show conformation of Glu341 or Glu354 in the respective binary structures. Black dotted lines indicate hydrogen bonding interactions; cyan balls denote water molecules.

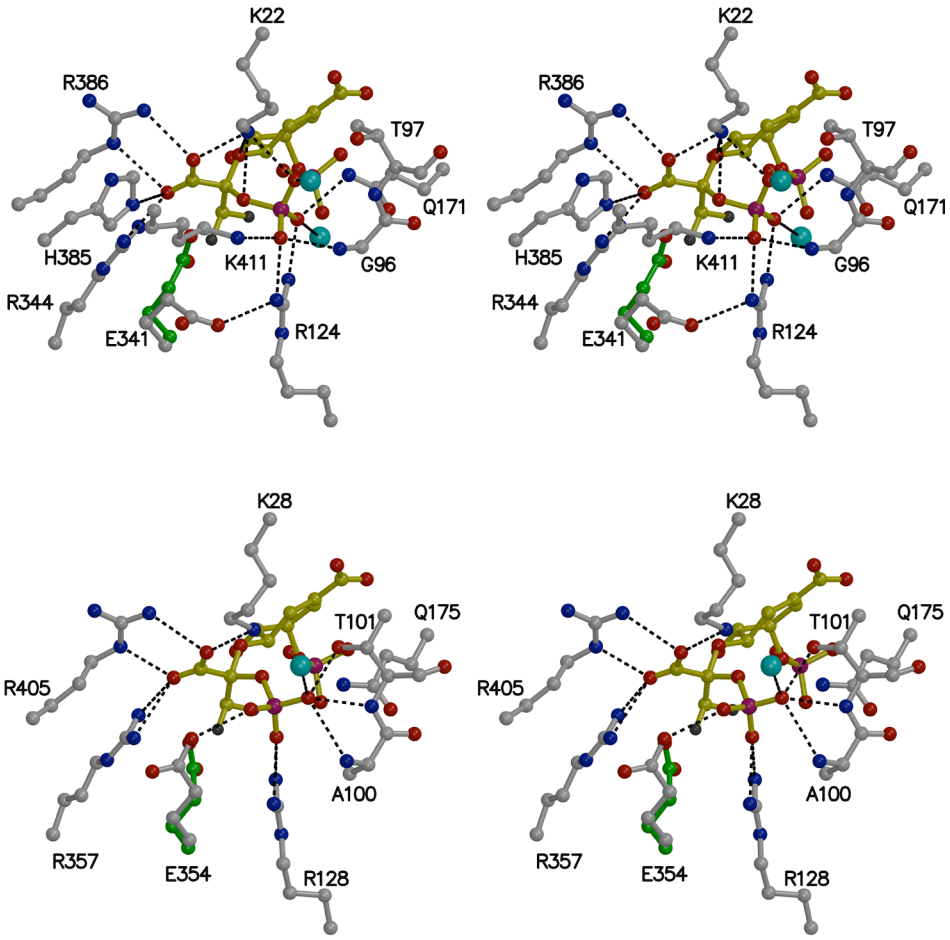

chain in the S3P-complexed enzyme is instead occupied by the difluoro group of 2F-TI. In comparison, the side chain conformations and bonding interactions of the CP4 active site are nearly identical in the S3P-bound or 2F-TI-bound structure and the equivalent glutamate (residue Glu354) shifts only slightly. Compared to the position of this side chain in the S3P-complexed enzyme the plane of the carboxyl moiety rotates slightly, the side chain clearly does not translate out of the active site. Aside from this glutamate residue, the other major difference observed when comparing the CP4 EPSPS•2F-TI active site to the *E. coli* EPSPS•2F-TI active site is the position of residue Thr101 (equivalent to Thr97 in the *E. coli* enzyme). The position of this residue in CP4 EPSPS appears to induce a slight conformational change in the 2F-TI molecule.

Comparison of RP-TI co-crystal structures- Fig. 8.6 shows the RP-TI liganded EPSPS structures in stereo (the *E. coli* EPSPS•RP-TI structure shown here was obtained previously). Again, the distinct conformational changes that are observed in the *E. coli* EPSPS•RP-TI active site are not reflected in the CP4 EPSPS structure. *E. coli* residues Glu341 and Arg124 shift out of the active site compared to their position in the S3P-binary structure. The equivalent residues in the CP4 EPSPS•RP-TI active site, Glu354 and Arg128, shift only slightly compared to their position in the CP4 EPSPS•S3P structure. The position of the Glu354 appears to cause a steric clash with respect to the RP-TI, providing one explanation for the dramatically reduced potency of this inhibitor. The Thr101 is in the same position as observed in the CP4 EPSPS•2F-TI structure, causing a slight shift in the 3'-phosphate orientation, and a

Fig. 8.6: RP-TI, active site structures and bonding interactions. Stereofigure shows inhibitor (yellow) bound to active site of EPSPS enzymes. (*Top*) RP-TI•*E. coli* EPSPS; (*Bottom*) RP-TI•CP4 EPSPS. Green residues show conformation of Glu341 and Arg124 or Glu354 in the respective binary structures. Black dotted lines indicate hydrogen bonding interactions; red dotted lines indicate steric clashes; cyan balls denote water molecules.

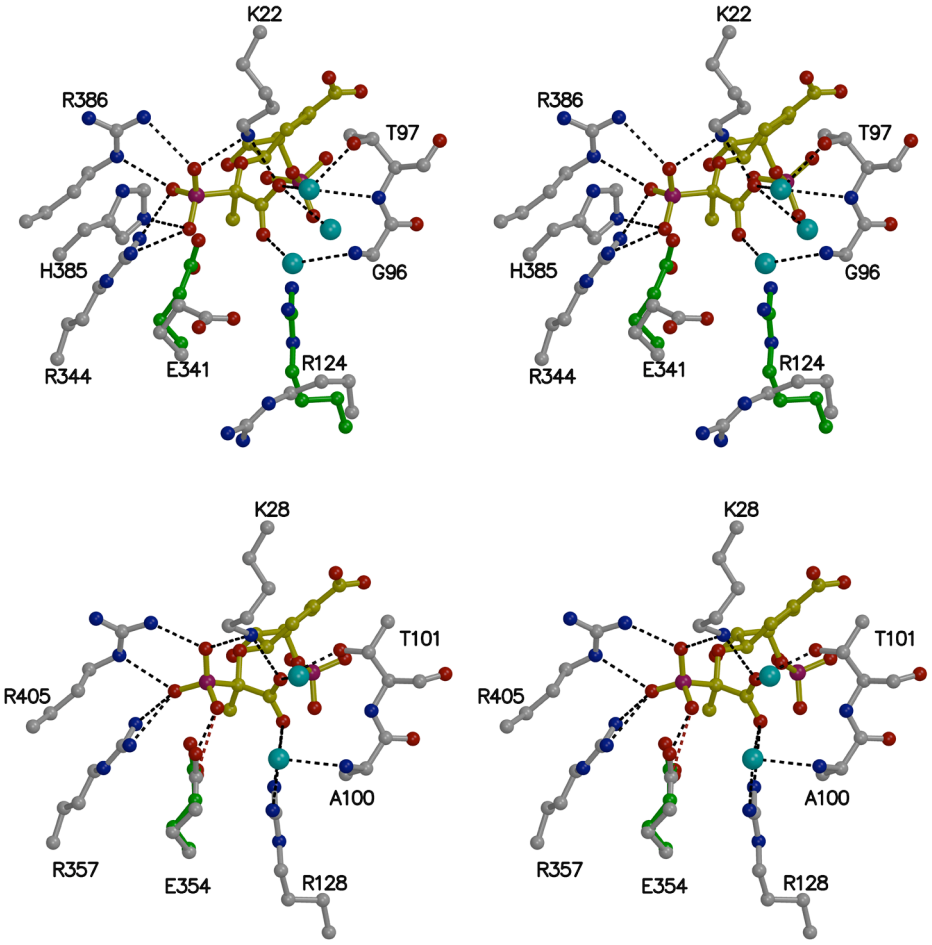

conformational change is observed in the RP-TI molecule. It appears that the conformational flexibility exhibited by active site residues of *E. coli* EPSPS is an important determinant of the binding of the TI analogs. Alternatively, one may say that the conformational rigidity displayed by the active site of CP4 EPSPS prevents binding of the favored conformations of these TI analogs. The idea that CP4 EPSPS has a more rigid structure is correlated by the results of the thermal denaturation studies we previously performed, which indicated that CP4 EPSPS is more thermostable than the *E. coli* enzyme. Fig. 8.7 highlights the conformational change observed for the TI analogs bound the *E. coli* or CP4 enzymes. In both cases, higher-energy inhibitor conformations are observed with CP4 EPSPS again suggesting that the conformational rigidity of the CP4 EPSPS may require conformational flexibility of the inhibitor molecule.

Analysis of SP-TI and EPSPS interactions- The basis for the low inhibitory potency of the SP-TI for CP4 EPSPS is difficult to assess in the absence of structural data. Repeated crystallization trials simply failed to produce crystals. The crystallization conditions utilized are specific to the "closed"-form CP4, so it is possible that the SP-TI failed to produce the required conformational change, perhaps due to intrinsic properties of the SP-TI itself, insufficient inhibitor concentration, or perhaps a contaminant from the synthesis process that interferes with crystallization at the high concentrations utilized. Docking experiments performed by Huijong Han (utilizing the closed-form CP4 EPSPS and the SPTI conformation as obtained with the *E. coli* enzyme) indicated that several electrostatic interactions observed in the *E. coli*

Fig. 8.7: Conformational change of TI analogs: The TI analogs bound to the CP4 enzyme adopt higher-energy conformations.

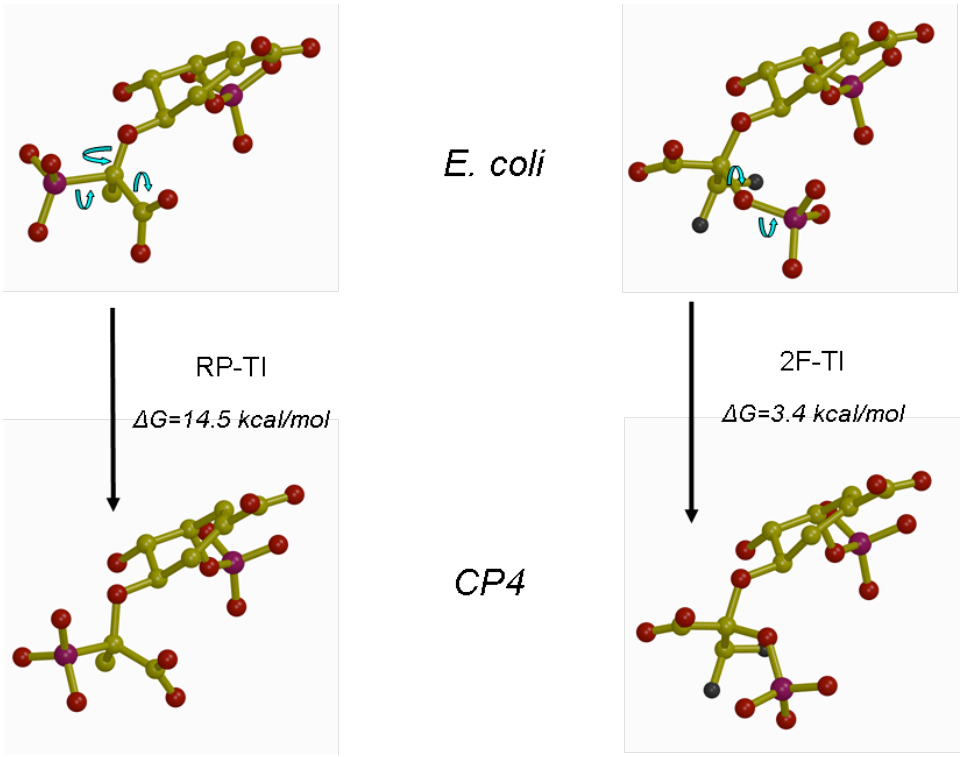

EPSPS•SP-TI complex would be lost in the complex of CP4 EPSPS•SP-TI, suggesting one possible basis for the weak inhibition observed in our inhibition studies.

Formation of dead-end complex- The global induced fit mechanism of EPSPS complicates the analysis and modeling of inhibition. Fig. 8.8 shows the two-step process that is required for formation of the closed-form inhibitor bound enzyme (also simply for binding of S3P). The initial binding of the S3P-moiety of these inhibitors with the N-terminal globular domain of the open-form EPSPS results in formation of a "collision complex". The enzyme then undergoes the open-closed transition, and this step may, in fact, be a rate-limiting step, in which case the observed K_i would not be equivalent to the K_d of these inhibitors. The differential inhibition that we observe with respect to the inhibition of *E. coli, S. aureus* and CP4 EPSPS may result in part from alteration of the rate of the global open-closed transition.

Conclusions:

Previous EPSPS-inhibition studies have focused on class I EPSPS enzymes. Here, we have shown that the 2F-TI, a nanomolar-range inhibitor of class I EPSPS, is also a potent inhibitor of the class II EPSPS from CP4 and *S. aureus* (K_i = 63 and 30 nm, respectively). In general however, the results of this work show that TI structure-activity-relationship studies conducted utilizing one EPSPS enzyme are not necessarily applicable to other EPSPS enzymes. The differential inhibition also suggests that the genuine TI of these enzymes may differ somewhat in energy and conformation. To probe this, we produced a D326A mutant of the CP4 enzyme

Fig. 8.8: Two steps are required to form the dead-end complex. Proposed molecular mode of action of TI analogues on EPSPS. On the basis of the structural data available to date, TI analogues (TIAs) would initially interact with the open state of EPSPS to form a *collision complex*, determined by the dissociation constant $K_{d(TIA)}$, followed by an open-closed transition to the *dead-end complex*, determined by the rate constants k_3* and k_4*. Under the steady-state conditions applied here, the measured K_i values represent the K_d only if the ratio of k_3* and k_4* is not altered as a result of the inhibitor's interaction with the enzyme.

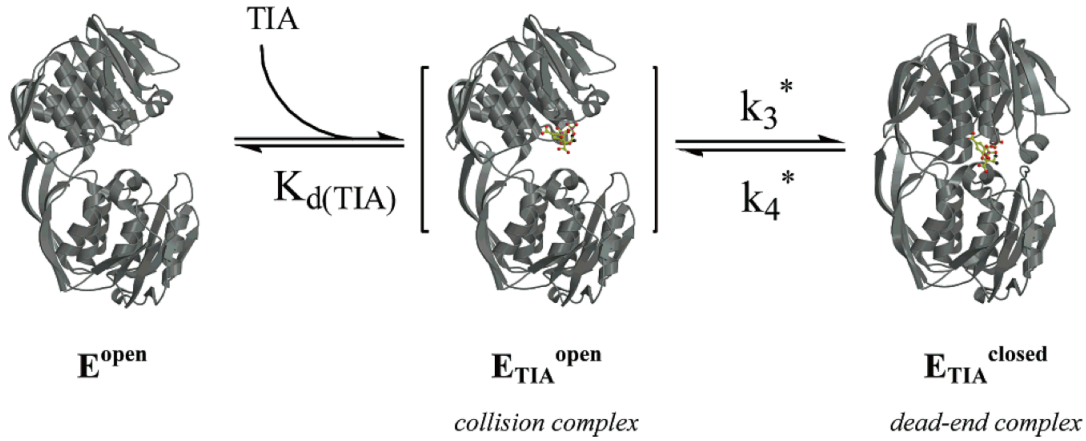

(equivalent to the D313A mutation that allowed trapping of the TI in *E. coli* EPSPS). While this enzyme was indeed inactive, crystals were never observed. Very recently, the coordinates of the *M. tuberculosis* EPSPS bound to the genuine tetrahedral intermediate were reported by another group (PDB 2o0x, unpublished); a simple alignment of the carbon atoms of the S3P rings (Fig. 8.9) indeed shows some conformational changes. Our hypothesis that the properties of CP4 may allow it to be used as a structural model of the *S. aureus* EPSPS does not appear to be supported, and our study suggests that, for antibiotic purposes, inhibitor design and development is best conducted using EPSPS from pathogenic sources.

Fig. 8.9: The genuine TI may exist in different conformations. Shown are the structures of the tetrahedral reaction intermediates found in *E. coli* D313A EPSPS (PDB 1q36) (green) and *M. tuberculosis* EPSPS (PDB 2o0x) (cyan). The cyclohexene moieties of each molecule were aligned using PyMol.

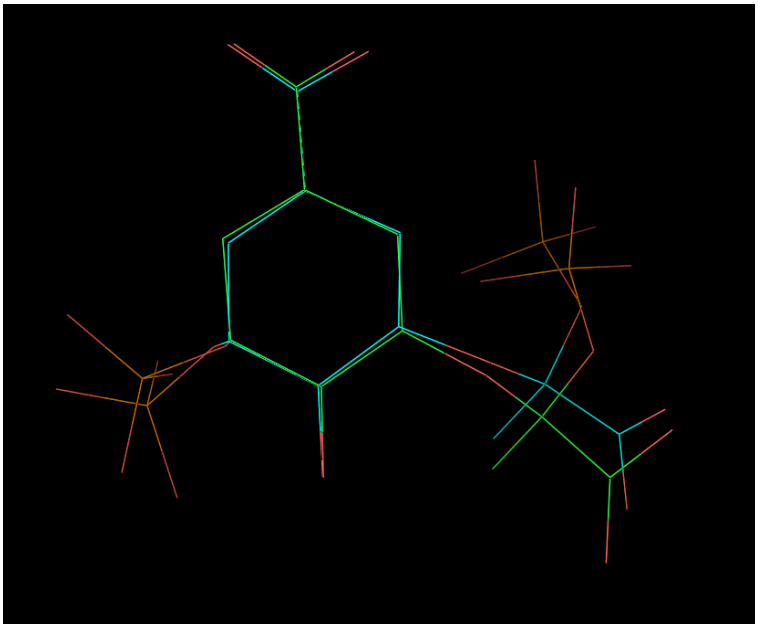

Chpt. 9: Synthesis of S3P or S3P-analogs from Shikimate or Shikimate-analogs using a Monitored Enzymatic Phosphorylation

(*unpublished)*

Introduction:

The enzyme shikimate kinase (SK) catalyzes the phosphorylation of shikimate, producing ADP and S3P (see Fig. 9.1). S3P is a key intermediate in the shikimate pathway toward the biosynthesis of aromatic compounds. As the substrate of EPSPS, S3P is required to examine the structure, function, and inhibition of this enzyme. S3P has been isolated from culture[123, 124], obtained from chemical synthesis[125], and produced by enzymatic synthesis[45]. While S3P can be obtained commercially (Toronto Research Chemicals, Inc.) the cost of $125 per milligram limits the experiments that can be contemplated; for example, screening of the 100,000+ compound collection at the KU HTS laboratory for inhibitors of *E. coli* EPSPS consumed nearly 200 milligrams of S3P. To enable such experiments, an enzymatic synthesis developed by Dr. Melanie Priestman[45] (see General Protocols, Chapter 1) was utilized, to produce S3P from shikimate and ATP, using *Methanococcus jannaschii* SK[46], and S3P was then purified using anion-exchange. This process was time-consuming, reproducibility was poor, and the process was inefficient (overall yield of approximately 25%).

An optimized synthesis of S3P was desired to increase yield, simplify procedures and improve reproducibility. Further, a variety of shikimate analogs had been produced (see Fig. 9.2) with the goal of utilizing S3P-analogs to probe the catalytic mechanism

Fig. 9.1: The reaction catalyzed by Shikimate Kinase (SK)

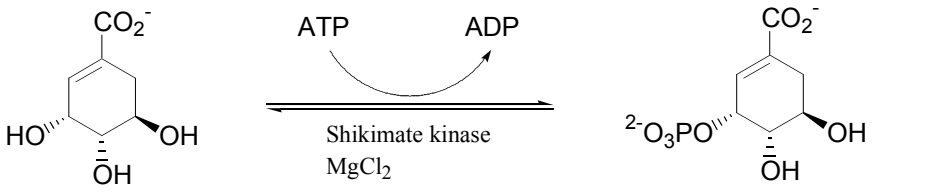

Shikimate Shikimate-3-phosphate

Fig. 9.2: Structure of shikimate and the analogs examined here.

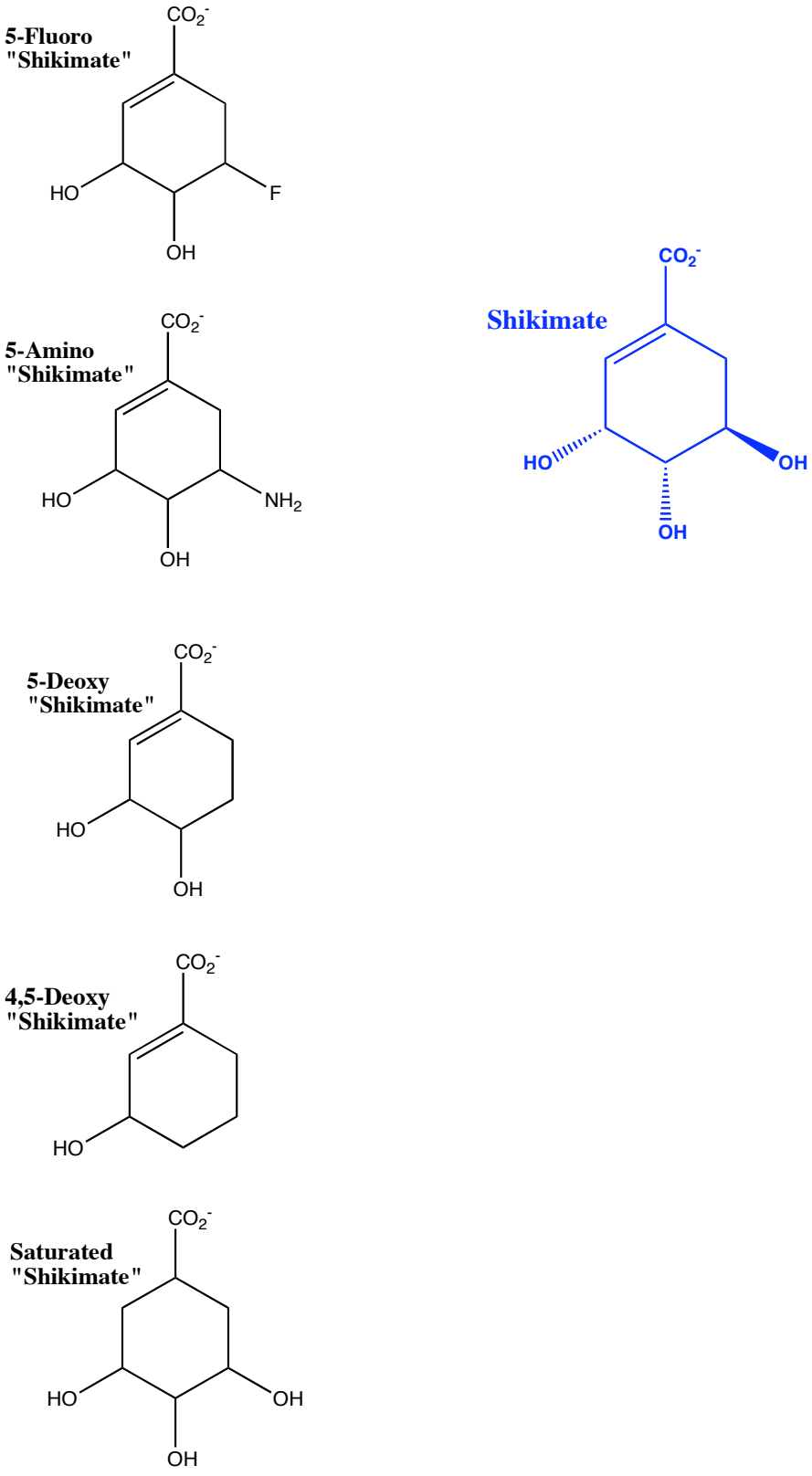

and inhibition of EPSPS. Chemical synthesis methods were found to result in non-specific phosphorylation of theses shikimate analogs, resulting in unresolvable mixtures. We hypothesized that SK enzymes could be used to phosphorylate these shikimate analogs at the proper position and with the desired stereochemistry. To meet these needs, two new SK genes were obtained, an assay was developed to monitor S3P production, and a more efficacious method was developed for removing nucleotides from the crude reaction mixture.

SK enzymes are quite diverse. Two types of SK have been characterized (SK I and SK II), and many organisms have genes for both. In *E. coli*, for example, the SK I is encoded by the *aroK* gene, while SK II is encoded by the *aroL* gene. These two genes are not highly similar, and it is believed that only SK II normally functions in the shikimate pathway[126, 127]. The structure of SK II from *E. coli* is not known. *Mycobacterium tubercuolosis*, on the other hand, has only the *aroK*-encoded SK I. This enzyme is not highly similar (optimal global alignment: 28% identity and 45% similarity) to SK II of *E. coli,* but more resembles SK I[128, 129]. Extensive structural data are available concerning the *M. tuberculosis* SK[130-132], but little functional data exist. The *M. jannaschii* SK enzyme previously utilized has very low sequence homology compared to other SK enzymes (optimal global alignment: 11% identity and 21% similarity to *aroL* from *E. coli*; 4% identity and 5% similarity to *aroK* of *M. tuberculosis*) (three-way alignment, Fig. 9.3). While *M. jannaschii* is not a pathogen, the SK enzymes are, in general, considered promising drug targets[27, 101, 133]. In order to improve the S3P synthesis, effect the phosphorylation of the shikimate analogs,

Fig. 9.3: Three-way alignment of SK enzymes. Three sources: *E. coli* SK II, *M. tuberculosis* SK I, and *M. jannaschii* SK

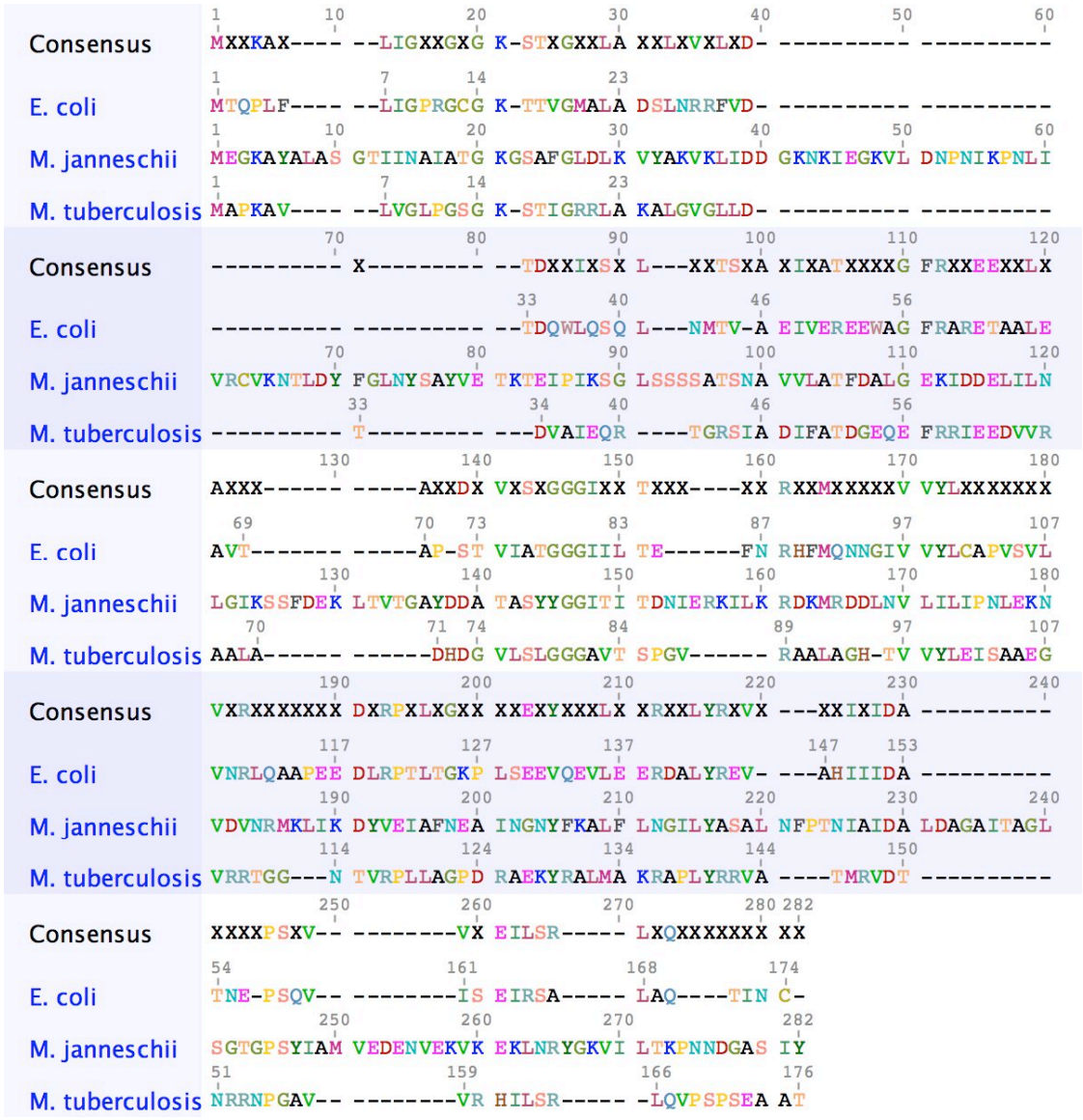

and probe the activity of diverse SK enzymes, the *E. coli aroL* (SK II) gene and the *M. tuberculosis aroK* (SK I) gene were obtained, a SK activity assay was developed, and the phosphorylation and product purification procedures were optimized.

Experimental Procedures:

Materials- All materials were purchased from Sigma except as otherwise stated. Shikimate analogs were provided by Dr. Apurba Dutta. Synthetic genes encoding *E. coli* SK II (*aroL*) and *M. tuberculosis* SK I (*aroK*), with codon usage optimized for high-level overexpression in bacteria, were purchased from GeneArt (Frankfurt, Germany).

Molecular biology- The GeneArt-produced construct was subjected to restriction digest using *Nde*I and *Xho*I restriction endonucleases in NEBuffer 2 + BSA (New England BioLabs), according to the manufacturer's instructions. The products of the digest were separated by size using agarose gel electrophoresis and the *aroL* and *aroK* genes were isolated using the QIAquick Gel Extraction Kit (Qiagen), according to the manufacturer's instructions. Empty pET-24c vector (Novagen) was linearized and purified by the same restriction digest and gel extraction process, and the *aroL* and *aroK* genes were ligated into this pre-digested vector using T4 DNA ligase from the Quick Ligation kit (New England BioLab), again according to the manufacture's instructions. The product of this cohesive-end ligation was utilized directly to transform chemically competent *E. coli* DH5-α. These cells were plated on LB-Agar plates containing 30 μg/ml kanamycin and incubated overnight. The resulting

bacterial colonies with kanamycin-resistance were picked and grown in LB media overnight, and the plasmids were isolated using the QIAprep Spin Miniprep kit (Qiagen) according the manufacturer's instructions. Samples of the isolated plasmids were subjected again to restriction digest by *Nde*I and *Xho*I and analyzed by DNA agarose gel electrophoresis. Several of the restriction digest analysis displayed properly-sized genes; these were submitted for sequence analysis at the Idaho State University Molecular Research Core Facility.

Protein production- The sequences obtained utilizing the T7 primer confirmed the presence of the open reading frame of the *aroL* and *aroK* genes, and the *aroK*-pET-24c and *aroL*-pET-24c constructs were transformed into *E. coli* BL21(DE3)Star cells (Invitrogen). Small-scale studies showed that soluble expression of both enzymes could by induced, at 37 °C, by addition of 0.5 mM IPTG. Large scale cultures were grown to log stage (OD_{600} = 0.4 to 0.6) at 37 °C in LB media in the presence of 30 μg/ml kanamycin, induced with 0.5 mM IPTG, and harvested by centrifugation 4-6 hours post-induction.

E. coli SK purification- *E. coli* SK II purification was performed first. As the $(NH_4)_2SO_4$ effects were unknown, the ammonium sulfate precipitation step was avoided. Instead, (much as in initial purifications of *S. aureus* or CP4 EPSPS) cells were lysed in extraction buffer and the clarified lysate was loaded directly onto the Q-sepharose column and eluted along a linear gradient from 100% - 0% buffer A, over 10 CV. The SK II enzyme was found in the flow through, likely due to the salt

content of the extraction buffer (0.1 M NaCl). The flow through was collecteted and concentrated by Amicon apparatus overnight using a 10 kDa Millipore filter. Q-sepharose Buffer A was added to dilute the salt content of the solution, and a precipitate was observed to form. SDS-PAGE indicated that this precipitate was (in fact nearly pure) *E. coli* SK II. Re-addition of NaCl did not re-solubilize the enzyme. Prior to performing a new overexpression and purification procedure, the gene sequence was checked again. This time, four extraneous residues, two methionines and two alanines, were noted at the N-terminus of the protein, an artifact of the restriction/ligation process (the gene product is thus N-term-MetAlaMetAla-*aroL*-C-term). Mutation of the methionine codons to something other than "ATG" will correct this defect, but this work has not been performed. Due to difficulties in purification and gene sequence, this project was set aside.

M. tuberculosis SK purification- *M. tuberculosis* SK I was purified by essentially the same process. Again, the enzyme was found in the flow through of the first anion-exchange column, again likely due to the NaCl content of the extraction buffer used for resuspension and lysis of the cell pellet. However, the flow-thru showed significant enrichment of the SK I enzyme. The flow through was concentrated by Amicon apparatus overnight using a 10 kDa Millipore filter. Q-sepharose Buffer A was added repeatedly to dilute the salt content of the solution, with no precipitation observed. The desalted and partially purified SK I preparation was applied to the Resource-Q anion exchange column and eluted over a 20 CV, 100 - 0 % Buffer A gradient. This time, the enzyme was found in the collected fractions. The *M.*

tuberculosis SK I enzyme was pooled analyzed by SDS-PAGE, and determined to be approximately 90% homogenous; a high molecular-weight contaminant was observed. The total yield was about 12 mgs of purified SK I from a 7 g cell pellet.

SK activity assay- To compare this *M. tuberculosis* SK to the *M. jannaschii* SK, and to monitor the phosphorylation of the shikimate analogs, an SK couple-enzyme activity assay was developed based on that used by Miller *et al* (1986)[134]. SK activity is coupled to the formation of NAD^+ from NADH, resulting in a change in absorbance at 340 nm (Fig. 9.4) using the enzymes pyruvate kinase and lactic dehydrogenase (from rabbit muscle; ammonium sulfate suspensions from Sigma). The total assay volume was 250 μL to facilitate 96-well microtiter plate-based kinetic experiments. For maximal activity SK activity, the ingredients in each assay sample were: 4 mM shikimate, 5 mM ATP, 2.5 mM PEP, 2.5 mM $MgCl_2$, 0.25 mM NADH, 2.5 U Pyruvate Kinase, and 2.5 U Lactic Dehydrogenase in a buffer of 100 mM Tris-HCl pH 8.5, 50 mM KCl, and 2 mM DTT. Typically, 0.0002 mg SK were added to start each reaction, and the ΔAbs_{340} was monitored as a function of time. In this reaction, oxidation of NADH is stoichiometrically equivalent to the production of ADP (and S3P) by SK; from linear portions of the graphs showing absorbance versus time (not shown), the ΔAbs_{340} per minute was calculated. Based on the extinction coefficient of NADH, the SK enzyme activity is equivalent to 0.089 micromoles product formed per unit of absorbance change at 340 nm, per minute of reaction, per milligram of enzyme. Put another way, SK activity = 0.089 μmol product * ΔAbs_{340} / min / mg.

Fig. 9.4: Coupled enzyme assay for monitoring reaction progress. S3P (or S3P analog) formation is stoichimetric with NADH consumption.

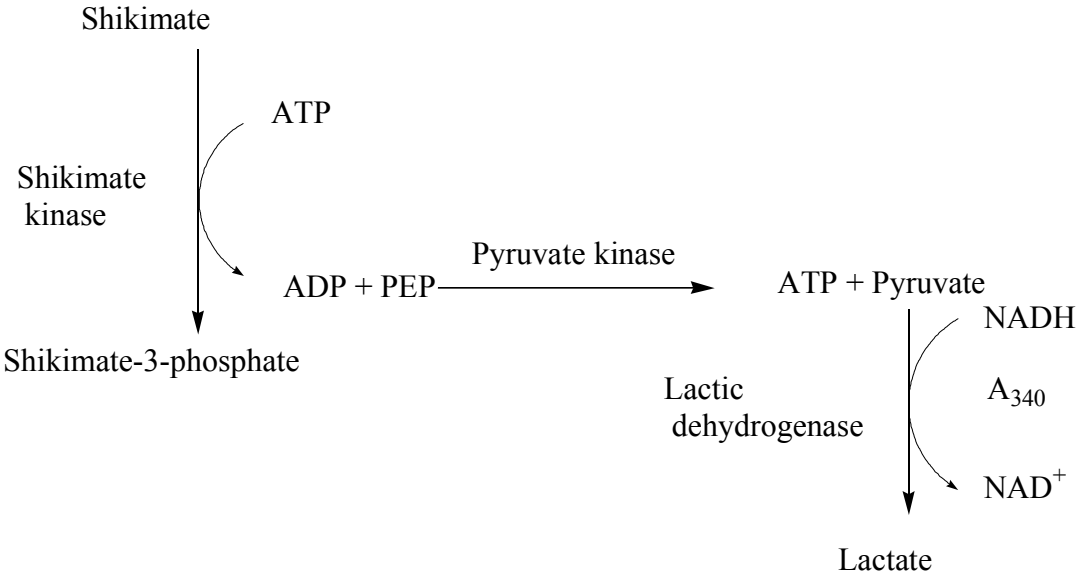

Substrate saturation experiments- To test these SK enzymes and this assay, enzyme activity was determined as a function of shikimate concentration and the data were fit to ***Equation 1:*** $v = V_{max} * [S] / (K_m + [S])$
to determine the K_m and V_{max} for each enzyme. The same procedure was utilized to study the phosphoryl transfer reaction with each shikimate analog; these data were also fit to Equation 1. The results of these assays were used to optimize the preparative phosphorylation of shikimate and shikmate-analogs.

Purification of S3P and S3P analogs- The purification of S3P and S3P analogs was simplified. At the suggestion of Dr. Andreas Becker, activated carbon was utilized to remove excess nucleotides from the synthesis reaction. Following preparative reactions, activated carbon (10% w/v) was stirred into the reaction solutions, and then removed by filtration. This step resulted in removal of approximately 90% of the ATP and ADP from the sample. The crude mixture was then diluted with H_2O to achieve a conductivity reading of < 5 mS per cm^2, and applied to a 6-ml Resource-Q anion exchange column, pre-equilibrated with H_2O. This phosphorylated compound was then eluted by a TEAB gradient (0 to 0.5 M over 20 CV) and detected by EPSPS activity tests, UV absorbance ($\lambda = 215$), or simply by time of elution. TEAB is volatile and was removed from the sample by rotary evaporation, with methanol added repeatedly, as necessary, to increase the rate of evaporation and replace the TEAB as solvent. The product was evaporated until dry, massed, and resuspended in

H_2O. Concentration was determined using the EPSPS phosphate release assay in the case of S3P, or based on mass or UV extinction in the case of the S3P-analogs.

Preaparative synthesis of shikimate analogs- For the preparative synthesis of the shikimate analogs described in the results, all reactions were carried out in 100 mM Na-HEPES, 50 mM KCl, 10 mM $MgCl_2$ and 2 mM DTT. The ATP and AMP were removed using activated carbon, as described, prior to anion-exchange purification.

Results and Discussion:

Shikimate-utilizing SK activity assays- Considering the very low sequence homology of the SK enzymes from *M. jannaschii* and *M. tuberculosis* (Fig. 9.3), the activity of these enzymes is remarkably similar. For maximum activity, both enzymes prefer similar reaction conditions. The K_m shikimate determinations (see Fig. 9.5) showed that these enzymes have comparable affinities for shikimate, and similar reaction velocities. The *M. tuberculosis* SK shows somewhat greater activity, but the *M. jannaschii* organism is thermophilic, so it may be expected that the *M. jannaschii* SK is more stable, and this may be particularly significant with longer reaction times. Both of these enzymes have been utilized for preparative S3P syntheses (typically allowed to run overnight); in both cases, the reactions ran to near-completion. Helpfully, the ADP-production assay allows one to verify that the reaction has been started, and also to determine the initial rate of the reaction and to estimate how much time is required to reach completion. Regarding preparative syntheses, it should be noted that substantial substrate inhibition was observed when using 10 mM ATP.

Fig. 9.5: SK utilization of Shikimate

(○) *M. tuberculosis* SK: V_{max} = 7.2 U/mg; K_m = 0.56 mM

(●) *M. jannaschii* SK: V_{max} = 4.7 U/mg; K_m = 0.50 mM

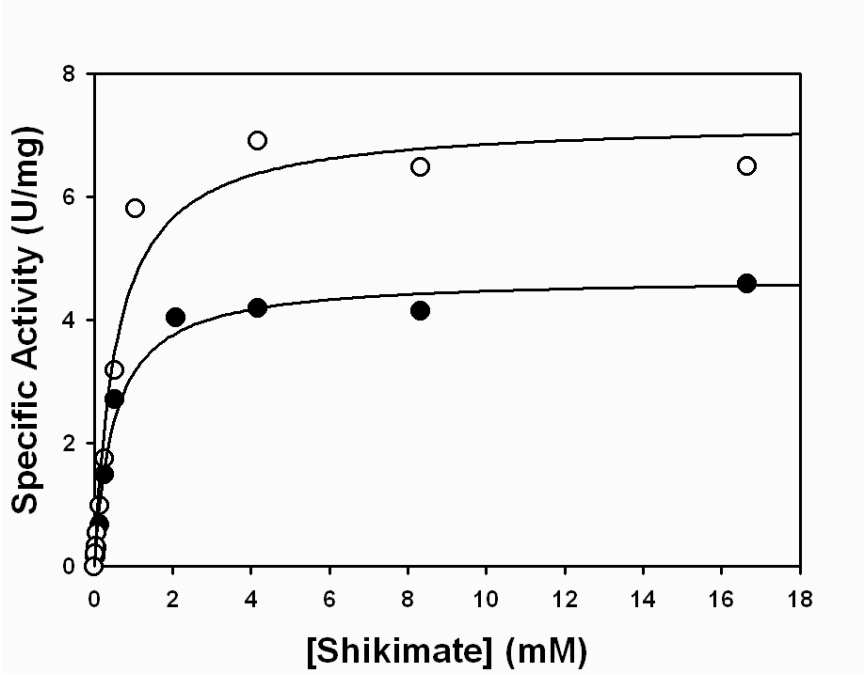

This suggests that to scale the enzymatic reactions, one should typically adjust the reaction volume, rather than the substrate concentration.

Shikimate analog phosphorylation trials- The assay described was used to probe the ability of these enzymes to phosphorylate analogs of shikimate. Only small amounts of the analog were available, precluding extensive testing, but the results were enlightening. Our hypothesis was that the divergent SK sequences were indicative of differences in the active-site structures; these in turn could result in differential affinity for the substrate analogs. While the *E. coli aroL* gene product, SK II, was not obtained, the results of our studies with the other two SK enzymes bear out this hypothesis.

Phosphorylation of the saturated analog of shikimate - Fig. 9.6 shows utilization of the saturated analog of shikimate by *M. tuberculosis* and *M. jannaschii* SK (see also Fig. 9.2). While the V_{max} of the enzymes is similar (*ca.* 1 U/mg), the K_m indicates that *M. jannaschii* binds this analog better (K_m = 1.4 mM, versus 3.5 mM for the *M. tuberculosis* SK). Based on this data, the *M. jannaschii* SK was utilized to phosphorylate the saturated shikimate analog.

For the preparative synthesis, an 11 ml overnight synthesis reaction was set up, containing 9 mM of the saturated shikimate, 12 mM ATP, and 0.1 mgs of *M. jannaschii* SK. The yield was estimated the following day using an endpoint assay to determine total ADP formation; the estimated yield was 56%, or 55.4 micromoles. This estimated yield is quite high considering the racemic character of the shikimate

Fig. 9.6: SK utilization of Saturated shikimate

(○)*M. tuberculosis* SK: V_{max} = 0.98 U/mg; K_m = 3.4 mM

(●) *M. jannaschii* SK: V_{max} = 1.1 U/mg; K_m = 1.4 mM

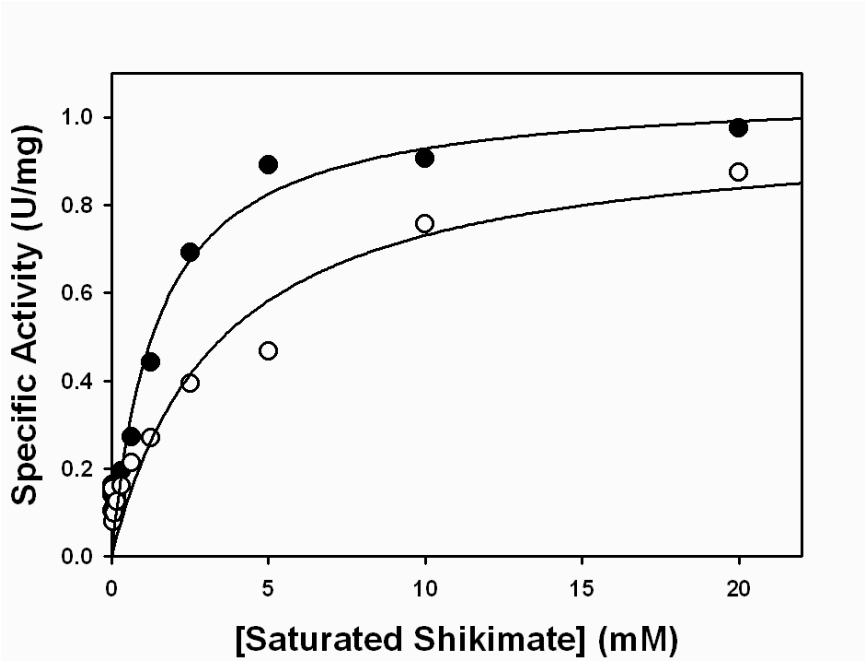

analogs. The saturated-S3P-analog was purified by anion exchange, as described. Since this compound has essentially no absorbance, the fractions where S3P normally elutes were collected.

Phosphorylation of the 5-Fluoro analog of shikimate- Fig. 9.7 shows utilization of the 5-fluoro analog of shikimate. In this case, the activity of the *M. tuberculosis* enzyme is 5-fold higher, and the K_m is halved compared to that exhibited by *M. jannaschii* SK. For the preperative synthesis of this analog, an 11 ml overnight synthesis reaction was set up, containing 9 mM of the 5-Fluoro shikimate, 12 mM ATP, and 0.1 mgs of *M. tuberculosis* SK. An additional 0.1 mgs of enzyme was added the following morning. The yield was estimated the following day using an endpoint assay to determine total ADP formation; the estimated yield was 41%, or 40.6 micromoles. Again, the analog was racemic, so this yield is very good. The 5-Fluoro-S3P-analog was purified by anion exchange, as described, and detected by UV scanning of the fractions.

Phosphorylation of the 5-deoxy analog of shikimate- Fig. 9.8 shows utilization of the 5-deoxy analog of shikimate. In this case, the activity of both enzymes is very low, but *M. tuberculosis* shows greater ability to utilized this substrate. The K_m values are indicate that this compound binds 10-fold better to these enzymes than does shikimate. It may be that the low signal-to-noise ratio produced aberrant data. Another possibility is that a synthetic contaminant was present and reduced enzyme activity at high concentrations. Further experiments would be helpful in determining

Fig. 9.7: SK utilization of 5-Fluoro-Shikimate

(○)*M. tuberculosis* SK: V_{max} = 1.2 U/mg; K_m = 0.53 mM

(●) *M. jannaschii* SK: V_{max} = 0.23 U/mg; K_m = 1.26 mM

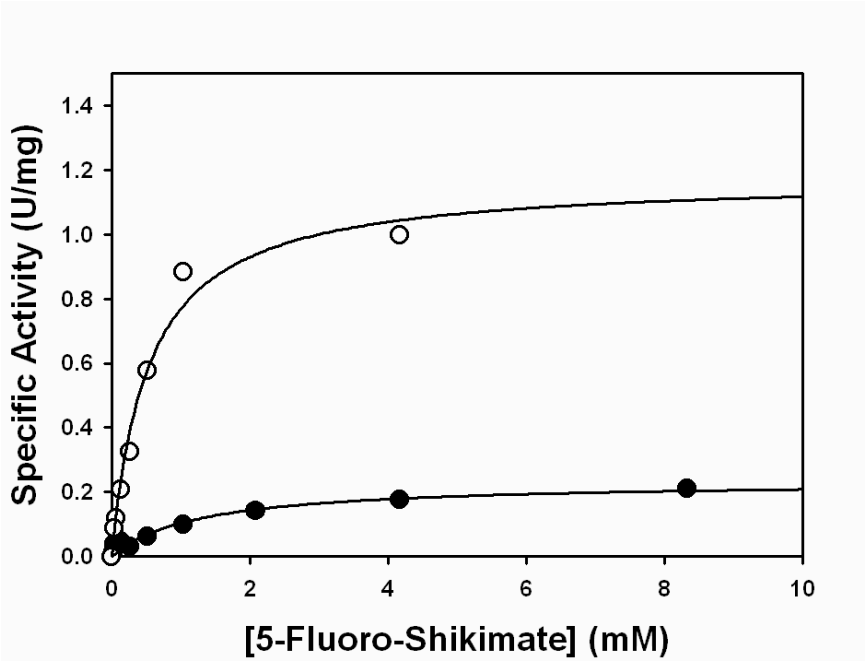

Fig. 9.8: SK utilization of 5-deoxy Shikimate

(○)*M. tuberculosis* SK: V_{max} = 0.22 U/mg; K_m = 0.041 mM

(●) *M. jannaschii* SK: V_{max} = 0.13 U/mg; K_m = 0.021 mM

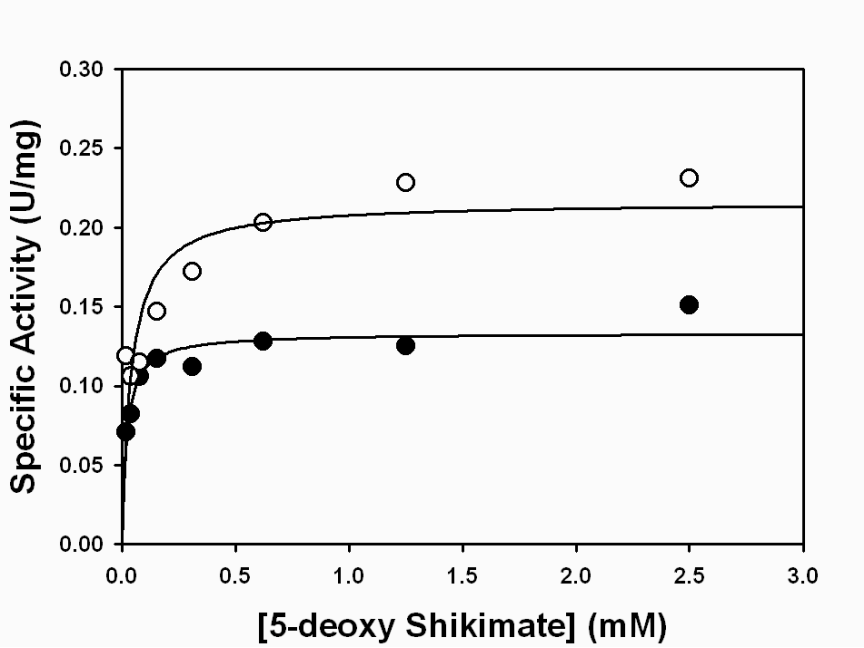

the basis for these unusual data. For the preparative synthesis of this analog, a 33 ml overnight synthesis reaction was set up, containing 3 mM of the 5-deoxy-shikimate analog, 6 mM ATP, and 0.2 mgs each of *M. tuberculosis* SK and *M. jannaschii* SK. An additional 0.1 mgs of each enzyme was added the following morning. The rationale for the large amount of enzyme was the low specific activity observed. The yield was estimated the following day using an endpoint assay to determine total ADP formation; the estimated yield was 24%, or 23.8 micromoles. This was better than expected based on the peculiar kinetic data. The 5-deoxy-S3P-analog was purified by anion exchange, as described, and detected by UV scanning of the fractions.

Phosphorylation of the 5-amino and the 4,5-deoxy analogs of shikimate- Not shown are the data concerning the utilization of the 5-amino analog of shikimate and the 4,5-deoxy analog of shikimate. Both of these showed no activity at concentrations of up to 20 mM. Preparative phosphorylation was not performed using the 5-amino shikimate analog. A single, possibly erroneous data point suggested that the 4,5-deoxy analog of shikimate could be phosphorylated by *M. jannaschii* SK if the analog were very concentrated (*ca*. 40 mM). A 7 ml overnight preparative synthesis reaction was set up, containing 30 mM 4,5-deoxy shikimate, 40 mM ATP, and 0.2 mgs of *M. jannaschii* SK. A precipitate formed, and no product was observed the following day. On the hypothesis that the precipitate was interfering with assay for detecting product formation, purification was attempted by anion exchange. The sample did not bind to the column, likely indicating the absence of the phosphate moiety. Additionally, the

ADP peak was not observed, suggesting that no ADP, and hence no S3P analog, were produced. The flow through was collected and frozen for later use. It is possible that another SK enzyme (such as *E. coli* SK II) could phosphorylate these compounds. More testing remains to be done.

Phosphorylation of Shikimate- As a control for these shikimate analog phosphorylation experiments, a 40 ml overnight reaction was set up containing 9 mM shikimate, 12 mM ATP, and 0.1 mgs *M. jannaschii* SK. The yield was estimated at 109%. This result is likely due to ATP auto-hydrolysis and variance resulting from single data points obtained after serial dilution. The yield of this 40 ml S3P synthesis reaction was 360 micromoles, nearly 90 mgs of S3P, demonstrating the utility of this enzymatic synthesis for the production of S3P.

Conclusions:

The production of the *E. coli* SK requires further analysis and troubleshooting, and the purification procedure for the *M. tuberculosis* SK should be modified to improve reproducibility. The production and purification procedures described here for S3P do work well and offer significant advantages in comparison to those utilized previously. This optimized procedure allows monitoring of the phosphoryl transfer reaction, requires only a one-column purification, uses significantly less TEAB, and achieves yields of over 90% with respect to shikimate. Further, the SK activity assay

developed here can be used to study SK enzymes from diverse species, and should aid investigation of these drug targets. Finally, three of the five shikimate analogs tested were successfully phosphorylated and purified. Testing and co-crystallization experiments will be conducted to examine the interaction of these S3P-analogs with EPSPS.

Chpt. 10: Summary and Conclusions

The results presented here summarize our work toward understanding the structure, function, and inhibition of EPSPS enzymes, toward an overall goal of the development of novel inhibitors with antimicrobial and herbicidal properties.

Prior to this work, very little information was available concerning the structure, function, or inhibition of class II EPSPS enzymes. We biochemically characterized two class II enzymes, EPSPS from the pathogen *S. aureus* and the economically important EPSPS from *Agrobacterium sp.* strain CP4. We succeeded in determining the structure of CP4 EPSPS, revealing the structural basis of glyphosate insensitivity exhibited by this enzyme. It is believed that this enzyme can be a useful model, facilitating comparative analyses with respect to other EPSPS enzymes. Significant structural and functional differences must be accounted for in attempts to develop broad-spectrum EPSPS inhibitors, as indicated by the differential inhibition observed with respect to the TI analogs studied in chapter 8.

Our analysis of mutation-induced glyphosate resistance shows that glyphosate tolerance can be induced without decreasing substrate affinity, but reduced catalytic activity is observed. Such mutations were studied previously in efforts to develop glyphosate-resistant crops, and will likely continue to be examined due to the emergence of glyphosate-tolerant weeds. Our studies suggest that more global coverage of the active site may delay the development of resistance; this should be

considered for the design of durable second-generation EPSPS. Until suitable glyphosate replacements are available, strategies should be implemented to slow the development and reduce the spread of glyphosate resistant weeds.

The use of alternate (non-substrate) ligands can be useful for exploration of substrate recognition and induced fit mechanisms. This approach was utilized using a precursor (shikimate), TI analogs (SP-TI, RP-TI, and 2F-TI), using and extrinsic fluorophore (ANS), and using a variety of drug-like compounds (HTS experiment). This course of study should be further expanded by the utilization of the S3P analogs produced in Chapter 9 to probe EPSPS, and our hope is that these results will provide a theoretical framework to facilitate structure-based drug design.

These studies have greatly improved our understanding of the structure, function, and inhibition of EPSPS. It is our belief that further efforts toward the development of novel EPSPS inhibitors will be crucial to the on-going struggle against agricultural pests and human pathogens.

References Cited:

1. Schonbrunn, E.; Eschenburg, S.; Luger, K.; Kabsch, W.; Amrhein, N., Structural basis for the interaction of the fluorescence probe 8- anilino-1-naphthalene sulfonate (ANS) with the antibiotic target MurA. *Proceedings of the National Academy of Sciences of the United States of America* **2000,** 97, (12), 6345-6349.

2. Herrmann, K. M.; Weaver, B., The shikimate pathway. *Annual Review of Plant Physiology and Plant Molecular Biology* **1999,** 50, 473-503.

3. Campbell SA; Richards TA; Mui EJ; Samuel BU; Coggins JR; McLeod R; Roberts CW, A complete shikimate pathway in Toxoplasma gondii: an ancient eukaryotic innovation. *Int J Parasitol.* **2004,** 34, (1), 5-13.

4. Woese, C. R.; Balch, W. E.; Magrum, L. J.; Fox, G. E.; Wolfe, R. S., An ancient divergence among the bacteria. *Journal of Molecular Evolution* **1977,** 9, 305-311.

5. Richards, T. A.; Dacks, J. B.; Campbell, S. A.; Blanchard, J. L.; Foster, P. G.; McLeod, R.; Roberts, C. W., Evolutionary Origins of the Eukaryotic Shikimate Pathway: Gene Fusions, Horizontal Gene Transfer, and Endosymbiotic Replacements. *Eukaryotic Cell* **2006,** 5, 1517-1531.

6. Roberts, C. W.; Roberts, F.; Lyons, R. E.; Kirisits, M. J.; Mui, E. J.; Finnerty, J.; Johnson, J. J.; Ferguson, D. J.; Coggins, J. R.; Krell, T.; Coombs, G. H.; Milhous, W. K.; Kyle, D. E.; Tzipori, S.; Barnwell, J.; Dame, J. B.; Carlton, J.; McLeod, R., The shikimate pathway and its branches in apicomplexan parasites. *Journal of Infectious Diseases* **2002,** 185, S25-S36.

7. Starcevic, A.; Akthar, S.; Dunlap, W. C.; Shick, J. M.; Hranueli, D.; Cullum, J.; Long, P. F., *Proc Natl Acad Sci U S A.* **2008,** 105, (7), 2533-7.

8. Herrmann, K. M., The Shikimate Pathway: Early Steps in the Biosynthesis of Aromatic Compounds. *Plant Cell* **1995,** 7, (7), 907-919.

9. Steinrucken, H. C.; Amrhein, N., The herbicide glyphosate is a potent inhibitor of 5-enolpyruvyl- shikimic acid-3-phosphate synthase. *Biochemical and Biophysical Research Communications* **1980,** 94, (4), 1207-1212.

10. Jaworski, E. G., Mode of action of N-phosphonomethylglycine. Inhibition of aromatic amino acid biosynthesis. *Journal of Agricultural and Food Chemistry* **1972,** 20, (6), 1195-1198.

11. Boocock, M. R.; Coggins, J. R., Kinetics of 5-enolpyruvylshikimate-3-phosphate synthase inhibition by glyphosate. *FEBS Letters* **1983,** 154, (1), 127-133.

12. Bentley, R., The shikimate pathway--a metabolic tree with many branches. *Critical Reviews in Biochemistry and Molecular Biology* **1990,** 25, (5), 307-384.

13. Haslam, E., *Shikimic acid: metabolism and metabolites*. John Wiley & Sons: Chichester, UK, 1993.

14. Kishore, G. M.; Shah, D. M., Amino acid biosynthesis inhibitors as herbicides. *Annual Review of Biochemistry* **1988,** 57, 627-663.

15. Buzzola, F. R., Barbagelata, M.S., Caccuri, R.L., and Sordelli, D.O., Attenuation and Persistence of and Ability To Induce Protective Immunity to a Staphylococcus aureus aroA Mutant in Mice. *Infection and Immunity* **2006,** 74, (6), 3498-506.

16. McDevitt, D.; Payne, D. J.; Holmes, D. J.; Rosenberg, M., Novel targets for the future development of antibacterial agents. *Journal of Applied Microbiology* **2002,** 92, (Suppl), 28S-34S.

17. McArthur, J. D.; West, N. P.; Cole, J. N.; Jungnitz, H.; Guzman, C. A.; Chin, J.; Lehrbach, P. R.; Djordjevic, S. P.; Walker, M. J., An aromatic amino acid auxotrophic mutant of *Bordetella bronchiseptica* is attenuated and immunogenic in a mouse model of infection. *FEMS Microbiology Letters* **2003,** 221, (1), 7-16.

18. Ferreras, J. A.; Ryu, J.-S.; Lello, F. D.; Tan, D. S.; Quadri, L. E. N., Small-molecule inhibition of siderophore biosynthesis in Mycobacterium tuberculosis and Yersinia pestis. *Nat Chem Biol* **2005,** 1, (1), 29-32.

19. Crosa, J. H.; Walsh, C. T., Genetics and Assembly Line Enzymology of Siderophore Biosynthesis in Bacteria. *Microbiol. Mol. Biol. Rev.* **2002,** 66, (2), 223-249.

20. Roberts, F.; Roberts, C. W.; Johnson, J. J.; Kyle, D. E.; Krell, T.; Coggins, J. R.; Coombs, G. H.; Milhous, W. K.; Tzipori, S.; Ferguson, D. J.; Chakrabarti, D.; McLeod, R., Evidence for the shikimate pathway in apicomplexan parasites. *Nature* **1998,** 393, (6687), 801-805.

21. Park, H.; Hilsenbeck, J. L.; Kim, H. J.; Shuttleworth, W. A.; Park, Y. H.; Evans, J. N.; Kang, C., Structural studies of *Streptococcus pneumoniae* EPSP synthase in unliganded state, tetrahedral intermediate-bound state and S3P-GLP-bound state. *Molecular Microbiology* **2004,** 51, (4), 963-971.

22. Schonbrunn, E.; Eschenburg, S.; Shuttleworth, W. A.; Schloss, J. V.; Amrhein, N.; Evans, J. N.; Kabsch, W., Interaction of the herbicide glyphosate with its target enzyme 5- enolpyruvylshikimate 3-phosphate synthase in atomic detail. *Proceedings of the National Academy of Sciences of the United States of America* **2001,** 98, (4), 1376-1380.

23. Stallings, W. C.; Abdel-Meguid, S. S.; Lim, L. W.; Shieh, H. S.; Dayringer, H. E.; Leimgruber, N. K.; Stegeman, R. A.; Anderson, K. S.; Sikorski, J. A.; Padgette, S. R.; Kishore, G. M., Structure and topological symmetry of the glyphosate target 5- enolpyruvylshikimate-3-phosphate synthase: a distinctive protein fold. *Proceedings of the National Academy of Sciences of the United States of America* **1991,** 88, (11), 5046-5050.

24. Eschenburg, S.; Kabsch, W.; Healy, M. L.; Schonbrunn, E., A new view of the mechanisms of UDP-N-acetylglucosamine enolpyruvyl transferase (MurA) and 5-

enolpyruvylshikimate-3-phosphate synthase (AroA) derived from X-ray structures of their tetrahedral reaction intermediate states. *Journal of Biological Chemistry* **2003,** 278, (49), 49215-49222.

25. An, M.; Maitra, U.; Neidlein, U.; Bartlett, P. A., 5-Enolpyruvylshikimate 3-phosphate synthase: chemical synthesis of the tetrahedral intermediate and assignment of the stereochemical course of the enzymatic reaction. *Journal of the American Chemical Society* **2003,** 125, (42), 12759-12767.

26. Alberg, D. G.; Lauhon, C. T.; Nyfeler, R.; Fassler, A.; Bartlett, P. A., Inhibition of EPSP synthase by analogues of the tetrahedral intermediate and EPSP. *Journal of the American Chemical Society* **1992,** 114, 3535-3546.

27. Coggins, J. R.; Abell, C.; Evans, L. B.; Frederickson, M.; Robinson, D. A.; Roszak, A. W.; Lapthorn, A. P., Experiences with the shikimate-pathway enzymes as targets for rational drug design. *Biochem. Soc. Trans.* **2003,** 31, (Pt 3), 548-552.

28. Priestman, M. A.; Healy, M. L.; Becker, A.; Alberg, D. G.; Bartlett, P. A.; Lushington, G. H.; Schonbrunn, E., The interaction of phosphonate analogs of the tetrahedral reaction intermediate with 5-enolpyruvylshikimate-3-phosphate synthase (EPSPS) in atomic detail. *Biochemistry* **2005,** 44, 3241-3248.

29. Franz, J. E.; Mao, M. K.; Sikorski, J. A., *Glyphosate: a unique global herbicide*. American Chemical Society: Washington DC, 1997; Vol. 189.

30. Williams, G. M.; Kroes, R.; Munro, I. C., Safety Evaluation and Risk Assessment of the Herbicide Roundup and Its Active Ingredient, Glyphosate, for Humans. *Regulatory Toxicology and Pharmacology* **2000,** 31, (2).

31. Smith, E. A.; Oehme, F. W., The biological activity of glyphosate to plants and animals: a literature review. *Veterinary and human toxicology* **1992,** 34., (6), 531-43.

32. Board, A. S., Acreage. *U.S. Department of Agriculture, National Agricultural Statistics Service* **2007**.

33. Schulz, A.; Krueper, A.; Amrhein, N., Differential sensitivity of bacterial 5-enolpyruvylshikimate 3-phosphate synthetases to the herbicide glyphosate. *FEMS Microbiology Letters* **1985,** 28, (3), 297-301.

34. Powell, H. A.; Kerby, N. W.; Rowell, P., Natural tolerance of cyanobacteria to the herbicide glyphosate. *New Phytologist* **1991,** 119, (3), 421-426.

35. Barry, G. F., Kishore, G. M. , Padgette, S. R. Glyphosate Tolerant 5-Enolpyruvylshikimate-3-phosphate synthases. 1992.

36. Fitzgibbon, J. E.; Braymer, H. D., Cloning of a gene from Pseudomonas sp. strain PG2982 conferring increased glyphosate resistance. *Applied and Environmental Microbiology* **1990,** 56, (11), 3382-3388.

37. Schulz, A.; Kruper, A.; Amrhein, N., Differential sensitivity of bacterial 5-enolpyruvylshikimate-3-phosphate synthases to the herbicide glyphosate. *FEMS Microbiology Letters* **1985,** 28, (3), 297-301.

38. McDonald, L., Trends in antimicrobial resistance in health care-associated pathogens and effect on treatment. *Clin Infect Dis.* **2006,** 42, (Suppl 2), S65-71.

39. Service, R. F., AGBIOTECH: A Growing Threat Down on the Farm. *Science* **2007,** 316, (5828), 1114-1117.

40. Service, R. F., AGBIOTECH: Glyphosate--The Conservationist's Friend? *Science* **2007,** 316, (5828), 1116-1117.

41. Gardner, J.; Nelson, G., Herbicides, glyphosate resistance and acute mammalian toxicity: simulating an environmental effect of glyphosate-resistant weeds in the USA. *Pest Management Science* **2008,** 64, (4), 470-8.

42. Duke SO, P. S., Glyphosate: a once-in-a-century herbicide. *Pest Management Science* **2008,** 64, (4), 319-25.

43. Eschenburg, S.; Healy, M. L.; Priestman, M. A.; Lushington, G. H.; Schonbrunn, E., How the mutation glycine96 to alanine confers glyphosate insensitivity to 5-enolpyruvyl shikimate-3-phosphate synthase from *Escherichia coli*. *Planta* **2002,** 216, (1), 129-135.

44. Bradford, M. M., A rapid and sensitive method for the quantitation of microgram quantities of protein utilizing the principle of protein-dye binding. *Analytical Biochemistry* **1976,** 72, 248-254.

45. Priestman, M. A.; Funke, T.; Singh, I. M.; Crupper, S. S.; Schonbrunn, E., 5-Enolpyruvylshikimate-3-phosphate synthase from *Staphylococcus aureus* is insensitive to glyphosate. *FEBS Letters* **2005,** 579, 728-732.

46. Daugherty, M.; Vonstein, V.; Overbeek, R.; Osterman, A., Archaeal shikimate kinase, a new member of the GHMP-kinase family. *Journal of Bacteriology* **2001,** 183, (1), 292-300.

47. Lanzetta, P. A.; Alvarez, L. J.; Reinach, P. S.; Candia, O. A., An improved assay for nanomole amounts of inorganic phosphate. *Analytical Biochemistry* **1979,** 100, 95-97.

48. Kabsch, W., Automatic procession of rotation diffraction data from crystals of initially unknown symmetry and cell constrants. *Journal of Applied Crystallography* **1993,** 26, 795-800.

49. Otwinowski, Z.; Minor, W., Processing of x-ray diffraction data collected in oscillation mode. *Methods in Enzymology* **1997,** 276, 307-326.

50. Brünger AT; Adams PD; Clore GM; DeLano WL; Gros P; Grosse-Kunstleve RW; Jiang JS; Kuszewski J; Nilges M; Pannu NS; Read RJ; Rice LM; Simonson T; GL, W., Crystallography & NMR system: A new software suite for macromolecular

structure determination. *Acta crystallographica. Section D, Biological crystallography* **1998,** 54, (part 5), 905-921.

51. Jones, T. A.; Zou, J. Y.; Cowan, S. W.; Kjeldgaard, Improved methods for building protein models in electron density maps and the location of errors in these models. *Acta Crystallographica. Section B, Structural Science* **1991,** 47, (Pt 2), 110-119.

52. Funke, T.; Han, H.; Healy-Fried, M. L.; Fischer, M.; Schoenbrunn, E., Molecular Basis for the Herbicide Resistance of Roundup Ready Crops. *Proceedings of the National Academy of Sciences of the United States of America* **2006,** 103, (35), 13010-13015.

53. DeLano, W. L., The PyMOL molecular graphics system. *DeLano Scientific, http://www.pymol.org* **2003**.

54. Kraulis, P. J., MOLSCRIPT: a program to produce both detailed and schematic plots of protein structures. *Journal of Applied Crystallography* **1991,** 24, 946-950.

55. Esnouf, R. M., An extensively modified version of MolScript that includes greatly enhanced coloring capabilities. *Journal of Molecular Graphics and Modelling* **1997,** 15, (2), 132-134.

56. Merrit, E. A.; Bacon, D. J., Raster3D: Photorealistic Molecular Graphics. *Methods in Enzymology* **1997,** 277, 505-524.

57. Miller, M. J.; Anderson, K. S.; Braccolino, D. S.; Cleary, D. G.; Gruys, K. J.; Han, C. Y.; Lin, K.-C.; Pansegrau, P. D.; Ream, J. E.; Sammons, D.; Sikorski, J. A., EPSP synthase inhibitor design II. The importance of the 3-phosphate group for ligand binding at the shikimate-3-phosphate site and the identification of 3-malonate ethers as novel 3-phosphate mimics. *Bioorganic and Medicinal Chemistry Letters* **1993,** 3, (7), 1435-1440.

58. Stauffer, M. E.; Young, J. K.; Helms, G. L.; Evans, J. N., Chemical shift mapping of shikimate-3-phosphate binding to the isolated N-terminal domain of 5-enolpyruvylshikimate-3-phosphate synthase. *FEBS Letters* **2001,** 499, (1-2), 182-186.

59. Priestman MA; Healy ML; Funke T; Becker A; E., S., Molecular basis for the glyphosate-insensitivity of the reaction of 5-enolpyruvylshikimate 3-phosphate synthase with shikimate. *FEBS Letters* **2005,** 579, (25), 5773-80.

60. An, M.; Bartlett, P. A., Enzymatic synthesis of a ring-contracted analogue of 5-enolpyruvylshikimate-3-phosphate. *Organic Letters* **2004,** 6, (22), 4065-4067.

61. Gruys, K. J.; Walker, M. C.; Sikorski, J. A., Substrate synergism and the steady-state kinetic reaction mechanism of EPSP synthase from *Escherichia coli*. *Biochemistry* **1992,** 31, 5534-5544.

62. Funke, T.; Healy-Fried, M. L.; Han, H.; Alberg, D. G.; Bartlett, P. A.; Schonbrunn, E., Differential Inhibition of Class I and Class II 5-

Enolpyruvylshikimate-3-phosphate Synthases by Tetrahedral Reaction Intermediate Analogues. *Biochemistry* **2007,** 46, (46), 13344-13351.

63. Casey, A. L.; Lambert, P. A.; Elliot, T. S. J., Staphylococci. *International Journal of Antimicrobial Agents* **2007,** 29, (Suppl. 3), S23-S32.

64. Rice, L. B., Antimicrobial resistance in gram-positive bacteria. *American Journal of Infection Contro* **2006,** 34, (5, supplement 1), S11-S19.

65. Barrett, C. T.; Barrett, J. F., Antibacterials: are the new entries enough to deal with the emerging resistance problems? *Current Opinion in Biotechnology* **2003,** 14, (6), 621-626.

66. Norrby SR; Nord CE; R;, F., Lack of development of new antimicrobial drugs: a potential serious threat to public health. *The Lancet Infectious Diseases* **2005,** 5, (2), 115-9.

67. Fischer, R. S.; Rubin, J. L.; Gaines, C. G.; Jensen, R. A., Glyphosate sensitivity of 5-enol-pyruvylshikimate-3-phosphate synthase from Bacillus subtilis depends upon state of activation induced by monovalent cations. *Archives of Biochemistry and Biophysics* **1987,** 256, (1), 325-34.

68. Du, W.; Wallis, N. G.; Mazzulla, M. J.; Chalker, A. F.; Zhang, L.; Liu, W. S.; Kallender, H.; Payne, D. J., Characterization of *Streptococcus pneumoniae* 5-enolpyruvylshikimate 3- phosphate synthase and its activation by univalent cations. *European Journal of Biochemistry* **2000,** 267, (1), 222-227.

69. Healy-Fried, M. L.; Funke, T.; Priestman, M. A.; Han, H.; Schonbrunn, E., Structural Basis of Glyphosate Tolerance Resulting from Mutations of Pro101 in Escherichia coli 5-Enolpyruvylshikimate-3-phosphate Synthase. *J. Biol. Chem.* **2007,** 282, (45), 32949-32955.

70. Powles, S. B.; Preston, C., Evolved Glyphosate Resistance in Plants: Biochemical and Genetic Basis of Resistance. *Weed Technology* **2006,** 20, (2), 282-289.

71. Stalker, D. M.; Hiatt, W. R.; Comai, L., A single amino acid substitution in the enzyme 5-enolpyruvylshikimate-3- phosphate synthase confers resistance to the herbicide glyphosate. *Journal of Biological Chemistry* **1985,** 260, (8), 4724-4728.

72. Barry, G. F.; Kishore, G. M.; Padgette, S. R.; C., S. W. Glyphosate-Tolerant 5-Enolpyruvylshikimate-3-Phosphate Synthases. 5633435, 1997.

73. Duke, S. O.; Powles, S. B., Glyphosate-Resistant Weeds and Crops. *Pest Management Science* **2008,** 64, (4), 317-318.

74. Amrhein, N.; Deus, B.; Gehrke, P.; Steinruecken, H. C., The site of the inhibition of the shikimate pathway by glyphosate. II. Interference of glyphosate with chorismate formation in vivo and in vitro. *Plant Physiology* **1980,** 66, (5), 830-4.

75. Comai, L.; Sen, L. C.; Stalker, D. M., An altered aroA gene product confers resistance to the herbicide glyphosate. *Science* **1983,** 221, (4608), 370-371.

76. Rogers, S. G.; Brand, L. A.; Holder, S. B.; Sharps, E. S.; Brackin, M. J., Amplification of the aroA gene from *Escherichia coli* results in tolerance to the herbicide glyphosate. *Applied and Environmental Microbiology* **1983,** 46, (1), 37-43.

77. Nafziger, E. D.; Widholm, J. M.; Steinrucken, H. C.; Killmer, J. L., Selection and characterization of a carrot cell line tolerant to glyphosate. *Plant Physiology* **1984,** 76, 571-574.

78. Sost, D.; Schulz, A.; Amrhein, N., Characterization of a glyphosate-insensitive 5-enolpyruvylshikimic acid-3-phosphate synthase. *FEBS Letters* **1984,** 173, (1), 238-242.

79. Smart, C. C.; Johanning, D.; Muller, G.; Amrhein, N., Selective overproduction of 5-enol-pyruvylshikimic acid 3-phosphate synthase in a plant cell culture which tolerates high doses of the herbicide glyphosate. *Journal of Biological Chemistry* **1985,** 260, (30), 16338-16346.

80. Spencer, M.; Mumm, R.; Gwyn, J., Glyphosate resistant maize lines. *US Patent 6040497* **1997**.

81. Gasser, C. S.; Winter, J. A.; Hironaka, C. M.; Shah, D. M., Structure, expression, and evolution of the 5-enolpyruvylshikimate-3- phosphate synthase genes of petunia and tomato. *Journal of Biological Chemistry* **1988,** 263, (9), 4280-4287.

82. Duke, S. O., Herbicide-Resistant Crops: Agricultural, Environmental, Economic, Regulatory, and Technical Aspects. *Book* **1996**, Chapter 4, pages 53-80.

83. Steinrucken, H. C.; Amrhein, N., 5-enolpyruvylshikimate-3-phosphate synthase of *Klebsiella pneumoniae* 2. Inhibition by glyphosate [N-(phosphonomethyl)glycine]. *European Journal of Biochemistry* **1984,** 143, (2), 351-357.

84. Preston, C.; Wakelin, A. M., Resistance to glyphosate from altered herbicide translocation patterns. *Pest Management Science* **2008,** 64, (4), 372-376.

85. Perez-Jones, A.; Park, K.-W.; Polge, N.; Colquhoun, J.; Mallory-Smith, C., Investigating the mechanisms of glyphosate resistance in Lolium multiflorum. *Planta* **2007,** 226, (2), 395-404.

86. Wakelin, A. M.; Lorraine-Colwill, D. F.; Preston, C., Glyphosate resistance in four different populations of Lolium rigidum is associated with reduced translocation of glyphosate to meristematic zones. *Weed Research* **2004,** 44, (6), 453-459.

87. Amrhein, N.; Johanning, D.; Schab, J.; Schulz, A., Biochemical basis for glyphosate-tolerance in a bacterium and plant tissue culture. *FEBS Letters* **1983,** 157, (1), 191-196.

88. Shyr, Y. Y.; Hepburn, A. G.; Widholm, J. M., Glyphosate selected amplification of the 5-enolpyruvylshikimate-3-phosphate synthase gene in cultured carrot cells. *Molecular and General Genetics* **1992,** 232, (3), 377-382.

89. Reinbothe, S.; Ortel, B.; Parthier, B., Overproduction by gene amplification of the multifunctional arom protein confers glyphosate tolerance to a plastid-free mutant of *Euglena gracilis*. *Molecular and General Genetics* **1993,** 239, (3), 416-424.

90. Sost, D.; Amrhein, N., Substitution of Gly-96 to Ala in the 5-enolpyruvylshikimate-3-phosphate synthase of *Klebsiella pneumoniae* results in a greatly reduced affinity for the herbicide glyphosate. *Archives of Biochemistry and Biophysics* **1990,** 282, (2), 433-436.

91. Alan, E. D.; Scott, G. C.; Kishore, G. M. Modified gene encoding glyphosate-tolerant 5-enolpyruvyl-3-phosphoshikimate synthase. 6,225,114, May 1, 2001, 2001.

92. Kahrizi, D.; Salmanian, A. H.; Afshari, A.; Moieni, A.; Mousavi, A., Simultaneous substitution of Gly96 to Ala and Ala183 to Thr in 5-enolpyruvylshikimate-3-phosphate synthase gene of E. coli (k12) and transformation of rapeseed (Brassica napus L.) in order to make tolerance to glyphosate. *Plant Cell Rep* **2007,** 26, (1), 95-104.

93. Tan S, E. R., Singh B, Herbicidal inhibitors of amino acid biosynthesis and herbicide-tolerant crops. *Amino Acids* **2006,** 30, (2), 195-204.

94. Jacob, G. S.; Garbow, J. R.; Hallas, L. E.; Kimack, N. M.; Kishore, G. M.; Schaefer, J., Metabolism of glyphosate in *Pseudomonas sp.* strain LBr. *Applied and Environmental Microbiology* **1988,** 54, (12), 2953-2958.

95. Balthazor, T.; Hallas, L., Glyphosate-Degrading Microorganisms from Industrial Activated Sludge. *Appl Environ Microbiol.* **1986,** 51, (2), 432-434.

96. Obojska, A.; Ternan, N.; Lejczak, B.; Kafarski, P.; McMullan, G., Organophosphonate utilization by the thermophile Geobacillus caldoxylosilyticus T20. *Appl Environ Microbiol* **2002,** 68, (4), 2081-4.

97. Padgette, S. R.; Kolacz, K. H.; Delannay, X.; Re, D. B.; LaVallee, B. J.; CTinius, C. N.; Rhodes, W. K.; Otero, Y. I.; Barry, G. F.; Eichholz, D. A.; Peshke, V. M.; Nida, D. L.; Taylor, N. B.; Kishore, G. M., Development, Identification, and Characterization of a Glyphosate-Tolerant Soybean Line. *Crop Science* **1995,** 35, 1451-1461.

98. Schmidt, M. W.; Baldridge, K. K.; Boatz, J. A.; Elbert, S. T.; Gordon, M. S.; Jensen, J. H.; Koseki, S.; Matsunaga, N.; Nguyen, K. A.; Su, S.; Windus, T. L.; Dupuis, M.; J.A. Montgomery, J., General atomic and molecular electronic structure system. *J. Comput. Chem.* **1993**, (14), 1347–1363.

99. Schroeder, J. I.; Ward, J. M.; Gassmann, W., Perspectives on the Physiology and Structure of Inward rectifying K Channels in Higher Plants: Biophysical

Implications for K Uptake. *Annual Review of Biophysics and Biomolecular Structure* **1994,** 23, (1), 441-471.

100. Baerson, S. R.; Rodriguez, D. J.; Tran, M.; Feng, Y.; Biest, N. A.; Dill, G. M., Glyphosate-resistant goosegrass. Identification of a mutation in the target enzyme 5-enolpyruvylshikimate-3-phosphate synthase. *Plant Physiology* **2002,** 129, (3), 1265-1275.

101. McConkey, G. A., Targeting the shikimate pathway in the malaria parasite *Plasmodium falciparum*. *Antimicrobial Agents and Chemotherapy* **1999,** 43, (1), 175-177.

102. Alibhai, M. F.; Stallings, W. C., Closing down on glyphosate inhibition--with a new structure for drug discovery. *Proceedings of the National Academy of Sciences of the United States of America* **2001,** 98, (6), 2944-2946.

103. Board, A. S., Acreage. In U.S. Dept. of Agriculture, N. A. S. S., Ed. 2005.

104. Padgette, S. R.; Re, D. B.; Gasser, C. S.; Eichholtz, D. A.; Frazier, R. B.; Hironaka, C. M.; Levine, E. B.; Shah, D. M.; Fraley, R. T.; Kishore, G. M., Site-directed mutagenesis of a conserved region of the 5- enolpyruvylshikimate-3-phosphate synthase active site. *Journal of Biological Chemistry* **1991,** 266, (33), 22364-22369.

105. He, M.; Nie, Y. F.; Xu, P., A T42M substitution in bacterial 5-enolpyruvylshikimate-3-phosphate synthase (EPSPS) generates enzymes with increased resistance to glyphosate. *Bioscience, Biotechnology, and Biochemistry* **2003,** 67, (6), 1405-1409.

106. Spencer, M.; Mumm, R.; Gwyn, J., Glyphosate resistant maize lines. *U.S. Patent 6,040,497* **2000**.

107. Lebrun, M.; Sailland, A.; Freyssinet, G.; Degryse, E., Mutated 5-enolpyruvylshikimate-3-phosphate synthase, gene coding for said protein and transformed plants containing said gene *U.S Patent 6,566,587* **2003**.

108. Ng, C. H.; Wickneswari, R.; Salmijah, S.; Teng, Y. T.; Ismail, B. S., Gene polymorphisms in glyphosate-resistant and -susceptible biotypes of Eleusine indica from Malaysia. *Weed Research* **2003,** 43, (2), 108-115.

109. Yu, Q.; Cairns, A.; Powles, S., Glyphosate, paraquat and ACCase multiple herbicide resistance evolved in a Lolium rigidum biotype. *Planta* **2007,** 225, (2), 499-513.

110. Eichholtz, D. A.; Scott, G. C.; Murthy, K. G., Modified gene encoding glyphosate-tolerant 5-enolpruvyl-3-phosphoshikimate synthase. *U.S Patent 6,225,114* **2001**.

111. Reddy, K. N., Weed control and species shift in bromoxynil- and glyphosate-resistant cotton. *Weed Technology* **2004,** 18, 131-139.

112. Behrens MR; Mutlu N; Chakraborty S; Dumitru R; Jiang WZ; Lavallee BJ; Herman PL; Clemente TE; Weeks DP, Dicamba resistance: enlarging and preserving biotechnology-based weed management strategies. *Science* **2007,** 316, (5828), 1185-8.

113. Du, W.; Liu, W. S.; Payne, D. J.; Doyle, M. L., Synergistic inhibitor binding to *Streptococcus pneumoniae* 5- enolpyruvylshikimate-3-phosphate synthase with both monovalent cations and substrate. *Biochemistry* **2000,** 39, (33), 10140-10146.

114. Spencer, M.; Mumm, R.; Gwyn, J. Glyphosate resistant maize lines. 6040497, March 21, 2000.

115. Sidhu, R. S.; Hammond, B. G.; Fuchs, R. L.; Mutz, J.-N., Holden, ; L.R., G., B., ; Olson, T., *J. Agric. Food Chem.* **2000,** 48, (6), 2305-2312.

116. Wang, Y. X.; Jones, J. D.; Weller, S. C.; Goldsbrough, P. B., Expression and stability of amplified genes encoding 5-enolpyruvylshikimate-3-phosphate synthase in glyphosate-tolerant tobacco cells. *Plant Molecular Biology* **1991,** 17, (6), 1127-1138.

117. Alberg, D. G.; Bartlett, P. A., Potent inhibition of 5-enolpyruvylshikimate-3-phosphate synthase by a reaction intermediate analogue. *Journal of the American Chemical Society* **1989,** 11, 2337-2338.

118. Shah, A.; Font, J. L.; Miller, M. J.; Ream, J. E.; Walker, M. C.; Sikorski, J. A., New aromatic inhibitors of EPSP synthase incorporating hydroxymalonates as novel 3-phosphate replacements. *Bioorganic and Medicinal Chemistry* **1997,** 5, (2), 323-334.

119. Peterson, M. L.; Corey, S. D.; Font, J. L.; Walker, M. C.; Sikorski, J. A., New simplified inhibitors of EPSP synthase: the importance of ring size for recognition at the shikimate 3-phosphate site. *Bioorganic and Medicinal Chemistry Letters* **1996,** 6, (23), 2853-2858.

120. Pansegrau, P. D.; Anderson, K. S.; Widlanski, T.; Ream, J. E.; Sammons, D.; Sikorski, J. A.; Knowles, J. R., Synthesis and evaluation of two new inhibitors of EPSP synthase. *Tetrahedron Letters* **1991,** 32, (23), 2589-2592.

121. Marzabadi, M. R.; Gruys, K. J.; Pansegrau, P. D.; Walker, M. C.; Yuen, H. K.; Sikorski, J. A., An EPSP synthase inhibitor joining shikimate 3-phosphate with glyphosate: synthesis and ligand binding studies. *Biochemistry* **1996,** 35, (13), 4199-4210.

122. Jude, D. A.; Ewart, C. D.; Thain, J. L.; Davies, G. M.; Nichols, W. W., Transport of the antibacterial agent (6S)-6-fluoroshikimate and other shikimate analogues by the shikimate transport system of *Escherichia coli*. *Biochimica et Biophysica Acta* **1996,** 1279, (2), 125-129.

123. He M; Yang ZY; Nie YF; Wang J; P., X., A new type of class I bacterial 5-enopyruvylshikimate-3-phosphate synthase mutants with enhanced tolerance to glyphosate. *Biochim Biophys Acta.* **2001,** 1568, (1), 1-6.

124. Reinbothe S; Nelles A; B., P., N-(phosphonomethyl)glycine (glyphosate) tolerance in Euglena gracilis acquired by either overproduced or resistant 5-enolpyruvylshikimate-3-phosphate synthase. *Eur J Biochem.* **1991,** 198, (2), 365-73.

125. Chahoua, L.; Baltas, M.; Gorrichon, L.; Tisnee, P.; Zedde, C., Synthesis of (-)-Shikimate and (-)-Quinate-3-phosphates by Differentiation of the Hydroxyl Functions of (-)-Shikimic and (-)-Quinic acids. *J. Org. Chem.* **1992,** 57, 5798-5801.

126. DeFeyter, R. C.; Pittard, J., Genetic and molecular analysis of aroL, the gene for shikimate kinase II in *Escherichia coli* K-12. *Journal of Applied Bacteriology* **1986,** 165, (1), 226-232.

127. De Feyter, R., Shikimate kinases from Escherichia coli K12. *Methods Enzymol.* **1987,** 142, 355-61.

128. Romanowski, M.; Burley, S., Crystal structure of the Escherichia coli shikimate kinase I (AroK) that confers sensitivity to mecillinam. *Proteins.* **2002,** 47, (4), 558-62.

129. Hartmann, M.; Bourenkov, G.; Oberschall, A.; Strizhov, N.; Bartunik, H., Mechanism of phosphoryl transfer catalyzed by shikimate kinase from Mycobacterium tuberculosis. *J Mol Biol.* **2006,** 364, (3), 411-23.

130. Pereira, J.; de Oliveira, J.; Canduri, F.; Dias, M.; Palma, M.; Basso, L.; Santos, D.; de Azevedo, W. J., Structure of shikimate kinase from Mycobacterium tuberculosis reveals the binding of shikimic acid. *Acta Crystallogr D Biol Crystallogr.* **2004,** 60, (Pt 12 Pt 2), 2310-9.

131. Gan, J.; Gu, Y.; Li, Y.; Yan, H.; Ji, X., Crystal structure of Mycobacterium tuberculosis shikimate kinase in complex with shikimic acid and an ATP analogue. *Biochemistry* **2006,** 45, (28), 8539-45.

132. Dhaliwal, B.; Nichols, C.; Ren, J.; Lockyer, M.; Charles, I.; Hawkins, A.; Stammers, D., Crystallographic studies of shikimate binding and induced conformational changes in Mycobacterium tuberculosis shikimate kinase. *FEBS Letters* **2004,** 574, (1-3), 49-54.

133. Abergel, C.; Coutard, B.; Byrne, D.; Chenivesse, S.; Claude, J.; Deregnaucourt, C.; Fricaux, T.; Gianesini-Boutreux, C.; Jeudy, S.; Lebrun, R.; Maza, C.; Notredame, C.; Poirot, O.; Suhre, K.; Varagnol, M.; Claverie, J., Structural genomics of highly conserved microbial genes of unknown function in search of new antibacterial targets. *J Struct Funct Genomics.* **2003,** 4, (2-3), 141-57.

134. Millar, G.; Lewendon, A.; Hunter, M. G.; Coggins, J. R., The cloning and expression of the aroL gene from *Escherichia coli* K12. Purification and complete

amino acid sequence of shikimate kinase II, the aroL-gene product. *Biochemical Journal* **1986,** 237, (2), 427-437.